

# 博士論文

Ultimate lateral pile resistance characterization using  
active pile length

(杭の有効長を考慮した極限水平抵抗特性に関する研究)

アグリペイ メリー ロクサーヌ インファンテ

AGLIPAY MARY ROXANNE INFANTE



# Ultimate Lateral Pile Resistance Characterization using Active Pile Length

(杭の有効長を考慮した極限水平抵抗特性に関する研究)

Mary Roxanne I. AGLIPAY

A Thesis

Submitted to the University of Tokyo  
in Partial Fulfilment of the Requirement for  
The Degree of Doctor of Engineering

Supervisor

Associate Professor Takashi KIYOTA

Advisory Committee:

Professor Kazuo KONAGAI<sup>1</sup>

Professor Junichi KOSEKI<sup>2</sup>

Associate Professor Kohei NAGAI<sup>2</sup>

Associate Professor Taro UCHIMURA<sup>2</sup>

<sup>1</sup> Yokohama National University, <sup>2</sup> University of Tokyo

Department of Civil Engineering  
The Graduate School of the University of Tokyo  
Tokyo, Japan



## 論文の内容の要旨

論文題目 Ultimate lateral pile resistance characterization using active pile length

(杭の有効長を考慮した極限水平抵抗特性に関する研究)

氏名 アグリペイ メリー ロクサーヌ インファンテ  
AGLIPAY MARY ROXANNE INFANTE

It is noted that the deformation of piles is predominantly governed by the soil-pile interaction. This is for the simple reason that the movement of the piles and the surrounding soil is mutually dependent. Piles subjected to lateral loads deforms relative to the surrounding soil and conversely, the surrounding soil deforms relative to the deformation of the piles. In common engineering practice, long and flexible piles are used. For this type of piles subjected to lateral loads, its deformation is not observed over its entire length as it attenuates with increasing depth. Significant pile deformation is rather observed to occur only at the upper region near the ground surface. Therefore, this length covering the region of significant deformation, called the active pile length,  $L_a$ , is important in developing solutions for laterally loaded pile. This active pile length is a parameter reflective of the soil-pile interaction as it is characterized by the stiffness of the pile relative to the stiffness of the surrounding soil.

Along this active pile length, a soil wedge in the passive region can be fully mobilized with large external lateral loading. This wedge is indicative of the ultimate side soil resistance and hence, the ultimate lateral pile resistance. Therefore, this study intends to establish relationship of the ultimate lateral pile resistance and the simple soil-pile interaction parameter, active pile length,  $L_a$ .

The active pile length,  $L_a$ , is said to be proportional to the characteristic length,  $L_c$ , which is a ratio of the pile stiffness and the soil stiffness. In this study, Konagai's formula is used. This formula is a function of the pile stiffness,  $EI_p$  and shear modulus,  $G$ . The main difference with the expression commonly used in engineering (Chang's formula) is the use of shear modulus to represent the soil stiffness rather than relying on the coefficient of horizontal subgrade reaction,  $k_h$ . The substitution of the shear modulus for the characteristic length allows to capture inherently the stiffness of the soil and provide more convenient in-situ test for getting the shear modulus through shear velocity without the need for size effect correction.

The research takes off with the numerical simulation of laterally loaded piles in two-dimensional (2D) system. In this simulation, the elasto-plastic behaviour of sand is considered with elastic piles embedded in it. It is acknowledged that in reality, the soil-pile problem is innately a three-dimensional (3D) problem and having soil-pile interaction in 2D and in out-of-plane direction. Hence, in this case, piles considered is limited to capture behavior of walls, row piles or sheet piles. Nevertheless, the main intention is to simply investigate the formation of the passive soil wedge during nonlinear scenario and relate it to the active pile length. Moreover, the behavior of the active pile length can be established varying the contributing parameters such as the pile and soil stiffness. Results show a proportional relationship of the active pile length with the characteristic length. More importantly, there is a high correlation with the relationship of active pile length and the ultimate lateral pile capacity.

Hence, the concept of active pile length is applied in the three-dimensional platform for single piles embedded in sand. From the results of the rigorous solution, a simplified method to evaluate the ultimate lateral resistance of single piles in sand using the key parameter,  $L_{ai}$  is presented.

In the progressive formation of the active pile length, two stages are highlighted: the initial stage and the ultimate stage. First, the active pile length at the initial stage,  $L_{oi}$  is determined on the basis of known parameters such as the pile stiffness,  $EI_p$ , and small-strain shear stiffness,  $G_{max}$ . Capturing the elasto-plastic behavior of the surrounding soil, where there is degradation of surrounding soil stiffness, the active pile length at the ultimate stage or at larger deformations,  $L_{au}$ , can be determined by application of a correction factor. This parameter together with other pile and soil parameters that describes the mobilized passive soil wedge such as the outer pile radius,  $R_o$ , unit weight,  $\gamma$ , and Rankine passive earth pressure coefficient,  $K_p$ , is presented to be highly correlated with the ultimate lateral pile resistance,  $P_{ult}$ .

With these findings for single piles, the concept of active pile length is extended to closely-spaced grouped pile which could be analyzed as an equivalent single vertical pile. Grouped piles having spacing to diameter,  $s/d_p$ , equal to 1.5, 2.5, 3.5 and 4.5 is considered as closely grouped piles in this study. The relative pile stiffness to the surrounding soil stiffness is similarly the predominant driving parameter to describe the lateral deformation along the length of the grouped piles. Generally, results show that similar relationships and processes can be found with the single piles in evaluating the ultimate lateral pile resistance. Special attention must be made to the definition of parameters such as the grouped pile stiffness,  $EI_g$  and  $R_o$  which is derived specifically for closely grouped piles. There is a difference of 13% for evaluating the ultimate lateral pile resistance of single and closely grouped pile. However, superimposing all cases considered for the single and closely-spaced grouped piles, a very high correlation ( $R^2=0.97$ ) is still observed.

Thus, the determination of the ultimate lateral pile capacity using simple parameters with physical basis and reflective of the mechanisms of the laterally loaded piles provides more practical approach in the seismic design and assessment of piles and can be extended to different soil-pile configurations under more complex loadings and conditions.

# ACKNOWLEDGMENT

To Assoc. Prof. Takashi Kiyota, my sincerest gratitude to you for giving me the opportunity to be part of your laboratory, do research and have exposure on various laboratory activities even outside the realm of my research. Thank you for always keeping track on me as your student, for your relentless support, and scholarly and life advices. You inspire me to be more hardworking and do my best.

Thank you to Prof. Kazuo Konagai for providing the thrusts, great insights and expertise on my research. Thank you so much for your overflowing generosity, for sharing your knowledge and enriching me with your life stories. Thank you for being so passionate about your work. You send out energy and drive to your students. Thanks for the inspiration and motivation.

To Assoc. Prof Takashi Kiyota and Prof. Kazuo Konagai, you have definitely marked a great impression in my life more than you can imagine. Thank you.

Thank you to my advisory committee: Prof. Junichi Koseki, Assoc. Prof. Kohei Nagai and Assoc. Prof. Taro Uchimura for your invaluable inputs and guidance.

To Dr. Hiroyuki Kyokawa, thank you for being a great mentor of the numerical simulation. Thank you for your time and effort in helping me with the formulation, modification, debugging and implementation of the codes. You have greatly helped me a lot especially in jumpstarting my research. I will be forever indebted to you.

To Dr. Rama Mohan Pokharel and Dr. Gabriel Chiaro, thank you for your comments and recommendations in the journey of my research. You have greatly helped me a lot in the direction of my research. More than that, thank you for the talks, for your stories, for sharing your PhD life back then, and for making me look forward to making the finish line.

To my labmates, thank you so for all the fun memories from the small talks to the unforgettable moments during parties. You have made research life more bearable and my stay here in Japan a blast!

To Takasaki-san and Katagiri-san, thank you for being so nice, patient and accommodating of my needs and my queries. You simply made it easier for me to settle in the laboratory and help me survive my lack of Nihongo skills.

To MEXT (Monbukagakusho), thank you for the opportunity to be a scholarship grantee. Your financial support has made all these possible. With this kind of enrichment, you've definitely made a big difference in my life and hopefully to my future colleagues and the society.

Above all, thank you God, for the spiritual strength to carry on, to believe in myself and pursue my heart's desires all for your glory.

Thank you to my family, who have always been supportive since day 1. Thank you for allowing me to explore opportunities and just have this experience of a lifetime.

To Jason, Mayen and Ralph and all my friends, thank you for keeping me sane in this crazy world. Despite being a hermit most of the time, you never cease to check on me, bug me for some fun or just give me space when I need to. Thank you all for just being so good friends.

And lastly, to Ed, thank you for always being there, near or far! Thank you for being a buffer of all my disappointments, frustrations, rants and self-doubts. Thank you for being my rock. Thank you for just being there to listen and celebrate the little successes along the way. Thank you for all your help. Thank you for being such a great partner in everything. Glad it's you I shared this journey with.

# CONTENTS

LIST OF FIGURES.....	ix
LIST OF TABLES.....	xiii
LIST OF SYMBOLS USED .....	xiv
Chapter 1 Introduction.....	1
1.1 Background.....	1
1.2 Research Significance .....	3
1.3 Objectives.....	3
1.4 Methodology.....	4
1.5 Scope of Research.....	5
1.6 Organization of the Thesis.....	7
Chapter 2 Review of Related Literature.....	9
2.1 Lateral Pile Resistance .....	9
2.2 Methods for predicting the lateral resistance .....	10
2.2.1 Limit States .....	10
2.2.2 Semi-Empirical (Subgrade Reaction Method) .....	10
2.2.3 Elastic Continuum Solutions.....	11
2.2.4 Numerical Approach .....	11
2.3 Experiments.....	11
2.3.1 Pile Deformation.....	12
2.3.2 Soil Deformation .....	12
2.4 Summary and Conclusion .....	12
Chapter 3 Characteristic Length, $L_c$ .....	14
3.1 Introduction.....	14
3.2 Definition of Characteristic Length, $L_c$ .....	14
3.3 Current Practice in Japan .....	15
3.3.1 Chang's Formula .....	15
3.3.2 Coefficient of horizontal subgrade reaction.....	17
3.4 Doubts and limitation of current practice.....	19
3.5 Improvements of Proposed Characteristic Length Parameter .....	20
3.5.1 Shear Modulus as an Inherent Soil Characteristic: A Parameter for More Practical Field Test.....	20
3.5.2 Performance-Based Design.....	22
3.6 Summary .....	23

Chapter 4 Preliminary Study on the Concept of the Active Pile Length for Piles Embedded in Sand using Two-Dimensional System Analysis .....	24
4.1 Introduction .....	24
4.2 Active pile length.....	24
4.2 Numerical Analysis.....	25
4.2.1 Soil-Pile Idealization.....	25
4.2.2 Material Model and Elements.....	26
4.2.2.1 Pile Model.....	26
4.2.2.2 Joint Model.....	28
4.2.2.3 Soil Model .....	30
(a) Background of Subloading $t_{ij}$ .....	30
(b) Soil Model Parameters .....	33
4.3 Parametric Analysis .....	35
4.3.1 Effect of Pile Stiffness.....	35
4.3.2 Effect of Pile Length.....	36
4.3.3 Effect of Soil Stiffness.....	37
4.4 Application to the Ultimate Lateral Pile Resistance .....	39
4.5 Summary and Conclusion.....	41
Chapter 5 Application of Active Pile Length in the Ultimate Lateral Resistance of Single Fixed Head Piles Embedded in Sand .....	42
5.1 Introduction .....	42
5.2 Definitions.....	42
5.2.1 Active Pile Length .....	42
5.2.2 Ultimate Lateral Pile Resistance.....	43
5.3 Numerical Simulations of Laterally Loaded Single Pile.....	43
5.3.1 Soil-Pile System Idealization.....	44
5.3.1.1 Geometry of the Model.....	44
5.3.1.2 Boundary Conditions .....	45
5.3.1.3 Soil- Pile Interface .....	46
5.3.1.4 Material Model and Elements.....	47
(1) Pile Modeling.....	47
(2) Soil Modelling .....	49
(a) Background of the hypoplastic model .....	50
(b) Soil Model Parameters.....	51
5.3.1.5 Loading Procedure.....	54
5.3.2 Simple Validation of FEM Techniques from Elastic Case.....	56

5.3.3 Validation of FEM Techniques from Field Test using Elasto-plastic Case .....	58
5.3.4 Summary of Cases Considered .....	62
5.4 Results and Discussion of Numerical Simulations: On Active Pile Length.....	63
5.4.1 Active Pile Length Progression with Increasing Pile Head Displacement .....	64
5.4.2 Establishment of Criteria of the Slenderness Ratio for Long Piles.....	65
5.4.3 Initial Active Pile Length .....	65
5.4.3.1 Active Pile Length in Elastic Soil Medium and Non-linear Soil Medium .....	66
5.4.3.2 Relationship of Characteristic Length and Initial Active Pile Length ..	67
5.4.4 Active Pile Length at the Ultimate Stage.....	68
5.5 Application of Active Pile Length on Ultimate Lateral Pile Resistance.....	71
5.5.1 Derivation of the Ultimate Lateral Pile Resistance .....	71
5.5.2 Simplified Expression of the Ultimate Side Soil Resistance .....	72
5.6 Summary and Conclusions .....	73
Chapter 6 Extension of the Applicability of Active Pile Length for the Ultimate Lateral Resistance of Closely Grouped Piles.....	75
6.1 Introduction .....	75
6.2 Definition of Closely Grouped Piles .....	75
6.3 Numerical Simulation of Grouped Piles.....	76
6.3.1 Soil-pile system idealization of closely grouped piles .....	77
6.3.2 Summary of Cases Considered .....	79
6.4 Results and Discussion of Numerical Simulations: On Active Pile Length.....	80
6.4.1 Characteristic Length.....	81
6.4.2 Active Pile Length in Grouped Piles .....	81
6.4.2.1 Passive Soil Mobilization in Grouped Piles .....	81
6.4.2.2 Effect of Spacing and Number of Piles in a Group in Active Pile Length .....	84
6.4.3 Initial Active Pile Length .....	87
6.4.4 Active Pile Length at the Ultimate Stage.....	87
6.5 Application of Active Pile Length on Ultimate Lateral Pile Resistance.....	89
6.5.1 Derivation of the Ultimate Lateral Pile Resistance .....	89
6.5.2 Simplified Expression of the Ultimate Resistance.....	91
6.5.3 Superposition of Single and Closely Grouped Piles .....	92
6.6 Summary and Conclusion .....	92
Chapter 7 Conclusions and Recommendations.....	94
7.1 Conclusions .....	94

7.2 Recommendations .....	95
7.2.1 On piles.....	95
7.2.2 On soils.....	96
7.2.3 On loading conditions .....	96
REFERENCES.....	98
APPENDIX A. Subloading $t_{ij}$ constitutive model code .....	105
APPENDIX B. User defined material code for the hypoplastic model.....	114
APPENDIX C. Sample Input code for the abaqus model with the user defined material.....	131
APPENDIX D. Element Test Abaqus for the hypoplastic model.....	138

# LIST OF FIGURES

Figure 1 - 1. Piles as deep foundation for important structures: (a) buildings (IHA), (b) bridges (SIRA) consulting engineers), (c) powerplant (Alamy, 2014)and (d) turbines (Alamy, 2013) .....	1
Figure 1 - 2. Girders dislocated in Luanghe bridge after Tangshan Earthquake (from Wei et al., 2008) .....	2
Figure 1 - 3. Lateral load transfer mechanism.....	2
Figure 1 - 4. Schematic diagram of the main objective .....	4
Figure 1- 5. Overview of the research process .....	4
Figure 1- 6. Scope and limitation of this research.....	6
Figure 3-1. Schematic representation and relationship of active pile length and characteristic length.....	15
Figure 3- 2. Winkler Model (Beam on Elastic Foundation) .....	16
Figure 3 - 4. Load-deformation curve for determination of coefficient of subgrade reaction .....	18
Figure 3 - 3. Schematic diagram of horizontal plate loading test (based on Yoshida and Yoshinaka, 1972) .....	18
Figure 3- 5. Equivalent uniform distribution .....	20
Figure 3- 6. Derivation of $E_{50}$ and $v_{50}$ .....	20
Figure 3- 7. Chang's Formula vs $L_c(EI,G)$ .....	21
Figure 4 - 1. Soil-pile configuration .....	26
Figure 4 - 2. The concept of the continuum-mechanics based beam finite element. (a) the 3D beam used discretised at the cross-section and in the longitudinal axis. (b) discretization along the longitudinal axis. (c) cross-sectional area discretization (after Yoon et al., 2012).....	27
Figure 4 - 3. SMP Plane (a) Definition of $t_N$ and $t_S$ (b) Definition of $d\varepsilon_N^*$ and $d\varepsilon_S^*$ (after Nakai, 2007) .....	31
Figure 4- 4. Failure criteria surface of different constitutive models in octahedral plane (Adopted from Nakai, 2007).....	32
Figure 4 - 5. Drained compression and extension test for Toyoura Sand (Taken from Kyokawa 2011) .....	34
Figure 4 - 6. Stress ratio- $\varepsilon_a$ and $\varepsilon_v$ - $\varepsilon_a$ relationship of Toyoura sand with varying void ratios, $e_o$ at $p'_o=98kPa$ .....	34
Figure 4 - 7. Variation of pile thickness, $b_t$ , with the active pile length, $L_a$ .....	35
Figure 4 - 8. Effect of pile stiffness, $EI_p$ , on active pile length, $L_a$ .....	36
Figure 4 - 9. Variation of active pile length, $L_a$ with pile length, $L_p$ .....	37
Figure 4 - 10. $L_a/L_p$ with actual pile length, $L_p$ .....	37
Figure 4 - 11. Variation of active pile length, $L_a$ , with the $L_o$ for all cases at different lateral pile head deformation.....	38
Figure 4 - 12. Variation of the ratio of the active pile length to the initial characteristic length with respect to the lateral pile head displacement. ....	39
Figure 4 - 13. Force-deformation curve.....	40
Figure 4 - 14. Correlation between $P_{ult}$ and $K_p\gamma L_{au}^2$ .....	41

Figure 5 - 1. Active pile length .....	42
Figure 5 - 2. Soil wedge formation around laterally loaded pile.....	43
Figure 5 - 3. X-ray CT scan of the failure deformation around laterally loaded pile .....	43
Figure 5 - 4. Soil-pile geometric properties and meshing in (a) plan view, (b) 3D Perspective view and (c) cross-sectional view .....	44
Figure 5 - 5. Boundary planes of the soil-pile system.....	45
Figure 5 - 6. Master-slave surface definition .....	46
Figure 5 - 7. Comparison of surface-to-surface discretization and node-to-surface discretization .....	46
Figure 5 - 8. Types of hexahedral elements (C3D8R and C3D20R) .....	47
Figure 5 - 9. Maximum deflection for a cantilever beam subjected to a concentrated force at the end .....	47
Figure 5 - 10. Load-deflection curve of a cantilever beam using C3D8 and C3D20 elements.....	48
Figure 5 - 12. Maximum deflection for cantilever beam with constrained rotation at end and applied with concentrated force .....	48
Figure 5 - 11. Constrained FEM techniques .....	48
Figure 5 - 13. Numerical solution vs. analytical solution of fixed-head pile .....	49
Figure 5 - 14. Void ratio vs. mean pressure in logarithmic scale (after Herle and Gudehus, 1999) .....	52
Figure 5 - 15. Comparison between experimental and numerical result for the stress-strain relationship of Toyoura sand (after (Kyokawa, 2011)) .....	53
Figure 5 - 16. Loading Process: (1) Initial Stress Condition Simulation: (a) Vertical Stress Condition (b) Vertical Displacement Distribution (c) Horizontal Stress Condition and (2) Application of Lateral Load.....	55
Figure 5 - 17. Comparison of the pile deformation along the pile depth (after (Lu et al., 2011)).....	57
Figure 5- 18. Arkansas Field Test Set-up (after Fan(1996)) .....	58
Figure 5 - 19. Arkansas Field Test FEM Model.....	60
Figure 5- 20. Comparison of Lateral Load - Deflection curves of the Arkansas Field Test and Numerical Simulations (Observed results from Alizadeh and Davisson (1970) and Fan (1996)) .....	61
Figure 5 - 21. Lateral Pile Head Deformations vs. Depth for the Arkansas Field Test (Observed results from Alizadeh and Davisson (1970) and Fan (1996)).....	61
Figure 5 - 22. Active pile length progression in the Arkansas Field Test .....	62
Figure 5 - 23. Definition of active pile length.....	63
Figure 5 - 24: Active pile length progression with increase in pile head deformation.....	64
Figure 5 - 25. Slenderness criteria for long piles .....	65
Figure 5- 26. Sample comparison of active pile length progression for piles embedded in elastic and elasto-plastic behaviour .....	66
Figure 5- 27. Comparison of initial active pile length between soil medium considered as elastic and elasto-plastic.....	66
Figure 5 - 28. Relationship of $L_c$ and $L_0$ using $G=G_{max}$ .....	67
Figure 5- 29. Relationship of normalized active pile length with pile head displacement for piles embedded in $e_0=0.73$ .....	68
Figure 5- 30. Relationship of normalized active pile length with pile head displacement for piles embedded in $e_0=0.80$ .....	68
Figure 5- 31. Relationship of normalized active pile length with pile head displacement for piles embedded in $e_0=0.90$ .....	69

Figure 5- 32. Relationship of normalized active pile length with the shear strain for piles embedded in $e_0=0.73$ .....	69
Figure 5- 33. Relationship of normalized active pile length with the shear strain for piles embedded in $e_0=0.80$ .....	70
Figure 5- 34. Relationship of normalized active pile length with the shear strain for piles embedded in $e_0=0.90$ .....	70
Figure 5- 35. Relationship of the $L_a/L_0$ with the initial void ratio.....	71
Figure 5 - 36. Load deformation curve.....	72
Figure 5- 37. Relationship of ultimate lateral pile resistance with active pile length and other soil parameters.....	72
Figure 5 - 38. Flowchart for the simplified expression of ultimate lateral pile resistance.....	74
Figure 6 - 1 Schematic illustration of the patterns of stress and deformation around laterally loaded grouped piles (a) closely grouped piles (b) widely spaced grouped piles (after Bogard and Matlock (1983)) .....	75
Figure 6 - 2 Equivalent Single Beam from Lateral Field Test (after (Konagai et al., 2003)) .....	75
Figure 6 - 3 Lateral pile group effects for different $s/d$ ratios (after Konagai et al. (2003) ) .....	76
Figure 6 - 4. Soil-pile configuration for 2x2 grouped piles. (a) 3D Perspective View, (b) Plan View. Note: Pile cap not shown and (c) Cross-sectional view.....	78
Figure 6 - 5. Soil-pile configuration for 3x3 grouped piles. (a) 3D perspective view, (b) Plan view. Note: Pile cap not shown and (c) Cross-sectional view.....	78
Figure 6 - 6. Soil-pile interface for grouped piles .....	79
Figure 6 - 7. Equivalent single beam analogy idealization .....	80
Figure 6- 8. Soil lateral displacement distribution at the passive region for 2x2 grouped piles ...	82
Figure 6- 9. Soil lateral displacement distribution at the passive region for 3x3 grouped piles ...	82
Figure 6 - 10. Active pile length progression at lead piles for closely grouped piles embedded in dense sand.....	83
Figure 6 - 11. Active pile length progression at lead piles for closely grouped piles embedded in medium dense sand .....	83
Figure 6 - 12. Active pile length progression at lead piles for closely grouped piles embedded in loose sand.....	83
Figure 6- 13. Average active pile length progression for grouped piles embedded in dense sand, $e_0=0.73$ .....	84
Figure 6- 14. Active pile length progression of the individual piles in the 2x2 grouped piles embedded in dense sand, $e_0=0.73$ .....	85
Figure 6- 15. Active pile length progression of individual piles in 3x3 grouped piles embedded in $e_0=0.73$ .....	86
Figure 6- 16. Active pile length progression of individual piles in 3x3 grouped piles embedded in $e_0=0.80$ .....	86
Figure 6- 17. Active pile length progression of individual piles in 3x3 grouped piles embedded in $e_0=0.90$ .....	86
Figure 6- 18. Relationship of characteristic length to the initial active pile length for closely grouped piles.....	87
Figure 6- 19. Relationship of $L_a/L_0$ with average shear strain for grouped piles embedded in soil with $e_0=0,73$ .....	88
Figure 6- 20. Relationship of $L_a/L_0$ with average shear strain for grouped piles embedded in soil with $e_0=0,80$ .....	88

Figure 6- 21. Relationship of $L_a/L_0$ with average shear strain for grouped piles embedded in soil with $e_0=0,90$ .....	88
Figure 6- 22 Load deformation curves for grouped piles .....	90
Figure 6- 23. Simulation of the laterally loaded grouped pile without the soil. ....	90
Figure 6- 24 Relationship of ultimate lateral pile resistance with active pile length and other soil parameters .....	91
Figure 6- 25 Superposition of the simplified approach for the single and closely grouped piles .	92
Figure 6 - 26. Flowchart for determining the ultimate lateral pile capacity of grouped piles .....	93

# LIST OF TABLES

Table 1- 1. Soil-pile system general configuration.....	5
Table 2- 1. Existing methods in determining the lateral response of piles.....	13
Table 3 - 1. Correction factor, $\alpha$ , for the following methods and load case (after Table 9.6.1 in Japan Road Association, 2012) .....	18
Table 3 - 2. Acceptable level of damage in performance-based design (from Iai, 2001) .....	23
Table 4 - 1. Comparison between tensors and scalars related to stress and strain in ordinary concept and $t_{ij}$ concept (after Nakai, 2007) .....	31
Table 4 - 2. Toyoura sand (TS) material parameters for the subloading $t_{ij}$ .....	34
Table 4- 3. Soil Parameters of Toyoura Sand (TS) ( $G_s = 2.65$ ).....	40
Table 5 - 1. Material parameters for Toyoura sand.....	53
Table 5 - 2. Pile properties .....	56
Table 5 - 3. Soil Properties .....	56
Table 5 - 4. Pile properties of the Arkansas Field Test Pile.....	58
Table 5 - 5. Soil properties at the Arkansas Field Test Site.....	59
Table 5 - 6. Soil parameters for the Arkansas Field Test.....	60
Table 5 - 7. Summary of pile and soil properties.....	62
Table 6 - 1 Summary of cases considered for grouped piles .....	79
Table 6 - 2. $L_a/L_0$ values for the single and grouped piles embedded in $e_0=0.73, 0.80$ and $0.90$ ..	89
Table 6 - 3. $L_a/L_0$ values normalized with $L_a/L_0$ (single piles) .....	89

## LIST OF SYMBOLS USED

- $a$  - One of the factor determining the critical state surface in the stress space for hypoplastic model given by equation 5.7
- $a_F$  - Parameter for controlling decay rate of the influence of density in subloading  $t_{ij}$  model
- $A$  -Cross-sectional area
- $b_t$  - Pile thickness (Length)
- $B$  - Plate width (Length)
- $B_H$  - Equivalent loading width (Length)
- $d_p$  - Pile diameter (Length)
- $D$  - Stretching Tensor
- $D^e$  - Elastic stiffness matrix at joint
- $e$  - Current void ratio
- $e_o$  - Initial void ratio
- $e_{cs}$  - Void ratio at normal consolidation at atmospheric pressure,  $P_a=98\text{kPa}$  (subloading  $t_{ij}$ )
- $e_c$  -Characteristic void ratio at critical state
- $e_{c0}$  - Reference characteristic void ratio at critical state at mean pressure =0 (hypoplastic model)
- $e_d$  -Characteristic void ratio, lower limit (Figure 5- 8)
- $e_{d0}$  - Reference characteristic minimum void ratio at mean pressure =0 (hypoplastic model)
- $e_i$  -Characteristic void ratio, upper limit (Figure 5- 8)
- $e_{i0}$  - Reference characteristic maximum void ratio at mean pressure =0 (hypoplastic model)
- $E_0$  - Modulus of soil deformation (Force/Length<sup>2</sup>)
- $E_p$  - Young's elastic modulus of pile (Force/Length<sup>2</sup>)
- $E_{50}$  - Secant Young's modulus determined from triaxial stress-strain curve at 50% of maximum deviator stress.

- $EI_p$  – Pile stiffness (Force-Length<sup>2</sup>)
- $EI_g$  – Grouped Pile stiffness (Force-Length<sup>2</sup>)
- $f_e, f_b$  – Dimensionless factors representing the dependency on relative density in the hypoplastic model
- $f_d$  – Dimensionless factors representing the dependency on pressure in the hypoplastic model
- $F$  – One of the factor determining the critical state surface in the stress space for hypoplastic model given by equation 5.8
- $f$  – yield function
- $g$  – potential function
- $G$  – Shear modulus (Force-Length<sup>2</sup>)
- $G_{50}$  – Secant shear modulus determined from triaxial stress-strain curve at 50% of maximum deviator stress.
- $G_s$  – Specific gravity of soil
- $G_{max}$  – Small strain shear modulus (Force/Length<sup>2</sup>)
- $h$  – Pile wall thickness (Length)
- $h_k(r)$  – linear shape function
- $h_k(s, t)$  – quadratic shape function
- $h_s$  – Granular stiffness parameter of hypoplastic model for determining the normal compression line and critical state line (Force/Length<sup>2</sup>)
- $I_p$  – Moment of inertia of pile (Length<sup>4</sup>)
- $k$  – Spring modulus (Force/Length<sup>2</sup>)
- $k_H$  – Coefficient of horizontal subgrade reaction (Force/Length<sup>3</sup>)
- $k_s$  – shear stiffness at joint
- $k_n$  – normal stiffness at joint
- $k_{H0}$  – Coefficient of horizontal subgrade reaction from a plate load test (Force/Length<sup>3</sup>)
- $K_p$  – Rankine passive coefficient of earth pressure
- $K_{xxGP}$  – Static stiffness of the grouped pile

- $K_{xxSP}$  – Static stiffness of single pile
- $L$  – Plate length (Length)
- $L_c$  – Characteristic length (Length)
- $L_a$  – Active Pile length (Length)
- $L_0$  – Active Pile length at the initial stage (Elastic) (Length)
- $L_{au}$  – Active Pile length at the ultimate stage (Length)
- $L_p$  – Actual Pile length (Length)
- $n$  – One of the parameters of hypoplastic model for determining the normal compression line and critical state line
- $n_p$  – Number of individual piles in a grouped pile
- $P$  – Load (Force)
- $P_a$  – Atmospheric pressure (kPa) (subloading  $t_{ij}$ )
- $P_{ult}$  – Ultimate lateral pile resistance (Force)
- $p(z)$  – Local force per unit length (Force/Length)
- $p_0$  – Initial mean stress
- $\boldsymbol{p}$  – Mean stress
- $q$  – Deviatoric stress
- $R_{cs}$  – Stress ratio at critical state (subloading  $t_{ij}$ )
- $R_0$  – Pile radius (Length)
- $s$  – Center-to-center spacing of piles in a grouped pile
- $t_s$  – Shear traction force at joint
- $t_n$  – Normal contact force at joint
- $p_0$  – Initial mean stress
- $\hat{\boldsymbol{T}}_s$  – Objective Jaumman stress rate tensor
- $\boldsymbol{T}_s$  – Cauchy stress tensor (hypoplastic model)
- $\hat{\boldsymbol{T}}_s$  – Stress ratio tensor (hypoplastic model)
- $\hat{\boldsymbol{T}}_s^*$  – Deviatoric stress ratio tensor (hypoplastic model)
- $u(z)$  – Deformation of the soil at any point (z coordinate)

- $\vec{V}_y^k$  – Direction vectors at y-axis
- $\vec{V}_z^k$  – Direction vectors at z-axis
- $\vec{x}^{(m)}$  – position vector of the solid element m in the Cartesian system  $r,s,t$
- $\bar{y}_k^{j(m)}$  – y nodal coordinates
- $y_{max}$  – Maximum deflection at the pile tip (Length)
- $\bar{z}_k^{j(m)}$  – z nodal coordinates
- $\alpha$  – Proportional constant for active pile length
- $\alpha_h$  – Parameter that controls the peak friction angle based on the relative density in hypoplastic model
- $\beta$  – Inverse of characteristic length (1/Length)
- $\beta_h$  – Parameter that controls the dependency of stiffness on the relative density in hypoplastic model
- $\beta^s$  – Shape of yield surface
- $\varepsilon_a$  – Axial strain (%)
- $\varepsilon_d$  – Shear strain (%)
- $\varepsilon_v$  – Volumetric strain (%)
- $\delta_s^p$  – Plastic shear strain
- $\delta^p$  – Incremental plastic strain
- $\delta$  – Incremental total strain
- $\delta^p$  – Incremental plastic strain
- $\delta^e$  – Incremental elastic strain
- $\kappa$  – Swelling Index (subloading  $t_{ij}$ )
- $\gamma$  – Dry Unit Weight (Force/Length<sup>3</sup>)
- $\gamma_w$  – Unit Weight of Water (Force/Length<sup>3</sup>)
- $\lambda$  – Compression Index (subloading  $t_{ij}$ )
- $\eta_L$  – Stiffness ratio of grouped piles to single piles
- $\nu$  – Poisson ratio
- $\nu_{50}$  – Poisson ratio at  $E_{50}$

- $\phi$  – Peak Angle of Internal Friction
- $\sigma'$  – Effective vertical stress
- $\varphi$  –Hardening parameter
- $\varphi_c$  – Parameter for critical angle of internal friction in hypoplastic model
- $\psi$  – One of the invariants in the hypoplastic model given by Equation 5.9
- $\theta$  – One of the invariants in the hypoplastic model given by Equation 5.10

# Chapter 1

## Introduction

### 1.1 Background

Piles are commonly used as deep foundations to transfer induced load down to deeper and harder stratum. They are usually used to support important structures such as building, bridges, and nuclear power plants, turbines, among others (see

Figure 1 - 1).



**Figure 1 - 1. Piles as deep foundation for important structures: (a) buildings (IHA), (b) bridges (SIRAJ consulting engineers), (c) powerplant (Alamy, 2014) and (d) turbines (Alamy, 2013)**

These piles are most susceptible to one or a combination of external lateral loads that could be in the form of wind, wave actions, earthquakes and/or large earth pressure. In the instance where the induced lateral loads are greater than the ultimate lateral capacity of piles, the structural integrity of the piles are at risk and leads to failure. This failure may be due to the loss of support from the resistance of the surrounding soil, which may allow excessive lateral deformations or formation of plastic hinges in the pile. An example showing failure of laterally loaded piles is shown in Figure 1 - 2 (Wei et al., 2008). In this photo of Luanghe bridge, taken after the 1976 Tangshan earthquake (M7.8) in China, pier deformations and dislocation of girders are observed due to the settlement and the lateral bending deformation of the piles. Given this actual disastrous scenario, it shows the importance of determining the ultimate lateral pile capacity. This definition allows to have an upper limit in the design and assessment of piles to resist the induced loads and realize the target performance.

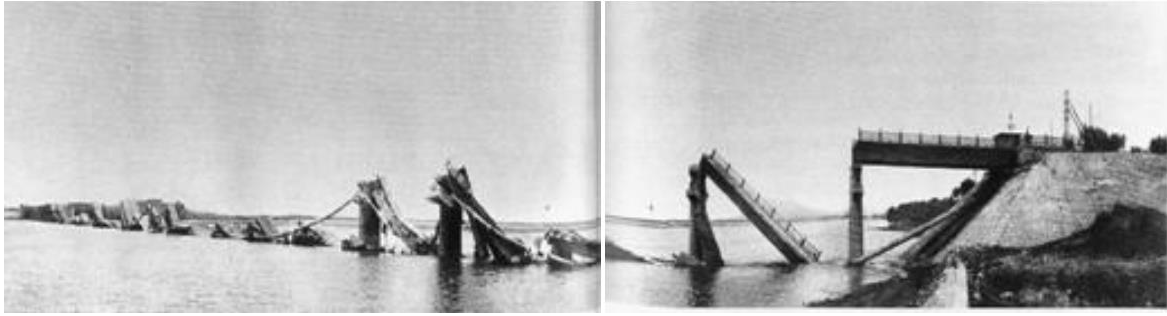


Figure 1 - 2. Girders dislocated in Luanghe bridge after Tangshan Earthquake (from Wei et al., 2008)

Practicing engineers have vital roles in the design of infrastructures in the society. Thus, the definition of the ultimate lateral pile capacity must appeal to them by being simple and practical. Yet more importantly, the salient feature of the definition of the ultimate lateral pile capacity is it should have physical basis and reflective of the mechanisms of the laterally loaded piles through simple parameters.

In deep foundations, there is the presence of two elements, the soil and the pile. When these piles are subjected to lateral load, the movements of the piles and their side soils are mutually dependent. The deformation of the piles is relative to the deformation of the soil. Conversely speaking, the deformation of the soil is relative to the deformation of the piles. Hence, the lateral resistance of piles is governed by soil-pile interaction. In common engineering practice, long and flexible piles are normally used. The deformations of these piles when subjected to lateral load does not transpire over the entire actual length. Instead, the pile deformation becomes negligible at some depth level from the ground surface (Figure 1 - 3). In effect, the actual pile length is not considered but rather the length that has significant deformation is ought to be the key parameter for developing solutions for laterally loaded piles to consider a more pragmatic approach. This length of significant deformation is called the *active pile length*, also referred as effective length by other researchers. This active pile length, is a parameter reflective of the soil-pile interaction as it is characterized by the stiffness of the pile relative to the stiffness of the surrounding soil.

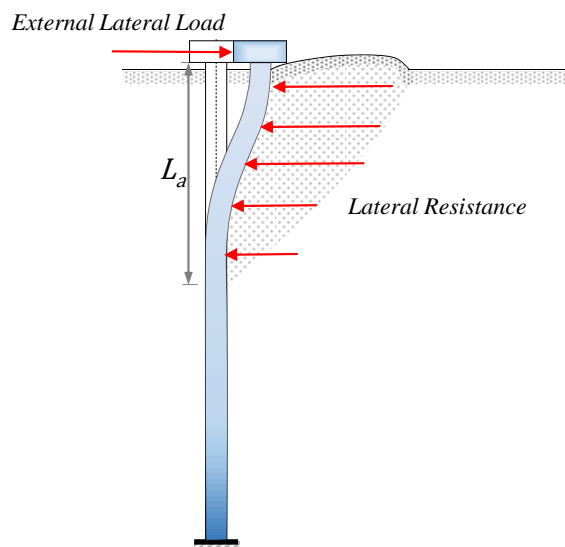


Figure 1 - 3. Lateral load transfer mechanism

In the scenario where piles are subjected to a lateral load especially under strong occurrences, the pile moves parallel to the direction of the load and pushing the front soil surrounding it (Figure 1 - 3). Consequently, compressive and shear stresses and strains are generated in the passive region of the soil, in consort with its nonlinear behaviour. A soil wedge is formed and mobilized along this active pile length. This side soil resistance, represented by the wedge, against the pile corresponds to the lateral pile capacity.

Therefore, it is inferred that the ultimate lateral pile resistance can be described by active pile length for the resiliency and response of piles within target structural and seismic performance.

## **1.2 Research Significance**

With the advent of high computing powers and advanced technology, rigorous tools have been developed to allow simple to complex soil-pile configurations to be modelled and simulated under different conditions. While it is indeed a powerful tool, fact remains that it is also a tedious job, not to mention the expert modelling skills and techniques needed to implement a careful, precise and correct simulation. To add to that, expensive computing time and memory is required with the increase in complexity of systems to simulate the scenario as close to reality. Thus, it is warranted that simple yet high calibre solutions are to be made available especially to practicing engineers.

Many attempts have been done to provide simplified approach in semi-empirical or analytical nature, despite the challenges in the complexity of pile design especially in the interest of the lateral pile capacity. However, with the simplifications comes the consideration of simple and conservative conditions like treatment of soil as an elastic medium.

This research proposes a method that echoes the simplistic nature of the existing methods yet at the same time, is founded on rigorous solutions offered by the more advanced and powerful tool. Problematic simplified treatment of soil as elastic medium of existing methods are addressed through consideration of the elasto-plastic behaviour of soil in the modelling and simulation of the system to produce rigorous solutions. The use of simple parameters with physical meaning such as the active pile length, reflective of the soil-pile interaction, provides a more valuable meaning and relevant to the practicing engineers.

The goal of this research to provide a simplified expression for the ultimate lateral pile resistance based on the active pile length parameter yields a more practical approach in the design and assessment of piles.

## **1.3 Objectives**

Generally, the objective of this study is to bridge the gap between the available rigorous methods and the world of practicing engineers by providing a rational simplified method for determining the ultimate lateral pile resistance and have the structures performed within target performance under expected loads (Figure 1 - 4).

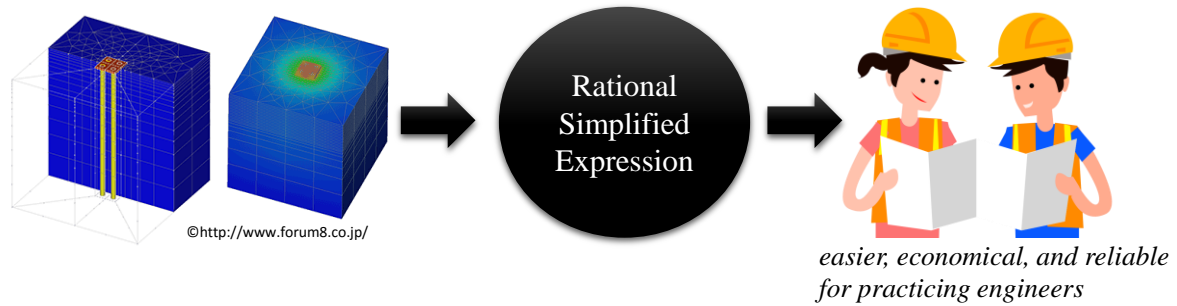


**Figure 1 - 4. Schematic diagram of the main objective**

Specifically, this study aims to do the following:

- Take advantage of the available rigorous methods like the finite element method (FEM) to model different soil-pile configurations with consideration of the elasto-plastic nature of the soil. This allows to simulate the soil-pile system as close to reality.
- Analyse the lateral deformation along the pile length in the interest to determine the active pile length progression with increasing load for several case studies from the results of these simulations. Correspondingly, describe the soil wedge formation around the laterally loaded pile represented by the side soil ultimate resistance.
- Finally, establish the relationship of the ultimate lateral pile resistance with the active pile length. In this way, a rational simplified expression for the ultimate lateral pile resistance based on a parameter indicative of the soil-pile interaction i.e. active pile length, and other soil properties could be provided for a more practical approach.

## 1.4 Methodology

This research entails a three-tier process as described in Figure 1- 5. The research process starts with the (1) numerical simulation followed by (2) the post-processing of the results and finally (3) the analysis to arrive at a rational simplified expression.

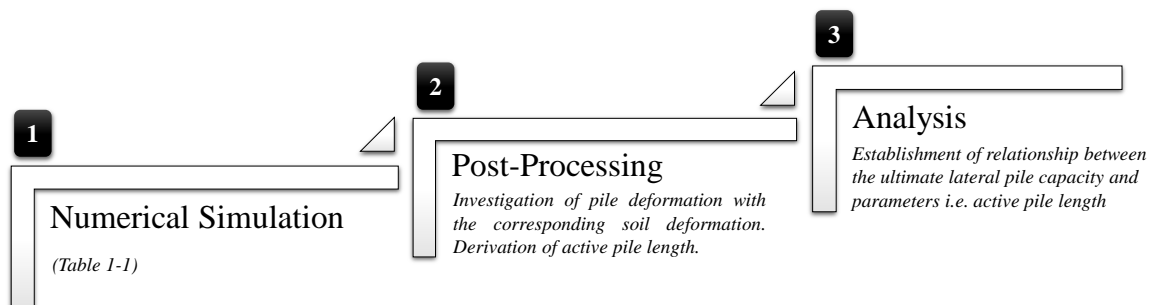


**Figure 1- 5. Overview of the research process**

To achieve the objectives abovementioned, a rigorous solution using finite element method (FEM) is initially performed. The modeling of the soil-pile system is intended to simulate the response of piles under lateral loading considering the general configuration listed in **Error! Reference source not found.** Parametric analysis considering variations of pile parameters and soil type is performed for different cases (i.e. single and grouped piles).

**Table 1- 1. Soil-pile system general configuration**

Soil	Homogeneous Sand
Soil Model	Elasto-plastic behavior
Pile Type	Fixed Head, Long, End bearing Piles
Pile Model	Linear Elastic
Analysis	FEM, static and monotonic loading

A post-processing is done from the results of the rigorous method. Investigation and analysis is done in terms of the pile deformation with the corresponding soil deformation around the laterally loaded pile. The active pile lengths are derived based on setting the criteria for the negligible deformation as the depth where the lateral displacement is only 3% of the pile head lateral displacement. Correspondingly, the ultimate side soil resistance is derived for all the cases.

Finally, the nonlinear response of piles embedded in sand, specifically in the interest of the side soil resistance is described by the active pile length. With the establishment of the relationship of these two parameters, a simplified expression could be provided for the ultimate lateral pile capacity.

## 1.5 Scope of Research

In this research, the interest is the use of active pile length as a key parameter in developing solutions for the ultimate capacity of laterally loaded piles. Hence, the focus of this research is on long and flexible piles. For short and stiff piles, a different behaviour and failure mechanism can be observed such that the concept of active pile length would be irrelevant.

Moreover, it is acknowledge that there are several combinations of soil-pile configuration under different conditions possible. To discuss and delved into all these issues would be impossible given the time constraint. Hence, this study aims to limit the study in way that it could still provide valuable contributions based on realistic scenarios. This research intends to provide a seed concept that could be built up on for extension to more complex ideas (see Figure 1- 6).

In modelling the piles, its behaviour is considered as an elastic case where the confinement of the soil around the pile is assumed to be a sufficient support even with formation of plastic hinges in the pile itself. For grouped piles, closely grouped piles are investigated on in the intention to extend the analysis for single fixed head piles to grouped piles that could be treated as equivalent single piles. Hence, the spacing to diameter ratio considered is small i.e.  $s/d_p = 1.5, 2.5$  and  $4.5$  to ensure grouped piles under the category of closely grouped piles. Moreover, a square configuration of the grouped piles is dealt with at this stage.

For treatment of soils, it is recognized that the stratigraphy of soil medium in existent is not homogeneous in terms of relative density, more so of the presence of various types of soil throughout the entire soil depth. However, given at this early stage, treating the soil medium as homogeneous puts a leverage in establishing the behaviour of the active pile length for a particular type of surrounding soil condition and its effect to the corresponding side soil resistance. In this particular research, the focus is on soil medium made up of a homogeneous dry clean sand. This could be related in the actual case where the top layer is made up of uniform sand and groundwater is not high, or perhaps a conservative approach for predominantly sandy soils, where the weighted average of soil properties along the entire depth is considered to be the equivalent homogeneous soil property. In any case, strain localization in the soil is not yet accounted for.

In terms of the load cases, the lateral load is applied on the pile heads in a static pushover method. In this case, the pile is subjected to a lateral load in a monotonic displacement-controlled pattern that continuously increases until large displacements are reached.

The cases considered for piles, soils and the loading condition in this research would serve as a jump-off in the analysis for more complex scenario. In a way, this perceived modularity of this research also makes it flexible to cater to specific problems once the whole system is built up.

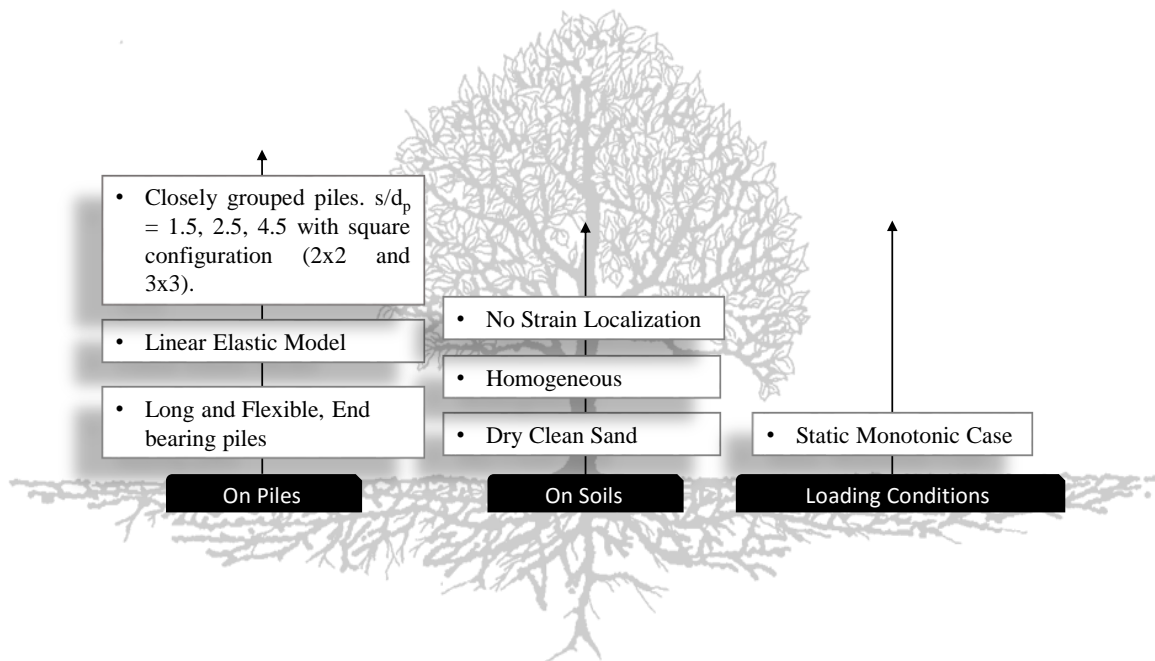


Figure 1- 6. Scope and limitation of this research

## **1.6 Organization of the Thesis**

The following summarizes the organization of thesis and a brief description of each chapter.

### **Chapter 1: Introduction**

Chapter 1 provides the overview of the study. This includes the background and thrusts of this research, the objectives, a view on the research investigation tools, and the outline of this research dissertation.

### **Chapter 2: Review of Related Literature**

Chapter 2 presents a comprehensive review of existing researches on the laterally loaded pile behaviour. This chapter presents the different approaches on determining the ultimate lateral pile resistance available in this aspect and highlight the need for this present study.

### **Chapter 3: Characteristic Length**

Chapter 3 presents the definition of the characteristic length which is proportional to the active pile length. The use of Chang's formula to determine this characteristic length as current practice in Japan is presented. Particularly, Chang's formula's dependency on the use of subgrade reaction is investigated on. This chapter highlights the physical basis, or the lack thereof, of this coefficient of horizontal subgrade reaction and proposes a more rational expression considering the shear modulus to represent the soil stiffness. The potential merits and solutions to improve the current practice using the new expression to determine the characteristic length is discussed.

### **Chapter 4: Preliminary Study on the Concept of Active Pile Length for Piles Embedded in Sand (2D)**

Chapter 4 delves on the concept of the active pile length in relation to the characteristic length. As a preliminary study, this chapter presents the study considering a 2D soil-pile system, to which piles could be deemed as sheet piles embedded in sand. Parameters affecting the active pile length is highlighted. The potential of active pile length to describe the ultimate lateral pile resistance is presented.

### **Chapter 5: Application of Active Pile Length in the Ultimate Lateral Resistance of Single Fixed Head Piles Embedded in Sand**

Chapter 5 discusses the applicability of the active pile length on determining the ultimate lateral pile resistance in a three-dimensional level. This chapter presents the process of arriving at the simplified expression based on the rigorous solution of simulating a long single fixed-head pile embedded in an elasto-plastic sand.

### **Chapter 6: Extension of the Applicability of Active Pile Length for the Ultimate Lateral Resistance of Closely Grouped Piles**

Considering the applicability of active pile length on determining the ultimate lateral pile resistance of single piles in sand, Chapter 6 extends this idea for closely grouped piles that could be considered as equivalent single pile.

### **Chapter 7: Conclusions and Recommendations**

Chapter 7 summarizes valuable contributions derived from this research and highlights the main findings for the simplified method to determine the ultimate lateral pile resistance based on simple active pile length parameter. This chapter also contains the recommendations on the potential extension on the use of active pile length on the same application considering more complex soil-pile configuration and under different kinds of loading.

## **References**

**Appendix A** Code for the subloading  $t_{ij}$  for 2D case

**Appendix B** Code for the user-defined material (hypoplastic) (Abaqus)

**Appendix C** Sample input file for the 3D numerical simulation (Abaqus)

**Appendix D** Sample input file for the element test using the hypoplastic model (Abaqus)

# Chapter 2

## Review of Related Literature

### 2.1 Lateral Pile Resistance

External lateral load is one of the components of the total external forces that engineers have to address when it comes in designing the piles under expected loads. One researcher (Rao et al., 1998) say that the percentage of lateral loads that may induce onshore structure are in the order of 10-15% and even worse for offshore structures, exceeding 30%. Perhaps, one of the common lateral forces that could induce on the pile supported structures are wind gusts (Basu et al., 2008). Other major sources of lateral loads are the horizontal forces generated from the horizontal ground shaking when earthquakes occur. A more obvious case would be the exposure of piles to lateral earth pressure, among others. However, there also structures, where the piles are intentionally designed to mainly resist the lateral loads, where deemed to be the critical loads. Examples of these structures are oil production platforms, wharfs and jetties and earth retaining structures (Basu et al., 2008). Particularly for earth retaining structures, the main role of pile to resist lateral forces is evident in the cases where piles are installed in slopes to impede ground movements and piles are used to support open excavations. All of these scenarios manifest exposure and vulnerability of piles to lateral loads.

The critical problem for the lateral loading is the loss of lateral bearing resistance of the soil in the passive region. When the lateral loads induced on the piles reaches the ultimate lateral capacity, failure happens. One actual example of this failure is the collapse of pile supported reinforced soil wall in a mixed-used development in the southern part of Malaysia (Shaw-shong et al., 2010). Investigations showed that the failure is caused by the rise of water table in the ground due to the perpetual heavy rainfall, where the saturation level of the soil is eventually reached causing excessive lateral load to the piles. The excessive lateral stress imposed on the pile exceeded the ultimate lateral resistance of the piles that resulted to the collapse of the central portion composite wall-pile structure. Another failure case is due to the lateral seismic loads generated from the 1976 Tangshan earthquake on Luanghe Bridge in China (Wei et al., 2008) as previously discussed in the introduction in Chapter 1. The imposed lateral loads reached the ultimate side soil resistance limit conditions that allowed for the excessive lateral displacements of piles, consequently, causing displacements of bridge spans from the seat decks.

To mitigate the potential disastrous failures, there are three criteria that need to be satisfied in addressing the lateral forces (Mokwa, 1999):(1) The ultimate side soil resistance should be adequate enough to resist the generated stresses and strains from the external lateral loads. (2) Pile deformations should be within acceptable limits and (3) there structural integrity of the foundation system should be kept intact.

It is indeed crucial to determine some limit conditions for the structures to perform the way they are intended to and provide safety to the users. Thus, the lateral resistance is an important element for the design of piles to consider (Abdrabbo and Gaaver, 2012).

## 2.2 Methods for predicting the lateral resistance

There are several methods in determining the lateral pile resistance and finding solutions for the response of laterally loaded pile. These methods can be categorized to (1) Limit States, (2) Semi-Empirical, (3) Elastic Continuum and (4) Numerical Simulations. Lateral response of piles is complicated to be evaluated, hence methods under (1) and (2) are attempts to provide simple solutions based on some basic idealizations. Methods under (3) made closed form continuum solutions available but limited to consideration of soil as elastic. Recent advances in technology offered methods under (4) that allow rigorous solutions and flexibility in dealing with various soil-pile configurations. These methods have its advantages and limitations. These will be discussed in the following sections and are summarized in **Error! Reference source not found.**

### 2.2.1 *Limit States*

The first criteria can be addressed during design using ultimate resistance theories such as those Broms (1965) or Brinch Hansen (1961). Brom's method is based on the earth pressure theory for elastic medium soils that may be applicable to the cohesionless or cohesive soils, short and long piles with fixed or free-condition. Similar development is made by Hansen, but is limited only for the rigid and cohesive soils only. Other researchers have also proposed similar limit states formulation ( Fleming et al., (2009), Reese et al., (1974), Meyerhof et al., (1988)). Noteworthy, is that these methods produce different values that may lead confusion to practicing engineers.

### 2.2.2 *Semi-Empirical (Subgrade Reaction Method)*

The concept is based on a beam resting on a soil medium represented by discrete springs. This is known as the Winkler model (Hetenyi, 1946). This is commonly used in analysing the behavior of foundations and where piles are treated as thin elastic strip. The difficulty in using this method is the determination of reasonable value of the modulus of the subgrade reaction. This is parameter is not a fundamental property of soil and is depended to many parameters such as the pile diameter, pile head conditions etc. Mostly, the coefficient of subgrade reaction is empirically derived. (Davisson and Prakash, 1963; Terzaghi, 1955) Hence, for the earlier developments of solutions to laterally loaded piles, soil medium are commonly treated as an elastic continuum or as Winkler spring medium. (Elson, 1989) Wot

This modulus of subgrade reaction is used and extended in developing the p-y curves (Matlock and Reese, 1960a). In this model, the soil is represented by a series of nonlinear p-y curves (load-deformation curves). This is semi-empirical in nature as these curves are derived from the field load tests. From the model initially developed by Matlock and Reese (1960), these has been modified by other researchers by representing p-y curve as hyperbolic curve (Kondner, 1963). Evans and Duncan (1982) modified it to account for the silty soils having cohesion and frictional angle properties. Mokwa (1999) applied p-multipliers to extend for the grouped piles. From here on forward, constant modifications have been done by researchers to come up with a p-y 0curve for improvement and dealing with different conditions like Abdrabbo and Gaaver (2012); Farid et al. (2013); Georgiadis and Georgiadis (2012); Guo et al. (2014); Han et al. (2015); Papadopoulou and Comodromos (2014); Salgado et al. (2014); Su and Yan (2013); Wu et al. (2015) among others.

The p-y method may lack some adequate theoretical background and may need back-calculation for reasonable prediction of suitable p-y curves. The accuracy of the output is highly dependent on the selection of p-y curve and reliable field test data.

### ***2.2.3 Elastic Continuum Solutions***

Contrary to the Winkler models, elastic and continuum solutions treat the soil as continuous medium. The analysis for both single and grouped piles for this particular approach assumes soil to be in linear elastic. Suitable secant modulus of soil is needed for satisfactory results. Researchers like Poulos, Banerjee and a more recent research Abedzadeh and Pak (Abedzadeh and Pak, 2004; Banerjee, 1978; Poulos, 1981) provide elastic solutions with these assumptions.

However, soil is more complex than being an elastic type of medium. It exhibits an elasto-plastic behaviour. Thus, treatment of a more realistic behaviour of soil is needed.

### ***2.2.4 Numerical Approach***

With the development of high computing tools, the rise of finite element method to model the response of laterally loaded piles in soil have been made available. Proper modelling techniques such as adequate discretization are needed to have reasonably accurate results. Complex systems, such as considering the non-linearity of the soil and the pile are made possible. Yet, one disadvantage is the cumbersome modelling, and the expensive computing time and memory with the complexity of systems. Thus, this type of approach is usually done by researchers and rarely used in the engineering practice. Many have used this with the pioneering works of Muqtadir and Desai (1986), Brown and Shie (1990), Kimura et al., (1991), Trochanis et al. (1991) until recent works of Wakai et al. (1999), Yang and Jeremi, (2002) Zhang, (2009) and Naveen et al. (2012) among many.

Though commonly among these models, the soil model used are elastic-perfectly plastic such as the Mohr-Coloumb model, Drucker-Prager and Von Mises constitutive soils.

## **2.3 Experiments**

Many lateral load tests have been conducted be it in the lab or field. For the lab, model tests in 1g and centrifuge tests are conducted. The lateral load – deformation curves are to be derived. The lateral load field tests originates from the works of Feagin (1937) along with the construction of pile-supported lock and dam along the Mississippi river. Another big pile data were derived during the construction of Arkansas River Navigation Project (Alizadeh and Davisson, 1970). These tests provide adequate enough to drive research studies in laterally loaded piles. From these experimental tests, it can be observed that with the increase of the load, the active length also increases considering some percentages of the pile head deformation as the negligible deformation.

The load deformation curves are easier observed through the laboratory tests where parameters are much under control. Lab tests in the form of 1g and centrifuge tests are commonly conducted.

Majority of the lab tests are conducted using the 1g as it is relatively cheaper than centrifuge tests. Different soil-pile configurations can be varied under different loading conditions. Cox et al. (1984) and Liu (1991) started the lab tests for large grouped piles. Models are careful used with scaling effect to model the behaviour of prototypes. Centrifuge model tests on pile groups have

been firstly conducted by (Barton, 1984). Other pioneering works are from Adachi et al. (1994), Zhang and Hu (1991) and (McVay et al., 1994) among many.

### ***2.3.1 Pile Deformation***

For performing lateral load test in the field, the pile lateral deformation along the soil depth is also of crucial interest along with the pile head deformation curves. This correspondingly determines the effect on the surrounding soil in the passive region. Normally, inclinometer probes are used at 0.6m interval installed at the pile. The displacements at the pile need to be held constant for 15-20 minutes while the deformations are being measured. Now, recent methods use the shape accelerometer consisting of triaxial chips at 0.3m interval. This can provide continuous reading of the displacement, velocity, acceleration and rotation at the location of the accelerometers (Rollins et al., 2008). In any case, these methods show the pile lateral deformation along the soil depth. Results show that the active pile length increases with increasing pile head displacement and not constant that can be observed when soils are treated as elastic medium.

### ***2.3.2 Soil Deformation***

Conventional failure passive wedge around laterally loaded piles are assumed as an inverse pyramidal shape (Reese et al., 1974a). However, recent model test using X-ray CT-scan (Otani et al., 2006) show that there is a conical wedge formed in the passive region with the increase of pile head loading. The X-ray CT scan results visualizes this wedge in progressive formation with the increase in pile head displacement. However, at larger displacements, the volume of this wedge reaches an ultimate value. Thus, this shows that the ultimate side soil resistance, hence the ultimate lateral pile resistance of piles can be represented by this failure wedge as the pile deformation pushes it.

## **2.4 Summary and Conclusion**

Several methods are available to determine solutions for laterally loaded piles. Researchers and engineers can choose from simple idealized models to rigorous models that can deal complex soil-pile configuration. For simple models, simplifications on the soil medium are assumed such as treating the soil as an elastic medium, in Winkler or continuum model. On the other hand, for complex models such as finite element method, tedious and meticulous handling of model is required and may require a lot of time and memory resources. That is why, this type of modelling is usually left for researchers and rarely used in practice. In the attempt to marry the advantages of simple and complex models, this study intends to provide solution that is rigorously and theoretically based i.e. can capture the soil natural behaviour but simple enough to use in the engineering practice. Establishing the relationship of the pile deformation with the corresponding soil deformation in the passive region is the major thrust in this study.

**Table 2- 1. Existing methods in determining the lateral response of piles.**

<b>Methods</b>	<b>Limit States</b>	<b>Semi-Emprical</b>	<b>Elastic Continuum Solutions</b>	<b>Numerical Approach</b>
Literataures	Broms (1965) Brinch Hansen (1961) Fleming et al., (2009) Reese et al., (1974) Meyerhof et al., (1988)	Hetenyi (1946) Davisson and Prakash (1963) Terzaghi (1955) Kondner (1963) Evans and Duncan (1982) Mokwa (1999) Abdrabbo and Gaaver (2012) Georgiadis and Georgiadis (2012) Farid et al. (2013) Salgado et al. (2014); Su and Yan (2013) Papadopoulou and Comodromos (2014) Guo et al. (2014); Han et al. (2015) Wu et al. (2015)	Banerjee (1978) Poulos (1981) Abedzadeh and Pak (2004)	Muqtadir and Desai (1986) Brown and Shie (1990) Kimura et al., (1991) Trochanis et al. (1991) Wakai et al. (1999), Yang and Jeremi, (2002) Zhang, (2009) Naveen et al. (2012)
Advantages	Simple solutions	Simple Solution	Treatment of Soil as Continuum	Flezible
Limitations	Elastic Case	Discrete, use of subgrade reaction	Elastic	Computationally expensive and memory, time, effort

# Chapter 3

## Characteristic Length, $L_c$

### 3.1 Introduction

The characteristic length,  $L_c$ , serves as the predominant criteria for estimating the deformation of piles. It is reflective of the soil-pile interaction, inherent in deep foundations or any structures embedded in soil. Chang's formula is known to estimate this characteristic length in common engineering practice. This formula is even used in Japan code (*Specifications for Highway Bridges*). This is based on the popular Winkler's theory or the subgrade reaction concept. In this model, the deformation of the piles are captured by the pile stiffness,  $EI_p$  and the soil stiffness is represented by the soil springs through the coefficient of subgrade reaction,  $k_H$ . However, the main question arises as to whether this coefficient of subgrade reaction,  $k_H$ , is considered to be a fundamental soil property. Having said that, a more rational expression for the characteristic length expression is proposed by Konagai considering the same pile stiffness,  $EI_p$ , but considers the shear modulus,  $G$ , to represent the soil property. Hereafter, this expression shall be called as Konagai formula.

In this chapter, the characteristic length in the form of Chang's formula and Konagai's formula (a function of  $EI_p$  and  $G$ ) are presented and compared. The current practice in Japan is delved into, particularly in the use of the Chang's formula, and more essentially in the derivation of the coefficient of horizontal subgrade reaction. Further questions drawn based on this review of conventional method, considering the more complex behaviour of soil, are investigated on. Lastly, given the Konagai's formula, the potential valuable improvements it could add on are discussed.

### 3.2 Definition of Characteristic Length, $L_c$

The characteristic length,  $L_c$ , is observed to be closely related to the active pile length,  $L_a$ , as seen in Figure 3-1 (Randolph, 1981; Velez et al., 1983). Such that, multiplying the characteristic length by a constant factor,  $\alpha$ , the active pile length can be derived as expressed in Equation 3.1.

$$L_a = \alpha L_c \quad (3.1)$$

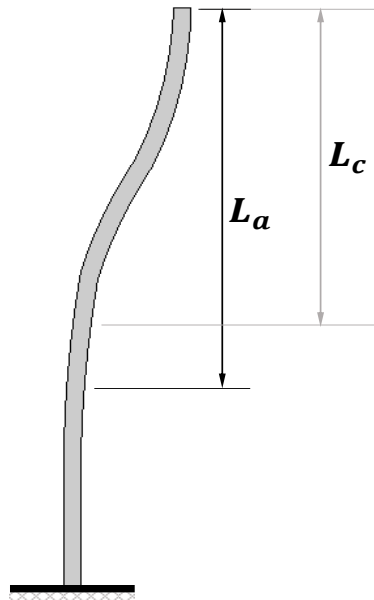
This characteristic length,  $L_c$ , from the name itself, characterizes the pile deformation. Knowing that the pile behaviour is predominantly governed by the soil pile interaction, this parameter describes the ratio of the pile stiffness relative to the surrounding soil stiffness.

There are two expressions of characteristic length presented in this section: (1) Chang's Formula (Chang, 1937) and (2): Konagai's formula, as a function of  $EI_p$  and  $G$ . (Konagai, 2000)

Chang's formula (Chang, 1937) given by Equation 3.2 is the common characteristic length parameter widely used in engineering practice. The ratio of the stiffness of pile to that of the soil is a function of the pile stiffness,  $EI_p$  and the soil stiffness represented by the spring stiffness

described by the product of the horizontal coefficient of subgrade reaction,  $k_H$  and pile diameter,  $d_p$ .

However, a more rational approach was proposed (Konagai, 2000) considering the soil stiffness to be represented by the shear modulus,  $G$  as it was arguable if the coefficient of horizontal subgrade coefficient is a fundamental soil property. This is expressed by Equation 3.4.



$$L_c = \frac{1}{\beta} \quad (3.2)$$

where,  $\beta$ : inverse of characteristic length

$$\beta = \sqrt[4]{k_H d / 4EI_p} \quad (3.3)$$

$k_H$ : horizontal coefficient of subgrade reaction

$d$ : diameter of the pile

$EI_p$ : pile stiffness

$$L_c = \sqrt[4]{\frac{EI_p}{G}} \quad (3.4)$$

Figure 3-1. Schematic representation and relationship of active pile length and characteristic length

where,  $EI_p$ : pile stiffness

$G$  : shear modulus

In summary, the main difference of expressions 3.2 and 3.4 is the representation of the soil property, probing on which has more of the physical basis and being the innate or fundamental property of the soil.

### 3.3 Current Practice in Japan

In this section, Chang's formula will be looked on more closely and its implementation in the specification of Japan Highway. Firstly, the background and the derivation of Chang's formula is discussed, then followed by the estimation of the coefficient of horizontal subgrade reaction that constitutes the Chang's formula.

#### 3.3.1 Chang's Formula

The simplistic appeal of Chang's formula has made it mainstream in the engineering practitioners' worlds then and now. This Chang's formula is based on the Winkler model or the subgrade reaction concept, which is one of the oldest and most popular methods for investigating the behaviour of laterally loaded pile (e.g. Davisson and Prakash, 1963; Hetenyi, 1946; Hirai, 2012; Huang, 2011; Kramer and Heavey, 1988; Matlock and Reese, 1960; Terzaghi, 1955). The Winkler

model assumes piles to behave like a horizontal beam resting on a half-space elastic foundation supported by discrete springs as shown in Figure 3-2.

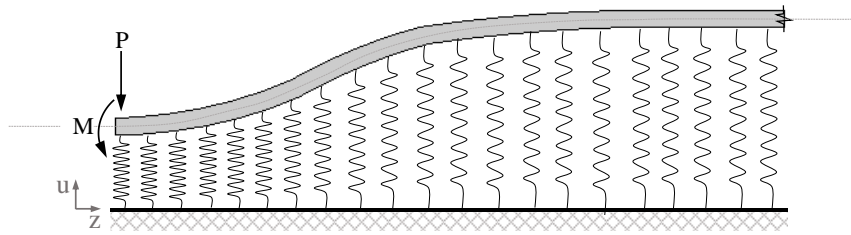


**Figure 3- 2. Winkler Model (Beam on Elastic Foundation)**

In any simple method that is based on the Winkler's model, the deformation of the soil at any point ( $z$  coordinate) depends on the local force per unit length given by Equation 3.5, where the  $k$ , is the stiffness of these springs, called as the modulus of subgrade reaction, (in force/length<sup>2</sup> unit) exhibiting the material property of the soil medium. Simply put, it assumes the soil-pile system to exhibit a linear elastic behaviour, where the deformation of the soil is linearly proportional to the external force.

$$p(z) = -ku(z) \quad (3.5)$$

The governing equation for a prismatic pile on a Winkler foundation is given by the differential equation in 3.6, where the spring modulus,  $k$ , is represented by the product of the coefficient of horizontal subgrade reaction (force per cubic length) and pile diameter given by  $k_H d_p$ .

$$EI_p \frac{d^4 u}{dz^4} + k_H d_p u = 0 \quad (3.6)$$

The equation above can be re-written as follows:

$$\frac{d^4 u}{dz^4} + 4 \frac{k_H d_p}{4EI} u = \frac{d^4 u}{dz^4} + 4\beta^4 u = 0 \quad (3.7)$$

where we note  $\beta$  to be one of the real part of the four complex roots for the solution as expressed below.

$$\beta = \sqrt[4]{k_H d_p / 4EI_p} \quad (3.8)$$

Then the general solution for this higher ordered differential equation is given by:

$$u(z) = e^{\beta z} (C_1 \cos \beta z + C_2 \sin \beta z) + e^{-\beta z} (C_3 \cos \beta z + C_4 \sin \beta z) \quad (3.9)$$

where constants  $C_1, C_2, C_3$  and  $C_4$  are integration constants that can be obtained based on given boundary conditions. And since  $\beta$  has a unit of one over length, then the inverse of it is thought to be the characteristic length.

### 3.3.2 Coefficient of horizontal subgrade reaction

The coefficient of horizontal subgrade reaction is assumed to be a property of the soil representative of the soil stiffness. The determination of the horizontal subgrade reaction can be in the form of in-situ tests like the horizontal plate loading test, the soil borehole investigation using the number of blows ( $N$ ) or from laboratory tests. Generally, the coefficient horizontal subgrade reaction is derived using “Equation 9.6.4” of the *Specification of Highway Bridges* (Japan Road Association, 2012) considering correction for the size effect of the small plate used to be applied on actual sized pile diameters. This is also given by the equation below, designated herein as Equation 3.10.

$$k_H = k_{H0} \left( \frac{B_H}{0.3} \right)^{-3/4} \quad (3.10)$$

where,  $B_H$ : Equivalent loading width (m)

$$B_H = \sqrt{d_p / \beta} \quad (3.11)$$

The expression for  $B_H$  as abovementioned is specifically for a pile foundation based on Table 9.6.2 (Japan Road Association, 2012)

$d_p$ : outer diameter of pile

$\beta$ : Chang’s formula given by Equation 3.8.

$k_{H0}$ : Coefficient of horizontal subgrade reaction from a plate load test ( $kN/m^3$ ).

The coefficient of the horizontal subgrade reaction can be derived normally by using the horizontal plate loading test. In this in-situ test, a vertical pit is excavated then lined with metal sheet for support. This sheet has a hole intended for the vertical plate. This plate has typical cross-sectional dimension ratio of  $B/L=2$ . Then, the vertical disk is loaded by a hydraulic jack. It pushes the vertical plate laterally on the side soil (as shown in Figure 3-3). From the incremental lateral load, the corresponding displacements are recorded. The lateral load – deflection curve is then plotted as seen in Figure 3 - 4. The coefficient of horizontal subgrade reaction,  $k_{H0}$ , is determined from the secant moduli of horizontal load-deformation curves at given displacement.

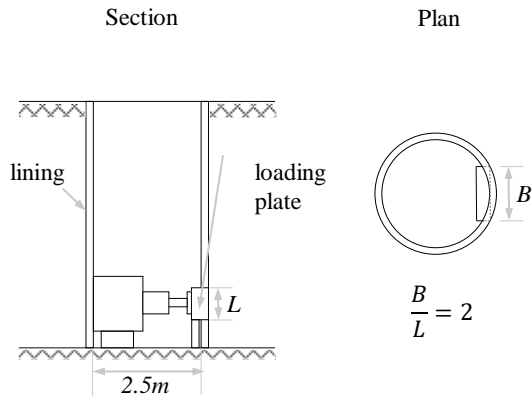


Figure 3 - 4. Schematic diagram of horizontal plate loading test (based on Yoshida and Yoshinaka, 1972)

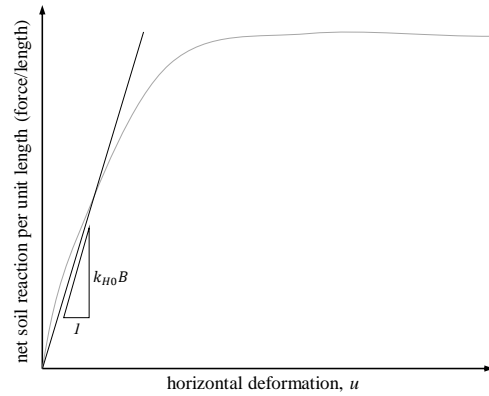


Figure 3 - 3. Load-deformation curve for determination of coefficient of subgrade reaction

If the modulus of soil deformation  $E_0$  ( $kN/m^2$ ) is known from performing one of the methods listed in Table 3-1 (Table 9.6.1 from (Japan Road Association, 2012) ), the following equation can be used:

$$k_{H0} = \frac{1}{0.3} \alpha E_0 \quad (3.12)$$

where,  $\alpha$ : correction factor dependent on the method and load case and listed in Table 3-1.

Implicitly, an iteration is needed to determine the coefficient of horizontal subgrade reaction as shown in Equation 3.10, where this expression would be dependent on Equation 3.11 and correspondingly to Equation 3.8.

Table 3 - 1. Correction factor,  $\alpha$ , for the following methods and load case (after Table 9.6.1 in Japan Road Association, 2012)

Methods for measuring $E_0$	correction factor $\alpha$ for	
	ordinary cases and typhoons	earthquakes
Half of the modulus of soil deformation obtained from cyclic plate load test	1	2
Modulus of soil deformation obtained from downhole horizontal loading test	4	8
Modulus of soil deformation obtained from either uniaxial or triaxial compression test	4	8
From blow count $N$ in a SPT, $E_0 = 2800 \cdot N$	1	2

### 3.4 Doubts and limitation of current practice

One of the obvious drawbacks of the models based on Winkler concept is the failure to account for the continuity of the soil since the soil medium is explicitly represented by discrete springs.

Coupled with this, is the more prevailing question on the physical basis of the coefficient of horizontal subgrade reaction. As previously said, the coefficient of horizontal subgrade reaction is intuitively thought to be a representative of the soil stiffness characteristics. However, it is noted that this is mainly derived through experiments and empirical equations. It has already been pointed out by other researchers (Kog et al., 2015; Reese and Van Impe, 2001; Teodoru and Toma, 2009; Terzaghi, 1955; Varghese, 2012) that this coefficient of horizontal subgrade reaction is influenced by several pile related factors such as bending stiffness and pile geometry. Still, the coefficient of the horizontal subgrade reaction derived using the code in the *Specifications of Highway Bridges* is closely examined.

From equation 3.10, it can be implicitly said that an iteration is needed to derive the characteristic length. Exactly speaking, the derivation of  $k_H$  is a function of the horizontal subgrade reaction from the plate load test,  $k_{H0}$  and the corresponding plate size correction factor,  $B_H$ . From equation 3.11, it is noted that,  $B_H$  is a function of pile diameter,  $d_p$  and  $\beta$ . Correspondingly,  $\beta$  is a function of pile stiffness and the coefficient of horizontal subgrade reaction,  $k_H$ . Hence in this case, it can be clearly seen that the coefficient of the horizontal subgrade reaction is not solely a function of soil characteristic as previously thought but also a function of the pile stiffness, hence, inherent of the influence of the soil-pile interaction.

Moreover, while the  $k_{H0}$  can be extracted directly from the plate load test, a size effect correction factor in the form of  $B_H$  is needed to be applied. This is for the reason that the spring stiffness reaction under a small rigid plate is representative only of the local deformations directly under the plate coverage but fails to capture the real soil response under bigger or real size foundations.

It is also known that Winkler-based models yields accurate results within ranges of small strains. This basically considers the soil in linear elastic. Similar limitations applies in the use of Equation 3.10, where it considers the ground to be within a linear elastic strain and perform under a certain allowable displacement. This served as the design philosophy for typical design calculation methods. The displacement of the foundation determined must be within the allowable displacement of 1% times the foundation pile width or less than or equal to 50mm (Japan Road Association, 2012). This assumes no cracking found within the depth of the pile and the possible onset of visible threats of crack markings to be observed in the surface only for immediate repair. However, even for elastic range, a study (Shirato et al., 2009) showed that the design threshold displacement based on field test data sets could be even larger than 1% of the pile diameter. It is proposed to be 2% to 4% of the pile diameter. The problem of laterally loaded pile is more complex because soils in real field situations behave nonlinearly, particularly in the upper region surrounding the pile. Also, the hard rule for the allowable target displacement can be very limiting for a wide range of type of structures of different purposes, allowing lapse of judgment on the balance of economy, safety and resiliency.

These limitations lead to study the characteristic length as a function of the pile stiffness and the shear modulus and explore its potential advantages.

### 3.5 Improvements of Proposed Characteristic Length Parameter

#### 3.5.1 Shear Modulus as an Inherent Soil Characteristic: A Parameter for More Practical Field Test

It is established that the coefficient of horizontal subgrade reaction is not a sole function of the soil property itself but is influenced by the stiffness of the pile, and consequently, a function of the soil-pile interaction. Thus, the shear stiffness is more appropriately represented by the shear modulus.

In this section, Chang's formula and the Konagai's formula (a function of pile stiffness,  $EI_p$  and shear modulus,  $G$ ) in an elastic medium is compared. From (Koseki et al., 2001), the derivation of the coefficient of horizontal subgrade reaction for a homogeneous soil medium that is completely in linear elastic is using the same equation with Equation 3.10 except with the exponent changed to -1 given by the expression below.

$$k_H = k_{H0} \left( \frac{B_H}{0.3} \right)^{-1} \quad (3.13)$$

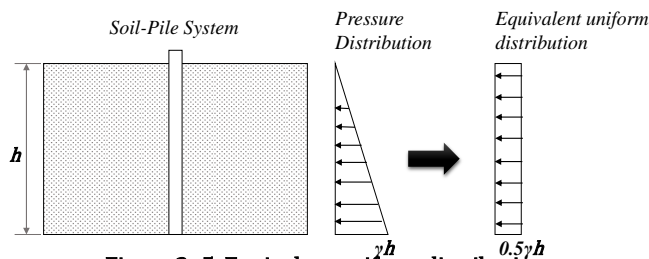


Figure 3- 5. Equivalent uniform distribution

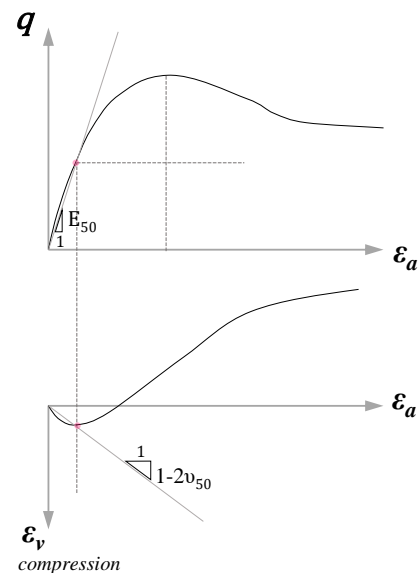


Figure 3- 6. Derivation of  $E_{50}$  and  $v_{50}$

The modulus of soil deformation,  $E_0$ , was used from a simulated drained compression triaxial test. In a more detailed discussion, the procedure of deriving the soil deformation is as follows: (1) The stress applied for the triaxial test is based on an equivalent uniform pressure distribution as shown in Figure 3-5 for  $h=1.45\text{m}$  (model test). (2) The  $E_{50}$  is derived from the deviator stress – axial strain relationship graph. The secant elastic modulus ( $E_{50}$ ) is equal to the slope from zero to half of the maximum deviator stress ( $q_{50}$ ). Correspondingly, the  $q_{50}$  is plotted down to the volumetric-axial strain relationship graph. Then,  $v_{50}$  is derived from the slope from 0 to the extended plot (red point). These steps are shown in Figure 3-6, where  $q$ : deviator stress,  $\epsilon_a$ : axial strain and  $\epsilon_v$ : volumetric strain.

This monotonic loading falls under the ordinary type of load case. Thus, referring to Table 3-1, correction factor,  $\alpha = 4$ , is used. This is then applied to equation 3.10.

From an iteration,  $k_H$  is derived then correspondingly the Chang's formula is derived for various pile diameters ( $d=10\text{mm}$ ,  $d=20\text{mm}$ ,  $d=25\text{mm}$ ,  $d=30\text{mm}$  and  $d=40\text{mm}$ ) embedded in three different soils. This is plotted on the y-axis of Figure 3-7.

The shear modulus is derived based on the relationship of  $E_{50}$  and  $\nu_{50}$  as shown in the equation 3.14:

$$G_{50} = \frac{4E_{50}}{2(1 + \nu_{50})} \quad (3.14)$$

This value is substituted to Equation 3.4 where  $G = G_{50}$  to get the characteristic length. Then plotted in the x-axis of Figure 3-7.

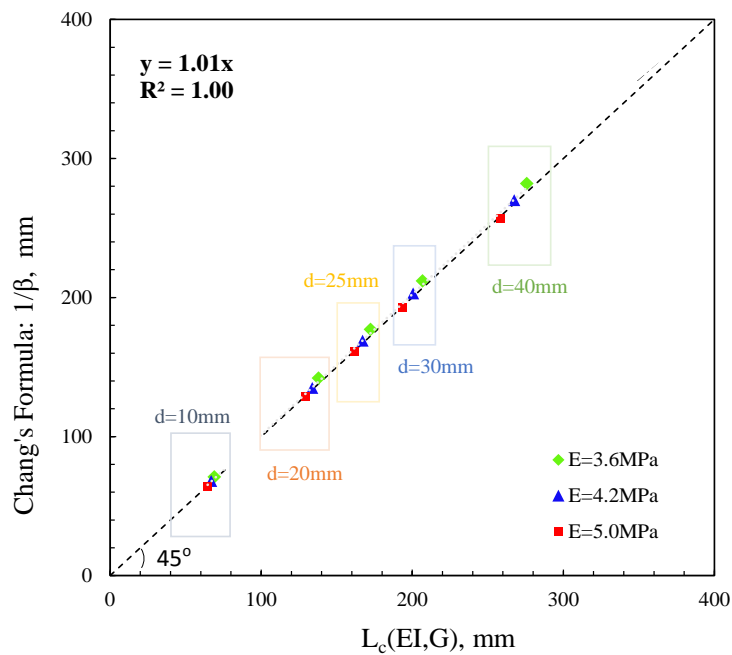


Figure 3- 7. Chang's Formula vs  $L_c(EI,G)$

It can be seen that there is a one to one correspondence between these two parameters: Chang's formula and  $L_c(EI,G)$ . The  $(4/k_H d)$  in Chang's formula eventually approaches the shear modulus,  $G$ . And it could be said that  $G$  automatically captures the size effect phenomenon. The current practice requires the use of the horizontal subgrade reaction which can be estimated using the in-situ static horizontal plate load test or the laboratory static load test. In conjunction with, is the prerequisite of accounting of the influence of loading width on the modulus of horizontal subgrade reaction. But with the use of shear modulus, there is no need to apply correction on the coefficient of subgrade reaction against the experimental plate used to capture the actual soil response from a real dimension diameter. With that said, it is indicative that shear modulus is a fundamental property of the soil.

So rather considering a soil constant, with the use of soil spring coefficients, the ground strength represented by shear modulus, could be of more important focus. This shear modulus can be determined from soil investigation methods through the shear wave velocity. To have an apple to

apple comparison with the Chang's formula,  $G_{50}$  is used in this instance. Note that in the next chapter of this paper, it will be illustrated how the  $L_c(EI, G)$  is related to the active pile length based on Equation 3.2a. The proportional factor,  $\alpha$ , will just change dependent on the type of  $G$  used. In the field, the small-strain shear modulus or maximum shear modulus is usually derived from the shear wave velocity. Therefore, it is utmost important to focus on this for practical purposes.

In-situ tests to derive this could be the PS logging, cross-hole, the down-hole, the SASW techniques or other new emerging techniques such as ReMi (Refraction Micrometer). Though they generally are in agreement with each other, the most accurate technique would be the PS logging (Pérez-santisteban et al., 2011). What is essential is for these methods to be performed properly and with integrity. In addition, in congruence with these soil investigation for shear modulus would be techniques to determine the type of soil inherent in the soil medium.

### ***3.5.2 Performance-Based Design***

The current practice has been defined that the deformation of the pile foundation is limited to 1% of the pile diameter or less than or equal to 50mm (Japan Road Association, 2012). This falls within the linear elastic case. This is based on the idea that no crack shall appear along the pile depth and can be seen only at the surface. Thus, it could just be pulled out with the onset of evidence of cracks found in the surface. However, considering the wide range of type of structures that demand different needs in terms of performance, life cycle and costs, this hard-lock rule of allowable displacement may not be reasonable to some projects. Thus, the thrust of performance-based design is initiated, where a target displacement is decided on discretion of the required performance.

Conventional designs are based on the demand capacity relationship given by a factor of safety. This means that to exceed the capacity of structure would be a worst case scenario. However, the severity of this worst scenario is not clearly defined (Kramer and Arduino, 2009). This is in agreement with what Bolton would say "Traditional approach is potentially wasteful". He instead encourages designers to explicitly consider and assess the possible capacity of deformation and strength of soil which should be within the expected deformation mechanism of geo-structure (Bolton, 2012). Hence, there's the need to push in the direction of performance based design.

The main design philosophy of this performance based design is to have a target deformation based on the strength and deformation mechanisms of the soil, as far as geo-structures are concerned. In this sense, it could also be based on the damage levels or losses on operation expectations on the structure. Currently, there are four level of damages that could serve as basis (Iai, 2004; Shinoda et al., 2009) as seen in Table 3-2. These are the acceptable level of damages based on structural resiliency and operational life required. In the economical point of view, this would become more reasonable as a balance is sought to find between how much damage a structure could take and how much cost is the client willing to spend for the repair and maintenance of the structure. Given these damage levels, a wide range of spectrum is possible for the required performance of a structure. The extreme damage level, degree IV, allows client the option of utilization of the entire life cycle of the structure, exhausting the residual deformation and providing a completely new structure after, which may be deemed more cost-efficient in this case. Meanwhile, on the safe side level, for degree I, where very important structures could be of structures in mind, i.e. nuclear power plants. The smallest deformation could be of critical one, therefore the target allowable displacement should fall within the linear elastic range.

**Table 3 - 2. Acceptable level of damage in performance-based design (from Iai, 2001)**

Acceptable level of damage	Structural	Operational
Degree I: Serviceable	Minor or so damage	Little or no loss of serviceability
Degree II: Repairable	Controlled Damage	Short-term of Serviceability
Degree III: Near Collapse	Extensive Damage in near collapse	Long term or Complete Loss of Serviceability
Degree IV: Collapse	Complete Loss of Structure	Complete Loss of Serviceability

However, the deformation criteria, based on the soil properties, is quintessential for the performance based design. Given an ultimate limit state, one could have the discretion to decide based on it. Hence, this is what the ultimate side soil resistance of piles offer. A criteria, where the option is not limited only to 1% the pile diameter or less than 50mm but at the same time, offers a knowledge or awareness of the critical state to which the lateral bearing resistance for the piles is reached.

Hence, the use of a simple parameter,  $L_c(EIp, G)$ , which is founded on fundamental properties of pile and soil, is of valuable study. It can be used to provide simple expression for the ultimate lateral pile resistance, useful for a performance-based design.

### 3.6 Summary

The use of Chang's formula is implemented in the *Specifications of Highway Bridges* in Japan. Acknowledging its simplistic approach and acceptable accuracy given the assumptions for the linear elastic case. It's still inherent that there are some questions in this model that could be answered with other parameters. These are:

- the obvious drawback of idealization of soil medium with discrete springs
- the physical basis and the intrinsic nature of the coefficient of horizontal subgrade reaction as a soil property.
- allowable displacement within the linear elastic range

A pragmatic approach is given by the substitution of the shear modulus for the characteristic length. This allows to:

- capture inherently the stiffness of the soil.
- provide more convenient in-situ test for getting the shear modulus through shear velocity without the need for size effect correction.
- be a good parameter to describe the pile behaviour in relation to the surrounding soil strength. Therefore, this can be used for describing ultimate limit states, i.e. lateral pile resistance which is useful for performance-based design.

This characteristic length,  $L_c(EI, G)$ , in relation to the active pile length can be applied to provide a simplified expression of ultimate lateral pile resistance for practical approach in the design and assessment of piles within target structural and seismic response. This will be shown in the next chapter.

# Chapter 4

## Preliminary Study on the Concept of the Active Pile Length for Piles Embedded in Sand using Two-Dimensional System Analysis

### 4.1 Introduction

The soil-pile configuration in this chapter is idealized in a plane strain condition similar to the works of Kok et al. (2008), Naveed et al. (2012) and Hazzar et al. (2013). It is acknowledged that inaccuracies are expected in this type of idealization given that the actual response of pile foundations is a principally a three-dimensional (3D) problem. This preliminary study is conducted to have an idea on the behaviour of active pile length varying the parameters of the piles and the surrounding soil condition. With the consideration of the 2D case, where the soil-pile interaction is not accounted for in the out-of-plane direction, this two-dimensional (2D) system may be limited only to capture the behaviour of piles considered as walls, row piles or sheet piles. Nevertheless, the intention to take this research off to a start using the 2D platform, is to simply investigate the formation of the passive soil wedge during nonlinear scenario and relate it to the active pile length. This idea is extended to a 3D platform in later chapters to realistically capture the behaviour of piles.

### 4.2 Active pile length

The behaviour of piles embedded in soil are generally governed by the deformation along its length. For long and flexible laterally loaded piles, significant deformation is observed near the ground surface. A clear cut-off criteria for negligible deformation is set considering the ranges from other researches (Velez et al., 1983; Wang and Liao, 1988). In this study, the  $L_a$  is defined from the ground surface down to the point where the deformation is equal to 3% of the maximum pile head deformation. Within this region of significant deformation, pile can be described as a cantilever beam, assuming fixity for the deeper region of negligible deformation. In common engineering practice as mentioned in Chapter 3, Chang's formula (Chang, 1937) (Equation 4.1) is used to define the characteristic length in Equation 4.20.

$$\beta = \sqrt[4]{\frac{k_h d_p}{4EI_p}} \quad (4.1)$$

$$L_c = \frac{1}{\beta} \quad (4.2)$$

In Equation 4.1,  $k_h$  is the coefficient of horizontal subgrade reaction,  $d_p$  is the pile width. However, in this 2D case, this pile width is set to  $b_b$  which is the side edges parallel to the loading direction, and  $EI_p$  is the pile stiffness. As previously discussed in Chapter 3, it is noted that the numerator  $k_h d$  is not an inherent property of the soil. Thus, a more rational expression is proposed by Konagai (2003) noting the stiffness of the pile relative to the surrounding soil (Equation 4.3).

$$L_c = \sqrt[4]{\frac{EI_p}{G}} \quad (4.3)$$

$$L_a = \alpha L_c \quad (4.4)$$

In Equation 4.3,  $EI_p$  refers to the pile stiffness and  $G$  represents the soil shear modulus. This Konagai's formula is deemed linearly proportional to the active pile length (Equation (4.4)). The  $L_a$  is closely investigated on by varying the parameters directly affecting it such as the  $EI_p$  and  $G$ . Particularly, the factors pile thickness,  $b_b$ , Young's modulus,  $E_p$ , pile length,  $L_p$ , and the initial void ratio,  $e_o$ , are varied.

## 4.2 Numerical Analysis

To simply investigate the idea of the formation of the soil wedge in the passive region of laterally loaded piles in relation to the active pile length,  $L_a$ , the soil-pile system is modelled as 2D plane strain condition using the finite element method. The simulation of the response of laterally loaded single piles in two-dimension were performed using a program named FEM2D developed by Kyokawa and Kikumoto (Kyokawa and Kikumoto, 2013) using a C++ platform. This software is for two-dimensional finite element analysis that is implemented with various elasto-plastic soil models including the subloading  $t_{ij}$  model. This software is modified to include continuum-beam based elements for the pile modelling and joint elements for simulation of the slipping in the interface of the soil and the pile elements. In this section, the procedure for the soil-pile idealization and the cases considered in this study is discussed in details.

### 4.2.1 Soil-Pile Idealization

Generally, the soil-pile system includes a single end bearing pile embedded in a homogeneous sandy soil subjected to a lateral load. The soil-pile configuration properties and techniques implemented are presented herein.

Figure 4 - 1 shows the general layout of the soil-pile system in 2D plane strain condition using the finite element method. A pile with width,  $b_b$  and a unit thickness in the out of plane direction and length,  $L_p$ , is embedded in a homogeneous soil having a width,  $b_s = 20\text{m}$ , on each opposite side of the pile.

A 2D solid quadrilateral-shaped element is used for the automated meshing for all the material type used – soil, pile and joint. Joint elements with zero thickness are used at the interface of the soil and pile elements.

The bottom end of the soil-pile system is considered as the hard strata, therefore, it is fixed in all degrees of freedom along the x and y-axis. On the other hand, the sides are fixed only in x direction.

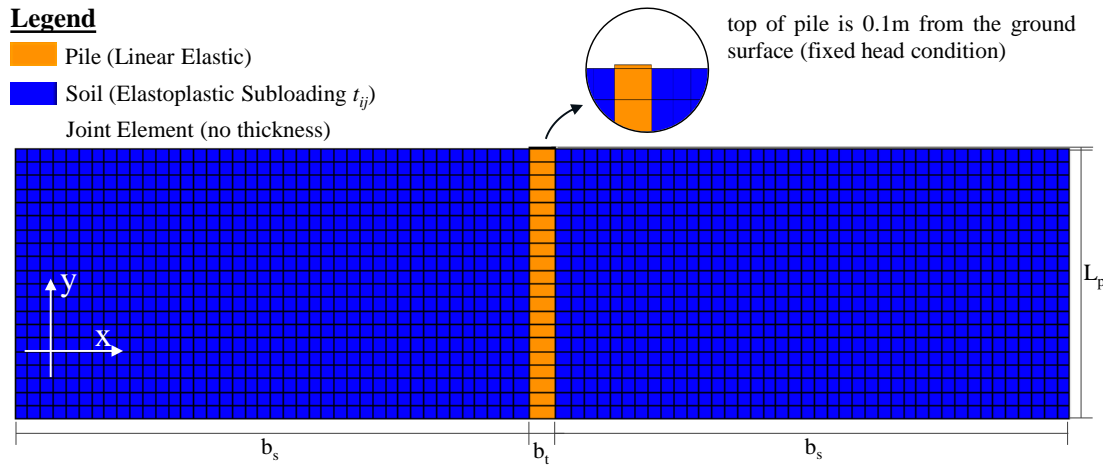


Figure 4 - 1. Soil-pile configuration

## 4.2.2 Material Model and Elements

### 4.2.2.1 Pile Model

A continuum based beam element (Yoon et al., 2012) is used for modelling the pile in elastic case. For 2D case, this coincides with the line beam elements but with the displacements and forces extrapolated to the nodes of the quadrilateral solid element. The salient feature of this model is the flexibility to handle various cross-sectional type of beams especially if this developed program is extended to three-dimensional platform. The advantage of this can be seen clearly and immensely in the three-dimensional case. This model uses much smaller number of elements compared to the conventional use of 3D solid elements. This model would allow to analyse the 3D case as a line, with displacements and forces extrapolated to the surface nodes of the pile cross section.

Because of the continuum mechanic formulation, where the cross-section is discretised with nodes, the cross-sectional properties are inherently accounted for. Thus, pre-calculation of area, second moment of area, etc. are not needed. In addition, the analysis of short, long, and deep beams is automatically considered.

Using the continuum beam based elements, geometry and displacements interpolation are made. First, the cross-section and the longitudinal section of the beam is discretised (see Figure 4 - 2). Detailed formulation and discussions can be found in Yoon (2012). Based on these nodes, geometry interpolation is made using interpolation polynomials for the usual isoparametric procedure. These are expressed by product of the linear and quadratic shape functions given by equation 4.5.

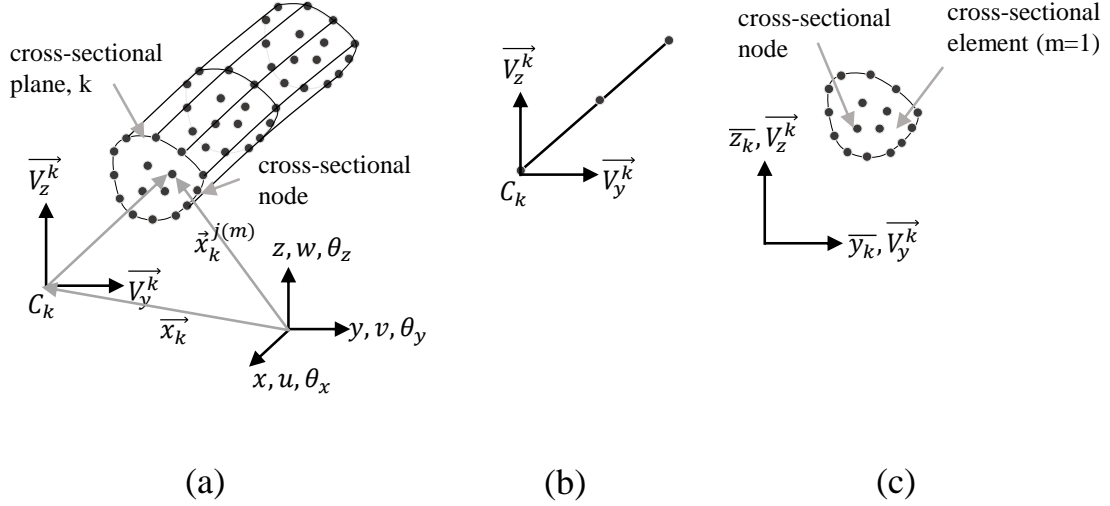


Figure 4 - 2. The concept of the continuum-mechanics based beam finite element. (a) the 3D beam used discretised at the cross-section and in the longitudinal axis. (b) discretization along the longitudinal axis. (c) cross-sectional area discretization (after Yoon et al., 2012)

$$\vec{x}^{(m)} = \sum_{k=1}^q h_k(r) \sum_{j=1}^p h_k(s, t) \vec{x}_k^{j(m)} \quad (4.5)$$

where  $\vec{x}^{(m)}$ : the position vector of the solid element  $m$  in the Cartesian system  $r, s, t$ . The  $h_k(r)$  and the  $h_k(s, t)$  are the linear and quadratic shape functions.  $\vec{x}_k^{j(m)}$  is the position vector of the  $j^{\text{th}}$  cross sectional nodes on plane  $k$ . Considering Figure 4 - 2, we note that:  $q=3$  (3 cross-sectional planes),  $p=16$  (16 nodes in each cross-section), and  $m=1$  (consider 1 serendipity element of 16 nodes).

The basic kinematic assumption of Timoshenko beam theory are implemented in this model, where plane remains plane even during deformations, though not necessarily perpendicular to the midline of the deformed beam. Considering this, equation 4.5 can be written as;

$$\vec{x}^{(m)} = \sum_{k=1}^q h_k(r) \vec{x}_k + \sum_{k=1}^q h_k(r) \bar{y}_k^{(m)} \vec{V}_y^k + \sum_{k=1}^q h_k(r) \bar{z}_k^{(m)} \vec{V}_z^k \quad (4.6)$$

and

$$\bar{y}_k^{(m)} = \sum_{j=1}^p h_j(s, t) \bar{y}_k^{j(m)} \quad (4.7)$$

$$\bar{z}_k^{(m)} = \sum_{j=1}^p h_j(s, t) \bar{z}_k^{j(m)} \quad (4.8)$$

where:  $h_j(s, t)$  is the quadratic shape function for the cross-sectional plane. In Figure 4 - 2c, the serendipity isoparametric function for 16 nodes is used.  $\bar{y}_k^{j(m)}$  and  $\bar{z}_k^{j(m)}$ : are the nodal coordinates in the cross-sectional plane,  $\bar{V}_y^k$  and  $\bar{V}_z^k$  are direction vectors and are perpendicular to each other.

Considering a beam with a unit dimension in the out-of-plane direction, the geometric interpolations are reduced as follows:

$$x = \sum_{k=1}^q h_k(r) x_k \quad (4.9)$$

$$y = \frac{b_t}{2} s \quad (4.10)$$

where:  $x_k$ : x coordinates of the longitudinal nodes,  $b_t$ : width of the beam section parallel to the loading.

Based on these, the displacement interpolation can now be made accordingly similar with Bathe (1996). For 2D case, we assume deflection is along v-axis and rotation along z, therefore the reduced equations are as follows.

$$u = \frac{s}{2} \sum_{k=1}^q b_t h_k(r) \theta_z \quad (4.11)$$

$$v = \sum_{k=1}^q h_k(r) v \quad (4.12)$$

where  $u, v$ : the translations at x and y axis and  $\theta_z$ : the rotation at z axis.

Given these equations, solutions are performed similar with conventional finite element method incorporating the Gauss quadrature.

#### 4.2.2.2 Joint Model

A joint element of virtual thickness is introduced between the soil and the pile to simulate the vertical slipping of soil against the pile during nonlinearity (Beer, 1985). The kinematic formulation is discussed in detailed by Beer (1985). The joint element is modelled using two-dimensional solid finite elements with isoparametric formulation or shape functions.

However, the slip occurring at the interface is described by an elasto-plastic constitutive model instead of the Mohr-Coulomb model used by Beer (1985). Irreversible slip at the interface happens when the shear strength of the joint is exceeded. The elasto-plastic yield function is defined by the expression below.

$$f = \frac{|t_s|}{t_n} - \tan\phi - \varphi\delta_s^p = 0 \quad (4.13)$$

where  $t_s$ : shear tractions,  $t_n$ : contract pressure,  $\phi$ : angle of internal friction,  $\varphi$ :hardening parameter , and  $\delta_s^p$ :plastic shear strain. In this case, the hardening parameter is considered as extremely small.

Meanwhile, the potential function for this model is defined by the expression below.

$$g = |t_s| = 0 \quad (4.14)$$

The strain increment of the slipping surface consists of the elastic,  $\delta^e$  and the plastic part,  $\delta^p$ .

$$\dot{\delta} = \delta^e + \delta^p \quad (4.15)$$

Considering the elastic part, the incremental traction forces and the incremental strains are relation by the equation below.

$$\begin{Bmatrix} \dot{t}_s \\ \dot{t}_n \end{Bmatrix} = \begin{bmatrix} k_s & 0 \\ 0 & k_n \end{bmatrix} \begin{Bmatrix} \delta_s^e \\ \delta_n^e \end{Bmatrix} \quad (4.16)$$

The values for shear and normal stiffness,  $k_s$  and  $k_n$ , should be extremely large since the stiffnesses of joints in contact are theoretically infinite. To define the large value, it should be adequate enough such that the elastic slip is negligible relative to the elements adjoined in the joint elements.

Equation 4.16 can be re-written as:

$$\dot{\mathbf{t}} = \mathbf{D}^e \dot{\delta}^e \quad (4.17)$$

Invoking the consistency condition,  $df = 0$ , gives the expression below:

$$df = \frac{\partial f}{\partial \mathbf{t}} \dot{\mathbf{t}} + \frac{\partial f}{\partial \delta_s^p} \dot{\delta}_s^p = 0 \quad (4.18)$$

Assuming a non-associated flow rule gives Equation 4.19.

$$\delta^p = \Delta \frac{\partial g}{\partial t} = 0 \quad (4.19)$$

where  $\Delta$ : proportional factor.

Re-writing equation 4.17 using equation 4.15 gives

$$\dot{\mathbf{t}} = \mathbf{D}^e (\dot{\boldsymbol{\delta}} - \dot{\boldsymbol{\delta}}^e) \quad (4.20)$$

Multiplying equation 4.20 with the  $\frac{\partial f}{\partial t}$  and substituting equation gives the following expression

$$\frac{\partial f}{\partial t} \dot{\mathbf{t}} = \frac{\partial f}{\partial t} \mathbf{D}^e (\dot{\boldsymbol{\delta}} - \Delta \frac{\partial g}{\partial t}) \quad (4.21)$$

Substituting equation 4.21 to equation 4.18, the proportional constant,  $\Delta$ , can be derived given in the equation below.

$$\Delta = \frac{\frac{\partial f}{\partial t} \mathbf{D}^e \dot{\boldsymbol{\delta}}}{\frac{\partial f}{\partial t} \mathbf{D}^e \frac{\partial g}{\partial t} - \frac{\partial f}{\partial t} \frac{\partial g}{\partial \delta_s^p}} \quad (4.22)$$

The deformation and strength of the interface can be evaluated already from the stress-strain increment expressed in the equation below using equations 4.20 and 4.22.

$$\dot{\mathbf{t}} = \left[ \mathbf{D}^e - \frac{\mathbf{D}^e \frac{\partial g}{\partial t} \frac{\partial f^T}{\partial t} \mathbf{D}^e}{\frac{\partial f}{\partial t} \mathbf{D}^e \frac{\partial g}{\partial t} - \frac{\partial f}{\partial \delta_s^p} \frac{\partial g}{\partial t}} \right] \dot{\boldsymbol{\delta}} \quad (4.23)$$

The angle of internal friction of the joint element considered is 25° (Wakai et al., 1999).

#### 4.2.2.3 Soil Model

##### (a) Background of Subloading $t_{ij}$

The subloading  $t_{ij}$  is a product of advanced researches on development of constitutive models to capture the elasto-plastic behaviour of the soil. This springs back from the onset of the Cam-clay model (Schofield and Wroth, 1968). The Cam clay model is essentially the first elasto-plastic model that requires few and simple material parameters with physical basis (Nakai, 2007). This simplistic nature of the Cam clay model leaves room for some limitations. At the very least, it could capture the shear deformation and consolidation of the soil in the field. Yet the more salient factors such as influence of the intermediate principal stresses and the influence of density and/or confining pressure are not accounted for. These limitations are addressed by the Subloading  $t_{ij}$  model, thus, showing its advantages. Moreover, it offers a simple model having material

parameters that are fundamentally similar with Cam clay model and just few departures even if it can simulate the complex behaviour of the soil.

Nakai and Matsuoka (1987) introduced the subloading  $t_{ij}$  based on the concept of SMP (spatially mobilized plane) (see Figure 4 - 3). The influence of the intermediate stresses on the deformation and strength of soil are accounted for by the modified stress  $t_{ij}$  from the SMP. The stress invariants,  $t_{ij}$ , represent the normal and shear stresses on the SMP. Correspondingly, the normal,  $\varepsilon_N$ , and shear,  $\varepsilon_S$ , strains are used. The comparison of the modified stress  $t_{ij}$  concept from the ordinary concept is summarize in Table 4 - 1 below.

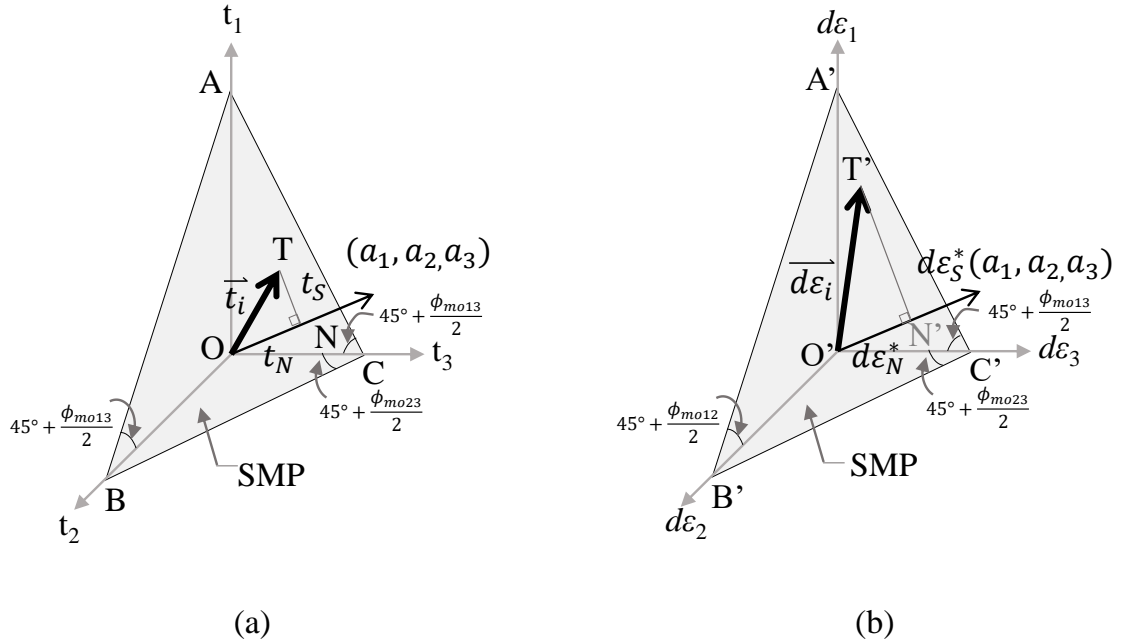
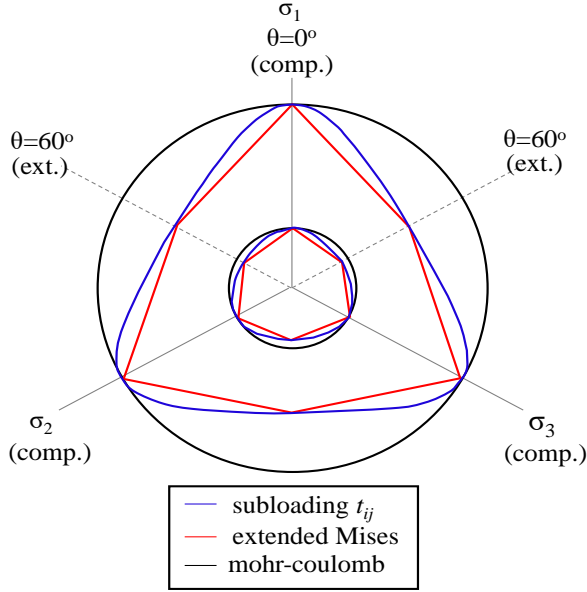


Figure 4 - 3. SMP Plane (a) Definition of  $t_N$  and  $t_S$  (b) Definition of  $d\varepsilon_N^*$  and  $d\varepsilon_S^*$  (after Nakai, 2007)

Table 4 - 1. Comparison between tensors and scalars related to stress and strain in ordinary concept and  $t_{ij}$  concept (after Nakai, 2007)

	ordinary concept	$t_{ij}$ concept
tensor normal to reference plane	$\delta_{ij}$	$a_{ij}$
stress tensor	$\sigma_{ij}$	$t_{ij}$
mean stress	$p = \sigma_{ij}\delta_{ij}/3$	$t_N = t_{ij}a_{ij}$
deviatoric stress tensor	$s_{ij} = \sigma_{ij} - p\delta_{ij}$	$t_{ij}' = t_{ij} - t_N a_{ij}$
deviatoric stress	$q = \sqrt{(3/2)s_{ij}s_{ij}}$	$t_S = \sqrt{t_{ij}'t_{ij}'}$
stress ratio tensor	$\eta_{ij} = s_{ij}/p$	$x_{ij} = t_{ij}'/t_N$
stress ratio	$\eta = q/p$	$X = t_S/t_N$
deviatoric strain increment tensor	$d\varepsilon_v = d\varepsilon_{ij}\delta_{ij}$	$d\varepsilon_N^* = d\varepsilon_{ij}a_{ij}$
strain increment parallel to reference plane	$d\varepsilon_{ij} = d\varepsilon_{ij} - d\varepsilon_v\delta_{ij}/3$	$d\varepsilon_{ij}' = d\varepsilon_{ij} - d\varepsilon_N^* a_{ij}$
strain increment parallel to reference plane	$d\varepsilon_d = \sqrt{(2/3)d\varepsilon_{ij}d\varepsilon_{ij}}$	$d\varepsilon_S^* = \sqrt{d\varepsilon_{ij}'d\varepsilon_{ij}'}$



**Figure 4- 4. Failure criteria surface of different constitutive models in octahedral plane (Adopted from Nakai, 2007)**

Moreover, this model follows a subloading surface that expands or contracts following the current stress point. Computation becomes stable considering the smooth transition from the elastic to the plastic formation from the continuous stress-strain rate described in the loading process. More so, the smooth triangular failure surface makes it a good modelling base. This compares favourably than that of conventional models such as Mohr-Coulomb and extended Mises as seen in **Error! Reference source not found.** This is indicative of the good performance of the model in capturing the behaviour of soil not only under compression, but also in triaxial extension, plain strain and true triaxial conditions.

In considering the intermediate stresses with influence of density and/or confining pressure to describe realistically the deformation and strength of soil, the yield function is formulated using the stress invariants from the SMP plane and density state variable,  $\rho$ , given by the expression below. These are derived and discussed in further details in the following references: (Kyokawa, 2011; Nakai and Matsuoka, 1987; Nakai, 2013, 2007; Nakai et al., 2011; Pedroso and Farias, 2005; Pedroso et al., 2005)

$$f = F - \{H + (\rho_0 - \rho)\} = 0 \quad (4.24)$$

where  $F = (\lambda - \kappa)\{(\ln(t_N/t_{N0}) + \zeta(X))\}$ ,  $H = (-\Delta e)^p$ ,  $\rho$ : current density function,  $\rho_0$ : density function at initial state,  $\lambda$ : compression index,  $\kappa$ : swelling index,  $t_N$ : mean stress tensor at current state,  $t_{N0}$ : mean stress at initial state,  $(-\Delta e)^p$ : irrecoverable plastic component of change of void ratio,  $\zeta(X) = \left(\frac{1}{\beta^S}\right)\left(\frac{X}{M^*}\right)^{\beta^S}$ , the stress ratio tensor,  $X = \frac{t_S}{t_N}$ , the intercept with vertical intercept of the stress dilatancy relationship for the modified  $t_{ij}$ ,  $M^* = (X_{CS}^{\beta^S} + X_{CS}^{\beta^S-1}Y_{CS})^{1/\beta^S}$ ,  $X_{CS} = (\sqrt{2}/3)(\sqrt{R_{CS}} - (1/\sqrt{R_{CS}}))$ ,  $Y_{CS} = (1 - \sqrt{R_{CS}})/(\sqrt{2}(\sqrt{R_{CS}} + 0.5))$ ,  $\beta^S$ : shape of yield surface, and the principal stress ratio at critical state in triaxial compression, and  $R_{CS} = (\sigma_1/\sigma_3)_{CScomp}$ .

Invoking the consistency condition, where the derivative of the yield function (Equation 4.24) is equal to zero ( $df = 0$ ), and considering associated flow rule assumed in  $t_{ij}$  space gives:

$$df = dF - (dH - d\rho) = \frac{\partial F}{\partial \sigma_{ij}} d\sigma_{ij} - \left\{ (1 + e_0)\Lambda \frac{\partial F}{\partial t_{kk}} - d\rho \right\} = 0 \quad (4.25)$$

where  $\Lambda$ : the proportionality constant which represents the magnitude of the plastic deformation.

Given that  $F$  is a dimensionless function, the proportional constant,  $\Lambda$ , has a unit of stress, hence, the term,  $(\partial F / \partial t_{kk})$  has the dimension of inverse of stress. Also, it is noted that the state variable  $\rho$  decreases with the development of the plastic deformation and finally reaches to  $\rho=0$ . Hence, satisfying these conditions, the evolution rule for the state variable,  $\rho$ , (Equation 4.26 ) can be represented using the monotonically increasing function,  $G(\rho)$ , which becomes 0 when  $\rho = 0$ .

$$d\rho = -\Lambda \cdot (1 + e_0) \cdot L(\rho, t_N) = \Lambda \cdot (1 + e_0) \frac{-G(\rho)}{t_N} \quad (4.26)$$

$G(\rho)$  is given as quadratic function of state variable expressed below.

$$G(\rho) = a_F \rho^2 \quad (4.27)$$

where  $a_F$  is the material constant parameter responsible in the influence of density. Substituting equation 4.26 to equation 4.25.

$$\Lambda = \left\langle \frac{\frac{\partial F}{\partial \sigma_{kl}} d\sigma_{kl}}{(1 + e_0) \left\{ \frac{\partial f}{\partial t_{kk}} + \frac{G(\rho)}{t_N} \right\}} \right\rangle = \left\langle \frac{dF}{h^p} \right\rangle \quad (4.28)$$

The plastic strain increment is calculated by substituting equation to the equation below.

$$d\varepsilon_{ij}^p = \Lambda \left( \frac{\partial F}{\partial t_N} \frac{\partial t_N}{\partial t_{ij}} + \frac{\partial F}{\partial X} \frac{\partial X}{\partial t_{ij}} \right) \quad (4.29)$$

### (b) Soil Model Parameters

The subloading  $t_{ij}$  model is used to describe the elasto-plastic behaviour of soils (Kyokawa, 2011; Nakai, 2013; Nakai et al., 2011). In this case, the homogeneous soil is taken as Toyoura sand, named as TS, hereafter. The material parameters used for this type of soil is summarized in Table 4 - 2. These are calibrated from the drained compression and extension tests shown in Figure 4-2 (Kyokawa, 2011).

A variation of initial void ratios ( $e_o = 0.6, 0.7, 0.8$  and  $0.9$ ) is considered. The relationship between the stress and strain, and volumetric strain-axial strain,  $\varepsilon_v - \varepsilon_a$ , relationship for the various initial void ratios considered are plotted in Figure 4-2. Generally, a more dilatant behavior is depicted

by the dense sand than that of the loose sand. Extreme relative density for the surrounding soil, loose ( $e_o = 0.9$ ) and dense ( $e_o = 0.6$ ) is considered to investigate its effect on the active pile length.

Table 4 - 2. Toyoura sand (TS) material parameters for the subloading  $t_{ij}$

Material Parameters	
Compression Index, $\lambda$	0.070
Swelling Index, $\kappa$	0.0045
Stress Ratio at critical state, $R_{CS}$	3.2
Shape of yield surface, $\beta^s$	2.0
Void Ratio at normal consolidation at $P_a=98\text{kPa}$ , $e_{NC}$	1.10
Atmospheric Pressure (kPa), $P_a$	98
Controlling Decay Rate of the influence of density, $a_F$	33
Poisson's Ratio, $\nu$	0.2

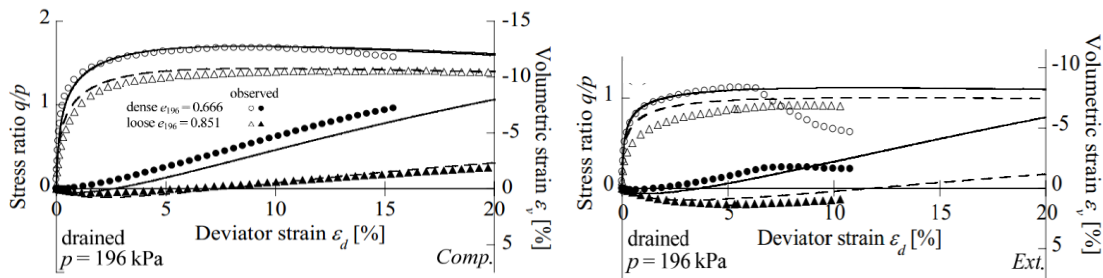


Figure 4 - 5. Drained compression and extension test for Toyoura Sand (Taken from Kyokawa 2011)

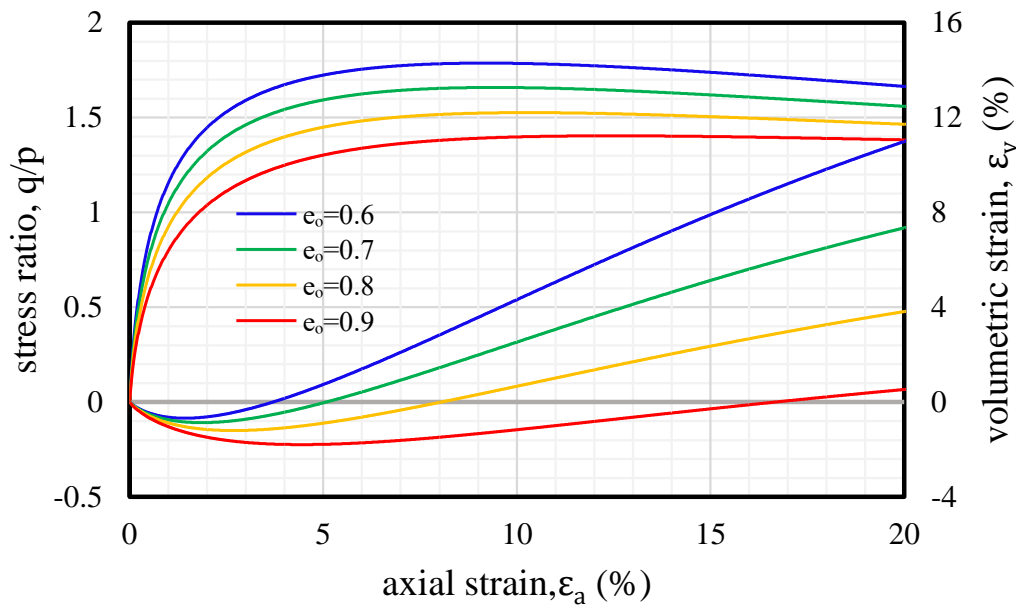


Figure 4 - 6. Stress ratio- $\epsilon_a$  and  $\epsilon_v$ - $\epsilon_a$  relationship of Toyoura sand with varying void ratios,  $e_o$  at  $p'_o=98\text{kPa}$ .

## 4.3 Parametric Analysis

### 4.3.1 Effect of Pile Stiffness

The  $L_a$  is predominantly influenced by the pile stiffness,  $EI_p$ . This pile stiffness is a function of the pile geometric properties, and hence, the effect of pile thickness,  $b_t$ , on the active length is investigated. A single pile with length,  $L_p$ , of 30m having  $E_p$  of 30GPa, is embedded in TS soil considering the initial void ratios of 0.6 and 0.9. The variable parameter in the analysis is the pile thickness,  $b_t$ . The parameter  $b_t$  is varied from 0.3m, 0.5m, 0.6m, 1.0m, 1.2m, 1.5m up to 2.0m, while the other parameters are kept constant. In effect, this variation also changes the pile stiffness with respect to the same surrounding side soils.

Figure 4-4 shows the relationship of the variation of the  $b_t$  and its corresponding  $L_a$ , where both parameters are normalized with the  $L_p$  for piles embedded in the dense and loose condition. Generally, an increasing in  $b_t$  gives an increase in  $EI_p$  and consequently, produces an increase in  $L_a$ . However, it can be closely observed that for piles with ratios of  $L_a/L_p < 0.75$  and  $b_t/L_p < 0.032$ , the difference in  $L_a$  of piles embedded in loose and dense sands increases with increasing  $b_t$  as seen by the divergence in Figure 4-4. But when the  $b_t/L_p$  reached 0.032, where the ratio,  $L_a/L_p$ , becomes greater than 0.75, the difference in the  $L_a$ 's for piles embedded in loose and dense sand starts to decrease and converges to a point. This scenario means that as the pile thickness increases, the pile stiffness increases, therefore, the active pile length increases eventually reaching a saturation point, where  $L_a$  is approximately equal to  $0.9L_p$ .  $L_a$  becomes constant with increasing lateral pile head deformations as restrained by the fixity at the bottom of pile. In this study, flexible piles are of interests. Thus, only piles having  $L_a/L_p < 0.75$  are considered.

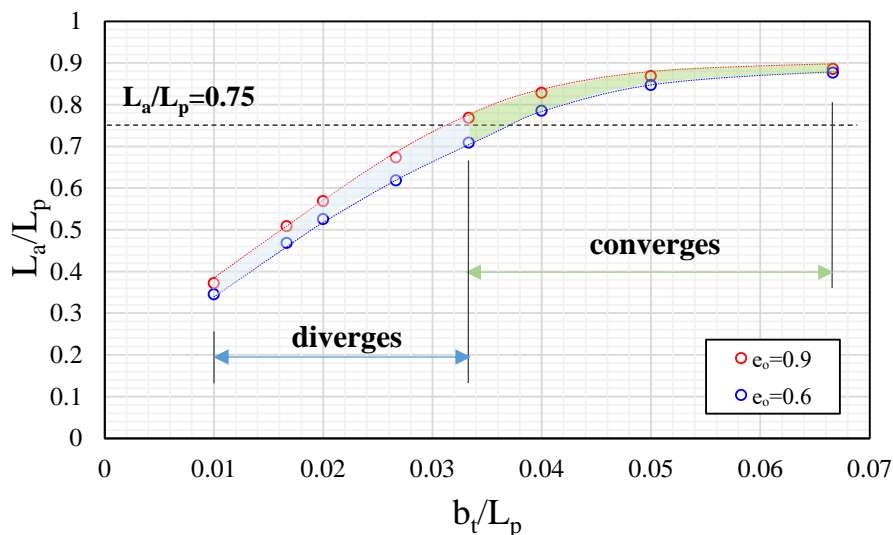


Figure 4 - 7. Variation of pile thickness,  $b_t$ , with the active pile length,  $L_a$

The piles having  $E_p = 200\text{GPa}$  with pile thickness,  $b_t$  equal to 0.3m, 0.35m, 0.4m and 0.5m and embedded in loose Toyoura sand were considered. The obtained active pile lengths were superimposed to those of piles having  $E_p = 30\text{GPa}$  with pile thickness,  $b_t$  equal to 0.3m, 0.5m, 0.6m and 0.8m. The combined effect of the Young's modulus,  $E_p$ , and the pile thickness,  $b_t$ , using the pile stiffness parameter,  $EI_p$ , is plotted against the active pile length for all the cases considered in this particular parametric analysis as seen in Figure 4-5. All the data points lie on a unique line defined by the linear function  $y = 2.891x + 3$ , where  $y$  and  $x$  are the active pile length and the fourth-root of the pile stiffness, respectively. Thus, there is indeed a linear relationship between the active pile length,  $L_a$  and the  $(EI_p)^{0.25}$ .

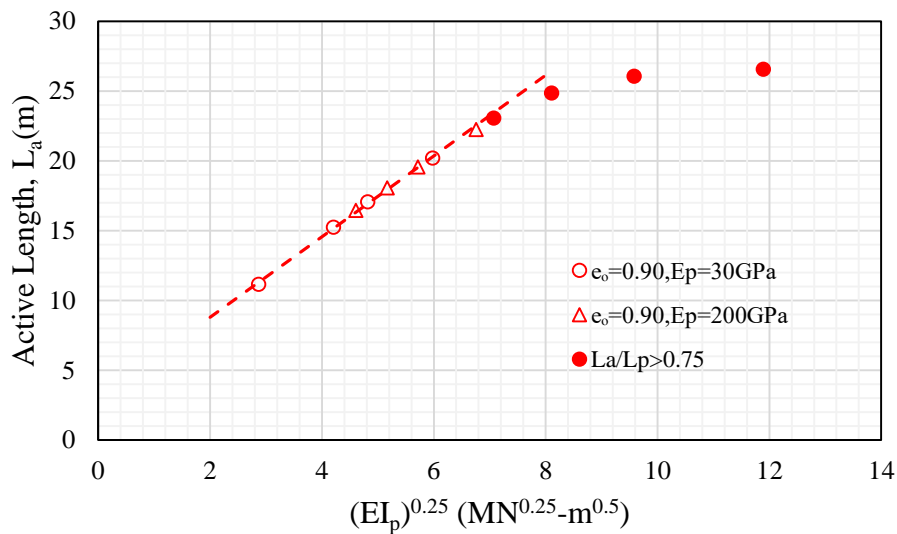


Figure 4 - 8. Effect of pile stiffness,  $EI_p$ , on active pile length,  $L_a$

### 4.3.2 Effect of Pile Length

The effect of pile length on the active pile length is investigated. In this case, the single pile having  $EI_p$  equal to  $312.5\text{MN-m}^2$  and  $2500\text{MN-m}^2$  were taken into consideration. Each pile is embedded in the loose sand with  $e_0 = 0.90$ , varying the pile lengths to 10m, 20m, 30m, 60m and 100m.

In Figure 4-6, for piles with stiffness  $EI_p$  of  $2500\text{MN-m}^2$  (red line), the  $L_a$  continues to increase with increasing  $L_p$  until it reaches to a ratio of  $L_a/L_p = 0.77$ , where the  $L_p$  is at 30m. The increase in active pile length means that it may actually need to be longer than the actual pile length but is restricted with the bottom boundary conditions, thus behaving as stiff piles. But when it reached the  $L_p$  of 60m, the effect of  $L_p$  on the  $L_a$  becomes negligible. This point is more prominent for the pile stiffness equal to  $312.5\text{MN-m}^2$  given by the blue line. Similar trend shows that as  $L_a/L_p$  becomes less than 0.76, the active pile length,  $L_a$ , becomes constant despite increasing the actual pile length,  $L_p$ . This means that the expected active pile length has been reached given the pile's actual pile length. Figure 4-7 shows the relationship between  $L_a/L_p$  and the actual pile length,  $L_p$ . For  $L_a/L_p < 0.75$  approximately, there is an asymptotic behavior with increasing  $L_p$ .

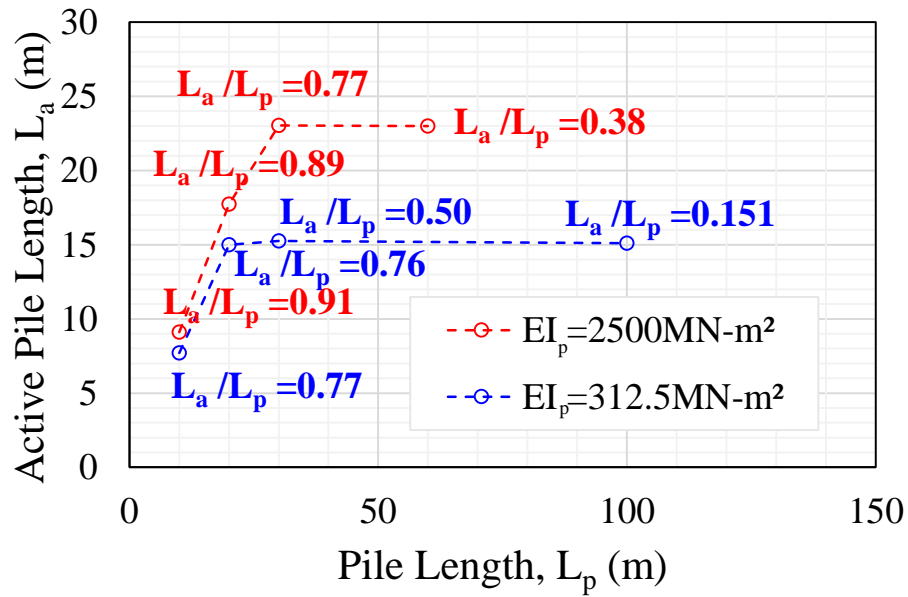


Figure 4 - 9. Variation of active pile length,  $L_a$  with pile length,  $L_p$

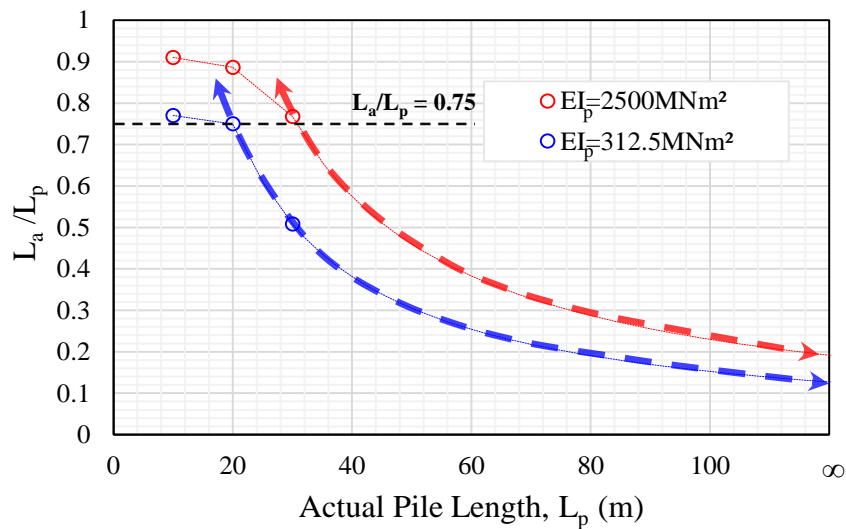


Figure 4 - 10.  $L_a/L_p$  with actual pile length,  $L_p$

### 4.3.3 Effect of Soil Stiffness

The shear modulus also needs to take account the shear degradation of the soil with increasing pile head deformation. In view of this, the following steps were undertaken. For each case considered, the shear strain is derived by dividing the current pile head displacement with the corresponding deformed  $L_a$ . Then, this shear strain is plotted in the shear degradation curves to get the corresponding shear modulus. Figure 4-8 plots the variation of the  $L_a$ , with the  $L_o$  given by the fourth-root of the ratio of  $EI_p$  with shear modulus  $G$  at the progressive pile head deformation (particularly at  $u_y = 0.009\text{m}$ ,  $0.036\text{m}$ ,  $0.135\text{m}$ ,  $0.45\text{m}$ ,  $1.575\text{m}$ ) for all the cases of piles with

varying  $b_b$ ,  $E_p$  embedded in dense and loose sand. It can be deduced from this figure, that there is a linear relationship with the active pile length and characteristic length for various pile head displacements. Thus, at this stage, it can be established that  $L_a = \alpha L_c$ . Moreover, there is a linear function describing the relationship between  $L_a$  and  $(EI_p/G)^{0.25}$ .

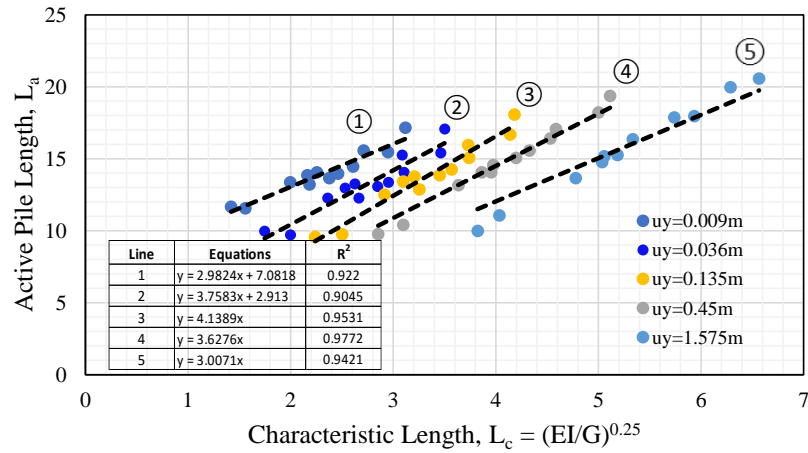
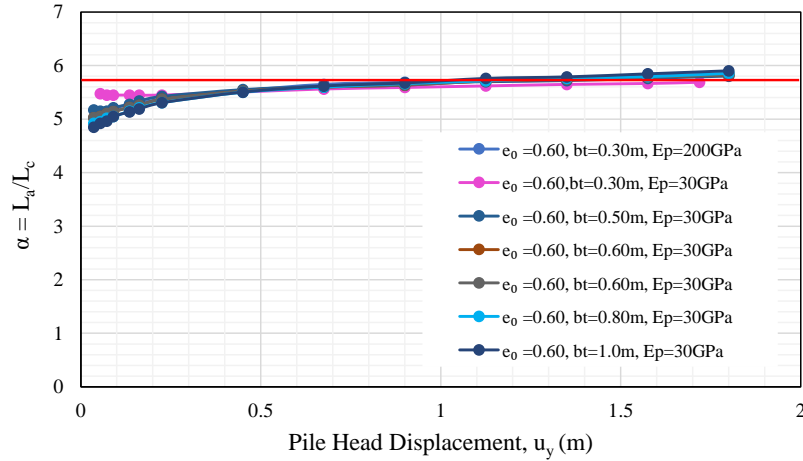
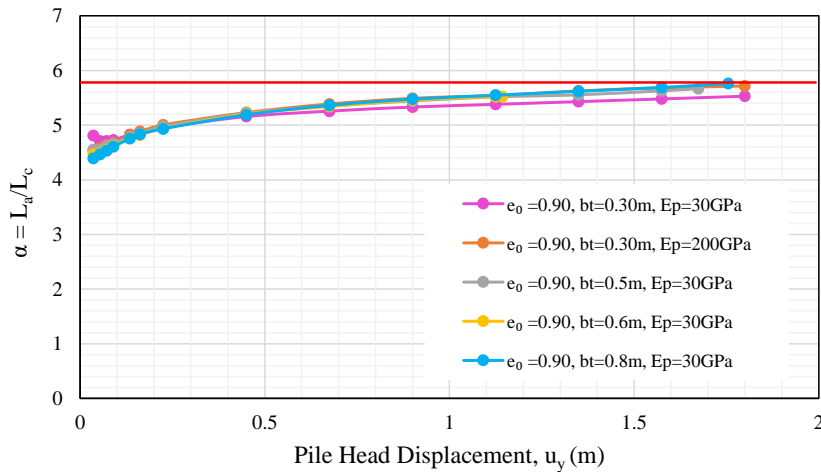


Figure 4 - 11. Variation of active pile length,  $L_a$ , with the  $L_c$  for all cases at different lateral pile head deformation

The progressive active pile length with the corresponding lateral pile head deformations were derived for piles embedded in dense and loose sand. These active pile length are normalized with the characteristic length,  $L_c = (EI/G)^{0.25}$ , where the shear modulus,  $G$ , is the maximum shear modulus,  $G_{max}$  which can be easily obtained in the field. The variation of the ratio of the active pile length to this initial characteristic length with the lateral pile head deformation is plotted in Figure 4-9. It can be seen that the curves reaches to a constant line at around  $\alpha = 5.8$ . Therefore, it can be said the initial active pile length is important as it can determine the active pile length at the ultimate stage by a factor of 5.8. It can be observed though that the piles in dense sand reaches the plateau line faster, with the small rate of change in the progression of the active pile length with increasing lateral pile head displacements (Figure 4-9a) while the rate of change of active pile length is larger for piles in the loose sand (Figure 4-9b).



(a) piles in dense sand



(b) piles in loose sand

Figure 4 - 12. Variation of the ratio of the active pile length to the initial characteristic length with respect to the lateral pile head displacement.

#### 4.4 Application to the Ultimate Lateral Pile Resistance

The numerical simulations done in this research show that a soil wedge is progressively formed at the passive region upon application of lateral load to the pile head. Figure 4-10 plots the lateral force at the pile head given by the black line. The pile resistance based on the active pile length at 1m pile head displacement (where the  $L_a$  starts to become constant and shear strain is approximately greater than 5%) given by the blue line. The side soil resistance is derived by the difference of the lateral force at the pile head and the pile resistance. The soil resistance increases with increase in the pile head displacement and approaches a constant value. This is where the ultimate lateral pile resistance,  $P_{ultimate}$ , is derived for all cases.

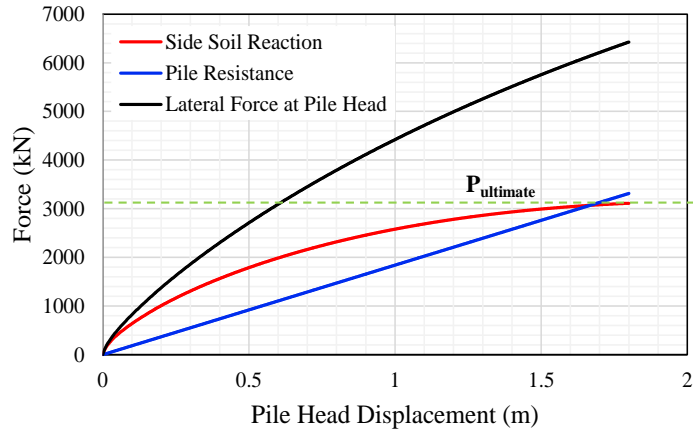


Figure 4 - 13. Force-deformation curve

The force representation of the wedge can be described by the unit weight,  $\gamma$ , and the Rankine passive earth pressure coefficient,  $K_p$ . The values for the  $\gamma$  and  $K_p$  are given in Table 4-2 based on the following expressions:

$$\gamma = \frac{G_s \gamma_w}{1 + e_o} \quad (4.30)$$

$$K_p = \tan^2 \left( 45^\circ + \frac{\phi}{2} \right) \quad (4.31)$$

where  $G_s$  specific gravity of soil

$\gamma_w$  unit weight of water (9.81kN/m<sup>3</sup>)

$\phi$  peak angle of internal friction

The following soil parameters are used for the cases taken into account. The  $\phi$  used is the peak angle of internal friction from the element test simulations.

Table 4- 3. Soil Parameters of Toyoura Sand (TS) ( $G_s = 2.65$ )

Initial void ratio, $e_o$	$\phi$ (deg)	$\gamma$ (kN/m <sup>3</sup> )
0.60	43.51	16.25
0.70	40.53	15.29
0.80	37.47	14.44
0.90	34.67	13.68

Together with the  $L_{au}$ , the soil parameters such as the unit weight of the soil,  $\gamma$ , Rankine passive coefficient,  $K_p$  are used to estimate the ultimate lateral resistance. Figure 4-11 shows the correlation of the ultimate side soil reaction force and the parameters  $K_p\gamma L_{au}^2$  for all the cases considered in this analysis having  $L_a/L_p < 0.75$ . In this figure, it can be observed that there is a high linear correlation between the  $P_{ult}$  and  $K_p\gamma L_{au}^2$  having an  $R^2=0.99$ . Therefore, the  $P_{ult}$  can be given by this equation:

$$P_{ult} = 0.153K_p\gamma L_{au}^2 \quad (4.32)$$

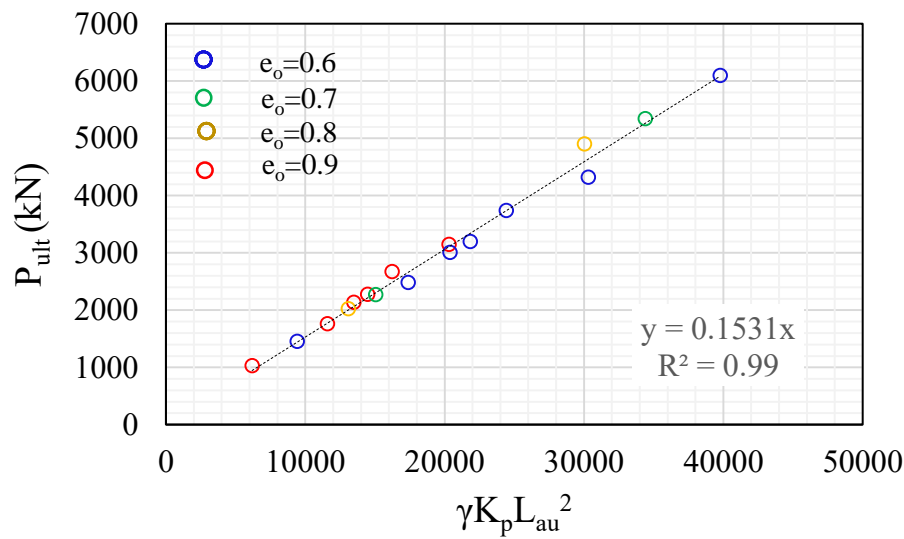


Figure 4 - 14. Correlation between  $P_{ult}$  and  $K_p\gamma L_{au}^2$

## 4.5 Summary and Conclusion

To ensure the use of flexible piles in the analysis, a  $L_a/L_p < 0.75$  were taken into consideration to discount the limiting effect of the bottom boundary condition for shorter piles. For flexible piles, the active pile length is generally governed by the stiffness of the pile relative to the surrounding soil stiffness. Particularly, there is a linear relationship with the fourth-root of the ratio of pile stiffness and soil stiffness at various lateral pile head deformation. Moreover, the active pile length at the initial stage is critical as it allows to estimate the active pile length at the ultimate stage. The use of active pile length to get the pile resistance and derive the side soil reaction from the load-deflection response curve at the pile head is indicative that the active pile length is a key parameter to define the ultimate lateral resistance. Together with other important soil parameters such as the soil unit weight and Rankine passive coefficient, the ultimate lateral resistance of the side soil can be estimated. This simplified expression can be useful for more practical approach in the seismic and assessment of piles. This idea can also be extended to the 3D case and for a more complicated scenario such as for group piles, among others.

# Chapter 5

## Application of Active Pile Length in the Ultimate Lateral Resistance of Single Fixed Head Piles Embedded in Sand

### 5.1 Introduction

The active pile length,  $L_a$ , governs the equivalent cantilever beam behaviour that can be derived from the deformation of long and flexible piles caused by the lateral loads applied at the pile head. This deformation is fully characterized by the ratio of the pile stiffness with the soil stiffness, represented by parameter,  $L_c$  (discussed in Chapter 3). Considering the soil wedge formed in the passive region from the lateral push as the pile deforms, the driving question is if this simple parameter can describe the ultimate lateral pile resistance. This chapter aims to address this question by presenting numerical simulations of laterally loaded single pile embedded in homogeneous sandy soil using the ABAQUSv6.13. In this soil-pile system, the elasto-plastic behavior of the soil is modeled using hypoplastic model of von Wolffersdorff while only the elastic nature of the pile is momentarily considered. From the results of the rigorous solution, the process of arriving at the simplified method to define the ultimate lateral resistance of single piles in sands using the active pile length,  $L_a$  as the key parameter, is discussed.

### 5.2 Definitions

Two concepts have been the driving force of this research: (1) Active pile length,  $L_a$  and (2) lateral pile resistance. The definitions of these concepts are discussed in this section.

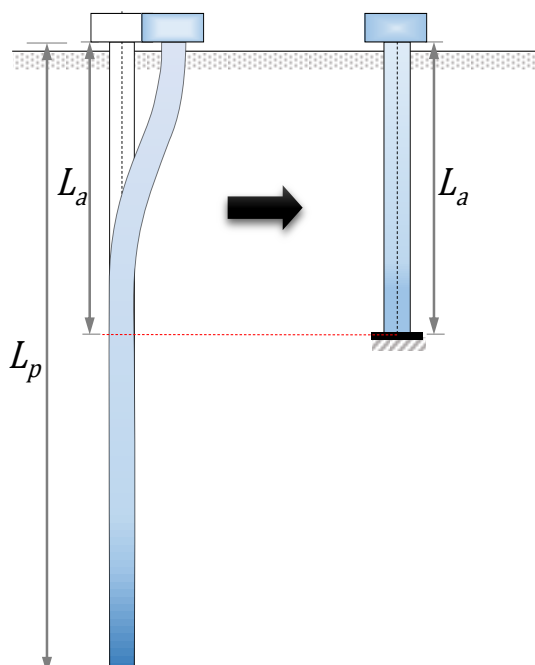


Figure 5 - 1. Active pile length

#### 5.2.1 Active Pile Length

Long and flexible piles are exposed to one or combinations of many lateral loads which may be in the form of wind, waves, large lateral earth pressure and/or seismic waves. The lateral pile resistance of piles is governed by the soil-pile interaction, simply because with the mere presence of piles and soil in the system. The deformation of the piles are relative to the deformation of the soil and vice versa. The deformation along the length of the piles can be described by the characteristic length,  $L_c$ , as defined in Chapter 3. The pile is observed to have large deformation at the region near the ground surface and becomes negligible with increasing depth. The fixity is assumed at the depths where the deeper embedment starts to have negligible deformation as seen in Figure 5 - 1. Therefore, the pile can be assumed as cantilever beam with

length,  $L_a$ . To derive the sole pile resistance would mean to get the product of the stiffness of this equivalent cantilever beam and the pile head deformation.

### 5.2.2 Ultimate Lateral Pile Resistance

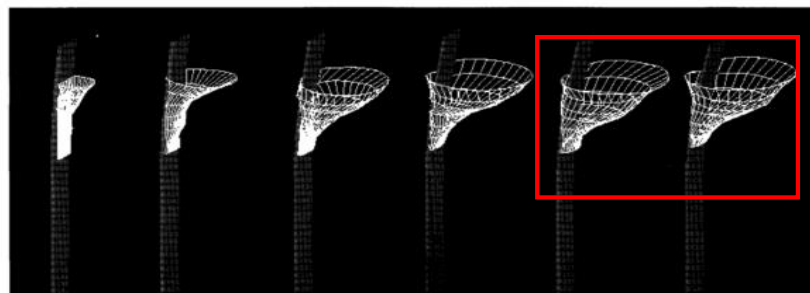
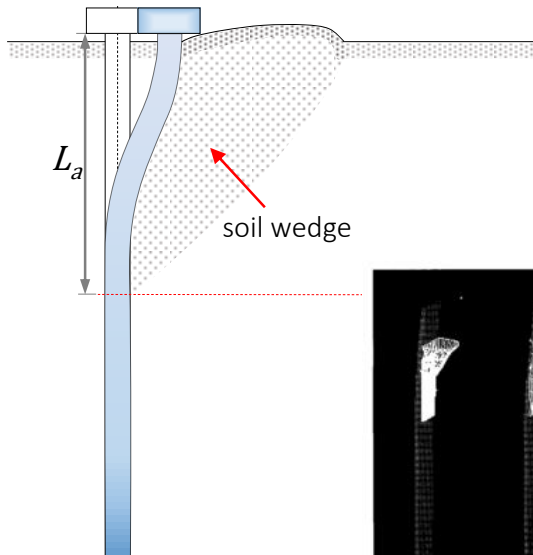


**Figure 5 - 2. Soil wedge formation around laterally loaded pile** **Figure 5 - 3. X-ray CT scan of the failure deformation around laterally loaded pile**

In the event when large lateral loads are applied on long and flexible piles, the lateral deformation of the pile pushes a soil wedge up in the passive region. The formed soil wedge along this active pile length is said to be the ultimate side soil resistance and correspondingly, the ultimate lateral pile resistance as seen in Figure 5 - 2.

As evidence, Otani et al. (2006) conducted a model test of a single flexible pile embedded in dense sand applied with a lateral force using Xray CT Scan. The research did a visualization of the lateral deformation around laterally loaded pile in the passive region as seen in Figure 5 - 3. It can be observed that with increasing pile head deformation, the soil wedge formation is progressively formed. However, with large displacements there appears to be an ultimate value where the soil wedge shape becomes constant.

## 5.3 Numerical Simulations of Laterally Loaded Single Pile

The simulation of the response of laterally loaded single piles in three-dimension (3D) were performed using the ABAQUS v6.13. The ABAQUS v6.13 is a commercial Finite Element Analysis (FEA) software (Dassault Systemes Simulia, 2013a) that allows rigorous simulations of the behaviour of simple model systems up to the more complicated ones. In this program, a user-friendly interface is built in to navigate smoothly through the modelling process. It also provides readily available interface models for cases of existence of contact surfaces of two-element models, necessary for the soil-pile interface. At the same time, it offers option to provide input in code command forms for more user-controlled environment. The modular nature of this software

allows the user to apply user-defined material constitutive models, perfect for incorporating soil constitutive models reflecting the elasto-plastic behaviour of soil.

In this section, the procedure for the soil-pile idealization and the cases considered in this study is discussed in details. The Finite Element Methods (FEM) implemented are validated through comparison of previous study as benchmark for simulating the cases.

### 5.3.1 Soil-Pile System Idealization

The soil-pile system includes a single end bearing pile embedded in a homogeneous sandy soil subjected to a lateral load. The soil-pile configuration properties and techniques implemented are presented herein.

#### 5.3.1.1 Geometry of the Model

While the programs based on FEM can rigorously model any soil-pile configurations, the computing time and memory requirement increases with complexity. Thus, only the half mesh of the soil-pile system is modelled in view of the symmetry (Figure 5 - 4). This soil-pile system is modelled with 3D solid deformable body. The maroon elements represent the soil medium, while the green elements represent the pile.

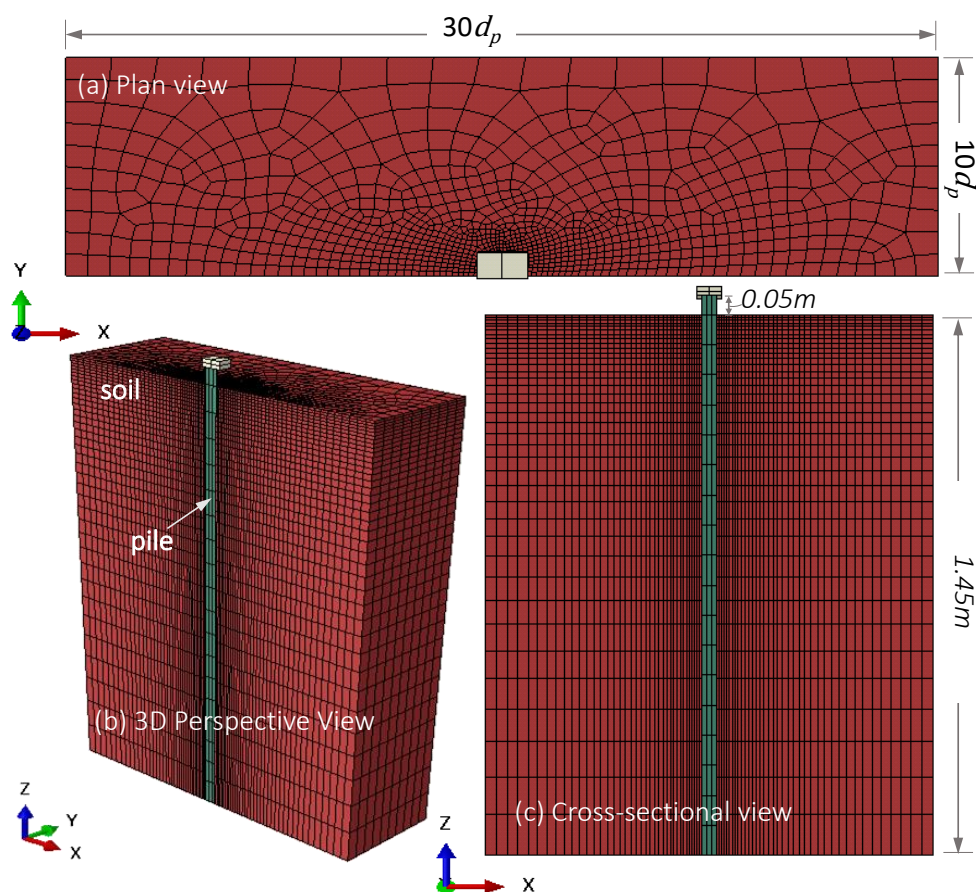


Figure 5 - 4. Soil-pile geometric properties and meshing in (a) plan view, (b) 3D Perspective view and (c) cross-sectional view

The soil models are dimensioned dependent on the size of the pile diameter,  $d_p$ , to minimize the boundary effects, though this is negligible for static cases. The soil is dimensioned as  $30 \times d_p$  in the

longitudinal direction (x-axis) and  $10x d_p$  in the transverse direction (y-axis) as seen in the plan view of Figure 5 - 4. The depth of the soil medium is 1.45m while the actual length of the pile,  $L_p$ , is 1.5m (Figure 5 - 4.c).

A 3d hexahedron-shaped element type used for the automated meshing. Non-uniform meshing is implemented to save computing time and memory. Finer meshing is done around the pile as seen in Figure 5-4a and near the ground surface as seen in Figure 5-4c.

### 5.3.1.2 Boundary Conditions

The boundary planes in the soil-pile system are designated as follows: (1) bottom (XY plane), (2) side (ZY plane), (3) back (ZX plane) and (4) plane of symmetry as shown in Figure 5 - 5. The plane designations is used to define the boundary conditions implemented in this section.

The bottom of the soil medium is considered as a hard stratum and the pile as an end bearing type. In this case, the bottom surface of the soil and the pile is considered fixed, where it is restrained at all degrees of freedom. The sides of the soil medium is restrained at the x-axis while the back is restrained at the y-axis. The plane of symmetry is enforced with symmetric boundary conditions, where the translations are restrained at the y-axis and rotations at z and x-axis.

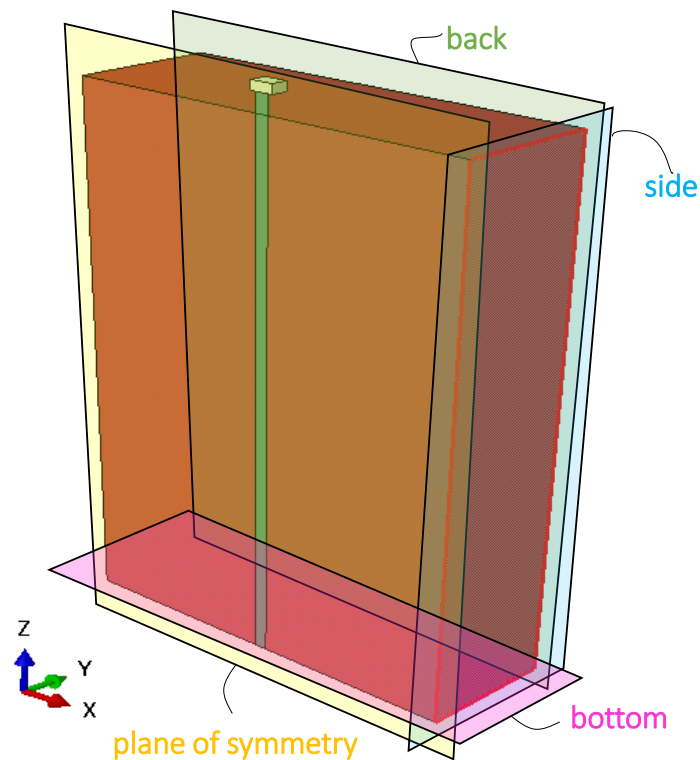


Figure 5 - 5. Boundary planes of the soil-pile system

### 5.3.1.3 Soil- Pile Interface

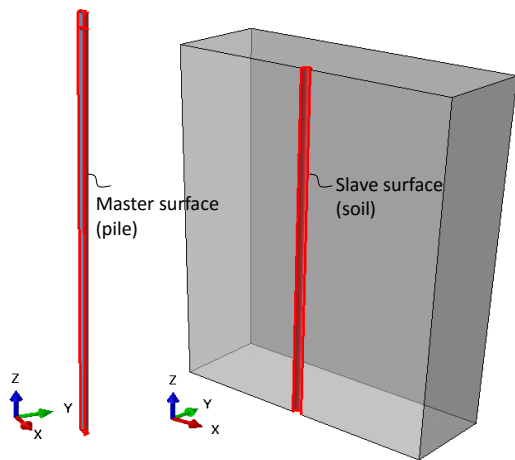


Figure 5 - 6. Master-slave surface definition

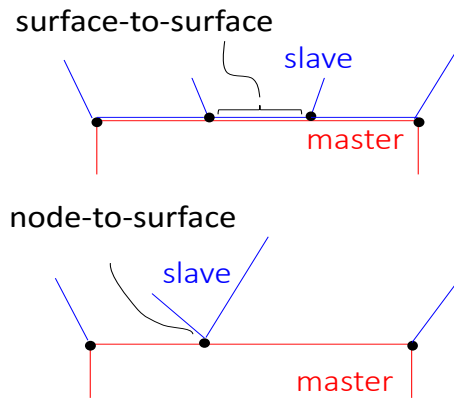


Figure 5 - 7. Comparison of surface-to-surface discretization and node-to-surface discretization

The contact pairs in the soil-pile system need to be identified to define the slipping and/or gapping behaviour between the soil and the pile. Specifically, each surface should be designated as either the master surface or the slave surface. The master surface is usually that of a stiffer body in which the slave surface behaviour tends to be dependent on. Thus for this case, the master surface is part of the pile in contact with the soil and the slave surface is part of the soil located at the hole intended for pile installation as seen in Figure 5 - 6.

Normally, numerical simulations dealing with models having contact pairs face difficulty for solutions to converge. Therefore, some suggested points are to consider for solving contact pair problems (King and Richards, 2013) especially for the soil-pile system considered in this study: (1) In modelling the contact pairs, the slave surface is suggested to be meshed finer than the master surface to avoid possible penetration of the master surface as implemented in Figure 5 - 4. (2) Considering the opposite normal direction of contact surfaces of the soil-pile interface, surface-to-surface discretization is deemed more appropriate (Figure 5 - 7). This type of discretization avoids penetration of surfaces to each other. It also need not require the matching of meshes of the master-slave surfaces as it inherently smoothens the contact surfaces through the coupling of nodes. With this action, good response to the behaviour of the master surface is more expected and thus allows improved convergence and accurate contact stresses. (3) In addition to the surface-to-surface discretization, extra reinforcement of “auto-smoothing” is implemented through adjustment of interference fit at the initial stage. Lastly, (4) Finite sliding between these two surfaces is chosen in consideration of large displacements.

The interaction between the soil and pile contact surface can be decomposed to the (1) normal component and (2) tangential component. The normal behaviour of the interface is modelled as “hard” contact. This means that separation between the contact surfaces occur when the contact pressure becomes zero or when there is tension deemed to happen given by a negative value. On the other hand, the tangential behaviour is modelled using the penalty algorithm characterized by a coefficient of friction between the surface of the pile and the soil. In this case, since the pile material is aluminium rested against a sandy soil, the coefficient of friction used is 0.47 or

equivalent to the soil-pile interface's internal angle of friction, equal to 25 degrees (Wakai et al., 1999). All other settings are set to default.

#### 5.3.1.4 Material Model and Elements

##### (1) Pile Modeling

The pile is modelled using 3d solid hexahedron elements. However, the question is whether to use an 8-node linear brick element or a 20-node quadratic brick element (Figure 5 - 8). To address this, sensitivity analysis is done to compare with the analytical solution of a simple cantilever beam with a concentrated force at the end. The following cases were considered: Two cases of using linear hexahedral elements with coarse mesh (C3D8R-152 elements) and finer mesh (C3D8R-6000 elements), and one case using quadratic hexahedral elements.

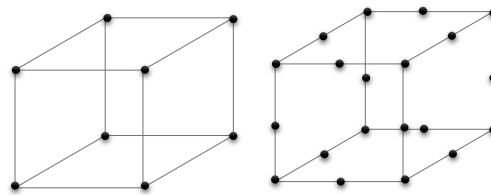


Figure 5 - 8. Types of hexahedral elements (C3D8R and C3D20R)

For a beam with bending stiffness  $EI_p$  of length  $L_p$ , subjected with a concentrated force,  $P$  at the end, the maximum deflection at the end (Figure 5 - 9) is given by the following equation:

$$y_{max} = \frac{PL_p^3}{3EI_p} \quad (5.1)$$

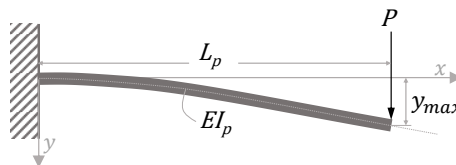


Figure 5 - 9. Maximum deflection for a cantilever beam subjected to a concentrated force at the end

The pile head deflections ( $y_{max}$ ) given the monotonic increase of load,  $P$  is plotted in Figure 5 - 10. It can be seen that using the linear hexahedral elements (C3D8R) with coarser mesh (152 elements), the difference of pile head displacements from the analytical solution considering a load of 1.5N is 28.20%. From the trend in Figure 5 - 10, this difference even increases with increasing load, hence accuracy fall short. But by making the mesh finer, using 6000 elements, the numerical solution gets nearer the same value of the analytical solution with a difference of 7%. Yet, this seems considerably tedious given that only piles are considered now. Imagine what the numerical scenario would look like when piles are embedded in the sand. Now, using the quadratic hexahedral elements of a very coarse mesh, with only 152 elements, the numerical solution is in agreement with the numerical solution. Therefore, to optimize the computing time, the C3D20R elements are used for the piles.

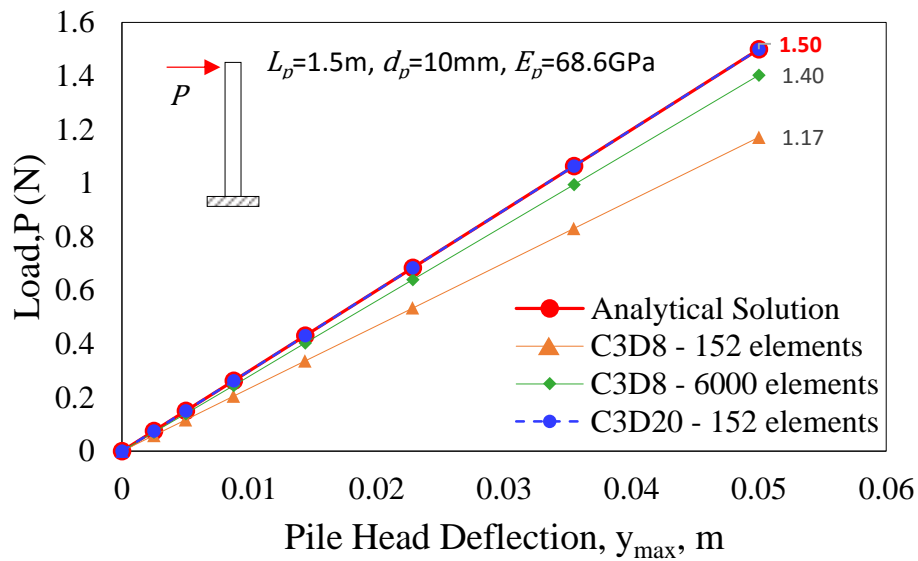


Figure 5 - 10. Load-deflection curve of a cantilever beam using C3D8 and C3D20 elements

Since the three-dimensional hexahedral elements has only the translational degrees of freedom, the rotational constraints at the head cannot be enforced directly. Therefore, a rigid mass is attached to the pile head as a cap, enforced with a rigid constraint, where the less stiff material is bound to have a deformation relative to it (Figure 5 - 11). In this case, the pile head nodes are tied with the rigid cap. Then, a reference point is set at the centroid of the cap, and set the node with symmetric condition and zero rotation. To verify if this approach suits the expected deformation, it is compared with analytical solution.

The analytical solution for the beam is as follows: For a beam (Figure 5 - 12) with bending stiffness  $EI_p$  of length  $L_p$ , with constrained rotation at the end and subjected with a concentrated force,  $P$ , the maximum deflection at the end is given by the Equation 5.2.

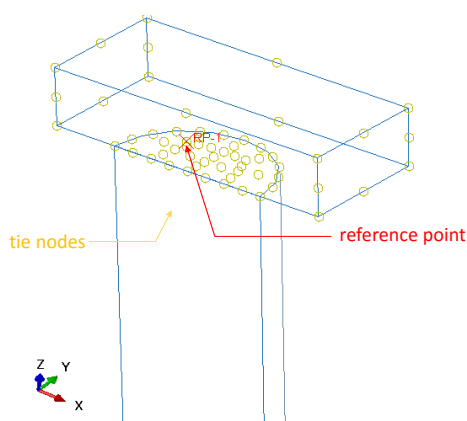


Figure 5 - 12. Constrained FEM techniques

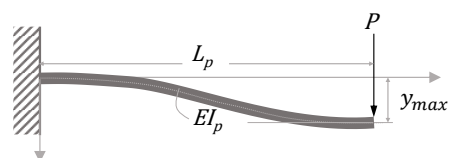


Figure 5 - 11. Maximum deflection for cantilever beam with constrained rotation at end and applied with concentrated force

$$y_{max} = \frac{PL_p^3}{12EI_p} \quad (5.2)$$

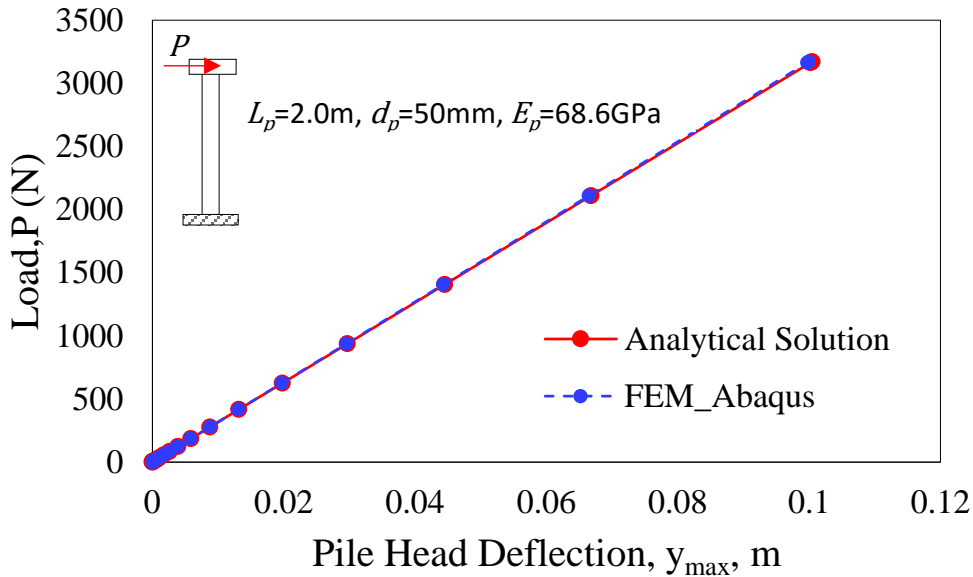


Figure 5 - 13. Numerical solution vs. analytical solution of fixed-head pile

From Figure 5 - 13, it can be seen that the numerical solution with the FEM techniques implemented is in agreement with the analytical solution. Therefore, this approach is implemented in the soil-pile system.

In this study, the piles considered are in elastic material which is defined by the following parameters: (1) Young's modulus,  $E_p$  and (2) Poisson's ratio,  $\nu$ .

## (2) Soil Modelling

In the soil-pile system, a homogeneous Toyoura sand is considered as the soil medium. A user-defined constitutive model is implemented in the Abaqus v6.13 to model the mechanical behaviour of the granular soil, particularly of Toyoura sand. This model is based on the Abaqus UMAT (User Material) (Dassault Systemes Simulia, 2013b) code from the soilmodels.info (Gudehus et al., 2008) with minor code alteration to be installed and run with the FEA program. The code is based on formulation of the basic model of hypo-plasticity model for granular materials (von Wolffersdorff, 1996) and small-strain extension (Niemunis and Herle, 1997) suitable for cyclic loading cases. In this study, only the basic model is utilized.

In this section, the description of the hypoplastic model and the required parameters are discussed. The calibration of parameters to simulate the behaviour of the Toyoura sand is presented.

**(a) Background of the hypoplastic model**

The nonlinear and inelastic behaviour of the soil, notwithstanding the elastic part, is captured using the hypoplastic model by von Wolffersdorff (von Wolffersdorff, 1996). This model is rooted from the elasto-plasticity theory models of the hypoplastic Drucker-Prager model (Drucker and Prager, 1952) with implementation of the yield criterion of the Matsuoka-Nakai failure surface (Matsuoka and Nakai, 1977). The difference of this model with the conventional elasto-plastic models is the formulation of only one tensorial function.

The general form of the constitutive equation for the current hypoplastic model is given by the expression:

$$\dot{\mathbf{T}}_s = \mathbf{F}(\mathbf{T}_s, e, \mathbf{D}) \quad (5.3)$$

where  $\dot{\mathbf{T}}_s$ : the objective Jaumman stress rate tensor. This tensor is a function of the Cauchy stress tensor,  $\mathbf{T}_s$ , the current void ratio,  $e$ , and the stretching tensor,  $\mathbf{D}$ . This equation clearly depicts the assumptions made by this constitutive model. The hypo-plasticity model treats the granular soil as a composition of grains, making up its skeleton. The current condition of skeleton of the granular soil is described by the contact between the grains, known as the effective stress,  $\mathbf{T}_s$  and the void ratio,  $e$ . The deformation of the granular soil is described by the stretching tensor,  $\mathbf{D}$  which is based on the rearrangement of the grains that includes evolution and decay of grain contact (Niemunis and Herle, 1997). It is noted together with these assumptions that the general form and size of the grains are kept as is, such that particle crushing, compression, abrasion, surface and thermal effects are not yet accounted for.

The function  $\mathbf{F}$  in equation 5.3 can be decomposed to two terms given by the function of  $\mathbf{A}$  and  $\mathbf{B}$ . The function of  $\mathbf{A}$  represents the hypoelastic behaviour (Bower, 2010) of the soil and the function of  $\mathbf{B}$  represents the nonlinearity and inelasticity. Therefore, equation 5.3 can be re-written as equation 5.4:

$$\dot{\mathbf{T}}_s = \mathbf{A}(\mathbf{T}_s, e, \mathbf{D}) + \mathbf{B}(e, \mathbf{T}_s) \|\mathbf{D}\| \quad (5.4)$$

where  $\|\mathbf{D}\|$  is the Euclidian norm  $\sqrt{\text{tr}\mathbf{D}^2}$ . It is warranted that functions  $\mathbf{A}$  and  $\mathbf{B}$  can be further decomposed to factors that would allow convenience in separating components for calibration of material parameters. Considering satisfaction of the sweep-out-of memory<sup>1</sup> (SOM) and critical states,  $\mathbf{A}$  and  $\mathbf{B}$  are replaced with dimensionless factors:  $f_e, f_b, f_d$ , depicting the dependence on the relative density and pressure. The dimensionless factors:  $f_e$  and  $f_b$  represent the pycnotropy (density) factor and  $f_d$  represents the barotropy (pressure).

$$\dot{\mathbf{T}}_s = f_e f_b (\mathbf{L}(\hat{\mathbf{T}}_s, \mathbf{D}) + f_d \mathbf{N}(\hat{\mathbf{T}}_s) \|\mathbf{D}\|) \quad (5.5)$$

where,  $\mathbf{L}$  and  $\mathbf{N}\|\mathbf{D}\|$  depend on the stretching tensor,  $\mathbf{D}$  and the stress ratio tensor,  $\hat{\mathbf{T}}_s = \frac{\mathbf{T}_s}{\text{tr}\mathbf{T}_s}$ . The stress ratio tensor is coaxial with the the principal axes of  $\mathbf{T}_s$ .

---

<sup>1</sup> Sweep-out- Memory state (SOM) is one of the boundary states of hypoplastic model. It means that for proportional strain paths, there are corresponding proportional stress paths. Influence of initial stresses and density vanishes with monotonic deformation (Anaraki, 2008; Mašín and Herle, 2006)

From equation 5.5, the Matusoka-Nakai yield surface condition is implemented and gives the equation 5.6.

$$\hat{\mathbf{T}}_s = f_e f_b \frac{1}{\text{tr} \hat{\mathbf{T}}_s^2} (F^2 \mathbf{D} + a^2 \text{tr}(\hat{\mathbf{T}}_s \mathbf{D}) \hat{\mathbf{T}}_s + f_d a F (\hat{\mathbf{T}}_s + \hat{\mathbf{T}}_s^*) \|\mathbf{D}\|) \quad (5.6)$$

where  $a$  and  $F$  are given by equations 5.7 and equation 5.8 respectively. Basically, these equations is primarily based on the critical angle of internal friction,  $\varphi_c$ , material parameter,

$$a = \sqrt{\frac{3(3 - \sin \varphi_c)}{8 \sin \varphi_c}} \quad (5.7)$$

$$F = \sqrt{\frac{1}{8} \tan^2 \psi + \frac{(2 - \tan^2 \psi)}{2 + \sqrt{2} \tan \psi \cos 3\theta}} - \frac{1}{2\sqrt{2}} \tan \psi \quad (5.8)$$

where the invariants are given by the following equations:

$$\tan \psi = \sqrt{3} \|\hat{\mathbf{T}}_s^*\| \quad (5.9)$$

$$\cos 3\theta = -\sqrt{6} \frac{\text{tr} \hat{\mathbf{T}}_s^{*3}}{(\text{tr} \hat{\mathbf{T}}_s^{*2})^{\frac{3}{2}}} \quad (5.10)$$

and  $\hat{\mathbf{T}}_s^*$  is the deviatoric stress ratio tensor given by equation 5.11.

$$\hat{\mathbf{T}}_s^* = \hat{\mathbf{T}}_s - \frac{1}{3} \mathbf{I} \quad (5.11)$$

where  $\mathbf{I}$  is the unit tensor.

### **(b) Soil Model Parameters**

One advantage of this model is that the parameters has physical basis and can be determined simply through conventional tests on dry sand to determine the mechanical behaviour of soil.

Considering the dependence of the model on the void ratio, three characteristic void ratios, namely,  $e_{c0}$ ,  $e_{i0}$  and  $e_{d0}$  are needed as parameters. These are the reference void ratios at mean pressure equal to zero, that characterize the position of limiting void ratio curves as seen in Figure 5 - 14.

The void ratio at the critical state is related to the mean pressure,  $p = -(\text{tr} \mathbf{T}_s)/3$  where  $\text{tr} \mathbf{T}_s < 0$  is for compression, by the following equation:

$$\frac{e_c}{e_{c0}} = \exp \left[ - \left( - \frac{\text{tr} \mathbf{T}_s}{h_s} \right)^n \right] \quad (5.12)$$

Other characteristic void ratio such as the minimum,  $e_{d0}$ , and maximum void ratio,  $e_{i0}$  are related with the mean pressure in similar form with the critical void ratio given by the equation below.

$$\frac{e_i}{e_{i0}} = \frac{e_d}{e_{d0}} = \exp \left[ - \left( - \frac{\text{tr} \mathbf{T}_s}{h_s} \right)^n \right] \quad (5.13)$$

where  $h_s, n$  are additional material constants.

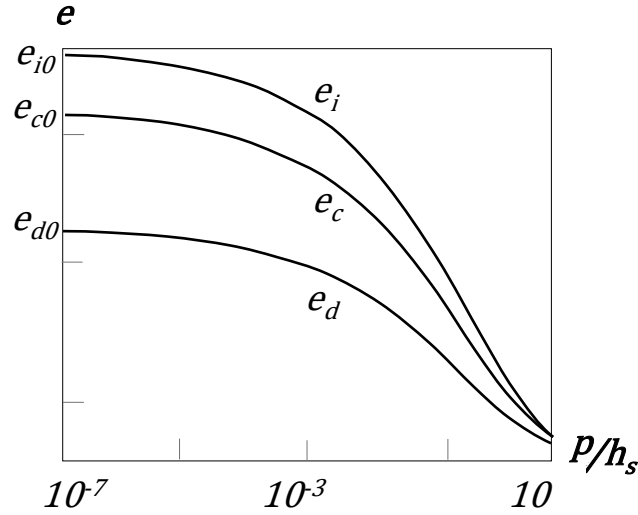


Figure 5 - 14. Void ratio vs. mean pressure in logarithmic scale (after Herle and Gudehus, 1999)

The granular stiffness,  $h_s$  and  $n$  also control the limiting void ratio curves and are two of the parameters that describe the normal compression and critical state line.

Equation 5.14 describes the pycnotropy factor,  $f_d$ . This controls the stress-strain relationship describing the transition to the peak friction angle, the dilative behaviour and critical state, with a material constant,  $\alpha_h$ . When,  $f_d = 1$ , the critical state is reached.

$$f_d = \left( \frac{e - e_d}{e_c - e_d} \right)^{\alpha_h} \quad (5.14)$$

The other pycnotropy factor,  $f_e$ , controls the influence of the void ratio  $e$  on the incremental stiffness. Considering that there is an increase in the stiffness with the decrease in void ratio, the density factor is related to the void ratio,  $e_c$ , of the soil by the following equation.

$$f_e = \left( \frac{e_c}{e} \right)^{\beta_h} \quad (5.15)$$

The barotropic factor,  $f_b$ , accounts for the increase of the stiffness with the increase of the mean stress. This can be directly determined from one-dimensional isotropic compression test or oedometer tests.

$$f_b = \frac{h_s}{n} \left( \frac{1 + e_i}{e_i} \right) \left( \frac{e_{i0}}{e_{c0}} \right)^{\beta_h} \left( - \frac{\text{tr} \mathbf{T}}{h_s} \right)^{1-n} \left[ 3 + a^2 - \sqrt{3}a \left( \frac{e_{i0} - e_{d0}}{e_{c0} - e_{d0}} \right)^{\alpha_h} \right]^{-1} \quad (5.16)$$

In summary, there are 8 parameters required for the basic hypoplastic model: (1) The critical friction angle,  $\varphi_c$ , (2) the granular stiffness,  $h_s$ , (3)  $n$ , the characteristic void ratios: (4)  $e_{d0}$ , (5)

$e_{c0}$  and (6)  $e_{i0}$ , (7)  $\alpha_h$ , that controls the peak friction angle based on the relative density and (8) the  $\beta_h$  that controls the dependency of stiffness on the relative density.

From Herle and Gudehus (1999), the materials can be calibrated from simple mechanical tests for dry sand. The critical friction angle is determined from the angle of repose of the loose material. On the other hand, the  $e_{i0}$  and  $e_{d0}$  correspond to the maximum and minimum void ratio respectively. The  $h_s$  and  $n$  can be determined from the oedometer tests.

Herle and Gudehus (1999) have performed calibration for the Toyoura sand yet are re-calibrated and compared with conventional drained compression triaxial test. The following parameters are used:

**Table 5 - 1. Material parameters for Toyoura sand**

Angle of internal friction at critical state, $\varphi_c$	30
Granular stiffness, $h_s$ [GPa]	2.6
Exponential material constant, $n$	0.35
Reference minimum characteristic void ratio, $e_{d0}$	.61
Reference characteristic void ratio at critical state, $e_{c0}$	.98
Reference maximum characteristic void ratio, $e_{c0}$	1.1
Parameter for controlling peak friction angle based on relative density, $\alpha_h$	0.18
Parameter for controlling dependence of stiffness on the relative density, $\beta_h$	1.1

A single element test was conducted using FEM in Abaqus, where the following material parameters are implemented with initial mean stress,  $p_0 = 196kPa$ . This simulation is compared with the experiment on the conventional drained compression triaxial test and numerical simulation of the elasto-plastic model, subloading  $t_{ij}$ .

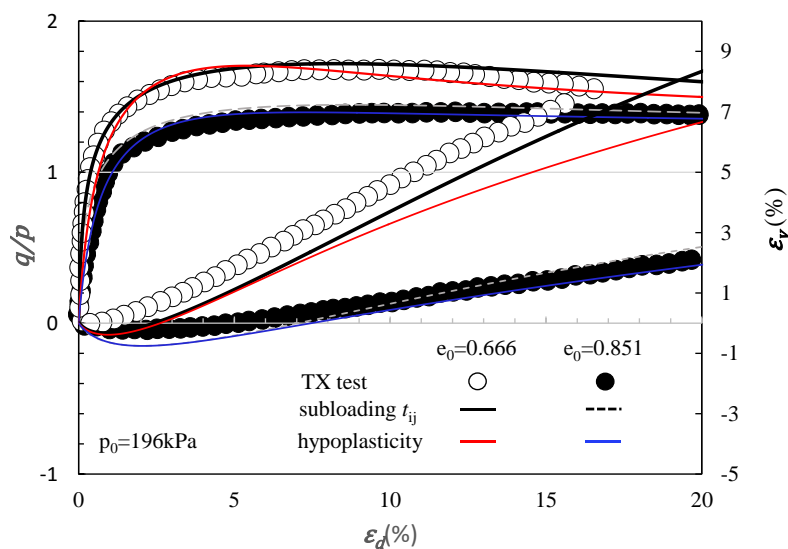


**Figure 5 - 15. Comparison between experimental and numerical result for the stress-strain relationship of Toyoura sand (after (Kyokawa, 2011))**

The stress ratio,  $q/p$  are plotted in Figure 5 - 15 with the corresponding shear strain,  $\varepsilon_{cb}$  for all cases considering loose and dense sand condition. Alongside with this is the dilative behaviour,  $\varepsilon_v - \varepsilon_d$  from all the tests. The colored lines are the simulations using the hypoplasticity model. This is superimposed with the results from the drained compression triaxial test and the numerical simulation using the subloading  $t_{ij}$ . It can be seen that the simulations are in agreement with the experimental results.

### *5.3.1.5 Loading Procedure*

Three steps were undertaken in the simulation of the lateral response of single piles. First, the initial conditions were defined which includes the boundary conditions, the interface properties and the pre-defined fields needed for the geostatic stresses and user-defined solutions.

In the first step, the initial conditions are called on. In the geostatic stresses, the expected vertical stresses at the top and bottom are entered and the horizontal factor,  $K_0$ . In the initial condition, the user-defined material is introduced and directed to.

Next, is the geostatic stresses  $s$  where initial soil stresses are to be developed but the strains are back to 0 and back to the equilibrium condition as seen in Figure 5-16. In this case, a selfweight analysis is conducted and the last stage is equal to the vertical stresses,  $\gamma h$  and horizontal stress,  $0.5\gamma h$ . In this case, the soil-pile interface properties are not yet activated, and the holes are constrained to move at x and y-axis, to assume the non-existence of the pile. Then a gravity load equivalent to the selfweight is applied to the whole soil medium. Vertical stresses (S33) are generated varying with depth (see Figure 5 - 16(1.a)) and with the horizontal stresses (S22) equal to 0.5(S33) (see Figure 5 - 16(1.c)). Then the strains generated are put back to the equilibrium state with zero or at the very least, very negligible displacements (U33) as seen in Figure 5 - 16(1.b).

Then, in the monotonic loading process under displacement controlled until it reaches, 0.5m or just to allow a large displacement. The lateral displacement is applied at the pile head as shown in Figure 5 - 16(2). In this step, the boundary conditions at the hole for the piles are removed and the interaction properties are activated.

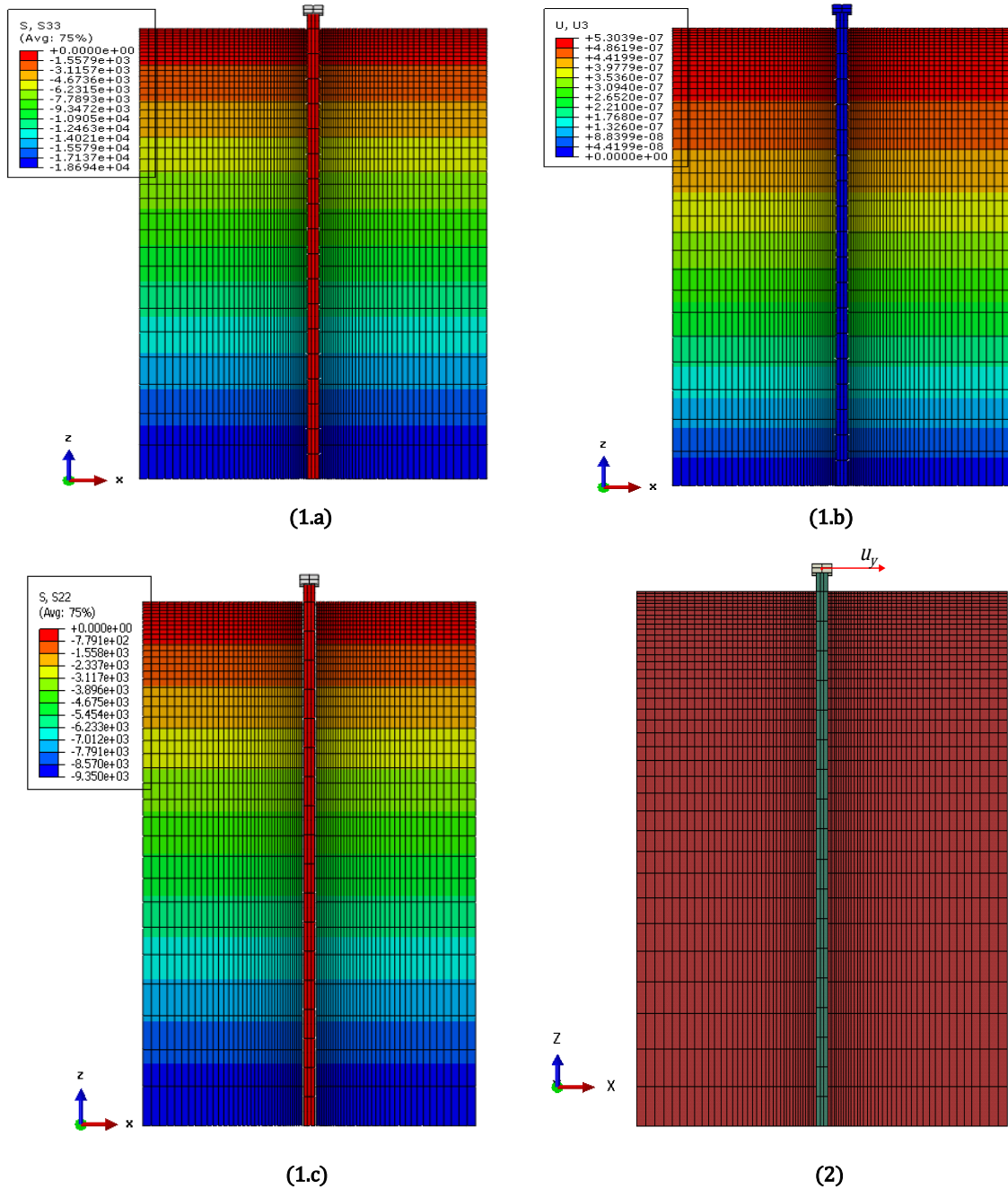


Figure 5 - 16. Loading Process: (1) Initial Stress Condition Simulation: (a) Vertical Stress Condition (b) Vertical Displacement Distribution (c) Horizontal Stress Condition and (2) Application of Lateral Load

### 5.3.2 Simple Validation of FEM Techniques from Elastic Case

The previously mentioned techniques are verified using a simple elastic case similarly used by the OpenSeesPL (Lu et al., 2011). This is done to serve as benchmark for the cases to be simulated.

This material parameters are used in this study is exactly the same parameters modelled by Lu et. al (2011) in the intention to compare with the analytic solution of Pak (2004) .

A cylindrical pile with hollow section having properties listed in Table 5-2 is considered. The soil domain where the pile is embedded is assumed to be homogeneous and in linear elastic with properties listed in Table 5-3. Also, the pile is assumed to be in perfect contact with the soil, therefore, rough tangential behaviour is implemented in the interface property.

**Table 5 - 2. Pile properties**

Outer Radius, $R_o$	8 in (0.203m)
Wall thickness, $h$	$0.1R_o$
Pile Length, $L_p$	33.3 ft (10.15m)
Young's Modulus of Pile, $E_p$	29000 ksi (200 GPa)
Moment of Inertia of Pile, $I_p$	1286.8 in <sup>4</sup> (5.356E-04 m <sup>4</sup> )
Poisson's Ratio, $\nu$	0.345

**Table 5 - 3. Soil Properties**

Shear Modulus of Soil, $G$	7.98 ksi (55MPa)
Poisson's Ratio, $\nu$	0.25
Submerged unit weight, $\gamma'$	62.8 pcf (9.865 kN/m <sup>3</sup> )

Initial stresses are generated using the selfweight analysis but the strains are put back to equilibrium. Then, the pile head with a free head condition is applied with a horizontal load of 31.5kips (140.12kN). The solution from the FEM using the Abaqus is compared with the elastic solution of Abedzadeh and Pak (2004) and the solutions using the OpenSees PL using different brick elements (8-node and 20-node) in terms of the pile deformation along the depth as seen in Figure 5-17.

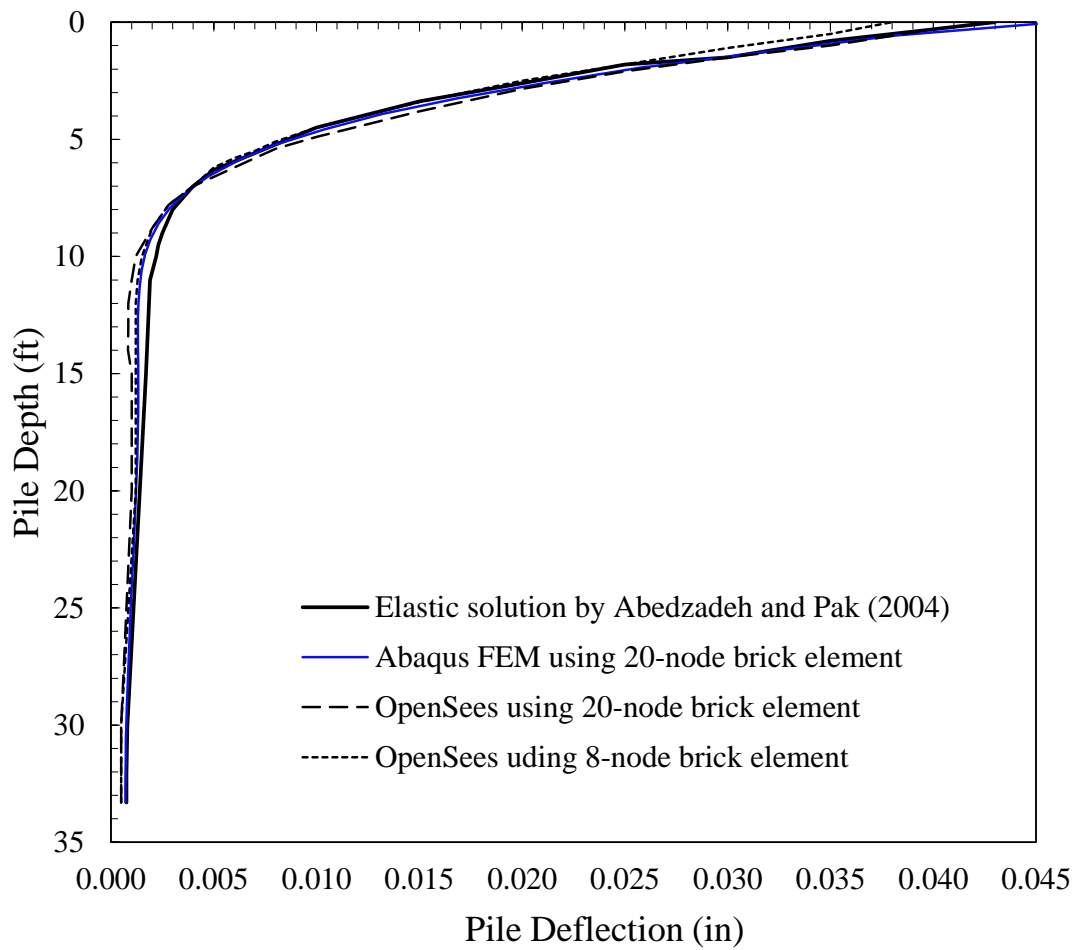


Figure 5 - 17. Comparison of the pile defomation along the pile depth (after (Lu et al., 2011))

Figure 5-17 shows that the pile deformation along the pile length from the results of FEM using Abaqus is in agreement with solutions using OpenseesPL and the elastic solution of Abedzadeh and Pak (2004). This deformation along the pile depth is of utmost focus since the active pile length is of interest. Therefore, the FEM techniques to simulate the response of laterally loaded piles are adequate.

### 5.3.3 Validation of FEM Techniques from Field Test using Elasto-plastic Case

The FEM techniques are also verified with the results from Arkansas Field Test conducted by the U.S. Army Engineer in the Arkansas River downstream from the Pine Bluff (Alizadeh and Davisson (1970) and Fan (1996)). This serves as benchmark model for the cases to be simulated.

The lateral load test set-up and configuration is illustrated in Figure 5- 18. The properties of the test piles and the in-situ surrounding soil are listed in Table 5 - 4 and Table 5 - 5 respectively.

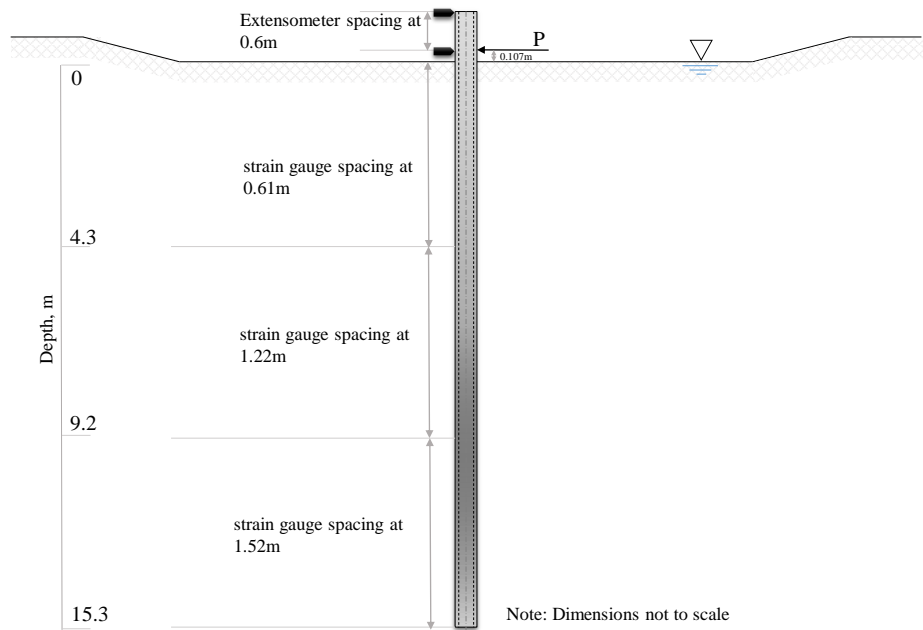


Figure 5- 18. Arkansas Field Test Set-up (after Fan(1996))

In the field test, the test steel pile ( $E_p=2.09 \times 10^8$  kN/m<sup>2</sup>) considered is a hollow cylinder having an outside diameter of 0.406 and a wall thickness of 7.925mm. The pile has a length equal to 15.3m. From flexural field test, the pile has an  $EI_p$  equal to  $6.998 \times 10^4$  kNm<sup>2</sup>.

Table 5 - 4. Pile properties of the Arkansas Field Test Pile

Outer Radius, $R_o$	0.203m
Wall thickness, $h$	7.925mm
Cross-sectional area, $A$	$1.539 \times 10^{-2}$ m <sup>2</sup>
Pile Length, $L_p$	15.3m
Young's Modulus of Pile, $E_p$	$2.09 \times 10^8$ kPa
Flexural stiffness, $EI_p$	$6.998 \times 10^4$ kNm <sup>2</sup>
Poisson's Ratio, $\nu$	0.345

The test pile is installed with electric strain gauges along the length of the piles and spaced as shown in Figure 5- 18. The test pile is installed with extensometers at the pile head to measure the lateral displacements. Then piles are driven in the soil. It should be noted that the protection on the pile consisting of the channels against potential damage from the pile driving has an additional contribution to the cross-sectional area of the piles, thus a total area of  $1.539 \times 10^{-2} \text{ m}^2$  is considered in the numerical modelling. The lateral load is then monotonically applied at the pile head which is 0.107m from the ground at a rate of 17.8 kN per minute. .

The soil properties were derived from exploratory borings and laboratory tests. Detailed descriptions of the soil profile, dry density and SPT values can be referred to (Alizadeh and Davisson (1970) and Fan (1996)) with English units and Metric units respectively.

The soil condition stated herein are based on the discussion of Fan (1996). Generally, the soil stratum is made up of relatively dense medium to fine sands with thin layers of silt and clay at depth levels of 12 to 19m. The average unit weight of the soil medium varies from 14.2 to 17.1 kN/m<sup>3</sup> and with soil medium submerged with groundwater, the submerged unit weight of sand is considered as 9.88kN/m<sup>3</sup>. Laboratory tests like the drained shear tests on the reconstituted soil samples taken from the site show the average friction angle of the sand ranging from 31 to 35 degrees and the friction angle at the interface of the pile and the soil is at 23-30 degrees. The soil properties at the site are summarized in Table 5 - 5.

**Table 5 - 5. Soil properties at the Arkansas Field Test Site**

Dry unit weight, $\gamma$	14.2 to 17.1 kN/m <sup>3</sup>
Submerged unit weight, $\gamma_{\text{sub}}$	9.88kN/m <sup>3</sup>
Average Angle of Internal Friction, $\phi$	31° – 35°
Friction angle at the soil-pile interface	23° – 30°

A three-dimensional modelling of the Arkansas Field test set-up is performed. The following Figure 5 - 19 shows the soil-pile idealization of the Arkansas Field Test.

The pile properties in the situ tests are exactly reflected in the numerical modelling. The soil-pile interface angle of friction used is 25°. The soil properties used are basically based on the SPT field tests and laboratory tests and mainly from back calculation based on the load-deflection curves of the Arkansas field tests given the many uncertainties in the soil properties and the possible effect of the pile driving. Similar with Fan (1996), the soil medium is treated as homogeneous soil. Given from the pile lateral deflection-depth curves, it can be seen that only the shallow layer is of importance as negligible deformation is observed at deeper levels. This shallow layer is considered to be the top 5.5m of the soil which is uniformly made up of sand. The average angle of friction for this layer is 41.5 degrees. This shows that the sand is dense with an initial void ratio of 0.73. Herle and Gudehus (1999) listed the critical angle of friction for various sands, this ranges from 30 to 33. Thus, the angle of friction chosen is 31°. Similarly, in terms of the characteristic void ratios ( $e_{d0}, e_{c0}, e_{i0}$ ), the minimum and the maximum void ratios were chosen within the usual range for sand. The rest of the parameters are calibrated to capture the results of the Arkansas Field Tests i.e. load-deflection curve at the pile head and the lateral pile deformation shown in Figure 5- 20 and Figure 5 - 21 respectively. Figure 5- 20 shows the lateral load applied at the pile head with the corresponding lateral displacements at the groundline. The red data shows the data

results from the field test and the black curve is from the output of the numerical simulation. It can be seen that the field test and the numerical simulation results are in agreement with each other. The soil parameters used for this simulation is summarized in Table 5 - 6. Furthermore, the lateral pile head displacement vs. depth are compared with the results of the numerical simulation for the lateral loads at 69kN, 109kN, 138kN, 172 kN and 208kN. The results are also in agreement with each other which establishes that the FEM techniques can be applied to do some simulations for different case scenarios.

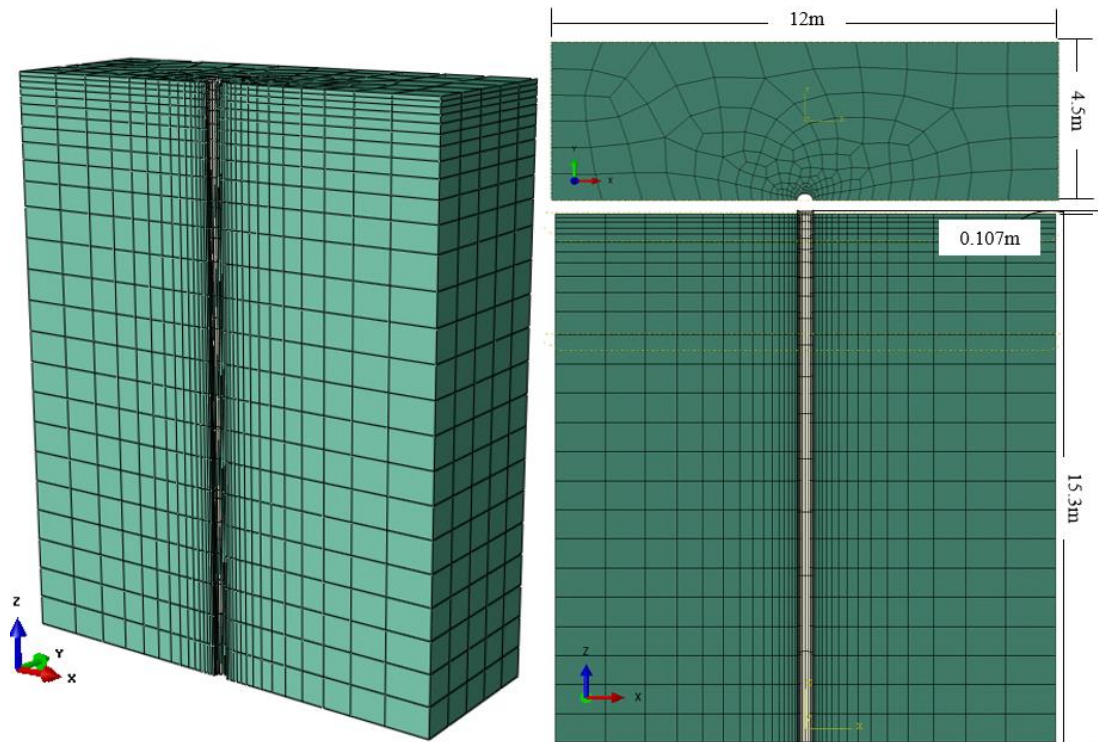


Figure 5 - 19. Arkansas Field Test FEM Model

Table 5 - 6. Soil parameters for the Arkansas Field Test

Angle of internal friction at critical state, $\varphi_c$	31
Granular stiffness, $h_s$ [GPa]	2.6
Exponential material constant, $n$	0.5
Reference minimum characteristic void ratio, $e_{d0}$	.61
Reference characteristic void ratio at critical state, $e_{c0}$	.98
Reference maximum characteristic void ratio, $e_{c0}$	1.1
Parameter for controlling peak friction angle based on relative density, $\alpha_h$	0.25
Parameter for controlling dependence of stiffness on the relative density, $\beta_h$	1.5

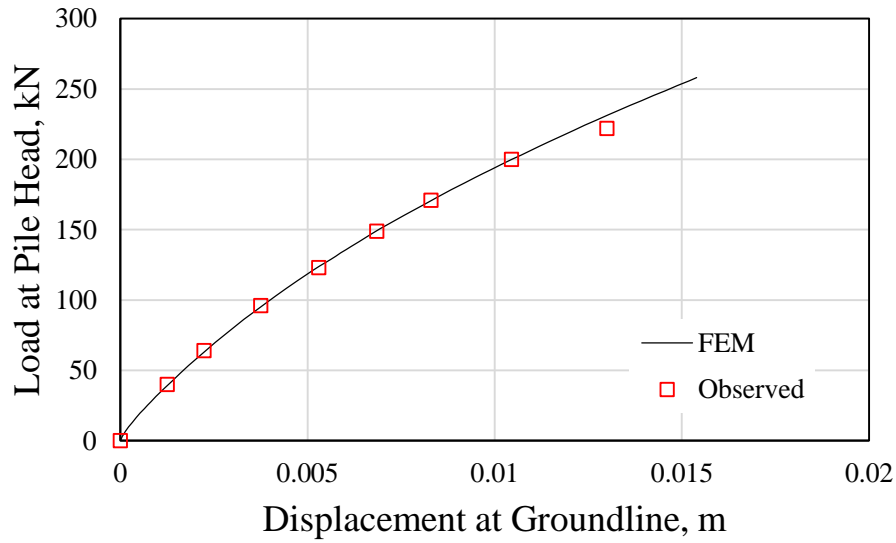


Figure 5- 20. Comparison of Lateral Load - Deflection curves of the Arkansas Field Test and Numerical Simulations (Observed results from Alizadeh and Davisson (1970) and Fan (1996))

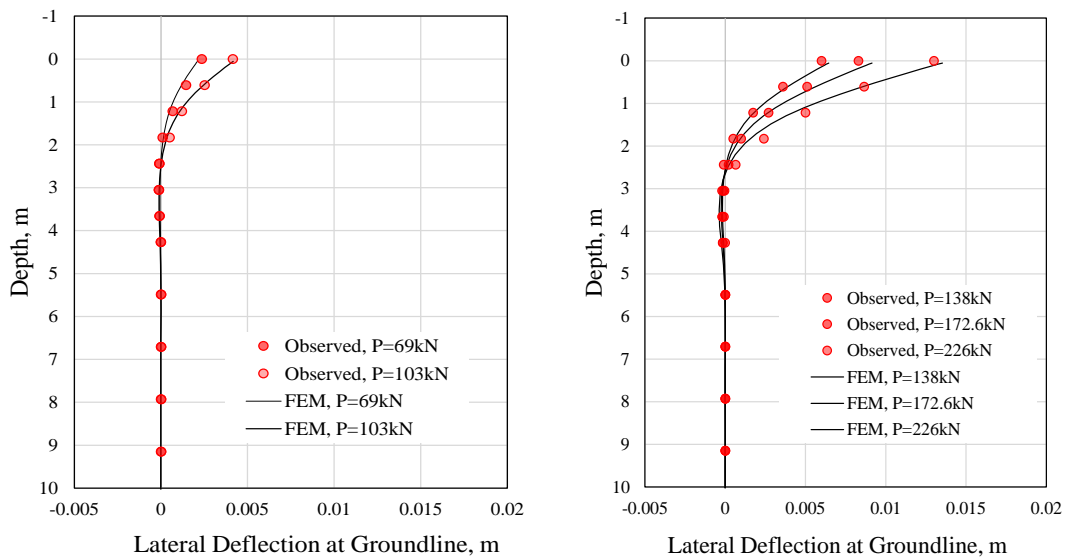


Figure 5 - 21. Lateral Pile Head Deformations vs. Depth for the Arkansas Field Test (Observed results from Alizadeh and Davisson (1970) and Fan (1996))

More notable in this simulations and field test, is the observed progression of the active pile length with increase of lateral loads. Based on the established definition of the active pile length until  $3\%u_y$  which is plotted in Figure 5 - 22, this trend can be seen.

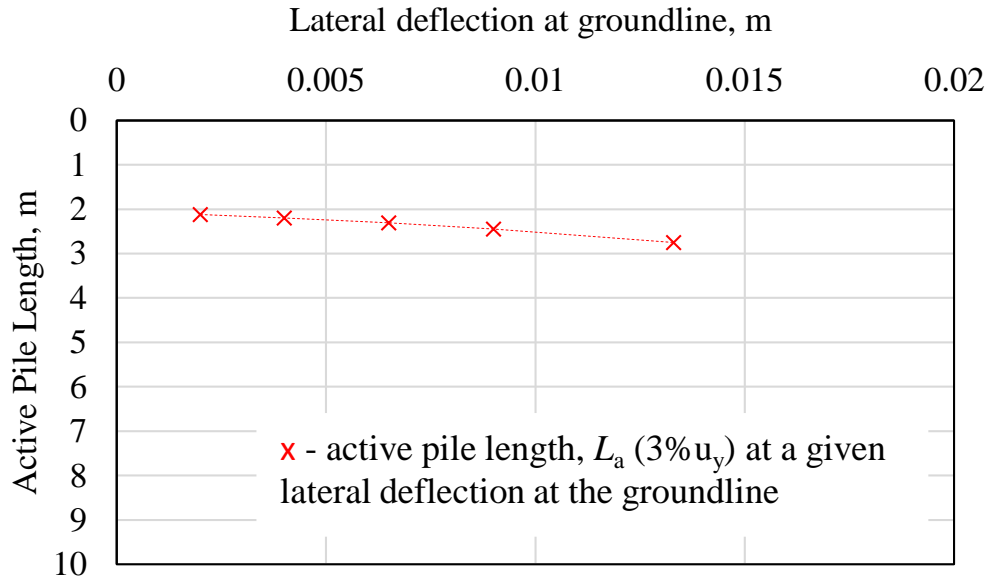


Figure 5 - 22. Active pile length progression in the Arkansas Field Test

### 5.3.4 Summary of Cases Considered

A number of static pushover tests for single end bearing pile embedded in a homogeneous Toyoura sand were simulated in this study. The static pushover test was conducted using a displacement control at pile head, where it is considered fixed. A lateral displacement is applied at the pile head until it reaches the final load of 0.5m. A total of 18 cases are considered where the diameter of a circular pile was varied from 10mm to 50mm. Table 5-4 summarizes the different geometric and material properties of the piles used in the simulation study. These piles are embedded in sands having initial void ratios,  $e_0=0.7392, 0.80$  and  $0.90$ . The material parameters of the corresponding sand is listed in Table 5-4.

Table 5 - 7. Summary of pile and soil properties

Case No.	Pile Properties			Soil Properties		
	$E_p$ (MPa)	$d_p$ (mm)	$EI_p$ (Nmm <sup>2</sup> )	$e_0$	$\gamma_d$ (N/mm <sup>3</sup> )	$\phi_{peak}$
1	68600	10	3.367E+07	0.7392	1.49E-05	41
2		20	5.388E+08			
3		25	1.315E+09			
4		30	2.728E+09			
5		40	8.621E+09			
6		50	2.105E+10			
7	68600	10	3.367E+07	0.80	1.44E-05	35
8		20	5.388E+08			
9		25	1.315E+09			
10		30	2.728E+09			

Case No.	Pile Properties			Soil Properties		
	$E_p$ (MPa)	$d_p$ (mm)	$EI_p$ (Nmm <sup>2</sup> )	$e_0$	$\gamma_d$ (N/mm <sup>3</sup> )	$\phi_{peak}$
11		40	8.621E+09			
12		50	2.105E+10			
13	68600	10	3.367E+07	0.90	1.37E-05	31
14		20	5.388E+08			
15		25	1.315E+09			
16		30	2.728E+09			
17		40	8.621E+09			
18		50	2.105E+10			

## 5.4 Results and Discussion of Numerical Simulations: On Active Pile Length

This active pile length is closely related to the characteristic length by factor  $\alpha$  as given by Equation 5.17 as observed in some formulas (Randolph, 1981; Velez et al., 1983).

$$L_a = \alpha L_c \quad (5.17)$$

The length from the pile head down to the point of negligible deformation is called the active pile length,  $L_a$ . Velez et al. (1983) defined the active length,  $L_a$ , to be the length until at a point along the pile length where the pile's lateral displacement is 5% of the pile head displacement. Wang and Liao (1988) used 0.3% of the pile head displacement as the fixity point. Therefore, in this paper, the point of fixity or zero bending is defined at midrange of previous literatures such as 3% of the maximum pile head displacement.

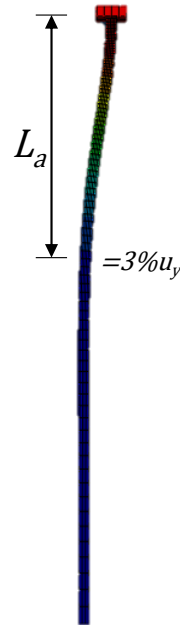


Figure 5 - 23. Definition of active pile length

### 5.4.1 Active Pile Length Progression with Increasing Pile Head Displacement

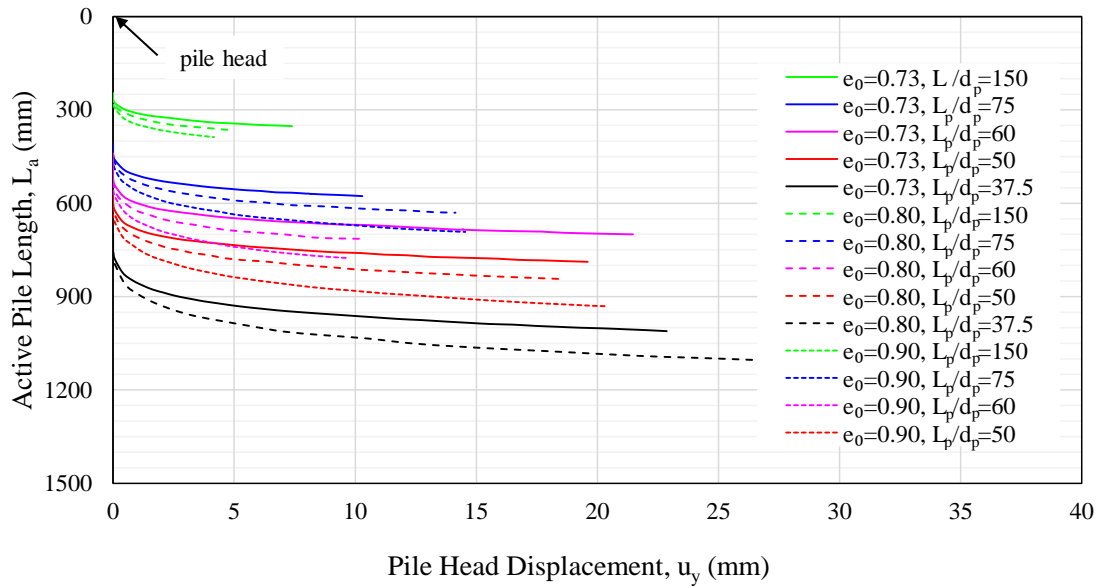


Figure 5 - 24: Active pile length progression with increase in pile head deformation

The active pile length based on the criteria of  $3\%u_y$  is determined for all cases considered in Table 5-4 and plotted in Figure 5 - 24 with the corresponding pile head deformation. The zero value in the vertical axis corresponds the ground surface, or the pile head. It can be observed in Figure 5-19 that as the pile head displacement applied increases, the active pile length progressively gets longer for all the cases considered and starts to stagnate at higher pile head deformation.

More importantly, some inherent trends can be observed considering the pile stiffness and the relative density of the soil. For the piles having the same pile stiffness, the active pile length is longer for piles embedded in loose sand than that of piles in dense sand. Furthermore, the rate of increase in active pile length is faster in loose soil than in dense soil due to the higher degree of softening of the soil. Conversely, given the same soil condition, the active pile length increases with increasing pile stiffness specifically for long and flexible piles.

### 5.4.2 Establishment of Criteria of the Slenderness Ratio for Long Piles

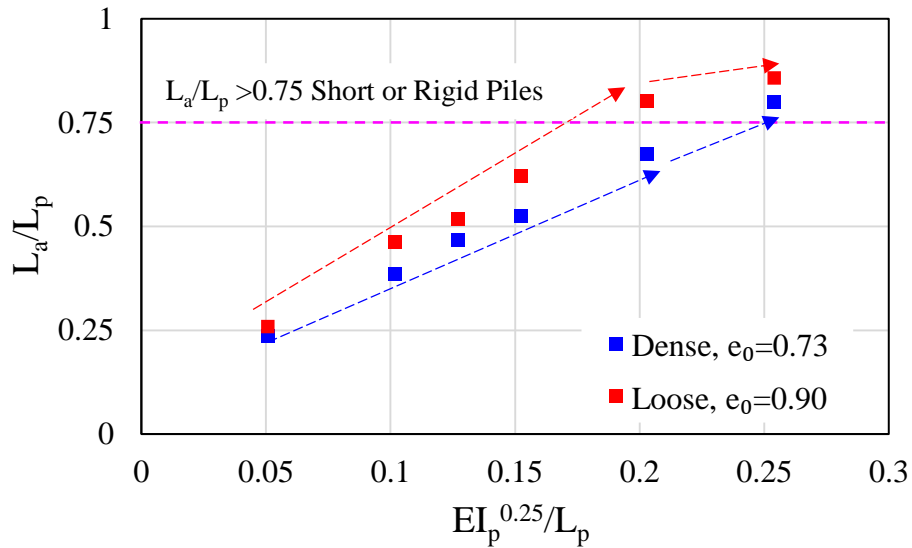


Figure 5 - 25. Slenderness criteria for long piles

A pile length,  $L_p= 1.45\text{m}$  of various diameters ( $d=10$  to  $50\text{mm}$ ) based on the list in the summary of cases embedded in both loose and dense sand is considered. Then the fourth root of the pile stiffness versus the active pile length at the ultimate stage is plotted in x and y axis respectively (Figure 5 - 25). These parameters are normalized with the actual pile length,  $L_p$ . In this case, it can be observed that difference in active pile length for piles embedded in dense and loose sand increases until the point where the ratio of  $L_a$  and  $L_p$  or the slenderness ratio is equal to 0.75 given by the red line. Beyond this ratio, the difference in the active pile length for increasing pile stiffness starts to have a converging behaviour. It reaches a saturation point, where despite the increase in pile head displacement, the active pile length is the same. This is due to the fact that the active pile length reaches the actual pile length. Given the bottom restraint of the actual pile length, the supposed active pile length that should have been formed is being restrained. In this case, the piles are considered short or stiff piles. For this study, only the long and slender piles will be considered where the concept of active pile length could be observed.

### 5.4.3 Initial Active Pile Length

The initial active pile length,  $L_0$ , is defined as the active pile length formed in the small strain region or at the elastic stage. In this section, the initial active pile length in relation with the characteristic length is discussed.

### 5.4.3.1 Active Pile Length in Elastic Soil Medium and Non-linear Soil Medium

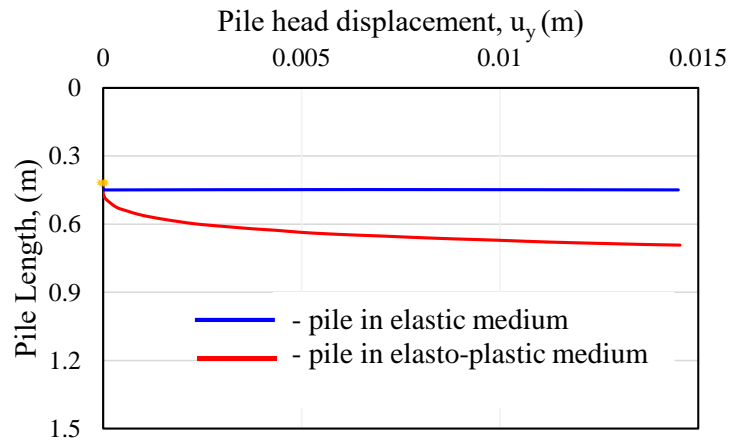


Figure 5- 26. Sample comparison of active pile length progression for piles embedded in elastic and elasto-plastic behaviour

The piles with  $d_p=25\text{mm}$  embedded in the loose condition is taken as an example to compare the active pile length for piles embedded in sand considered as elastic and elasto-plastic. The progression of active pile length with the increase in pile head displacements are plotted in Figure 5- 26. It can be seen that the active pile length progression for piles embedded in elastic is constant regardless of the increase in deformation at the pile head. However, considering the more realistic nature of the soil, which is in elasto-plastic, it can be seen that there is progression in the active pile length with an increase pile head and reaches an ultimate value. Nevertheless, it is noted that the initial active length for both cases is the same. The initial active pile lengths for all the cases for various pile diameters embedded in different soils in elastic and elasto-plastic case are plotted in x and y axis respectively as seen in Figure 5- 27. It can be seen that there's a 1:1 correspondence. It starts to deviate from the linear line as the diameter increases, since these diameters are already nearing the short and pile behaviour.

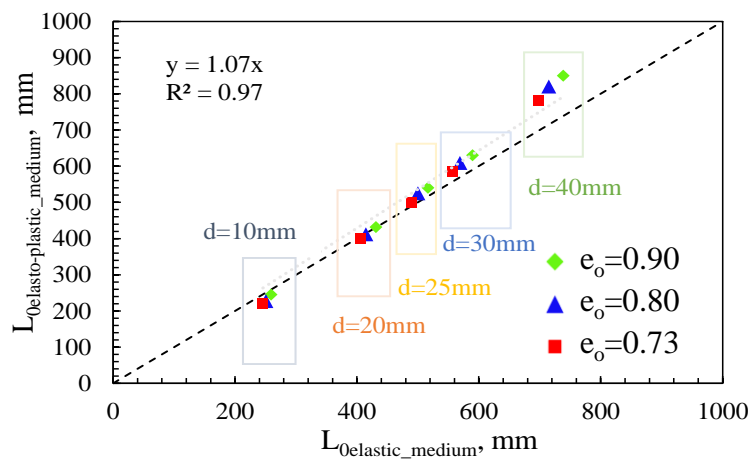


Figure 5- 27. Comparison of initial active pile length between soil medium considered as elastic and elasto-plastic

Therefore, at the initial stage, the active pile length is equal to the elastic active pile length.

#### 5.4.3.2 Relationship of Characteristic Length and Initial Active Pile Length

As defined in Chapter 3, the characteristic length is the ratio of the pile stiffness to the surrounding soil stiffness. The modified characteristic length (Konagai, 2000) is given by the equation below:

$$L_c = \sqrt[4]{\frac{EI_p}{G}} \quad (5.18)$$

The pile stiffness of piles,  $EI_p$ , can be easily computed just based on the cross sectional geometric properties and material of the piles. For the  $G_{max}$ , this can be easily derived in the site through the PS logging or other similar methods. Considering the small strain stiffness of the Toyoura sand that was used in the model. The empirical formula (Gu et al., 2013) is given in equation 5.19 which is fitted based on the series tests on Toyoura sand using resonant column (RC) apparatus with a torsional shear function and installed with bender elements.

$$G_{max} = 95.5(MPa) \left( \frac{\sigma'}{P_a} \right)^{0.41} \frac{(2.17 - e_0)^2}{1 + e_0} \quad (5.19)$$

Where  $\sigma'$ : the effective vertical stress,  $P_a$ =reference atmospheric pressure, 98kPa and  $e_0$ : initial void ratio of the sand. Similar trend can be seen with the discussion of Archer and Heymann (2015) plotting the shear stiffness versus depth for different relative densities of sand.

The characteristic length from Equation 5.18 using  $G=G_{max}$  is derived, and plotted in the x-axis as seen in Figure 5 - 28. There exists a linear relationship between the active pile length at the initial stage and the characteristic length. The proportional factor,  $\alpha$  equal to 6.38. This is described by the equation below:

$$L_0 = 6.38 L_c \quad (5.20)$$

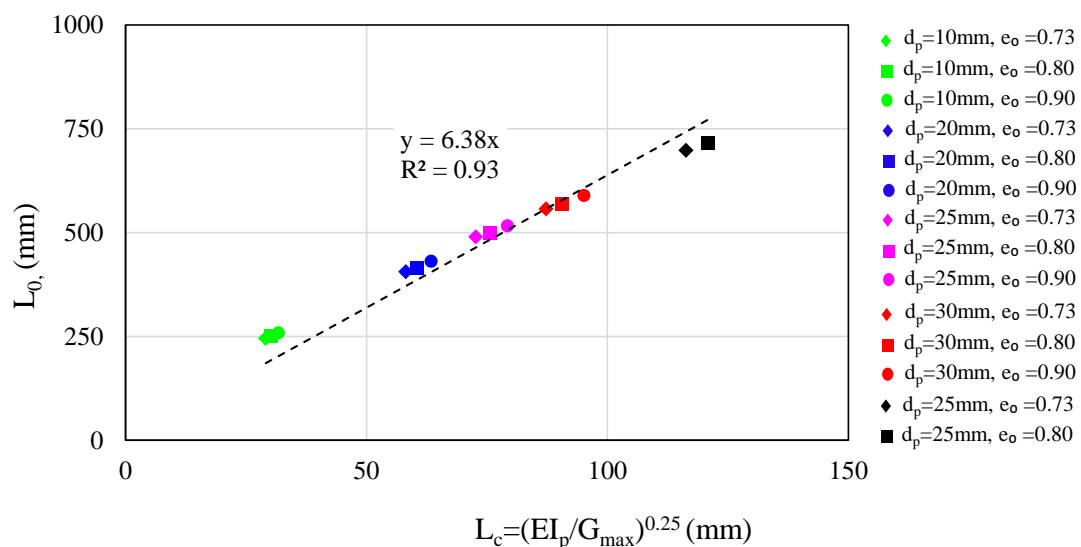


Figure 5 - 28. Relationship of  $L_c$  and  $L_0$  using  $G=G_{max}$

Therefore, given just the pile stiffness and the shear modulus, the initial active pile length can be determined. The active pile length formed at the initial stage can be the key parameter for describing the active pile length at the progressive stage due to increase in pile head deformations, more importantly at the ultimate stage.

#### 5.4.4 Active Pile Length at the Ultimate Stage

Given that the active pile length at the initial stage can be a determining factor in describing the active pile length at the ultimate stage, the progressive active pile length is normalized with the initial active pile length. This parameter,  $L_a/L_0$  for various pile diameters in each soil type,  $e_0=0.73$ ,  $e_0=0.80$  and  $e_0=0.90$  is plotted in the y-axis with the corresponding pile head displacement in x-axis. The plots are seen in Figure 5- 29, Figure 5- 30 and Figure 5- 31.

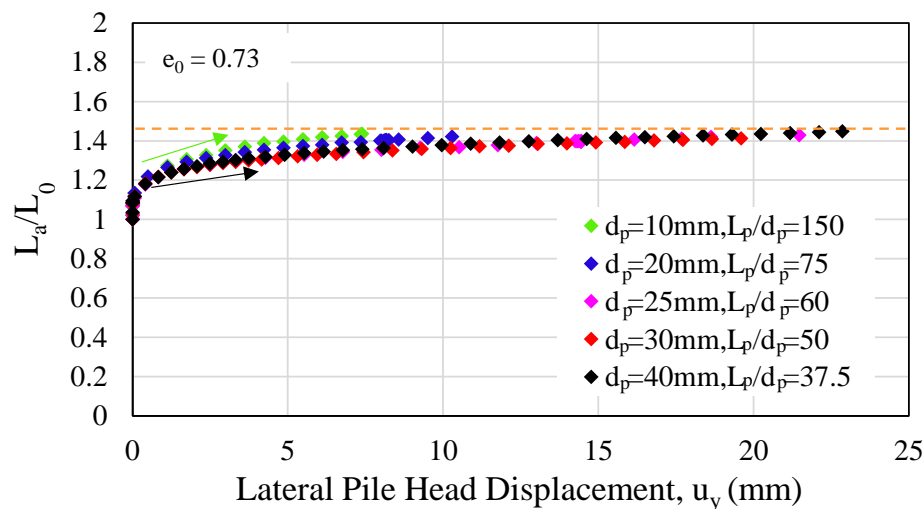


Figure 5- 29. Relationship of normalized active pile length with pile head displacement for piles embedded in  $e_0=0.73$

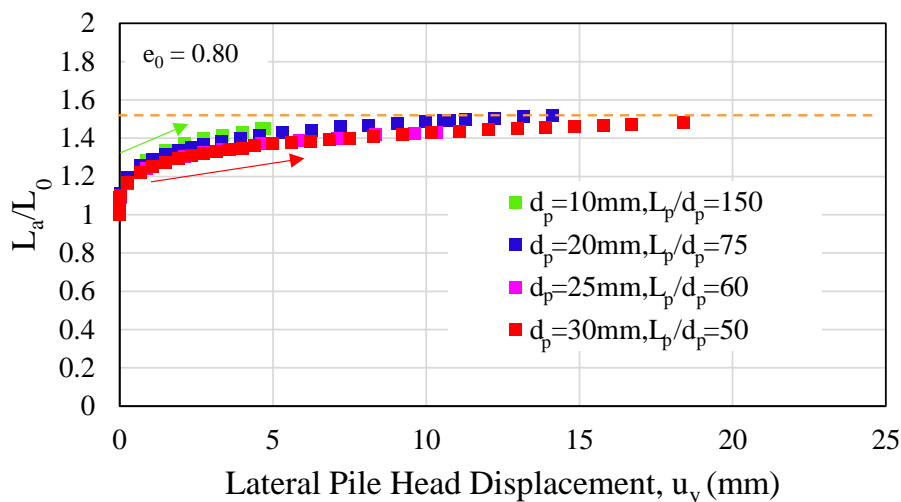


Figure 5- 30. Relationship of normalized active pile length with pile head displacement for piles embedded in  $e_0=0.80$

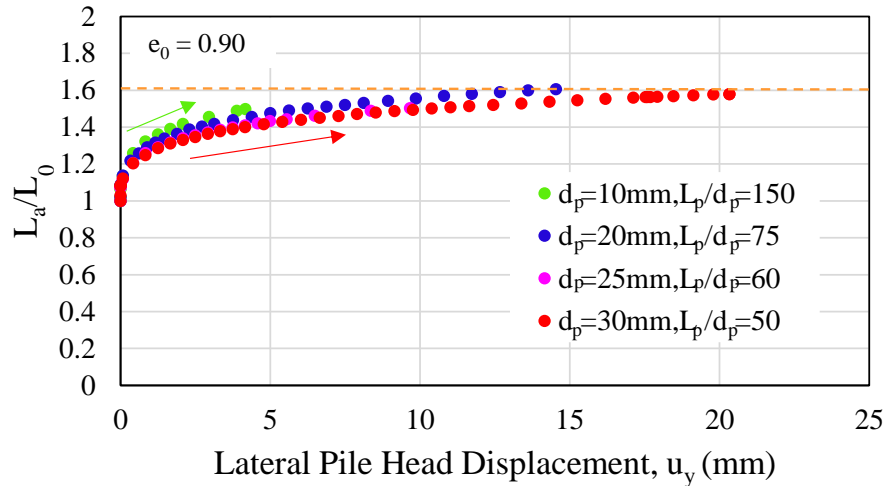


Figure 5- 31. Relationship of normalized active pile length with pile head displacement for piles embedded in  $e_0=0.90$

From these figures above, it can be observed that there is a constant value of the ratio of the active pile length to the initial active pile length where all the cases tend to converge on. The smaller the pile stiffness, the faster it reaches the constant value. At the same time, the looser the surrounding soil condition, the higher the  $L_a/L_0$  value. This behaviour means that the increase in the active pile length from the active pile length initially formed is large due to the softening of the soil.

The relationship of the average shear strain formed in the area of the mobilized wedge, which is the pile head displacement divided by the corresponding active pile length and the ratio of the active pile length to the initial active pile length ratio is of interest. For various cases of pile head diameter embedded in a specific type of sand, there exists a unique curve as seen in Figure 5- 32, Figure 5- 33 and Figure 5- 34. This unique approaches a constant value at higher shear strains. It can be observed that for all the surrounding soil type, the  $L_a/L_0$  parameter becomes constant at shear strain equal to around 2%. This means that at 2% average shear strain, the failure surface has already ruptured and the wedge fully formed. The constant ultimate active pile length job is to push the mobilized wedge in the passive region.

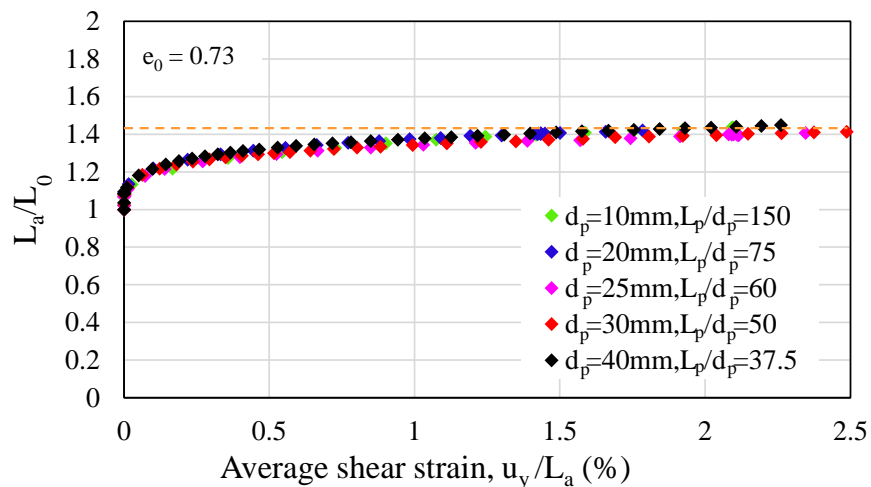


Figure 5- 32. Relationship of normalized active pile length with the shear strain for piles embedded in  $e_0=0.73$

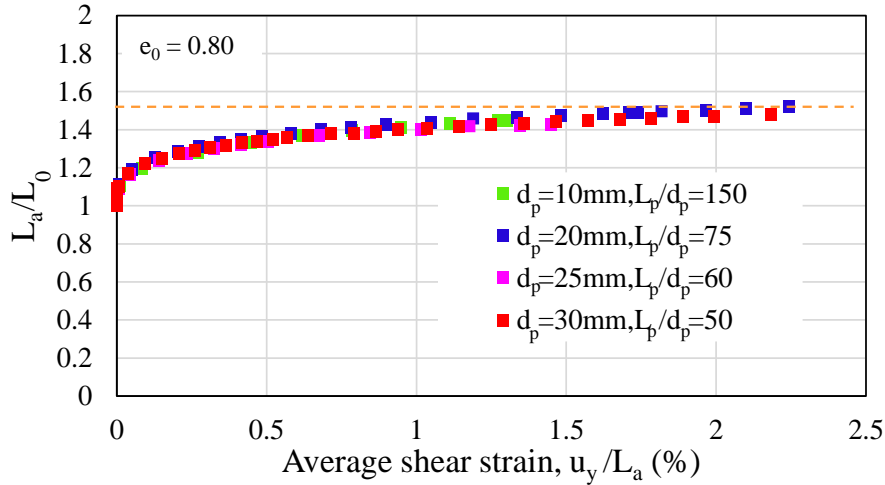


Figure 5- 33. Relationship of normalized active pile length with the shear strain for piles embedded in  $e_0=0.80$

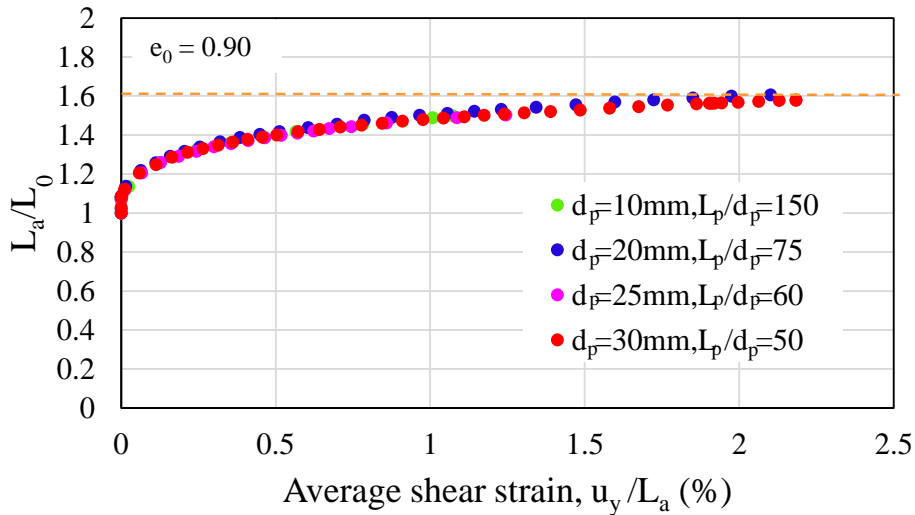


Figure 5- 34. Relationship of normalized active pile length with the shear strain for piles embedded in  $e_0=0.90$

The convergence value of  $L_a/L_0$  varies for each type of soil. Plotting the void ratio with the parameter  $L_a/L_0$ , there's a linear relationship given by the following equation (Figure 5- 35). It can be noted that the y-intercept could be related to the minimum void ratio of the type of soil and the coefficient 1.05 is close to the reference critical void used in the material parameter for this type of soil.

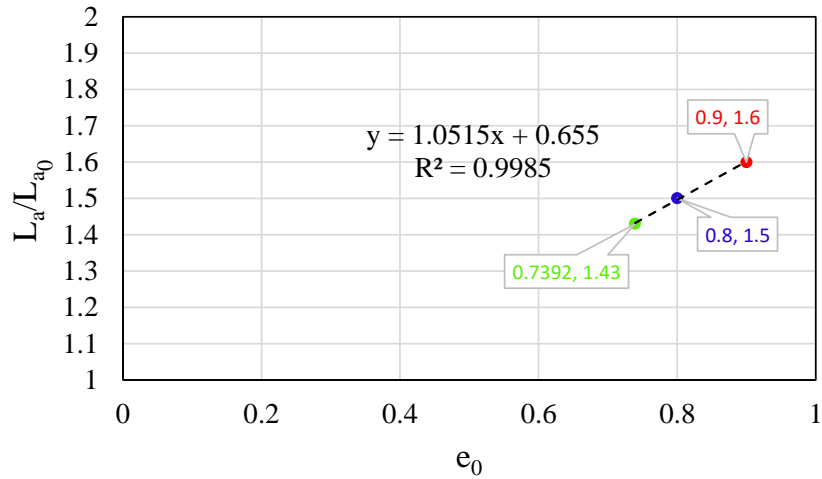


Figure 5- 35. Relationship of the  $L_a/L_0$  with the initial void ratio

The linear relationship for this soil, and generally for sands, can be described in the following equation.

$$L_{au} = L_0(1.0515e_0 + 0.655) \quad (5.21)$$

The active pile length can be determined based on the active pile length at the initial stage by applying this correction factor.

## 5.5 Application of Active Pile Length on Ultimate Lateral Pile Resistance

### 5.5.1 Derivation of the Ultimate Lateral Pile Resistance

Numerical simulations show that there exists a wedge formed in the passive region. The load displacement curve from the overall response of the soil-pile system subjected to the lateral load is plotted given by the black line shown in Figure 5 - 36.

Considering the active pile length concept. When piles subjected with lateral loads, the pile deforms significantly near the ground surface and decreases with increasing depth. Where at the start of negligible deformation, the point of fixity. For deeper depths or embedment length, the piles as negligible deformation. Therefore, up to this point the pile can be considered as cantilever beam. The pile resistance alone is based on the piles considering as cantilever length. The load deformation of pile resistance is plotted using the blue line in Figure 5 - 36.

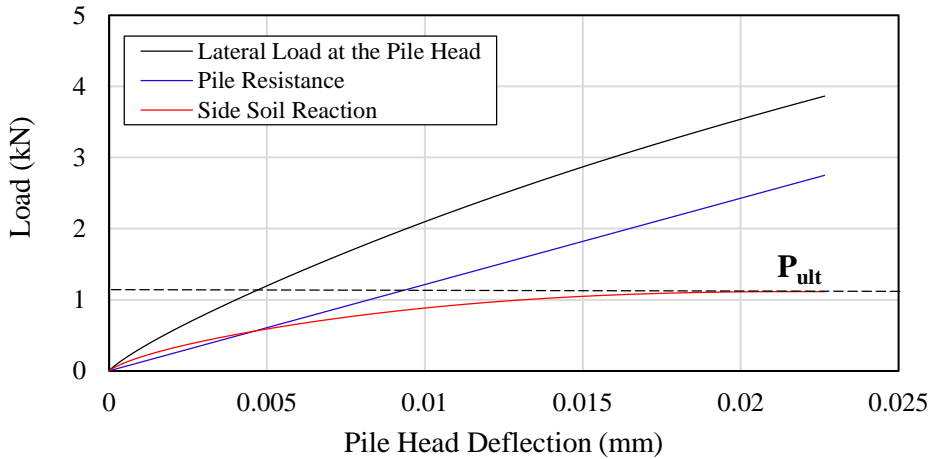


Figure 5 - 36. Load deformation curve

Subtracting the load-deformation of the pile resistance alone from the overall behaviour gives the side soil reaction as plotted by the red line seen in Figure 5 - 36. This side soil reaction reaches a constant line, the value of this line is called the ultimate side soil reaction. This is how the ultimate side soil reaction is derived for all cases.

### 5.5.2 Simplified Expression of the Ultimate Side Soil Resistance

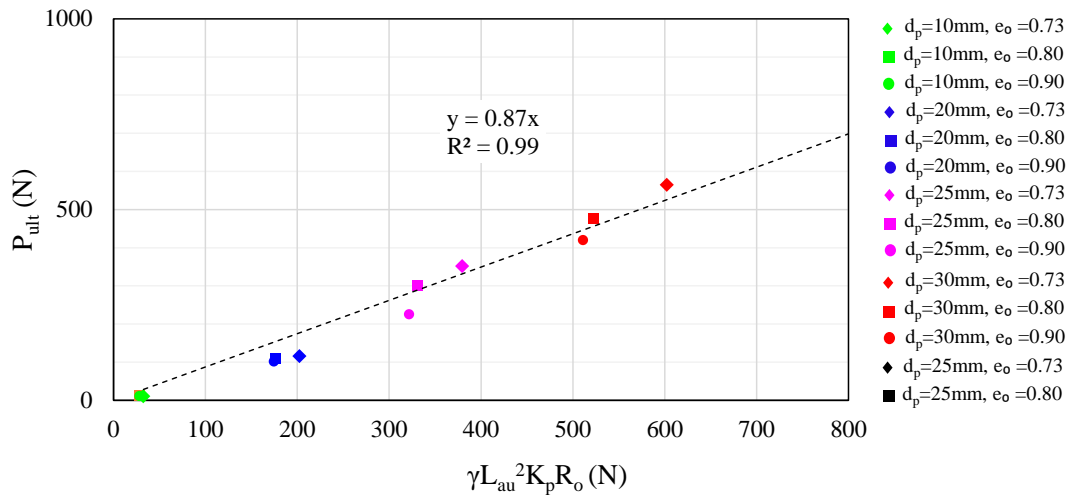


Figure 5- 37. Relationship of ultimate lateral pile resistance with active pile length and other soil parameters

The wedge formed at the passive region is indicative of the side soil reaction. The force representation of the soil wedge can be defined by the weight of the volume of the extent of this soil wedge. The extent of this soil wedge is represented by the following parameters: the active

pile length,  $L_a$ , Rankine passive earth coefficient,  $K_p$ , and the outer pile radius,  $R_o$  and multiplied with the unit weight,  $\gamma$ .

These simple parameters are plotted in the x-axis with the corresponding ultimate lateral pile resistance for all the cases as shown in Figure 5- 37. It can be seen that there is a linear relationship with high correlation between these terms. Thus, a simplified expression can describe the ultimate lateral pile resistance given by equation 5.22.

$$P_{ult} = 0.87\gamma L_a^2 K_p R_o \quad (5.22)$$

## 5.6 Summary and Conclusions

The active pile length is a simple parameter reflective of the soil-pile interaction. For long and flexible piles, the active pile length is established to be governed by the stiffness of the pile relative to the surrounding soil stiffness. Given known parameters  $EI_p$  and  $G_{max}$ , the active pile length initially formed at the elastic range can be easily determined.

Considering the elasto-plastic nature of the soil, the active pile length is progressively formed with an increase in the applied load. Once an average shear strain of 2% is reached at the passive region, the failure surface ruptures and the soil wedge is fully mobilized. This is evident of the constant active pile length at the ultimate stage. This active pile length at the ultimate stage is largely dependent on the initial active pile length, as this can be determined by applying a correction factor expressed as a function of the void ratio.

With the formation of the soil wedge at the passive region along this so-called active pile length, the ultimate lateral pile resistance is deemed to be dependent on this simple parameter. This is proven true with the high correlation of the ultimate side soil resistance and the parameters representative of the weight of this soil wedge. The ultimate lateral pile resistance of piles can be expressed by simple parameters such as  $L_{aw}$ ,  $\gamma$ ,  $K_p$  and  $R_o$ .

The summary of the simplified expression approach is shown in Figure 5 - 38. This simplified expression for the ultimate lateral pile resistance for flexible single end bearing piles embedded in sand can be useful for more practical approach in the seismic and assessment of piles. This idea can be extended to a more complicated scenario such as for group piles and other related cases.

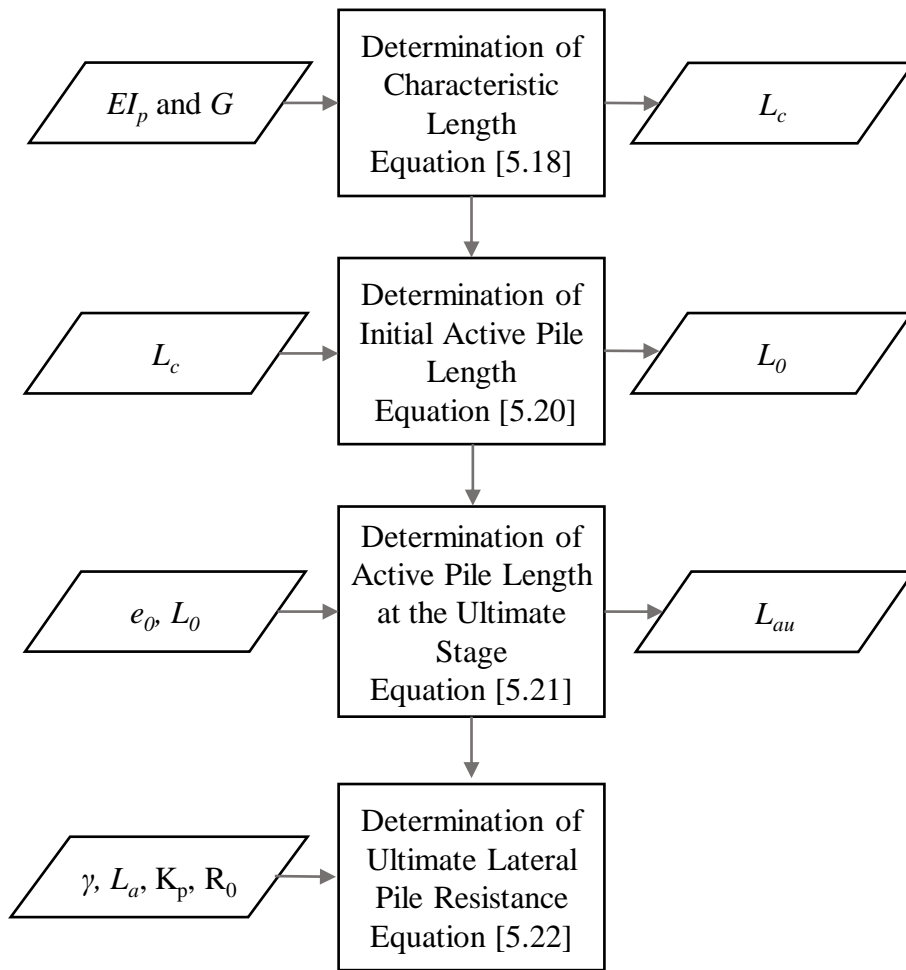


Figure 5 - 38. Flowchart for the simplified expression of ultimate lateral pile resistance

# Chapter 6

## Extension of the Applicability of Active Pile Length for the Ultimate Lateral Resistance of Closely Grouped Piles

### 6.1 Introduction

The active pile length has been established to be a key parameter in determining the ultimate lateral resistance of single piles embedded in sand in Chapter 5. This method is useful in giving insight into the mechanics of soil-pile interaction and the formation of the soil wedge in the passive region. However, piles are commonly used in practice as grouped piles in a foundation system. For grouped piles with wide spacing, piles can be treated as individual piles while for closely spaced grouped piles, it could be treated as an equivalent vertical single pile. Hence, this chapter presents the extension of concept of active pile length as key parameter in determining the ultimate lateral pile resistance developed for single piles to closely grouped piles embedded in sand.

### 6.2 Definition of Closely Grouped Piles

According to Bogard and Matlock (1983), the spacing in between or among piles dictates the stress formation and the deformation around the piles within this group. Lateral loads induced on the pile groups generate normal and shear stresses and strains in the passive region and diminishes radially outward the pile vicinity as response to the external loading. The group with piles widely spaced from each other tend to have localized plastic flow zones around them. The adequate space between and among piles within this group allow each to behave individually with negligible effect on the surrounding piles, or totally none for much wider space. Hence, the piles belonging in this widely spaced grouped pile could be treated as individual piles and the ultimate lateral resistance could just be the summation of these individual piles. The closely grouped piles' behaviour is different as the dense spacing results in a pile group effect. The mechanism behind this group effect for the closely spaced grouped piles is due to the overlapping and development of plastic zones around the piles within the group. Therefore, this brings stronger effect among the piles that allows the piles to act as a unit. Thus, closely grouped piles can be treated as an equivalent pile as can be seen in the Figure 6-1.

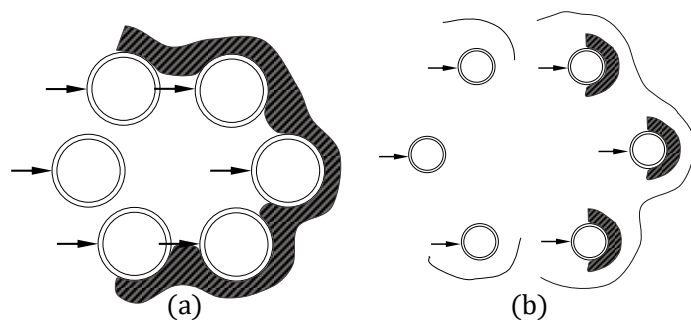


Figure 6 - 1 Schematic illustration of the patterns of stress and deformation around laterally loaded grouped piles (a) closely grouped piles (b) widely spaced grouped piles (after Bogard and Matlock (1983))

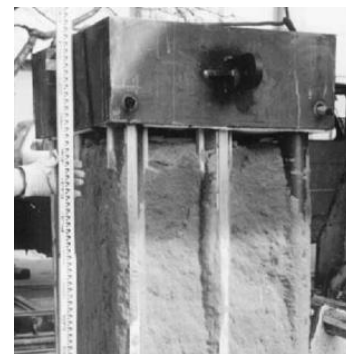


Figure 6 - 2 Equivalent Single Beam from Lateral Field Test (after (Konagai et al., 2003))

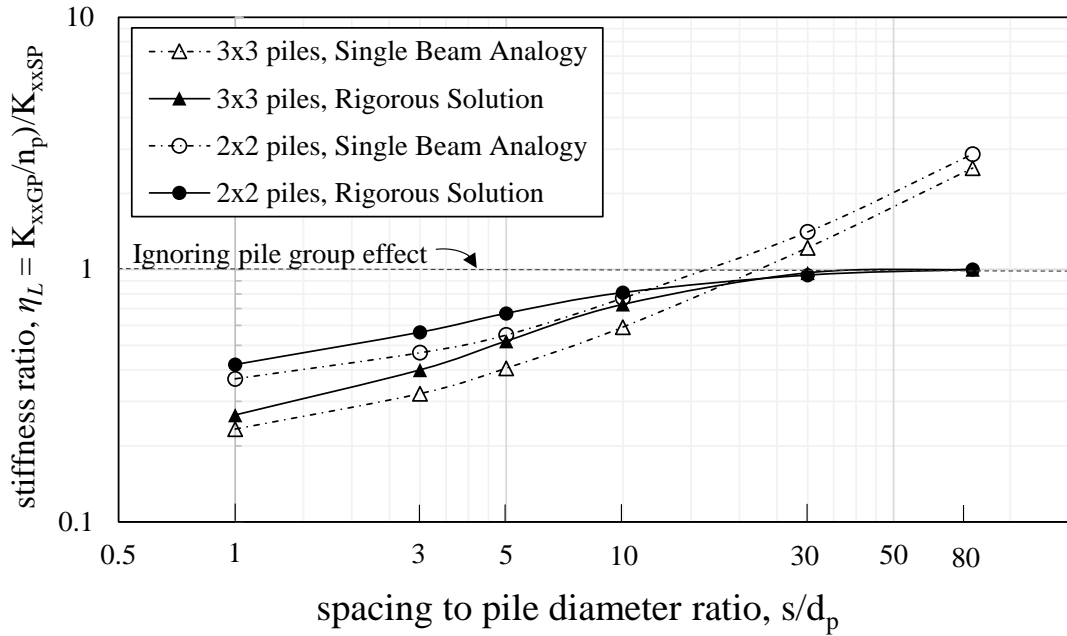


Figure 6 - 3 Lateral pile group effects for different  $s/d_p$  ratios (after Konagai et al. (2003) )

Konagai et. al. (2003) showed the tolerable limits for the pile-to-pile spacing to define the closely grouped piles and widely spaced grouped piles. The stiffness ratio,  $\eta_L$  with respect to the different spacing to diameter ( $s/d_p$ ) ratio is plotted in  $y$  and  $x$  axis, respectively (see Figure 6-3). The normalized grouped pile stiffness ratio,  $\eta_L$ , is given by the following equation.

$$\eta_L = \frac{(K_{xxGP}/n_p)}{K_{xxSP}} \quad (6.1)$$

where:  $K_{xxGP}$  is the static stiffness of the grouped pile,  $n_p$  is the number of piles in the group and  $K_{xxSP}$  is the static stiffness of a single pile. This parameter,  $\eta_L$ , dependent on the  $s/d_p$ , serves as an index in the consideration of pile group effect, where  $\eta_L < 1$  accounts for the pile group effect and  $\eta_L > 1$  means otherwise. Two geometric grouped pile configurations were taken into account: (1) 2 x 2 and (2) 3 x 3 where the  $s/d_p$  ratios are varied to 1, 3, 5, 10 and extreme cases such as 30 and 80. The stiffness of these grouped pile were derived using the rigorous method and the equivalent single beam analogy (Konagai et al., 2003). From Figure 6-3, it could be observed that for  $s/d_p < 20$ , the rigorous solution and the single beam analogy are well within considerable agreement and for  $s/d_p > 20$ , there is an obvious deviation between the two methods. This is because the piles within the grouped piles already have very wide spacing from each other that they behave as individual piles and can no longer be treated as a unit.

### 6.3 Numerical Simulation of Grouped Piles

The simulation of the response of laterally loaded closely grouped piles in three-dimension (3D) were also performed using the ABAQUS v6.13. This gives an advantage of allowing rigorous simulation of the additional complexity of the laterally loaded piles as they come in group. Basically, similar finite element method techniques implemented in the numerical simulation of the single piles are applied to the modelling of the grouped piles. In this section, the soil-pile

idealization of the closely grouped pile and the cases considered in this study are discussed in details.

### ***6.3.1 Soil-pile system idealization of closely grouped piles***

The additional complexity of the grouped pile demands a lot more computing time and memory. Hence, modelling the cases in view of their symmetry is of utmost importance. Similar with the case of single piles, the soil-pile system is modelled with 3D solid deformable body. The maroon elements represent the soil medium, the green elements represent the pile, and the grey elements represent the pile cap connecting the individual piles.

The diameter of the individual pile for all the cases of grouped pile is taken to be  $d_p=20\text{mm}$  to ensure having a case of long and flexible piles. The soil models are dimensioned dependent on the size of the pile diameter,  $d_p$ . For the 2x2 grouped pile, the longitudinal length (along the x-axis) is taken to be  $35d_p$  or equal to 0.7m as seen in Figure 6 - 4b. Covering a bigger area for the 3x3 grouped pile, the longitudinal length (along the x-axis) is taken to be  $55d_p$  or equal to 1.10m as seen in Figure 6 - 5b. The transverse length is dimensioned to maintain a longitudinal to transverse length ratio of approximately 2.35. Hence, the transverse length (along the y-axis) for the 2x2 and 3x3 grouped pile model is 0.35m and 0.45m respectively. In general, the geometric configuration the soil medium should be adequate enough to allow mobilization of soil and minimize the boundary effects, though this is negligible for static cases. The depth of the soil medium is 1.45m while the actual length of the pile,  $L_p$ , is 1.5m (Figure 6 - 4c and Figure 6 - 5c).

The piles in the grouped pile are separated with a center-to-center spacing,  $s$ . (Figure 6 - 4a and Figure 6 - 5a). Note that for the 2x2 grouped pile, the piles are positioned  $0.5s$  from the plane of symmetry and the cut at the pile cap is coplanar with it. For the 3x3 grouped pile, the plane of symmetry cuts through the middle of the center row of grouped piles, thus the farthest row of piles are positioned  $s$  from the plane of symmetry.

A 3d hexahedron-shaped element type used for the automated meshing. A linear hexahedron element type is adequate for the soil elements while a quadratic hexahedron element is used for the piles having 20 nodes to be in agreement with the kinematic action of the piles as a flexural structure discussed in Chapter 5. Non-uniform meshing is also implemented in the intention to cut down computing time and memory. Finer meshing is done around the pile as seen in Figure 6 - 4b and Figure 6 - 5b for the 2x2 and 3x3 grouped pile respectively. Also, similar case of meshing is implemented near the ground surface as seen in Figure 6 - 4c and Figure 6 - 5c. A total of 24671 elements are used for the 2x2 grouped pile and 40667 elements for the 3x3 grouped pile.

With reference to Figure 5 - 5, similar boundary planes are designed to that of the soil-pile model for the all the cases of grouped piles namely: (1) bottom (XY plane), (2) side (ZY plane), (3) back (ZX plane) and (4) plane of symmetry.

The following boundary conditions are implemented to the abovementioned boundary plane designations.

- (1) Bottom (XY plane) – Fixed. All the degrees of freedom are restrained
- (2) Side (ZY plane) – Restrained at x-axis
- (3) Back (ZX plane) – Restrained at y-axis
- (4) Plane of Symmetry – Translations are restrained at y-axis and Rotations at z- and x-axis

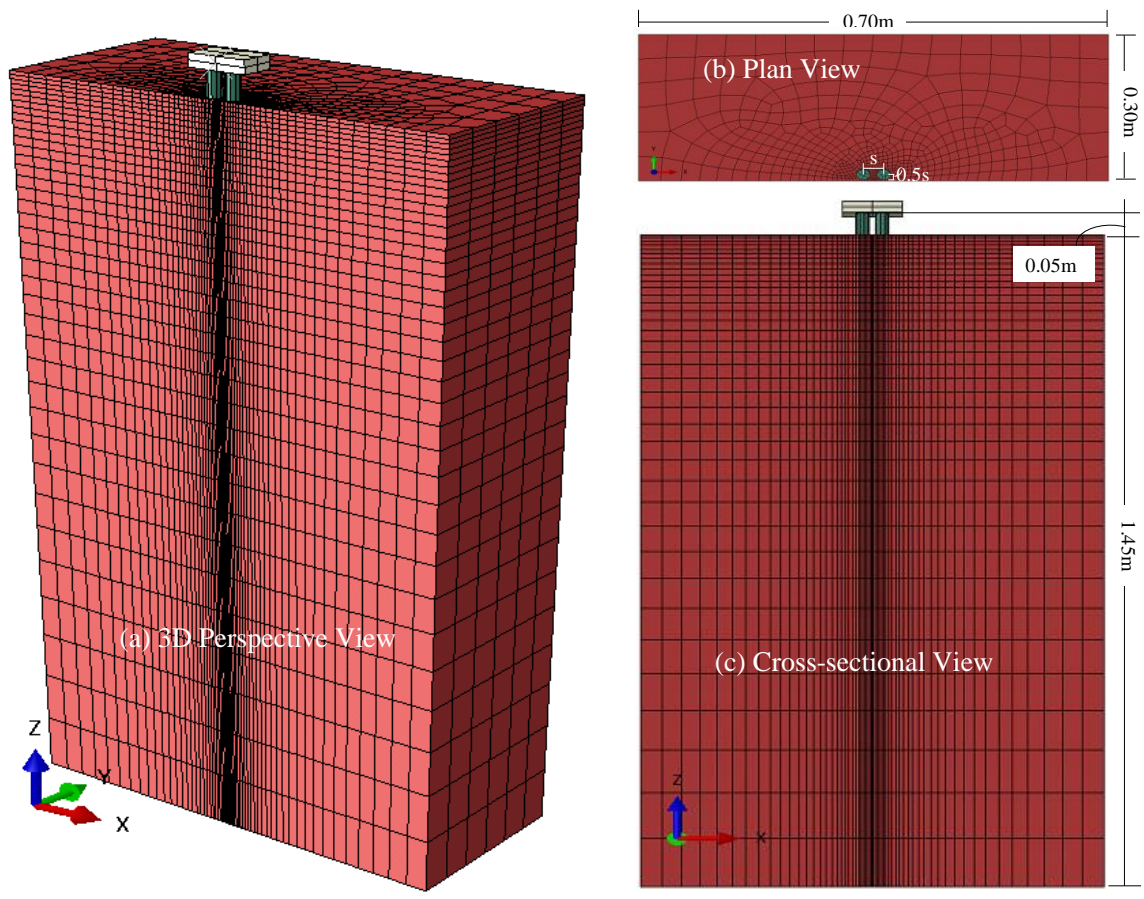


Figure 6 - 4. Soil-pile configuration for 2x2 grouped piles. (a) 3D Perspective View, (b) Plan View. Note: Pile cap not shown and (c) Cross-sectional view.

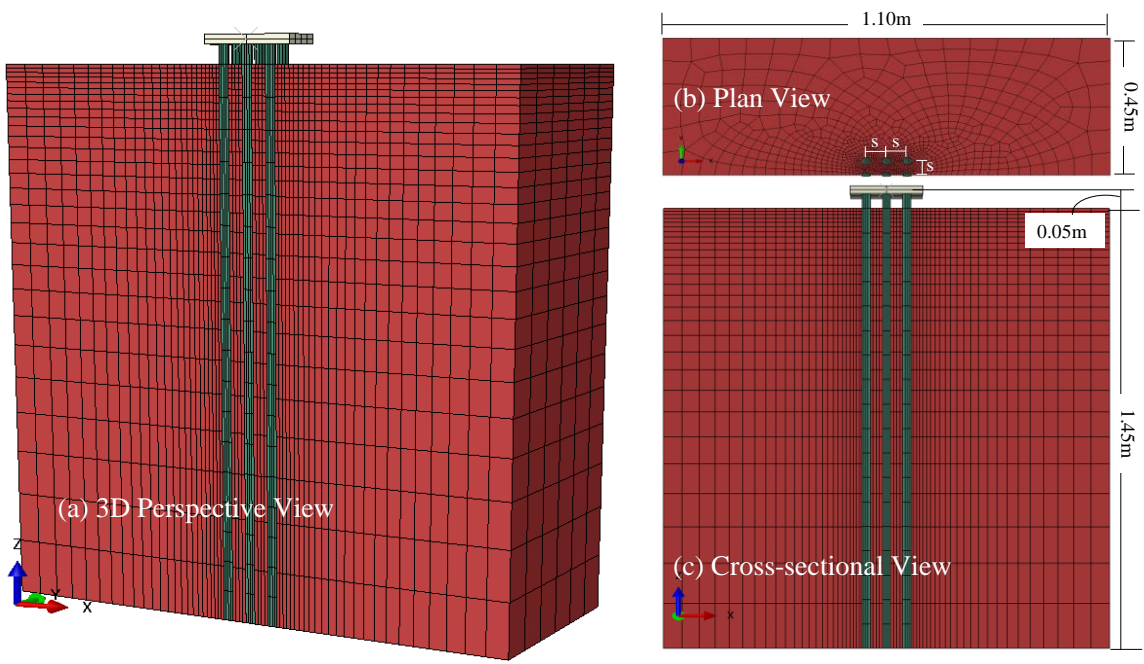


Figure 6 - 5. Soil-pile configuration for 3x3 grouped piles. (a) 3D perspective view, (b) Plan view. Note: Pile cap not shown and (c) Cross-sectional view

Another important model technique is the implementation of the slipping and gapping at the soil-pile interface. In this case, the contact pairs are present around each individual piles as seen in Figure 6 - 6. Similar with the single piles, the master and slave surface are identified being the pile and soil contact surface respectively. The same interface properties are implemented since the material of the pile and the soil conditions are not changed.

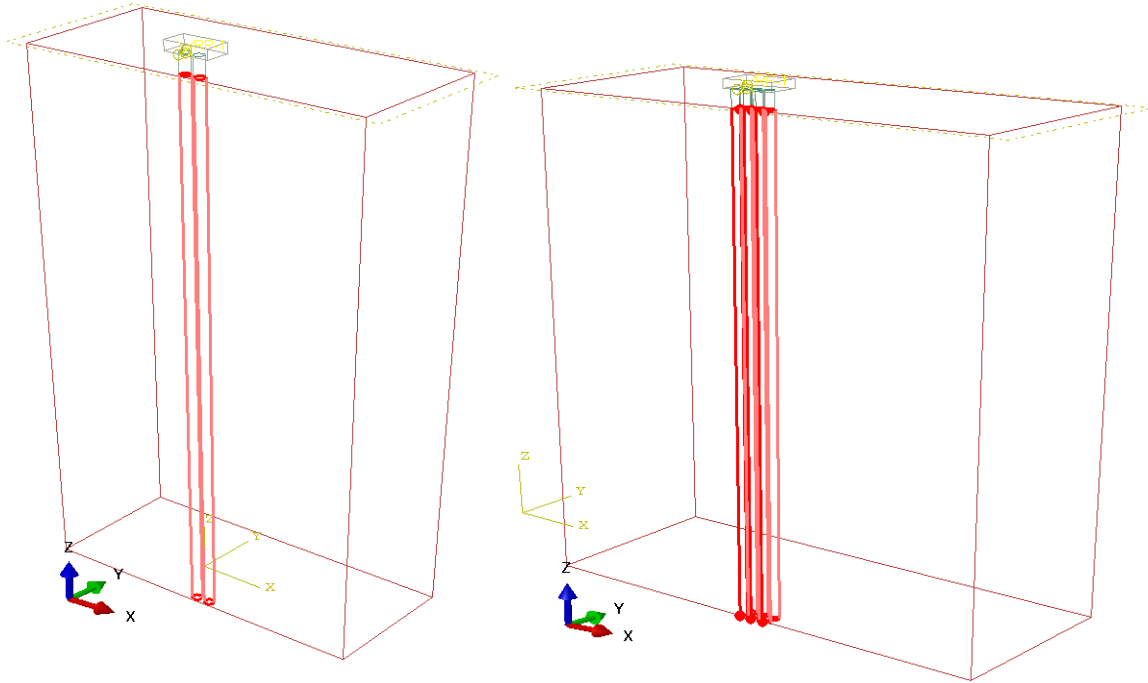


Figure 6 - 6. Soil-pile interface for grouped piles

### 6.3.2 Summary of Cases Considered

The spacing to diameter ratio of  $s/d_p < 10$  is chosen. Particularly  $s/d_p = 1.5, 2.5$  and  $4.5$  were considered for the following grouped piles: 2x2 and 3x3. This is to ensure that a set of closely grouped piles is considered based on the abovementioned definition. The summary of cases considered is listed in Table 6-1 along with the corresponding equivalent single beam parameters such as  $R_0$  and  $EI_g$ .

Table 6 - 1 Summary of cases considered for grouped piles

Grouped Pile	$s/d_p$	$R_0$ (mm)	$EI_g$ ( $\times 10^9$ mm <sup>4</sup> )	$e_0$
2x2	1.5	28.21	2.16	0.73
2x2	2.5	39.49	2.16	0.73
2x2	4.5	62.06	2.16	0.73
3x3	2.5	67.70	4.85	0.73
2x2	1.5	28.21	2.16	0.80
2x2	2.5	39.49	2.16	0.80
3x3	2.5	67.70	4.85	0.80
2x2	1.5	28.21	2.16	0.90
2x2	2.5	39.49	2.16	0.90
3x3	2.5	67.70	4.85	0.90

The idealization for the equivalent single beam analogy for grouped piles consisting of the composite number of piles,  $n_p$ , and the soil entrapped among these piles as illustrated in Figure 6 - 7.

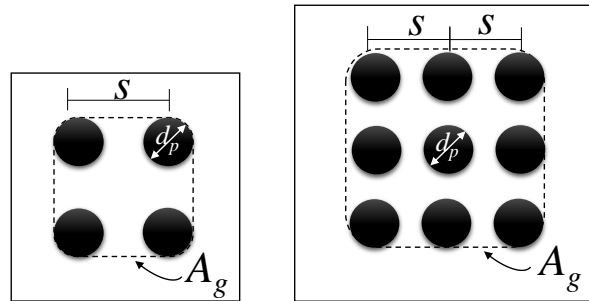


Figure 6 - 7. Equivalent single beam analogy idealization

From this idealization, the equivalent single beam parameters such as the cross-sectional area,  $A_g$ , and the grouped pile stiffness,  $EI_g$ , are defined given by Equation 6.2 and 6.3 respectively.

$$A_g = \pi R_o^2 \quad (6.2)$$

$$EI_g = n_p EI_p \quad (6.3)$$

The broken lines in Figure 6 - 7 circumscribing the outermost piles in the group determines its cross section  $A_g$ . This cross-sectional area is a square with the sides equal to the length running until the edges of the outermost piles. From this cross-sectional area, the equivalent radius,  $R_o$  is derived.

The stiffness of the grouped piles,  $EI_g$ , is defined by the product of the number of piles,  $n_p$ , and the stiffness of the individual piles,  $EI_p$  with the assumption that pile elements within a horizontal slice of soil deforms but keep their spacing constant and the entrapped soil moves with them. It is noted that to consider the cross-sectional area to calculate the bending stiffness of the grouped pile would mean an overestimation since the stiffness of the soil entrapped in the pile is much greater than the stiffness of the pile, and thus justifies the method. All the grouped piles are embedded in various sand with initial void ratios of 0.73, 0.80 and 0.90.

## 6.4 Results and Discussion of Numerical Simulations: On Active Pile Length

From these rigorous solutions, the lateral deformations along the length of the pile is observed. Noting that closely grouped piles can be treated as an equivalent single pile, the relationships established in determining the characteristic lengths, the initial active pile length and the ultimate active pile length for single fixed head pile is extended and applied for closely grouped piles. Finally, the established active pile length,  $L_a$ , is used to describe the relationship of the ultimate lateral pile resistance for the grouped pile.

### 6.4.1 Characteristic Length

The characteristic length is the ratio of the relative stiffness of the piles to the surrounding soil stiffness. The stiffness of the grouped pile treating the closely grouped pile as equivalent single pile is given by Equation 6.3. Therefore, the stiffness,  $EI_p$ , for the single fixed head pile is changed to  $EI_g$  and correspondingly, the characteristic length for closely grouped pile can be given by the equation below.

$$L_c = \sqrt[4]{\frac{EI_g}{G}} \quad (6.4)$$

Thus considering the  $s/d_p < 10$  within the definition of closely grouped piles, the spacing between the piles does not play significantly in the closely grouped pile lateral deformation. In this case, given the same number of piles in a closely grouped pile, the individual pile stiffness governs.

### 6.4.2 Active Pile Length in Grouped Piles

The same criteria of active pile length is implemented in this case. The progressive lateral deformation of piles with increasing pile head displacement is derived considering the point of negligible deformation equal to  $3\%u_y$ . Considering presence of composite number of single piles in grouped pile, the active pile length formation is initially observed in the passive side of each piles in the group. In this section, the definition of the active pile length used for this closely grouped pile is discussed. Moreover, the effect of spacing and number of piles in the progression of active pile length is shown.

#### 6.4.2.1 Passive Soil Mobilization in Grouped Piles

The soil mobilization in the passive region for single piles is observed at the passive edge of the single piles. In the case of closely grouped piles, the soil wedge mobilization in the passive region is due to the onset of the lateral deformation of the lead pile. The lead pile is defined to be the pile at the forefront of the lateral loading. To illustrate the case, sample cases are shown in Figure 6- 8 and Figure 6- 9 considering the grouped piles with geometric configurations of 2x2 and 3x3. Both cases have  $s/d_p$  ratio equal to 2.5 and embedded in dense sand. The lead piles in this figures are the pile (2x2 configuration in view of symmetry of the model) and the column of piles (3x3 configuration in view of symmetry of the model) located at the leftmost of the grouped pile. The soil lateral displacement distributions around the piles for 2x2 and 3x3 are illustrated in Figure 6- 8 and Figure 6- 9 respectively using isosurfaces. This shows that the active pile length of the lead piles at the passive side is deemed to be crucial as it leads the direction and progression of soil mobilization. For this reason, the active pile length of concern would be from the lead piles. The active pile length formulation at the initial stage and ultimate stage would be based on this active pile length. Noting that there are two piles as the lead piles for 2x2 grouped pile configuration and 3 lead piles for 3x3 grouped piles, the average of the active pile length of these piles are considered, though differences of the lateral deformation of among the piles in the lead column are negligible.

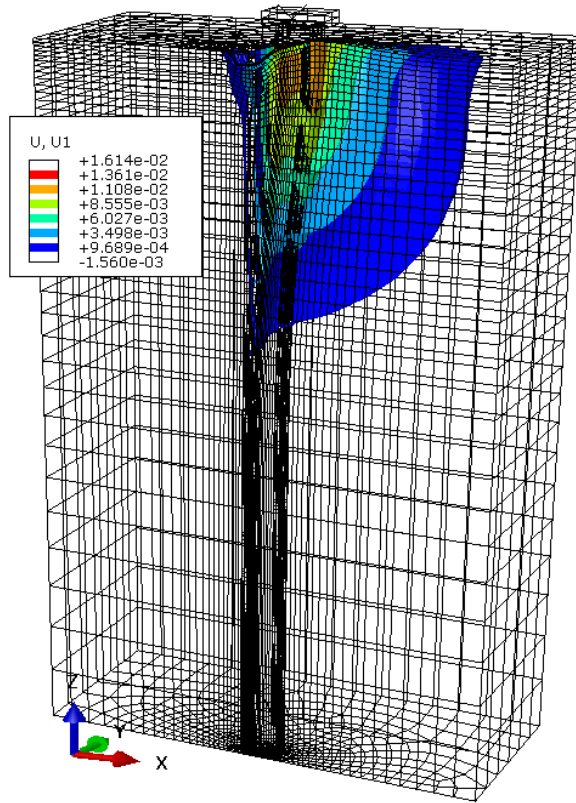


Figure 6- 8. Soil lateral displacement distribution at the passive region for 2x2 grouped piles

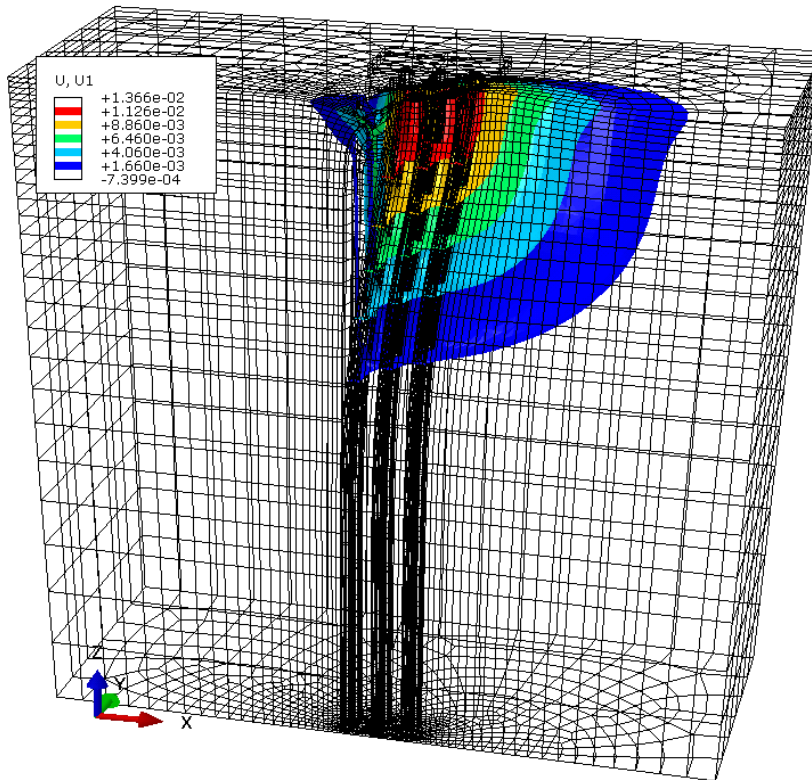


Figure 6- 9. Soil lateral displacement distribution at the passive region for 3x3 grouped piles

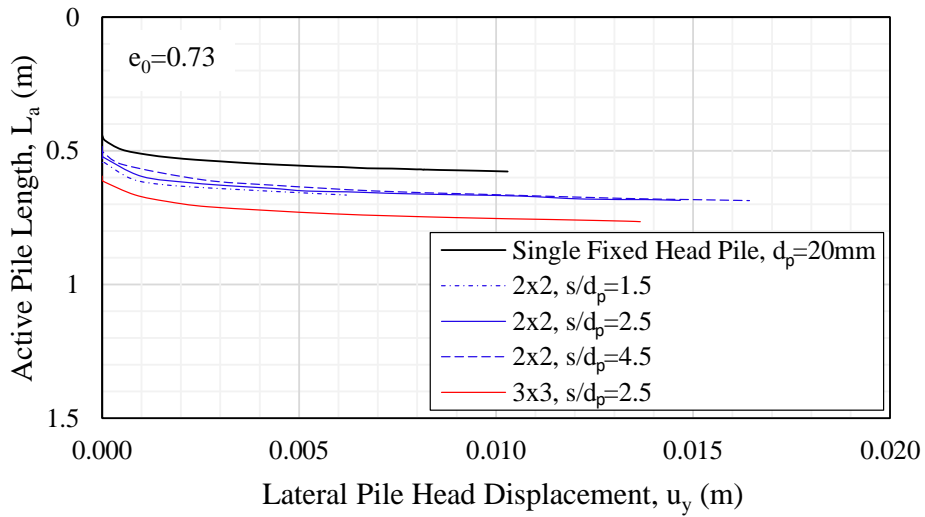


Figure 6 - 10. Active pile length progression at lead piles for closely grouped piles embedded in dense sand

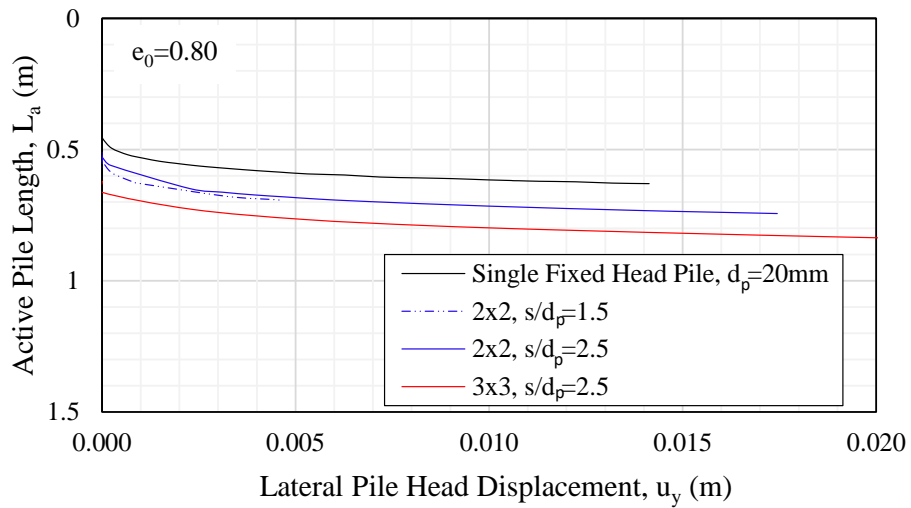


Figure 6 - 11. Active pile length progression at lead piles for closely grouped piles embedded in medium dense sand

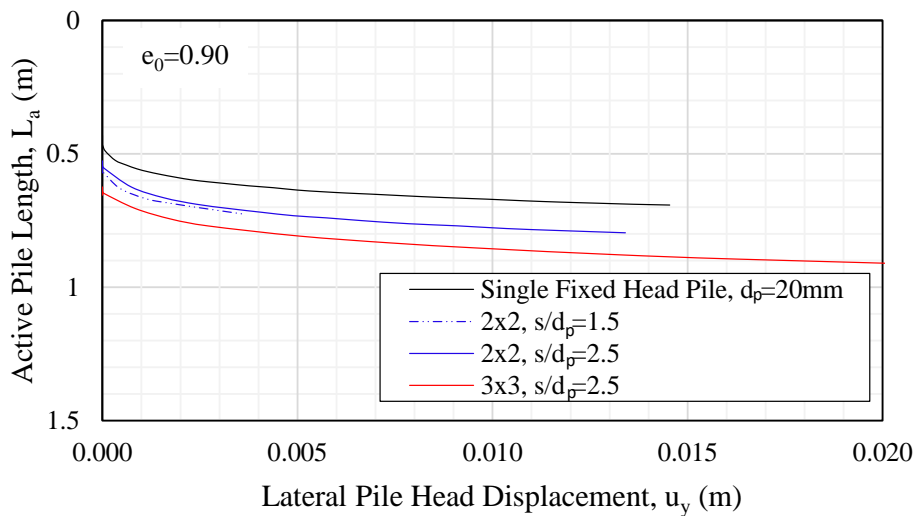


Figure 6 - 12. Active pile length progression at lead piles for closely grouped piles embedded in loose sand

A summary of the progression of the active pile length of the lead piles for all the pile configuration cases taken into consideration which are embedded in soils with initial void ratios of 0.73, 0.80 and 0.90 are presented in Figure 6 - 10, Figure 6 - 11 and Figure 6 - 12 respectively in reference to the single fixed head pile with diameter,  $d_p=20\text{mm}$ . All these data are plotted with reference to the definition of the active pile length as abovementioned.

In these figures, the zero value in the y-axis is the level of the pile head and the 1.5m level is equivalent to the bottom of the pile. From these illustrations, similar trends of active pile length progression, in terms of the effect of the pile stiffness and soil property is observed with the single fixed head piles. For piles embedded in the same soil condition, the higher the pile stiffness, the longer the active pile lengths. Hence, for grouped piles, the more number of piles, the longer the active pile length. On the other hand, given the same grouped pile configurations, longer active pile length is observed in loose condition due to the softening of the soil. Yet, it is noted that the spacing inherent in the pile group, do not have a contributing effect to the active pile length formation in the lead piles. This is highlighted in Figure 6 - 10. Looking at the 2x2 pile configuration, the active pile length progression is practically the same considering varied  $s/d_p$  ratios of 1.5, 2.5 and 4.5. This is also seen in the remaining two figures (Figure 6 - 11 and Figure 6 - 12), for the 2x2 pile configurations.

#### 6.4.2.2 Effect of Spacing and Number of Piles in a Group in Active Pile Length

Whilst the effect of the spacing is not shown in the active pile length of the lead piles, the extent of the grouped pile is looked at considering the average of the active pile length of all the piles in the grouped pile. By taking the average, this considers the range from the lead piles to the outer trailing piles. The average active pile length of the grouped piles is plotted against the lateral pile head displacements with reference to the single fixed head pile. A sample case is shown for grouped piles embedded in dense sand with initial void ratio,  $e_0=0.73$ . This figure shows that with the increase of spacing to diameter ratio,  $s/d_p$ , the average active pile length decreases and approaches the active pile length progression of the single fixed head pile. The average active pile length parameter supports claim that widely spaced grouped piles can be treated as individual single piles.

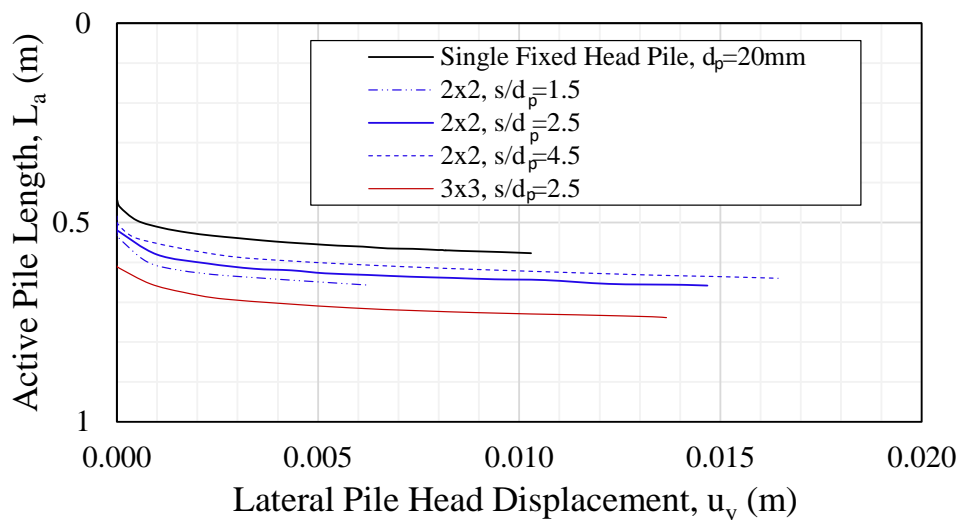
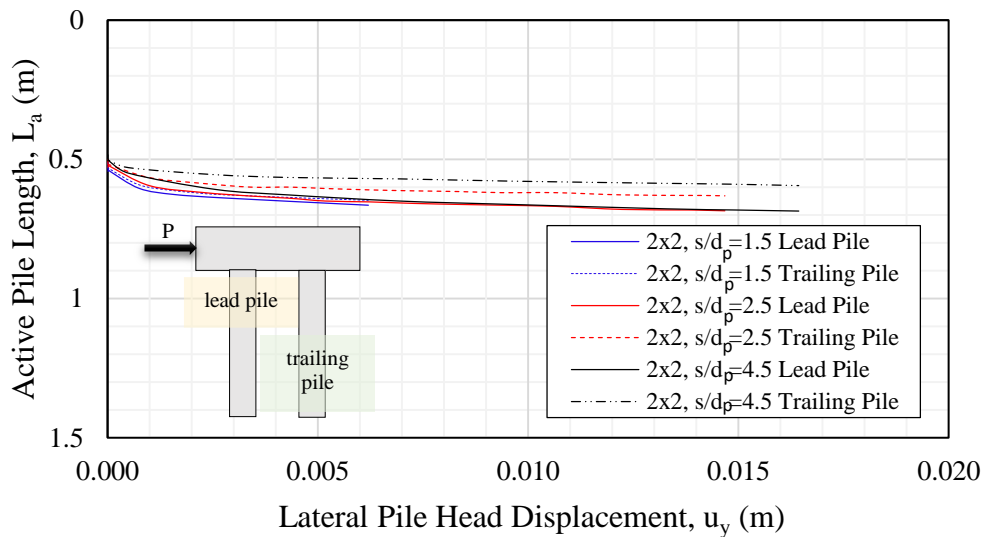


Figure 6- 13. Average active pile length progression for grouped piles embedded in dense sand,  $e_0=0.73$ .

The active pile length progression for each piles in the grouped pile are observed and plotted as seen in Figure 6- 14. This plot is case for the 2x2 grouped piles embedded in dense sand with varying spacing to diameter ratio. For the 2x2 pile configuration, the leftmost column of piles are termed as the lead piles and the rightmost column of piles are termed as the trailing pile. All the solid lines represent the active pile length progression at the lead piles and the all the dashed lines are for the active pile length progression of the trailing piles. Generally speaking, the active pile length of the lead piles are longer that those of the trailing piles. Moreover, spacing wise, it can be observed that considering low  $s/d_p$  ratio, say=1.5, given by the blue line in the graph below, the active pile length progressions are practically the same with that of the lead and trailing piles. This means that the spacing is not enough for the development of the mobilization of the soil within the grouped pile. With the increase of spacing to diameter ratio, the differences between the active pile length of the lead piles and the trail piles also increases i.e the active pile length of the trailing piles decreases. This spacing have allowed some soil mobilization already before reaching the trailing pile. Thus, given a widely spaced grouped pile, soil mobilization develops without the inhibition of the trailing pile.



**Figure 6- 14. Active pile length progression of the individual piles in the 2x2 grouped piles embedded in dense sand,  $e_0=0.73$**

The active pile lengths of individual piles in grouped piles having a 3x3 configuration embedded in soil with initial void ratios,  $e_0=0.73$ , 0.80 and 0.90 are observed and shown in Figure 6- 15, Figure 6- 16 and Figure 6- 17 respectively. The zero level at the y-axis is the pile head. The red, blue and green lines represent the active pile length in the lead piles, middle piles and outer piles respectively. Similar trend is seen where the active pile length is the longest at the lead pile and decreases with the trailing outer piles. It can be noted that the difference between the middle piles and the outer trailing piles is significantly lower compared to the difference between the lead piles with the middle piles and the lead piles with the outer trailing piles even for different soil conditions. On the other hand, the difference of the active pile length of the lead piles with the other trailing piles increases with decrease in soil stiffness.

In summary, the active pile length at the lead piles is a critical factor for the soil mobilization at the passive region. The spacing controls the extent of the soil mobilization within the grouped pile. The number of piles significantly increases the pile stiffness of the grouped piles.

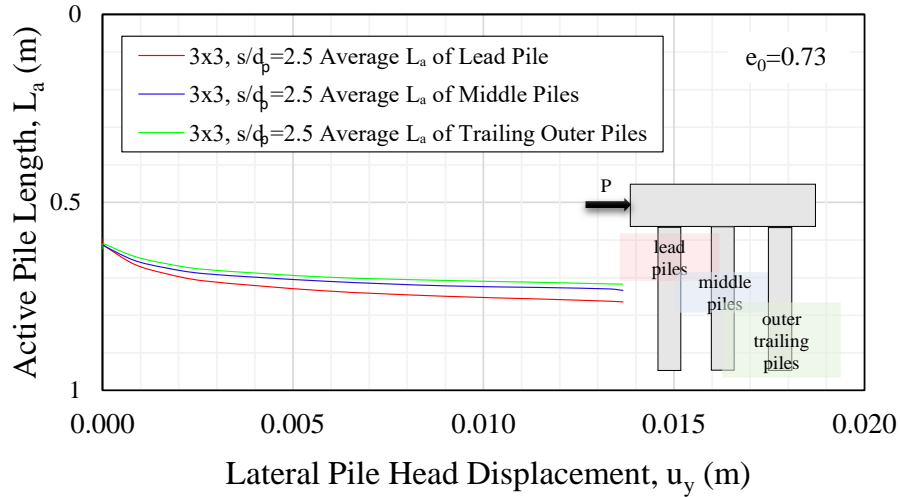


Figure 6- 15. Active pile length progression of individual piles in 3x3 grouped piles embedded in  $e_0=0.73$

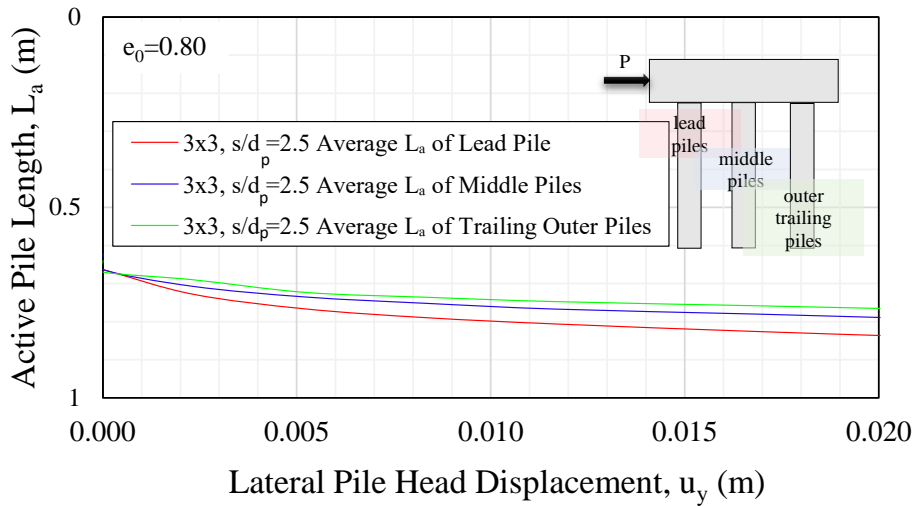


Figure 6- 16. Active pile length progression of individual piles in 3x3 grouped piles embedded in  $e_0=0.80$

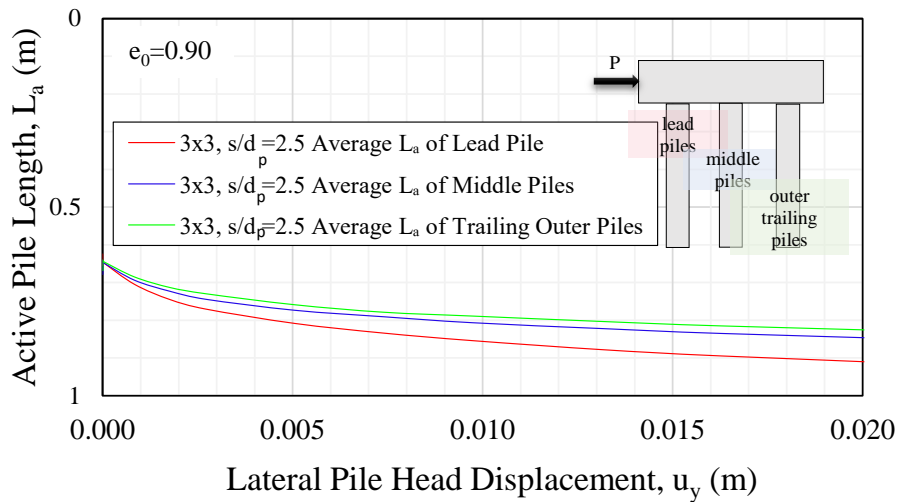


Figure 6- 17. Active pile length progression of individual piles in 3x3 grouped piles embedded in  $e_0=0.90$

### 6.4.3 Initial Active Pile Length

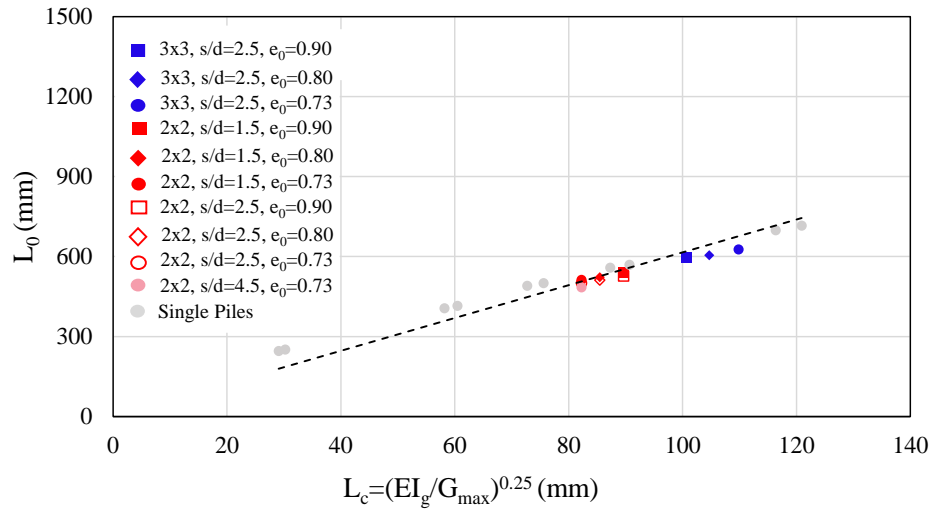


Figure 6- 18. Relationship of characteristic length to the initial active pile length for closely grouped piles.

Similar with the single fixed head piles, the active pile length is needed to derive the active pile length at the ultimate stage. It is warranted that this parameter be determined just with the basis of known parameters such as the pile and soil stiffness. Thus, the relationship of the characteristic length and the active pile length at the initial stage is established. The active pile length at the initial stage of the lead piles are plotted in the y-axis of Figure 6- 18. The characteristic length of all cases are derived using equation 6.4 similar with that of the single fixed head pile but using the grouped pile stiffness from equation 6.3. The plots for the cases of grouped piles are superimposed with the single fixed head piles represented by the gray dots. It can be seen that the data for the grouped pile lies within the relationship of  $L_c$  and  $L_0$  established for the single fixed head pile. This is given with the expression below:

$$L_0 = 6.38 L_c \quad (6.5)$$

### 6.4.4 Active Pile Length at the Ultimate Stage

Given that the active pile length at the initial stage has been established, the active pile length at the ultimate stage can be determined correspondingly. The average shear strain is plotted with the  $L_a/L_0$  for all the grouped piles embedded in soil with  $e_0=0.73, 0.80$  and  $0.90$  and with reference to the plots of the single fixed head piles represented by the grey dots as showed in Figure 6- 19, Figure 6- 20 and Figure 6- 21 respectively. Generally, the plots come close to the trend of that of the single fixed head pile. The active pile length at the ultimate stage is reached when the average shear strain is at 2%. For the same pile configuration, say 2x2 but with varying  $s/d_p$ , the data lie in a unique curve. However, it can be noted that the  $L_a/L_0$  ratio decreases with the increase of number of piles in a group. The  $L_a/L_0$  limits are summarized in Table 6 - 2. The  $L_a/L_0$  values for the grouped piles are normalized with that of the single piles to see the departure from the single piles. This is summarized in Table 6 - 3 in accordance with the number of piles in a grouped pile. It can be seen that a reduction factor of 0.96 and 0.92 is applied to the  $L_a/L_0$  of the single piles. Therefore, the difference from the relationship established with that of the single pile is just 4% and 8% for the 2x2 and 3x3 grouped pile respectively, which is practically small.

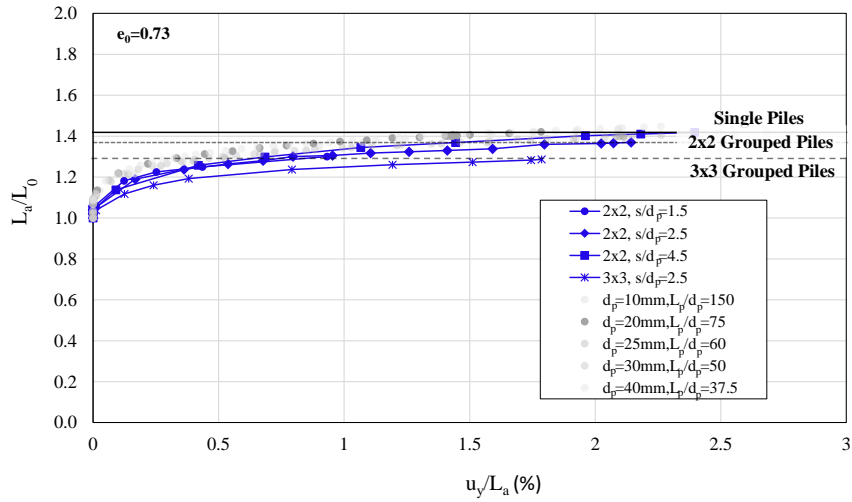


Figure 6- 19. Relationship of  $L_a/L_0$  with average shear strain for grouped piles embedded in soil with  $e_0=0,73$

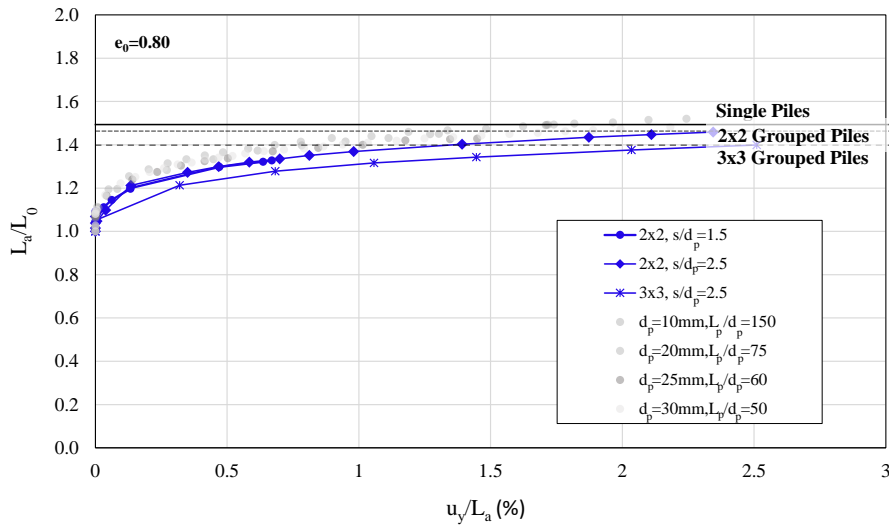


Figure 6- 20. Relationship of  $L_a/L_0$  with average shear strain for grouped piles embedded in soil with  $e_0=0,80$

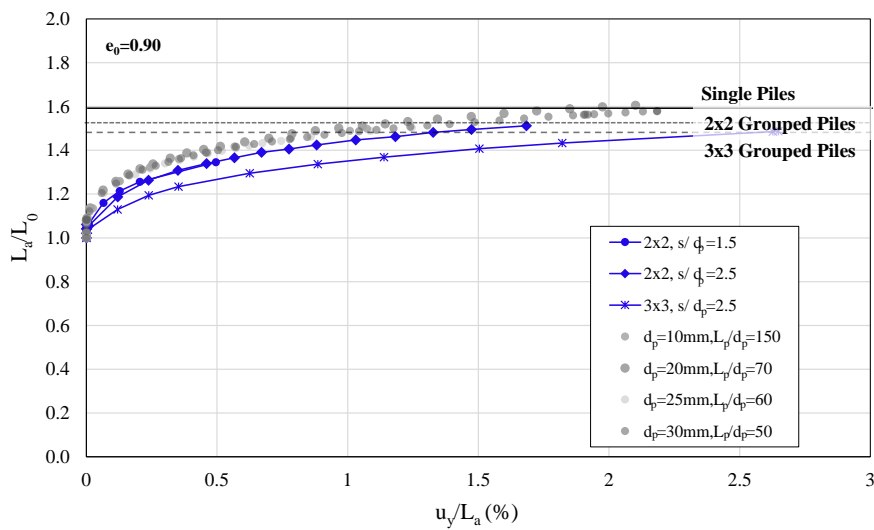


Figure 6- 21. Relationship of  $L_a/L_0$  with average shear strain for grouped piles embedded in soil with  $e_0=0,90$

**Table 6 - 2.  $L_a/L_0$  values for the single and grouped piles embedded in  $e_0=0.73, 0.80$  and  $0.90$**

Initial void ratio, $e_0$	$L_a/L_0$ value		
	Single	2x2	3x3
0.73	1.43	1.37	1.29
0.80	1.50	1.46	1.40
0.90	1.60	1.52	1.487

**Table 6 - 3.  $L_a/L_0$  values normalized with  $L_a/L_0$  (single piles)**

No. of Piles	Reduction Factor for Grouped Piles at the Ultimate Stage ( $\times L_a/L_0$ ) <sub>single piles</sub>
1	1.00
4	0.96
9	0.92

Hence, the equation to get the active pile length at the ultimate is given by the expression below:

$$L_{au} = L_0(1.0515e_0 + 0.655) \quad (6.6)$$

But if to be exact,

$$L_{au} = \chi L_0(1.0515e_0 + 0.655) \quad (6.7)$$

where  $\chi$  is the reduction factor dependent on the number of piles. This might matter if a huge number of piles is to be used.

## 6.5 Application of Active Pile Length on Ultimate Lateral Pile Resistance

Since the active pile length concept for the single fixed head piles has been established to be applicable for the closely grouped piles. This is implemented in describing the ultimate lateral pile resistance for grouped piles in this section.

### 6.5.1 Derivation of the Ultimate Lateral Pile Resistance

A similar way of the derivation of the ultimate lateral pile resistance for single piles is done with the closely grouped pile as shown in Figure 6- 22. The overall behaviour of the response of the grouped pile with the application pile head loading is described with the black line.

To determine the sole pile resistance of grouped pile is not as straightforward as the application of the analytical solution for single cantilever beam with fixed rotation at the end given the length,  $L_a$ . In order to calculate the grouped pile resistance, the grouped pile is modelled without the surrounding soil as seen in Figure 6- 23. The length of the piles is designated to be equal to the active pile length at the ultimate stage. Then, a pile head displacement is applied. The pile resistance is plotted in Figure 6- 22 represented by the blue line.

The side soil reaction is derived as the difference of overall behaviour minus the pile resistance. The constant line that appears at the larger displacement for the side soil reaction curve is the

ultimate side soil reaction or the ultimate lateral pile resistance for all cases of closely grouped piles.

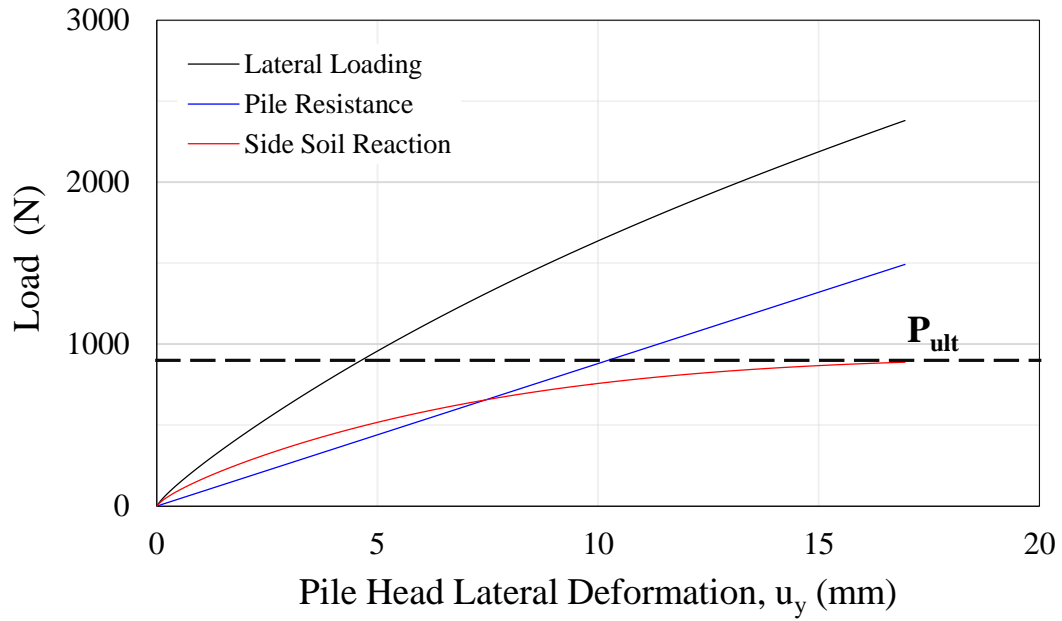


Figure 6- 22 Load deformation curves for grouped piles

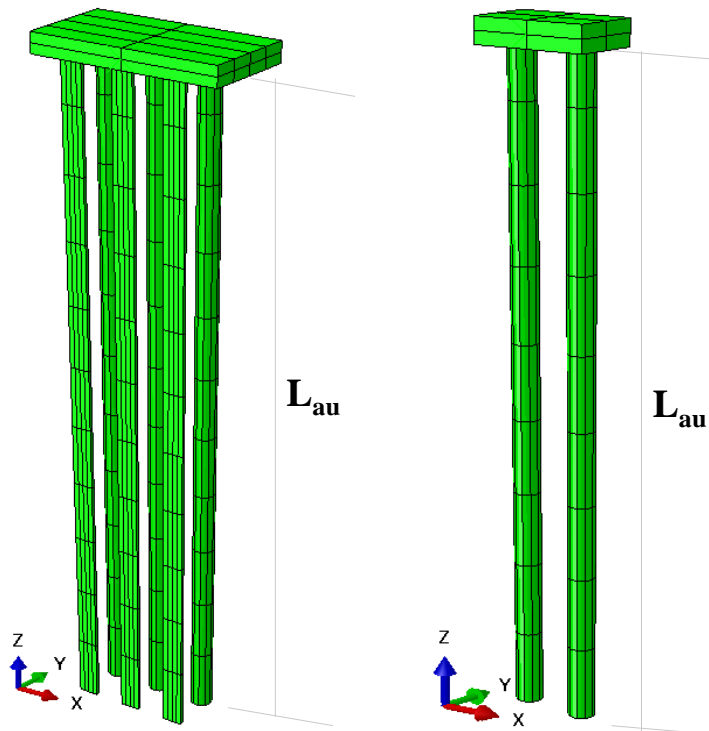


Figure 6- 23. Simulation of the laterally loaded grouped pile without the soil.

### 6.5.2 Simplified Expression of the Ultimate Resistance

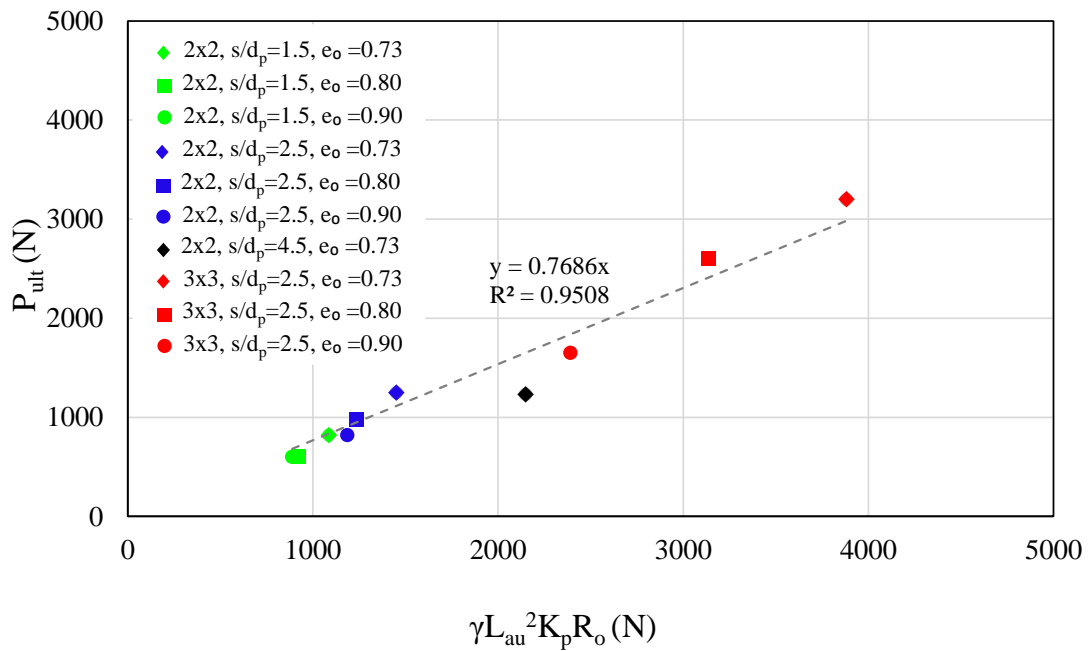


Figure 6- 24 Relationship of ultimate lateral pile resistance with active pile length and other soil parameters

The same set of parameters to describe to soil wedge in the passive region of a laterally loaded single piles is basically considered. The soil parameters used are the dry unit weight,  $\gamma$  and the Rankine passive coefficient,  $K_p$  describing the volume of the soil mobilized in the passive region. The pile radius in this case, is the equivalent radius of closely grouped pile,  $R_o$ , as shown in Figure 6- 24. The soil-pile interaction parameter used is the active pile length of the lead piles at the ultimate stage,  $L_{au}$ . From Figure 6- 24, there's a high correspondence with the linear relationship of the ultimate lateral pile resistance and the simple combination of parameters given in the x-axis. The relationship established with ultimate lateral pile resistance can be expressed in the equation below:

$$P_{ult} = 0.768\gamma L_{au}^2 K_p R_o \quad (6.8)$$

From the data plotted above, it can be seen that with increase in the number of piles in a grouped pile, the higher the ultimate pile resistance. Moreover, increasing the spacing could give the additional capacity because of the wider soil entrapment coverage represented by  $R_o$ , but limited to such spacing so that it is not under the category of widely spaced grouped pile. Ideally, the stiffer the soil and the stiffer the piles contributes to a big lateral pile capacity.

### 6.5.3 Superposition of Single and Closely Grouped Piles

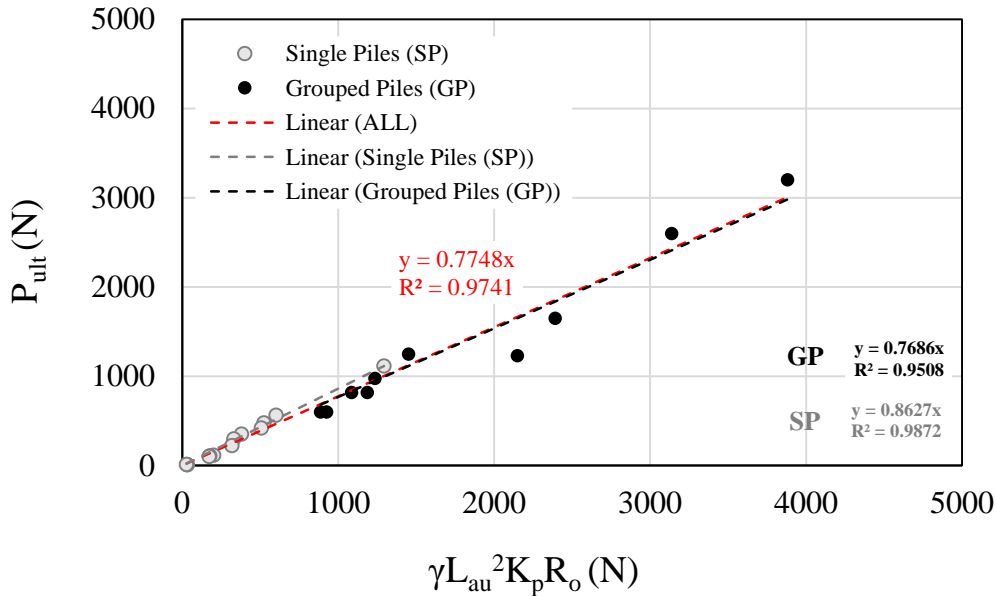


Figure 6- 25 Superposition of the simplified approach for the single and closely grouped piles

It has been established in Chapter 5 that the soil wedge for laterally loaded single pile, representative of the ultimate lateral pile resistance can be determined using the simple parameter,  $L_a$ , reflective of the soil-pile interaction and combining it with other soil parameters and pile parameter. Same relationship has been observed for the closely grouped piles. While there is 13% difference between the coefficients of the simplified expressions for single and closely grouped piles, it can be said that they are in agreement. Superimposing the data points for the single piles and grouped piles, and considering all the points, it can be noted that there is a high linear correlation between the ultimate lateral pile resistance and the simple parameters. Hence, overall, the ultimate lateral pile resistance can be expressed by the equation below.

$$P_{ult} = 0.77\gamma L_{au}^2 K_p R_o \quad (6.9)$$

## 6.6 Summary and Conclusion

Grouped piles behave as equivalent single piles where the spacing to diameter ratio is less than 10. The relative pile stiffness to the surrounding soil stiffness is similarly the predominant driving parameter to describe the lateral deformation along the length of the grouped piles. While the same number of piles gives the same pile group stiffness and correspondingly almost the same active pile length, the coverage of the soil entrapped in within the piles, indicative of the equivalent  $R_o$ , gives the additional lateral pile capacity. The concept of the active pile length for the single piles to the formation of the soil wedge in the passive region can be extended for closely grouped piles. While there is some discrepancy of about 13% for evaluating the ultimate lateral pile

resistance of single and closely grouped pile, a high correlation is still observed considering all the cases for both single and closely grouped piles.

Below is the flowchart for determining the ultimate lateral pile capacity for closely grouped pile.

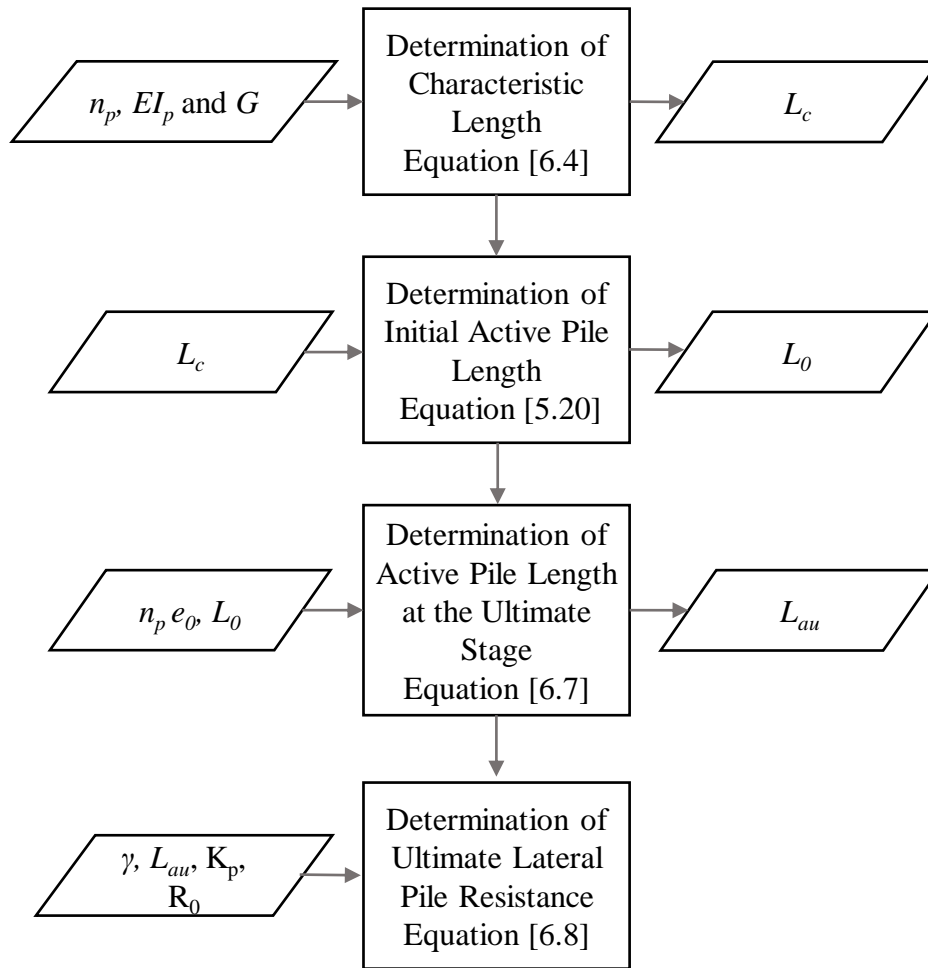


Figure 6 - 26. Flowchart for determining the ultimate lateral pile capacity of grouped piles

# Chapter 7

## Conclusions and Recommendations

### 7.1 Conclusions

Recent advances in numerical simulations have made it possible to simulate complex ideas. Case in point is the soil-pile interaction using tools such as finite element method. However, practitioners still clamour for the convenience and fast solutions especially for projects that need immediate attention. This for the reason, that even to this day simple formula is used. In common engineering practice, Chang's formula based on Winkler model is used in determining the characteristic length. In this case, the soil is assumed as an elastic medium discretised in springs representative of the soil stiffness. This soil stiffness is given by the coefficient of the subgrade reaction. The limitations of this model is that the continuum nature of the soil is not accounted for. More importantly, the coefficient of the subgrade reaction is not a fundamental property of the soil.

In Chapter 3, this point is elucidated. Although practitioners need simple and fast solutions, the accuracy and foundation on rigorous solution must not be compromised. Thus, the thrust for a more rational expression of the characteristic length is proposed. In this expression, the soil stiffness is changed to the shear modulus. This allows a more practical solution for field extraction without the need for size correction factor to capture the actual size of pile foundations. This characteristic length defines the relative stiffness of the pile to the surrounding soil stiffness. It predominantly characterizes the pile deformation relative to the surrounding soil that can be related to the passive soil wedge formation. Hence, it serves as a good parameter for describing the limit state useful in performance based design.

In Chapter 4, a preliminary study is done for the concept of the active pile length in two-dimensional analysis. It is established that the pile stiffness and soil stiffness predominantly affect the active pile length formation. It was observed that increasing the pile stiffness given the same surrounding soil stiffness increases the active pile length. The looser the surrounding soil medium for the same pile stiffness, the longer the active pile length. This behaviour is general for the long piles where  $L_a/L_p < 0.75$ . For practicality purposes, the active pile length is critical for developing solutions for the laterally loaded piles since deformations are not formed over its entire length i.e. once the active pile length is developed, increasing the pile length over and beyond this value does not matter.

The results derived in Chapter 4 are formidable and has showed potential for establishing the relationship of the active pile length with the ultimate lateral pile resistance. Thus, this concept is extended to the three-dimensional platform where a simplified approach is developed in describing the ultimate lateral pile resistance based on the active pile length as discussed in Chapter 5. For long and flexible piles, the characteristic length can be determined by both the known parameters: pile stiffness,  $EI_p$  and soil stiffness,  $G_{max}$ . The initial active pile length,  $L_0$ , formed at the elastic stage where the pile head displacements is small can be determined by this characteristic length by multiplying it with just the proportionality factor.

It is noted that in an elasto-plastic soil medium, the active pile length is progressively formed. The active pile length becomes constant when the average shear strain reaches 2%. This means that

the soil wedge is fully mobilized and this constant active pile length just continues to push it up. This is the active pile length at the ultimate stage. A relationship is established between the initial active pile length and the active pile length at the ultimate stage. This means that a correction factor applied to the active pile length formed at the elastic stage can yield the active pile length considering the nonlinearity and plasticity of the soil.

The formation of the soil wedge in the passive region with the increase of the pile head displacements along this so-called active pile length gives reasonable and physical basis for the ultimate lateral pile resistance to be dependent on this simple parameter. As evidence, a high correlation is seen with the ultimate side soil resistance and the parameters representative of the weight of this soil wedge. The ultimate lateral pile resistance of piles can be expressed by simple parameters such as  $L_{au}$ ,  $\gamma$ ,  $K_p$  and  $R_o$ .

In practice, grouped piles are commonly used. Considering the clear relationship of these simple parameters with the ultimate lateral pile resistance, this can be implemented similarly with closely spaced grouped piles. In Chapter 6, this idea is extended to closely grouped piles where it can be considered to be an equivalent single beam for grouped piles having spacing to diameter ratio ( $s/d_p$ )  $< 10$ . The pile stiffness considered for the group is equal to the product of the number of piles in the group and the individual stiffness. The increase in capacity contributed by the entrapped soil is represented by the equivalent radius,  $R_o$ . In comparison with the single piles, a 13% discrepancy is observed in the coefficient for determining the ultimate lateral pile resistance. Yet, if all data cases are to be considered, there is still a high correlation observed with the ultimate side soil resistance and the simple parameters including the active pile length and other soil parameters.

## 7.2 Recommendations

One valuable contribution of this research is establishing the relationship of the active pile length with the ultimate lateral pile resistance considering the non-linearity and plasticity behaviour of the soil. The main intention of this study is to provide a seed concept to start with laying out the foundations in terms of characterizing the limit states of the soil wedge formation in the passive region using the active pile length. It is recognized in this study that a lot of simplifications have been dealt with and limits the results for dealing with systems having soil as dry homogeneous sand with elastic piles embedded in it. Of course in reality, more complicated scenarios are inherent. Thus, this concept could be extended on those directions in the future studies. New research ideas could be built on this by just changing the material models for the piles, soils and loading conditions (see Figure 7- 1).

### 7.2.1 On piles

In this study, piles as elastic materials are considered. Also, it is assumed that the cross section of the piles remain the same from the start of the application of the load until the end. Thus, the material and geometric nonlinearities of the pile have not been accounted for. This assumption the pile may not be valid in many cases. One main dilemma in dealing pile as an elastic in this case would be piles reaching failure before reaching the ultimate lateral pile resistance. Hence, nonlinear behaviour of the pile in both its material and geometric properties could be the next step.

### ***7.2.2 On soils***

With the rise of finite element, comes more advance and efficient elasto-plastic constitutive materials for soils such that non-convergence numerical problem could be addressed. Advanced models could be used such as the SANISAND, the subloading  $t_{ij}$  and other models that are already in a sense a unification of dealing other properties of sand such as its structures, loading history, anisotropy, crushing, thermal effects etc.

Specific constitutive models could be applied dependent on the condition of the soil one is interest to capture. Liquefaction models, though in research working progress, are to be made available and may be implemented with FEM tools. In this case, with cyclic loading and undrained case, natural behaviour of soil could be captured.

Moreover, an interest for frozen soil may arise especially for structures located in cold regions. In this case, a multi-phase soil constitutive model could be implemented in the model. With the freezing of soil, comes the increase of the stiffness of soil in the upper part dependent on the depth of freezing. This could be treated as a multi-layered soil medium of different stiffness.

In lieu of that, the soil medium in reality is stratified and made up of different soil type per layer. Hence, the next step would be dealing with multi-layered soil system. For the current practice, the characteristic length using Chang's formula for multi-layered system is derived in iteration by getting the average of the coefficient of subgrade reaction up to the length of the characteristic length. For future work, this could be considered but with consideration of the position of the soil type. It is noted that the position of the layers is very important. Given the homogeneous soil medium, pile deformation appears to be significant in the upper region near the ground surface. Thus, taking for example a two-layered soil of same thickness, different behaviour is expected to be observed for piles where it has dense soil material above the loose soil as compared to the opposite case where loose soil is located above the dense soil. It is for this reason that an average of soil stiffness considering the thickness only is not adequate. Furthermore, different ground geometric configurations could be considered such as piles embedded in slopes.

### ***7.2.3 On loading conditions***

In this current study, a static monotonic loading is applied in the pile head system. In this case, the passive wedge is formed in just one side towards the direction of the loading. An interesting research would be the effect on the active pile length and the ultimate lateral pile resistance of the small back and forth application of the loading, which is called the ratcheting effect. In this case, the active and passive soil wedges are interchangeably formed with the application of loading. One issue with this type of phenomena is the settlement of the backfilled soil. An extension to this ratcheting would be the cyclic loading, which is needed to simulate the liquefaction case for undrained soil. An extension to dealing with the liquefaction would be the additional axial loads induced on embedded structures due to the liquefied layer sandwiched between non-liquefied soils. This consequently affect the active pile length deformations. A more complex scenario would be the natural loading orientation of the earthquakes which is random multi-directional lateral loading. Hence, this captures realistically the formation of the soil wedge indicative of the ultimate lateral pile resistance. In addition, real seismic load could be implemented.

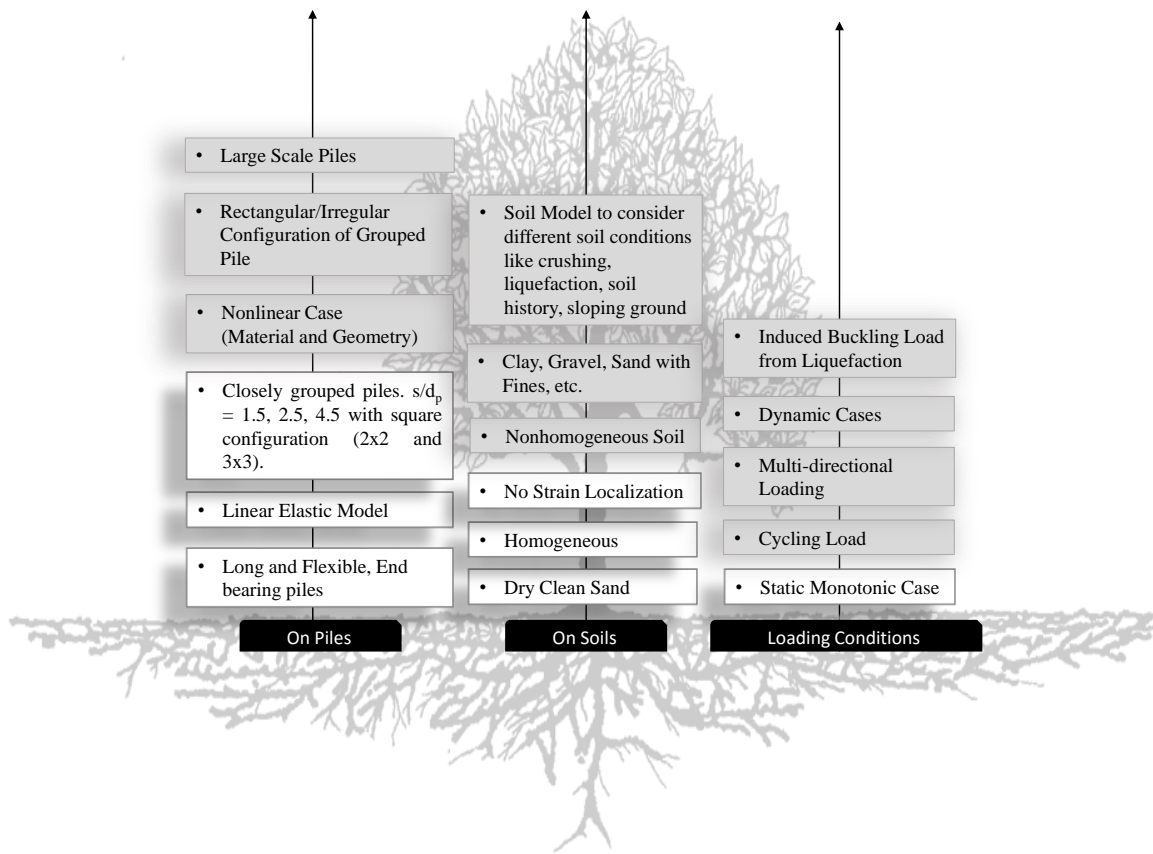


**Figure 7- 1. Future Direction of Research**

## REFERENCES

- Abdrabbo, F.M., Gaaver, K.E., 2012. Simplified analysis of laterally loaded pile groups. *Alexandria Eng. J.* 51, 121–127. doi:10.1016/j.aej.2012.05.005
- Abedzadeh, F., Pak, R.Y.S., 2004. Continuum Mechanics of Lateral Soil–Pile Interaction. *Engineering* 130, 1309–1318. doi:10.1061/(ASCE)0733-9399(2004)130
- Adachi, T., Kimura, M., Kobayashi, H., 1994. Behavior of laterally loaded pile groups in dense sand, in: *International Conference of Centrifuge 94*. Singapore, pp. 509–514.
- Alamy, 2014. Aerial view of Cattenom nuclear power plant in Lorraine, one of the French plants targeted by drones operated by unknown person [WWW Document]. *Guard*. URL <http://www.theguardian.com/environment/2014/nov/06/arrests-myster-drones-flying-french-nuclear-plants> (accessed 12.1.15).
- Alamy, 2013. China is covering its northern plains with wind turbines [WWW Document]. *Telegraph*. URL <http://www.telegraph.co.uk/news/earth/energy/windpower/10524840/Councils-waste-millions-on-ineffective-wind-turbines-that-will-take-190-years-to-repay.html> (accessed 12.1.15).
- Alizadeh, M., Davisson, M.T., 1970. Lateral load test on piles - Arkansas River Project. *J. Geotech. Eng. ASCE* 1583–1603.
- Anaraki, K.E., 2008. Hypoplasticity Investigated Parameter Determination and Numerical Simulation.
- Archer, A., Heymann, G., 2015. Using small - strain stiffness to predict the load - settlement behaviour of shallow foundations on sand 57, 28–35.
- Banerjee, P.K., 1978. The behavior of axially and laterally loaded single piles embedded in homogeneous soils. *Geotechnique* 28, 309–326.
- Barton, Y., 1984. Response of pile groups to lateral loading in the centrifuge, in: *Proceeding of a Symposium on the Application of Centrifuge Modeling to Geotechnical Design*. AA Balkema, Rotterdam, the Netherlands.
- Basu, D., Salgado, R., Prezzi, M., 2008. Analysis of laterally loaded piles in multilayered soil deposits. *Jt. Transp. Res. Progr.* 151. doi:10.5703/1288284313454.This
- Bathe, K.-J., 1996. *Finite Element Procedure*. Prentice Hall, New York.
- Beer, G., 1985. An isoparametric joint/interface element for finite element analysis. *Int. J. Numer. Anal. Methods Geomech.* 21, 585–600.
- Bogard, D., Matlock, H., 1983. Procedures for analysis of laterally loaded pile groups in soft clay, in: *Wright, S.G. (Ed.), Geotechnical Practice in Offshore Engineering*. American Society of Civil Engineers, New York, pp. 499–535.
- Bolton, M., 2012. Abstract of Performance-based design in geotechnical engineering for the 52nd Rankine Lecture.
- Bower, A., 2010. *Applied Mechanics of Solids, Chemistry & ....*
- Brinch Hansen, J., 1961. The ultimate resistance of rigid piles against transversal forces (No. 12), *Bulletin (Geoteknisk institut (Denmark))*. Copenhagen.
- Broms, B., 1965. Design of laterally loaded piles. *J. Soil Mech. Found. Div. ASCE* 91, 79–99.
- Brown, D. a., Shie, C., 1990. Three dimensional finite element model of laterally loaded piles. *Comput.*

Geotech. 10, 59–79. doi:10.1016/0266-352X(90)90008-J

- Chang, Y.L., 1937. Discussion on “lateral piles loaded tests” by Feagin Trans. ASCE 272, Paper no. 1959.
- Cox, W.R., Dixon, D.A., Murphy, B.S., 1984. Lateral-load tests on 25.4 mm diameter piles in very soft clay in side by side and in line groups, in: Laterally Loaded Deep Foundations: Analysis and Performance, ASTM STP 835. pp. 122–139.
- Dassault Systemes Simulia, 2013a. Abaqus 6.13 Online Documentation [WWW Document]. Dassault Systèmes. URL <http://129.97.46.200:2080/v6.13/> (accessed 1.1.14).
- Dassault Systemes Simulia, 2013b. UMAT: User subroutine to define a material’s mechanical behavior, in: Abaqus 6. 13 Documentation. p. Section 1.1.41.
- Davisson, M.T., Prakash, S., 1963. A reievew of soil-pole behavior, Transportation Research Board.
- Drucker, D.C., Prager, W., 1952. Soil Mechanics and Plastic-Analysis or Limit Design. Q. Appl. Math.
- Elson, W.K., 1989. Design of laterally-loaded piles (No. Report 103).
- Evans, L.T., Duncan, J.M., 1982. Simplified analysis of laterally loaded piles (No. UCB/GT/82-04). Berkley, CA.
- Fan, C.-C., 1996. The behavior of laterally loaded single piles and group piles in sand. University of Illinois.
- Farid, M., Salah, N.M., Cosentino, P.J., 2013. Pencil Pressuremeter Testing to Determining P-Y Curves for Laterally Loaded Deep Foundations. Procedia Eng. 54, 491–504. doi:10.1016/j.proeng.2013.03.045
- Feagin, L.B., 1937. Lateral pile-loading tests. Trans. ASCE 102, 236–254.
- Fleming, K., Weltman, A., Randolph, M.F., Elson, K., 2009. Piling engineering, Third. ed, Engineering Geology. Taylor & Francis, New York, USA.
- Georgiadis, K., Georgiadis, M., 2012. Development of p-y curves for undrained response of piles near slopes. Comput. Geotech. 40, 53–61. doi:10.1016/j.compgeo.2011.09.005
- Gu, X., Yang, J., Huang, M., 2013. Laboratory measurements of small strain properties of dry sands by bender element. Soils Found. 53, 735–745. doi:10.1016/j.sandf.2013.08.011
- Gudehus, G., Amorosi, A., Gens, A., Herle, I., Kolymbas, D., Mašín, D., Muir Wood, D., Niemunis, A., Nova, R., Pastor, M., Tamagnini, C., Viggiani, G., 2008. The soilmodels.info project. Int. J. Numer. Anal. Methods Geomech. 32, 1571–1572. doi:10.1002/nag.675
- Guo, P.X., Xiao, Y., Kunnath, S.K., 2014. Performance of laterally loaded H-piles in sand. Soil Dyn. Earthq. Eng. 67, 316–325. doi:10.1016/j.soildyn.2014.10.007
- Han, F., Salgado, R., Prezzi, M., 2015. Nonlinear analyses of laterally loaded piles – A semi-analytical approach. Comput. Geotech. 70, 116–129. doi:10.1016/j.compgeo.2015.07.009
- Herle, I., Gudehus, G., 1999. Determination of parameters of a hypoplastic constitutive model from properties of grain assemblies. Mech. Cohesive-frictional Mater. 4, 461–486. doi:10.1002/(SICI)1099-1484(199909)4:5<461::AID-CFM71>3.0.CO;2-P
- Hetenyi, M., 1946. Beams on elastic foundations. University of Michigan Press, Ann Arbor.
- Hirai, H., 2012. A Winkler model approach for vertically and laterally loaded piles in nonhomogeneous soil. Int. J. Numer. Anal. Methods Geomech. 36, 1869–1897. doi:10.1002/nag.1078
- Huang, J., 2011. Development of modified p-y curves for Winkler Analysis to characterize the lateral

- load behavior of a single pile embedded in improved soft clay. Iowa State University.
- Iai, S., 2004. Performance-Based Design Of Geotechnical Structures : Recent Advances, in: 5th International Conferences on Recent Advances in Geotechnical Earthquake Engineering. Missouri, p. Paper 7.
- IHA, n.d. North Vancouver [WWW Document]. URL <https://www.ihacom/Short-term-rentals-North-vancouver/4mE/> (accessed 12.1.15).
- Japan Road Association, 2012. Chapter IV: Foundations, in: Specifications for Highway Bridges. pp. 284–286, 406.
- Kimura, M., Yashima, A., Shibata, T., 1991. Three-dimensional finite element analysis of laterally loaded piles, in: Proceeding of 7th International Conference on Computer Method and Advance in Geomechanics. Cairns, Balkema, pp. 145–150.
- King, S., Richards, T., 2013. Solving Contact Problems with Abaqus, in: DS Simulia Abaqus Seminar. p. 325.
- Kog, Y.C., Kho, C., Loh, K.K., 2015. Tunnel Design and Modulus of Subgrade Reaction 29, 1–8. doi:10.1061/(ASCE)CF.1943-5509.0000537.
- Konagai, K., 2000. Shaking Table Test Allowing Interpretation of Damage to Structure in Terms of Energy Influx and Efflux through Soil-Structure Interface.
- Konagai, K., Yin, Y., Murono, Y., 2003. Single beam analogy for describing soil-pile group interaction. Soil Dyn. Earthq. Eng. 23, 213–221. doi:10.1016/S0267-7261(02)00212-9
- Kondner, R.L., 1963. Hyperbolic stress-strain response: cohesive soils. J. Soil Mech. Found. Div. ASCE 89, 115–143.
- Koseki, J., Kurachi, Y., Ogata, T., 2001. Dependency of horizontal and vertical subgrade reaction coefficients on loading width, in: Tatsuoka, Shibuya, Kuwano (Eds.), Advanced Laboratory Stress-Strain Testing of Geomaterials. Swets & Zeitlinger Publishers Lisse, Balkema, pp. 259–264.
- Kramer, S.L., Arduino, P., 2009. Development of performance criteria for foundations and earth structures, in: Performance-Based Design in Earthquake Geotechnical Engineering - from Case History to Practice. pp. 107–120.
- Kramer, S.L., Heavey, E.J., 1988. Lateral load analysis of nonlinear piles. J. Geotech. Eng. ASCE 114, 1045–1049. doi:10.1061/(ASCE)0733-9410(1988)114:9(1045)
- Kyokawa, H., 2011. Elastoplastic constitutive model for saturated and unsaturated soil considering the deposited structure and anisotropy. Nagoya Institute of Technology.
- Kyokawa, H., Kikumoto, M., 2013. FEM2D [WWW Document]. URL [h.kyokawa@gmail.com](mailto:h.kyokawa@gmail.com)
- Liu, J.L., 1991. Comprehensive effect coefficients calculating method for lateral bearing capacity of pile groups, in: Asian Regional Conference on Soil Mechanics and Foundation Engineering. pp. 247–250.
- Lu, J., Elgamal, A., Yang, Z., Diego, S., 2011. OpenSeesPL : 3D Lateral Pile-Ground Interaction.
- Mašin, D., Herle, I., 2006. State Boundary Surface in Hypoplasticity. pp. 117–128. doi:10.1007/978-3-540-35724-7\_7
- Matlock, H., Reese, L.C., 1960a. Generalized solution for laterally loaded piles. J. Soil Mech. Found. Div. ASCE 86, 63–91.
- Matlock, H., Reese, L.C., 1960b. Generalized solutions for laterally loaded piles. J. Soil Mech. Found. Div. 86, 63–94.

- Matsuoka, H., Nakai, T., 1977. Stress-strain relationship of soil based on the SMP, in: Proceedings of Specialty Session 9, 9th International Conference on Soil Mechanics and Foundation Engineering (ICSMFE). pp. 153–162. doi:10.1007/BF02092239
- McVay, M., Bloomquist, D., Vanderlinde, D., Clausen, J., 1994. Centrifuge modeling of laterally loaded pile groups in sands. *ASTM Geotech. Test. J.* 17, 129–137.
- Meyerhof, G.G., Sastry, V.V.R.N., Yalcin, A.S., 1988. Lateral resistance and deflection of flexible piles. *Can. Geotech. J.* 25, 511–522. doi:10.1139/t88-056
- Mokwa, R.L., 1999. Investigation of the resistance of the pile caps and integral abutments to lateral loading. Virginia Polytechnic Institute and State University.
- Muqtadir, A., Desai, C., 1986. Three-dimensional analysis of a pile-group foundation. *Int. J. Numer. Anal. Methods Geomech.* 10, 41–58. doi:10.1002/nag.1610100104
- Nakai, T., 2013. *Constitutive Modeling of Geomaterials - Principles and Applications*, CRC Press Taylor & Francis Group.
- Nakai, T., 2007. Modeling of soil behavior based on tij concept, in: 13th Asian Regional Conference on Soil Mechanics and Geotechnical Engineering Kolkata, India. Kolkata, India.
- Nakai, T., Matsuoka, H., 1987. Generalized elastoplastic constitutive model for clay in three-dimensional stresses. *Int. J. Rock Mech. Min. Sci. Geomech. Abstr.* 24, 107. doi:10.1016/0148-9062(87)90704-2
- Nakai, T., Shahin, H.M., Kikumoto, M., Kyokawa, H., Zhang, F., Farias, M.M., 2011. A Simple and Unified Three-Dimensional Model To Describe Various Characteristics of Soils. *Soils Found.* 51, 1149–1168. doi:10.3208/sandf.51.1149
- Naveen, B.P., Sitharam, T.G., Vishruth, S., 2012. Numerical Simulations of Laterally Loaded Piles, in: Indraratna, B., Cholachat, R., Vinod, J.S. (Eds.), *Proceedings of the International Conference on Ground Improvement & Ground Control*. Research Publishing Services, Singapore, pp. 1565–1570. doi:10.3850/978-981-07-3560-9\_09-0907
- Niemunis, A., Herle, I., 1997. Hypoplastic model for cohesionless soils with elastic strain range. *Mech. Cohesive-frictional Mater.* 2, 279–299. doi:10.1002/(SICI)1099-1484(199710)2:4<279::AID-CFM29>3.0.CO;2-8
- Otani, J., Pham, K.D., Sano, J., 2006. Investigation of failure patterns in sand due to laterally loaded pile using X-Ray CT. *SOILS Found.* 46, 529–535. doi:10.3208/sandf.46.529
- Papadopoulou, M.C., Comodromos, E.M., 2014. Explicit extension of the p-y method to pile groups in sandy soils. *Acta Geotech.* 9, 485–497. doi:10.1007/s11440-013-0274-z
- Pedroso, D., Farias, M., 2005. Implicit and explicit numerical integration schemes applied to elastoplastic constitutive laws for soils. *IWS-Fortaleza—2nd Int. ....*
- Pedroso, D.M., Farias, M., Nakai, T., 2005. An interpretation of subloading tij model in the context of conventional elastoplasticity theory. *Soils Found.* 45, 61–77. doi:http://doi.org/10.3208/sandf.45.4\_61
- Pérez-santisteban, I., García-mayordomo, J., Muñoz, A., Carbó, A., 2011. Comparison among SASW , ReMi and PS-logging techniques : Application to a railway embankment. *J. Appl. Geophys.* 73, 59–64. doi:10.1016/j.jappgeo.2010.11.006
- Poulos, H.G., 1981. Behavior of laterally loaded piles. *J. Soil Mech. Found. Div. ASCE* 31, 247–259.
- RAMON, V., KENJI, I., 1996. The Steady State of Sandy Soils. *Soils Found.* 36, 81–91. doi:10.3208/sandf.36.2\_81

- Randolph, M.F., 1981. The response of flexible piles to lateral loading. *Geotechnique* 31, 247–259.
- Rao, S.N., Ramakrishna, V.G.S.T., Rao, M.B., 1998. Influence of Rigidity on Laterally Loaded Pile Groups in Marine Clay. *J. Geotech. Geoenvironmental Eng.* 124, 542–549. doi:10.1061/(ASCE)1090-0241(1998)124:6(542)
- Reese, L., Van Impe, W., 2001. Single piles and pile groups under lateral loading.
- Reese, L.C., Cox, W.R., Koop, 1974a. Analysis of laterally loaded piles in sand, in: *Proceeding of Offshore Technology Conference*. OTC2080.
- Reese, L.C., Cox, W.R., Koop, F.D., 1974b. Analysis of laterally loaded piles in sand, in: *Offshore Technology Conference*. Offshore Technology Conference, OTC2080. doi:10.4043/2080-MS
- Rollins, K., Gerber, T., Cummins, C., Herbst, M., 2008. Monitoring Displacement vs . Depth in Lateral Pile Load Tests with Shape Accelerometer Arrays Suivi de déplacement c . profondeur en essais de charge latérale de pile avec des réseaux-.
- Salgado, R., Tehrani, F.S., Prezzi, M., 2014. Analysis of laterally loaded pile groups in multilayered elastic soil. *Comput. Geotech.* 62, 136–153. doi:10.1016/j.compgeo.2014.07.005
- Schofield, A.N., Wroth, C.P., 1968. Critical State Soil Mechanics. *Soil Use Manag.* 25, 310. doi:10.1111/j.1475-2743.1987.tb00718.x
- Shaw-shong, L., Seong-tatt, L., Kuan-seng, K., Bhd, P.G.S., Lumpur, K., 2010. Failure Investigation of Piled Reinforcement Soil Wall & Excessive Movements of Piled Embankment at Soft Ground , Malaysia 1–4.
- Shinoda, M., Watanabe, K., Kojima, K., Tateyama, M., 2009. Outline of performance-based design for railway earth structures in Japan, in: Kokusho, T., Tsukamoto, Y., Yoshimine, M. (Eds.), *Performance-Based Design in Earthquake Geotechnical Engineering - from Case History to Practice*. Taylor and Francis Group, London, pp. 137–148.
- Shirato, M., Shoichi, N., Matsui, K., Nakaura, T., 2009. Geotechnical criteria for serviceability limit state of horizontally loaded deep foundations. *Proc. Int. Symp. Geotech. Earthq. Eng.* 119–126. doi:doi:10.1201/9780203867310.ch13
- SIRAJ consulting engineers, n.d. Al Qardiya Bridge [WWW Document]. URL <http://siraj-int.com/bridgepro1.html> (accessed 12.1.15).
- Su, D., Yan, W.M., 2013. A multidirectional p–y model for lateral sand–pile interactions. *Soils Found.* 53, 199–214. doi:10.1016/j.sandf.2013.02.002
- Teodoru, I.-B., Toma, I.-O., 2009. Numerical Analyses of Plate Loading Test. *Bull. Polytech. Inst. Jassy, Constr. Arch. Sect. LV (LIX)*, 57–66.
- Terzaghi, K., 1955. Evaluation of Coefficient of Subgrade Reaction. *Geotech. London* 5, 41–50.
- Trochanis, B.A.M., Member, A., Bielak, J., Christiano, P., 1991. Three-dimensional nonlinear study of piles 117, 429–447.
- Varghese, P.C., 2012. *Foundation Engineering*. Asole K. Ghosh, PHI Learning Private Limited, New Delhi.
- Velez, A., Gazetas, G., Krishnan, R., 1983. Lateral Dynamic Response of Constrained-Head Piles. *J. Geotech. Eng.* 109, 1063–1081. doi:10.1061/(ASCE)0733-9410(1983)109:8(1063)
- von Wolffersdorff, P. a., 1996. A hypoplastic relation for granular materials with a predefined limit state surface. *Mech. Cohesive-Frictional Mater.* 1, 251–271. doi:10.1002/(SICI)1099-1484(199607)1:3<251::AID-CFM13>3.0.CO;2-3
- Wakai, A., Gose, S., Ugai, K., 1999. 3-D Elasto-Plastic Finite Element Analyses of Pile Foundations

- Subjected to Lateral Loading. SOILS Found. 39, 97–111. doi:10.3208/sandf.39.97
- Wang, M.C., Liao, W.P., 1988. Active Length of Laterally Loaded Piles. *J. Geotech Engg* 5, 1044–1048.
- Wei, X., Wang, Q., Wang, J., 2008. Damage Patterns and Failure Mechanisms of Bridge Pile, in: 14th World Conference on Earthquake Engineering. Beijing, China, pp. 1–7.
- Wu, G., Liam Finn, W.D., Dowling, J., 2015. Quasi-3D analysis: Validation by full 3D analysis and field tests on single piles and pile groups. *Soil Dyn. Earthq. Eng.* 78, 61–70. doi:10.1016/j.soildyn.2015.07.006
- Yang, Z., Jeremi, B., 2002. Numerical Analysis of Pile Behavior under Lateral Loads in Layered Elastic – Plastic Soils. *Int. J. Numer. Anal. Methods Geomech.* 02, 1–31.
- Yoon, K., Lee, Y., Lee, P.S., 2012. A continuum mechanics based 3-D beam finite element with warping displacements and its modeling capabilities. *Struct. Eng. Mech.* 43, 411–437. doi:10.12989/sem.2012.43.4.411
- Yoshida, I., Yoshinaka, R., 1972. A Method to Estimate Modulus of Horizontal Subgrade Reaction for a Pile. *Soils Found.* 12, 1–17.
- Zhang, L., 2009. Nonlinear analysis of laterally loaded rigid piles in cohesionless soil. *Comput. Geotech.* 36, 718–724. doi:10.1016/j.compgeo.2008.12.001
- Zhang, L., Hu, T., 1991. Modeling of residual stresses of large piles in centrifuge, in: *Centrifuge 91*. pp. 237–243.



## APPENDIX A.

### Subloading $t_{ij}$ constitutive model code

The main code done in C++ platform for the 2D analysis is mainly from Dr. Hiroyuki Kyokawa with modifications done to account for the slipping interface and the addition of 2D continuum beam-based elements. The whole program is very long and complicated with many layered functions. Hence, attached herein is the abridge code, intending to showcase the constitutive model used to simulate the elasto-plastic behaviour of soil. The code used here is the subloading  $t_{ij}$ .

```

/*****

MatSubloadingTij (FEAC Ver.0.00)
Copyright (C) 2012 Hiroyuki Kyokawa, All rights reserved.
e-mail: h.kyokawa@gmail.com

*****/

#include "MatSubloadingTij.h"
#include "PropSubloadingTij.h"

void MatSubloadingTij::eigenValueAndVector(Matrix& eigenValue, Matrix& eigenVector){
// [eigenVector.transpose()] * [generalCoordinate] * [eigenVector] = [eigenValue]
// eigenValue : general stress(strain) matrix to principal stress(strain) matrix
// eigenVector : orthogonal transform matrix from general to principal axis

#define EIGEN_ZERO 1.0E-12
    eigenVector = Matrix(3,3,
        1.0, 0.0, 0.0,
        0.0, 1.0, 0.0,
        0.0, 0.0, 1.0);
    double W1,W2,a,b,c;
    double tc,ts;
    Matrix trans;
    double sum = fabs(eigenValue[0][1]) + fabs(eigenValue[0][2]) + fabs(eigenValue[1][2]);
    double elimitss = 3.0*EIGEN_ZERO;
    while (sum > elimitss){
        if (fabs(eigenValue[0][1]) > EIGEN_ZERO){
            a = eigenValue[0][1]; b = eigenValue[0][0]; c = eigenValue[1][1];
            W1 = b - c;
            W2 = 2.0 * a / (fabs(W1)+sqrt(W1*W1+4.0*a*a));
            if(W1 < 0.0) W2 *= -1.0;
            tc = 1.0 / sqrt(1.0+W2*W2);
            ts = tc * W2;
            trans = Matrix(3,3,
                tc, -ts, 0.0,
                ts, tc, 0.0,
                0.0, 0.0, 1.0);
            eigenValue = trans.transpose() * eigenValue * trans;
            eigenVector *= trans;
        }
        if (fabs(eigenValue[0][2]) > EIGEN_ZERO){
            a = eigenValue[0][2]; b = eigenValue[0][0]; c = eigenValue[2][2];
            W1 = b - c;
            W2 = 2.0 * a / (fabs(W1)+sqrt(W1*W1+4.0*a*a));
            if(W1 < 0.0) W2 *= -1.0;
            tc = 1.0 / sqrt(1.0+W2*W2);
            ts = tc * W2;
            trans = Matrix(3,3,
                tc, 0.0, -ts,
                0.0, 1.0, 0.0,
                ts, 0.0, tc);
            eigenValue = trans.transpose() * eigenValue * trans;
            eigenVector *= trans;
        }
        if (fabs(eigenValue[1][2]) > EIGEN_ZERO){
            a = eigenValue[1][2]; b = eigenValue[1][1]; c = eigenValue[2][2];
            W1 = b - c;
            W2 = 2.0 * a / (fabs(W1)+sqrt(W1*W1+4.0*a*a));
            if (W1 < 0.0) W2 *= -1.0;
            tc = 1.0/sqrt(1.0 + W2*W2);
            ts = tc * W2;
            trans = Matrix(3,3,
                1.0, 0.0, 0.0,
                0.0, tc, -ts,
                0.0, ts, tc);
            eigenValue = trans.transpose() * eigenValue * trans;
            eigenVector *= trans;
        }
        sum = fabs(eigenValue[0][1]) + fabs(eigenValue[0][2]) + fabs(eigenValue[1][2]);
    }

// Set order of principal stresses, i.e., major, intermediate and minor principal stress
    int swapPos;
    for (int i=0; i<2; i++){
        sum = eigenValue[i][i];
        swapPos = i;
        for (int j=(i+1); j<3; j++){
            if (eigenValue[j][j] > sum){
                sum = eigenValue[j][j];
                swapPos = j;
            }
        }
        if (swapPos != i){
            eigenValue[swapPos][swapPos] = eigenValue[i][i];
            eigenValue[i][i] = sum;
            for (int j=0; j<3; j++){

```



```

Matrix MatSubloadingTij::getDeInverse(Prop* prop){
    //----- Compression is positive in soil mechanics -----
    Matrix stress = -prop->getStress();
    Matrix stressMatrix(3,3,
        stress(0,0), stress(3,0), stress(5,0),
        stress(3,0), stress(1,0), stress(4,0),
        stress(5,0), stress(4,0), stress(2,0));

    // unit tensor
    Matrix deltaij(3,3,
        1.0,0.0,0.0,
        0.0,1.0,0.0,
        0.0,0.0,1.0);

#ifdef WATER_COUPLED
    double uW = prop->getUw();
    stressMatrix -= uW*deltaij; // Effective stress
#endif

    //-----
    double p = stressMatrix.trace()/3.0;
    double youngModulus = youngModulus_d_p * p;
    double Ediv = 1.0/youngModulus;
    double EPdiv = -poissonRatio/youngModulus;
    double Gdiv = 1.0 / (G_d_p * p);
    return Matrix(6,6,
        Ediv , EPdiv , EPdiv , 0.0 , 0.0 , 0.0 ,
        EPdiv , Ediv , EPdiv , 0.0 , 0.0 , 0.0 ,
        EPdiv , EPdiv , Ediv , 0.0 , 0.0 , 0.0 ,
        0.0 , 0.0 , 0.0 , Gdiv , 0.0 , 0.0 ,
        0.0 , 0.0 , 0.0 , 0.0 , Gdiv , 0.0 ,
        0.0 , 0.0 , 0.0 , 0.0 , 0.0 , Gdiv);
}

char* MatSubloadingTij::getType(void){
    return "SubloadingTij";
}

void MatSubloadingTij::read(istream& is){
    is >> lambda // Compression index
    >> kappa // Swelling index
    >> Rcs // Principal stress ratio at critical state
    >> beta // Shpae of yield surface
    >> eNC // Void ratio on NCL under atmospheric pressure
    >> Pa // Atmospheric pressure
    >> a // Controlling decay rate of the influence of density
    >> poissonRatio // Poisson ratio
    >> gamma // Unit weight
    >> K_Zero // K0
    >> e0; // Initial void ratio

#ifdef WATER_COUPLED
    is >> kx // Permeability in x direction
    >> ky // Permeability in y direction
    >> densityOfWater; // Density of water
#endif

#ifdef DYNAMIC_ANALYSIS
    is >> densityOfSoil; // Density of soil
#endif

    // elasticity
    youngModulus_d_p = 3.0 * (1.0+e0) * (1.0-2.0*poissonRatio) / kappa;
    G_d_p = youngModulus_d_p / 2.0 / (1.0+poissonRatio);
    lambda_d_p = (poissonRatio * youngModulus_d_p) / ((1.0-2.0*poissonRatio) * (1.0+poissonRatio));
    lambda_p_2G_d_p = lambda_d_p + 2.0*G_d_p;
    // failure func.
    Xcs = sqrt(2.0) * (sqrt(Rcs)-1.0/sqrt(Rcs)) / 3.0;
    Ycs = (1.0-sqrt(Rcs)) / (sqrt(2.0) * (sqrt(Rcs)+0.5));
    Mstar = pow((pow(Xcs,beta) + pow(Xcs,beta-1.0)*Ycs),1.0/beta);
    Cp = (lambda-kappa)/(1.0+e0);
}

void MatSubloadingTij::show(ostream& os){
    os << "Material Type : MatSubloadingTij" << endl
    << "Lambda : " << lambda << endl
    << "Kappa : " << kappa << endl
    << "Stress Ratio at Critical State : " << Rcs << endl
    << "Beta : " << beta << endl
    << "eNC : " << eNC << endl
    << "Atmospheric pressure : " << Pa << endl
    << "Influence of density : " << a << endl
    << "e0 : " << e0 << endl
    << "Unit Weight : " << gamma << endl
    << "K_0 : " << K_Zero;
}

```

```

Matrix MatSubloadingTij::getDep(Prop* prop){
    Matrix De = getDe(prop);
    //----- Initial loading condition is elastic in first step of stage ---
    if(prop->getLoadingDirection() == -100){ // neutralized
        prop->setLoadingDirection(-1);
        prop->setDep(De);
        return De;
    }

    //----- Compression is positive in soil mechanics -----
    Matrix stress = -prop->getStress();
    Matrix dStrain = -prop->getDTotalStrain();
    Matrix stressMatrix(3,3,
        stress(0,0), stress(3,0), stress(5,0),
        stress(3,0), stress(1,0), stress(4,0),
        stress(5,0), stress(4,0), stress(2,0));

    // unit tensor
    Matrix deltaTij(3,3,
        1.0,0.0,0.0,
        0.0,1.0,0.0,
        0.0,0.0,1.0);

#ifdef WATER_COUPLED
    double uW = prop->getUw();
    stressMatrix -= uW*deltaTij; // Effective stress
#endif

    //+++++ calculate components of ordinary stress fDij ++++++
    double p = stressMatrix.trace()/3.0;
    // calculation of principal stress and axis
    Matrix principalStress = stressMatrix;
    Matrix principalAxis(3,3); // orthogonal transform matrix from general to principal axis
    eigenValueAndVector(principalStress,principalAxis);
    // invariant of stress tensor
    double I1 = stressMatrix.trace();
    double I2 = 0.5*(pow(stressMatrix.trace(),2.0)-(stressMatrix*stressMatrix).trace());
    double I3 = stressMatrix.determinant();
    //+++++ calculate components of modified stress tij ++++++
    // aii,aij,tii,tij
    Matrix aii(3,3, // PS = principalStress
        sqrt(I3/(I2*principalStress(0,0))), 0.0, 0.0,
        0.0, sqrt(I3/(I2*principalStress(1,1))), 0.0,
        0.0, 0.0, sqrt(I3/(I2*principalStress(2,2))));
    Matrix aij = principalAxis * aii * principalAxis.transpose();
    Matrix tii = aii*principalStress;
    Matrix tij = aij*stressMatrix;
    double tN = 3.0*I3/I2; // tN
    //-----
    Matrix dFdsVector = getDFds(prop);
    Matrix dFdtVector = getDFdt(prop);
    // hardening function
    double rho = prop->getRho();
    double G = a*rho*fabs(rho);
    double hp = 0.0;

#ifdef FINITE_DEFORMATION
    double J = prop->getF().determinant(); // Jacobian
    hp = (J*(dFdtVector(0,0)+dFdtVector(1,0)+dFdtVector(2,0)) + G/tN)/Cp;
#else
    hp = (dFdtVector(0,0)+dFdtVector(1,0)+dFdtVector(2,0) + G/tN)/Cp;
#endif

    //---- Loading judgement and Elasto-plastic stiffness matrix -----
    double dFe = dFdsVector.transpose() * De * dStrain;
    double capLambda = dFe/(hp+dFdsVector.transpose()*De*dFdtVector);
    if(prop->getLoadingDirection() == -1){
        if(capLambda<=0.0){
#ifdef CONVERGENCE_CALCULATION
            prop->setLoadingDirection(1);
#endif
            prop->setDep(De);
            return De;
        }
        else{
            Matrix Dep = De - De*dFdtVector*dFdsVector.transpose()*De/ (hp+dFdsVector.transpose()*De*dFdtVector);
#ifdef CONVERGENCE_CALCULATION
            prop->setLoadingDirection(2);
#endif
            prop->setDep(Dep);
            return Dep;
        }
    }
}

```

```

#ifdef CONVERGENCE_CALCULATION
    else if(prop->getLoadingDirection() == 1){
        prop->setDep(De);
        return De;
    }
    else{ //prop->getLoadingDirection() == 2
        Matrix Dep = De - De*dFdtVector*dFdsVector.transpose()*De
        / (hp+dFdsVector.transpose()*De*dFdtVector);
        prop->setDep(Dep);
        return Dep;
    }
#endif

Matrix MatSubloadingTij::getBuiltDep(Prop* prop){
    return prop->getBuiltDep();
}

Matrix MatSubloadingTij::getDFds(Prop* prop){
    //----- Compression is positive in soil mechanics -----
    Matrix stress = -prop->getStress();
    Matrix stressMatrix(3,3,
        stress(0,0), stress(3,0), stress(5,0),
        stress(3,0), stress(1,0), stress(4,0),
        stress(5,0), stress(4,0), stress(2,0));
    // unit tensor
    Matrix deltaij(3,3,
        1.0,0.0,0.0,
        0.0,1.0,0.0,
        0.0,0.0,1.0);

#ifdef WATER_COUPLED
    double uW = prop->getUw();
    stressMatrix -= uW*deltaij; // Effective stress
#endif

//+++++ calculate components of ordinary stress fDij ++++++
double p = stressMatrix.trace()/3.0;
// calculation of principal stress and axis
Matrix principalStress = stressMatrix;
Matrix principalAxis(3,3); // orthogonal transform matrix from general to principal axis
eigenValueAndVector(principalStress,principalAxis);
// invariant of stress tensor
double I1 = stressMatrix.trace();
double I2 = 0.5*(pow(stressMatrix.trace(),2.0)-(stressMatrix*stressMatrix).trace());
double I3 = stressMatrix.determinant();
//+++++ calculate components of modified stress tij ++++++
// aii,aij,tii,tij
Matrix aii(3,3, // PS = principalStress
    sqrt(I3/(I2*principalStress(0,0))), 0.0, 0.0,
    0.0, sqrt(I3/(I2*principalStress(1,1))), 0.0,
    0.0, 0.0, sqrt(I3/(I2*principalStress(2,2))));
Matrix aij = principalAxis * aii * principalAxis.transpose();
Matrix tii = aii*principalStress;
Matrix tij = aij*stressMatrix;
// tN
double tN = 3.0*I3/I2;
// xij,X
Matrix xij = tij/tN - aij;
double X = xij.getNorm();
//+++++ calculate derivative of failure function F ++++++
//+++++ with respect to modified stress tij ++++++
// • YF/• YtN
double dFdtN = 1.0/tN;
// □YfA/□YX
double dZetadX = 0.0;
if(X != 0.0)
    dZetadX = pow(X/Mstar,beta-1.0)/Mstar;
// • YF/• YX = • YZita/• YX
double dFDX = dZetadX;
//+++++ calculate derivative of failure function F ++++++
//+++++ with respect to ordinary stress fDij ++++++
// □YI1/□YfDij
Matrix dl1dsij = deltaij;
// □YI2/□YfDij
Matrix dl2dsij = I1*deltaij - stressMatrix.transpose();
// □YI3/□YfDij = 0.5*(Eist*Ejlm*fDsl*fDtm)□@
Matrix S = stressMatrix;
Matrix dl3dsij(3,3, // S = stress
    S(1,1)*S(2,2)-S(1,2)*S(2,1), S(1,2)*S(2,0)-S(1,0)*S(2,2), S(1,0)*S(2,1)-S(1,1)*S(2,0),
    S(2,1)*S(0,2)-S(2,2)*S(0,1), S(2,2)*S(0,0)-S(2,0)*S(0,2), S(2,0)*S(0,1)-S(2,1)*S(0,0),
    S(0,1)*S(1,2)-S(0,2)*S(1,1), S(0,2)*S(1,0)-S(0,0)*S(1,2), S(0,0)*S(1,1)-S(0,1)*S(1,0));
// □YtN/□YfDij = □Y(I3/I2)• YfDij
Matrix dtNdsij = 3.0*(1.0/I2*dI3dsij - I3/(I2*I2)*dI2dsij);
// □YX/□YfDij = □Y(sqrt(I1*I2/I3-1))/□YfDij
Matrix dXdsij(3,3);
if(X != 0.0)

```

```

        dXdsij = (I2*dI1dsij + I1*dI2dsij - I1*I2/I3*dI3dsij) / (18.0*X*I3);
// □Yf/□YfDij
Matrix dFdsij = dFdtN*dtNdsij + dFdX*dXdsij;
Matrix dFdsVector(6,1,dFdsij(0,0),dFdsij(1,1),dFdsij(2,2),2.0*dFdsij(0,1),2.0*dFdsij(1,2),2.0*dFdsij(2,0));
//-----
if(p < 0.0){ // Sm < 0
    return Matrix(6,1,
        -0.5773502691896257,
        -0.5773502691896257,
        -0.5773502691896257,
        0.0,
        0.0,
        0.0);
}
return dFdsVector;
}

Matrix MatSubloadingTij::getDFdt(Prop* prop){
//----- Compression is positive in soil mechanics -----
Matrix stress = -prop->getStress();
Matrix stressMatrix(3,3,
    stress(0,0), stress(3,0), stress(5,0),
    stress(3,0), stress(1,0), stress(4,0),
    stress(5,0), stress(4,0), stress(2,0));
// unit tensor
Matrix deltaij(3,3,
    1.0,0.0,0.0,
    0.0,1.0,0.0,
    0.0,0.0,1.0);

#ifdef WATER_COUPLED
    double uW = prop->getUw();
    stressMatrix -= uW*deltaij; // Effective stress
#endif

//+++++ calculate components of ordinary stress fDij ++++++
double p = stressMatrix.trace()/3.0;
// calculation of principal stress and axis
Matrix principalStress = stressMatrix;
Matrix principalAxis(3,3); // orthogonal transform matrix from general to principal axis
eigenValueAndVector(principalStress,principalAxis);
// invariant of stress tensor
double I1 = stressMatrix.trace();
double I2 = 0.5*(pow(stressMatrix.trace(),2.0)-(stressMatrix*stressMatrix).trace());
double I3 = stressMatrix.determinant();
//+++++ calculate components of modified stress tij ++++++
// aii,aij,tii,tij
Matrix aii(3,3, // PS = principalStress
    sqrt(I3/(I2*principalStress(0,0))), 0.0, 0.0,
    0.0, sqrt(I3/(I2*principalStress(1,1))), 0.0,
    0.0, 0.0, sqrt(I3/(I2*principalStress(2,2))));
Matrix aij = principalAxis * aii * principalAxis.transpose();
Matrix tii = aii*principalStress;
Matrix tij = aij*stressMatrix;
// tN
double tN = 3.0*I3/I2;
// xij,X
Matrix xij = tij/tN - aij;
double X = xij.getNorm();
//+++++ calculate derivative of failure function F ++++++
//+++++ with respect to modified stress tij ++++++
// • Yf/• YtN
double dFdtN = 1.0/tN;
// □Yf/□YX
double dZetadX = 0.0;
if(X != 0.0)
    dZetadX = pow(X/Mstar,beta-1.0)/Mstar;
// • Yf/• YX = • YZita/• YX
double dFdX = dZetadX;
// • YtN/• Ytij
Matrix dtNdtij = aij;
// • YX/• Ytij = • YX/• Yxkl * • Yxkl/• Ytij
Matrix dXdtij(3,3);
if(X != 0.0)
    dXdtij = (xij - X*X*aij) / (X*tN);
// • Yf/• Ytij
Matrix dFdtij = dFdtN*dtNdtij + dFdX*dXdtij;
Matrix dFdVector(6,1,dFdtij(0,0),dFdtij(1,1),dFdtij(2,2),2.0*dFdtij(0,1),2.0*dFdtij(1,2),2.0*dFdtij(2,0));
//-----
if(p < 0.0){ // Sm < 0
    return Matrix(6,1,
        -0.5773502691896257,
        -0.5773502691896257,
        -0.5773502691896257,
        0.0,
        0.0,
        0.0);
}
}

```

```

    }
    return dFdVector;
}

void MatSubloadingTij::initialize(Prop* prop){
    //----- Compression is positive in soil mechanics -----
    Matrix stress = -prop->getStress();
    // stress tensor
    Matrix stressMatrix(3,3,
        stress(0,0), stress(3,0), stress(5,0),
        stress(3,0), stress(1,0), stress(4,0),
        stress(5,0), stress(4,0), stress(2,0));
    // unit tensor
    Matrix deltaij(3,3,
        1.0, 0.0, 0.0,
        0.0, 1.0, 0.0,
        0.0, 0.0, 1.0);
#ifdef WATER_COUPLED
    double uW = prop->getUw();
    stressMatrix -= uW*deltaij;
#endif
// calculation of principal stress and axis
    Matrix principalStress = stressMatrix;
    Matrix principalAxis(3,3);
    eigenValueAndVector(principalStress,principalAxis);
    // invariant of stress tensor
    //double I1 = stressMatrix.trace();
    double I2 = 0.5*(pow(stressMatrix.trace(),2,0)-(stressMatrix*stressMatrix).trace());
    double I3 = stressMatrix.determinant();
    // aii,aij,tii,tij
    Matrix aii(3,3,
        sqrt(I3/(I2*principalStress(0,0))), 0.0, 0.0,
        0.0, sqrt(I3/(I2*principalStress(1,1))), 0.0,
        0.0, 0.0, sqrt(I3/(I2*principalStress(2,2))));
    Matrix aij = principalAxis * aii * principalAxis.transpose();
    Matrix tii = aii*principalStress;
    Matrix tij = aij*stressMatrix;
    // tN
    double tN = 3.0*I3/I2;
    Matrix xij = tij/tN - aij;
    double X = xij.getNorm();
    // tN1• Fsize of current subloading surface
    double tN1 = tN*exp(1.0/beta*pow(X/Mstar,beta));
    // e1 : void ratio on NCL under current stress
    double e1 = eNC - lambda*log(tN1/Pa);
    // tN0 : size of initial yield surface at tN-axis
    double tN0 = tN*exp((e1-e0)/(lambda-kappa));
    // f1• Fparamter representing the influence density (OCR)
    double rho = e1-e0;
    // update hardening parameters
    prop->setHardeningParameter(tN0);
    prop->setInitialHardeningParameter(tN0);
    prop->setRho(rho);
}

void MatSubloadingTij::update(Prop* prop){
    //----- Compression is positive in soil mechanics -----
    Matrix plasticStrain = -prop->getPlasticStrain();
    double plasticStrainV = plasticStrain(0,0)+plasticStrain(1,0)+plasticStrain(2,0);
    //
    Matrix stress = -prop->getStress();
    Matrix strain = -prop->getTotalStrain();
    Matrix stressMatrix(3,3,
        stress(0,0), stress(3,0), stress(5,0),
        stress(3,0), stress(1,0), stress(4,0),
        stress(5,0), stress(4,0), stress(2,0));
    Matrix strainMatrix(3,3,
        strain(0,0), 0.5*strain(3,0), 0.5*strain(5,0),
        0.5*strain(3,0), strain(1,0), 0.5*strain(4,0),
        0.5*strain(5,0), 0.5*strain(4,0), strain(2,0));
    // unit tensor
    Matrix deltaij(3,3,
        1.0,0.0,0.0,
        0.0,1.0,0.0,
        0.0,0.0,1.0);
#ifdef WATER_COUPLED
    double uW = prop->getUw();
    stressMatrix -= uW*deltaij; // Effective stress
#endif
// calculation of principal stress and axis
    Matrix principalStress = stressMatrix;
    Matrix principalAxis(3,3);
    eigenValueAndVector(principalStress,principalAxis);
    // invariant of stress tensor
    double I2 = 0.5*(pow(stressMatrix.trace(),2,0)-(stressMatrix*stressMatrix).trace());

```

```

double I3 = stressMatrix.determinant();
// aii,aij,tii,tij
Matrix aii(3,3,
           sqrt(I3/(I2*principalStress(0,0))), 0.0, 0.0,
           0.0, sqrt(I3/(I2*principalStress(1,1))), 0.0,
           0.0, 0.0, sqrt(I3/(I2*principalStress(2,2))));
Matrix aij = principalAxis * aii * principalAxis.transpose();
Matrix tii = aii*principalStress;
Matrix tij = aij*stressMatrix;
// tN
double tN = 3.0*I3/I2;
// xij : deviatoric stress tensor in modified stress tij space
Matrix xij = tij/tN - aij;
// X
double X = xij.getNorm();
//
double strainV = strainMatrix.trace();
double voidRatio0 = prop->getInitialVoidRatio();
double voidRatio = voidRatio0 - (1.0+voidRatio0)*strainV;
//-----
// p0• Fsize of initial yield surface
double tN0 = prop->getInitialHardeningParameter();
// p1e• Fsize of curent yield surface
double tN1e = tN0 * exp(plasticStrainV/Cp);
// p1• Fsize of subloading surface
double tN1 = tN * exp(pow(X/Mstar,beta)/beta);
// f1• Fparamter representing the influence density (OCR)
double rho = (lambda-kappa)*log(tN1e/tN1);
// update hardening parameters
prop->setVoidRatio(voidRatio);
prop->setHardeningParameter(tN1e);
prop->setRho(rho);
}

```

## **APPENDIX B.**

### **User defined material code for the hypoplastic model**

The user-defined soil material is available in <https://soilmodel.info> and modified a bit to be successfully implemented in the Abaqus. Moreover, user-defined initial state definition thru the subroutine SDVINI is added so that initial conditions could be defined and called by the code.

```

! Copyright (C) 2009 C. Tamagnini, E. Sellari, D. Masin, P.A. von
Wolffersdorff
!
! This program is free software; you can redistribute it and/or modify
! it under the terms of the GNU General Public License as published
! by
! the Free Software Foundation; either version 2 of the License, or
! (at your option) any later version.
!
! This program is distributed in the hope that it will be useful,
! but WITHOUT ANY WARRANTY; without even the implied warranty
! of
! MERCHANTABILITY or FITNESS FOR A PARTICULAR PURPOSE.
See the
! GNU General Public License for more details.
!
! You should have received a copy of the GNU General Public License
! along with this program; if not, write to the Free Software
! Foundation, Inc., 51 Franklin Street, Fifth Floor, Boston, MA 02110-
1301,
! USA.

```

```

-----
subroutine umat(stress,statev,ddsdde,sse,spd,scd,
& rpl,ddsddt,drplde,drpldt,
& stran,dstran,time,dtime,temp,dtemp,predef,dpred,cmname,
& ndi,nshr,ntens,nstatv,props,nprops,coords,drot,pnewdt,
& celent,dfgrd0,dfgrd1,noel,npt,layer,kspt,kstep,kinc)

```

```

c user subroutine for Abaqus

```

```

c Author: D. Masin, based on RKF23 implementation by C.
Tamagnini

```

```

c
c implicit none

```

```

c character*80 cmname
c integer ntens, ndi, nshr, nstatv, nprops, noel, npt,
& layer, kspt, kstep, kinc, inittension

```

```

c double precision stress(ntens), statev(nstatv),
& ddsdde(ntens,ntens), ddsddt(ntens), drplde(ntens),
& stran(ntens), dstran(ntens), time(2), predef(1), dpred(1),
& props(nprops), coords(3), drot(3,3), dfgrd0(3,3), dfgrd1(3,3)
double precision sse, spd, scd, rpl, drplde, dtime, temp,
& dtemp, pnewdt, celent

```

```

c
c ... 1. nasvdim = maximum number of additional state variables
c 2. tolintT = prescribed error tolerance for the adaptive
c substepping scheme
c 3. maxnint = maximum number of time substeps allowed.
c If the limit is exceeded abaqus is forced to reduce
c the overall time step size (cut-back)
c 4. DTmin = minimum substeps size allowed.
c If the limit is exceeded abaqus is forced to reduce
c the overall time step size (cut-back)
c 5. perturb = perturbation parameter for numerical computation of
Jacobian matrices
c 6. nfasv = number of first additional state variable in statev field
c 7. prsw = switch for printing information

```

```

c ... declaration of local variables
c logical prsw,elprsw

```

```

c integer i,error,maxnint,nfev,testnan,maxninttest
c integer nparms,nasvdim,nfasv,nydim,nasv,nyact,testing

```

```

c double precision dot_vect_h

```

```

c double precision parms(nprops),theta,tolintT,dsub,DTmin,perturb
double precision sig_n(6),sig_np1(6),DDtan(6,6),pore
double precision depts_np1(6),depsv_np1,norm_deps,tolintTtest
double precision norm_deps2,pp,qq,cos3t,I1,I2,I3,norm_D2,norm_D
double precision ameanstress,avoid,youngel,tdepel0,tdepel1,nuel
double precision Eyoung0,Eyoung1,nu0,nu1

```

```

c
parameter (nasvdim = 15)
parameter (nydim = 6+nasvdim)
parameter (tolintT = 1.0d-3) ...orig value...
parameter (tolintT = 1.0d-3)
parameter (tolintTtest = 1.0d-1)
c
parameter (maxnint = 1000) ...orig value...
parameter (maxnint = 10000)
parameter (maxninttest = 1000)
parameter (DTmin = 1.0d-17)
parameter (perturb = 1.0d-5)
parameter (nfasv = 1)
parameter (prsw = .true.)

```

```

c ... additional state variables
c
double precision asv(nasvdim)

```

```

c ... solution vector (stresses, additional state variables)
c
double precision y(nydim),y_n(nydim),dy(nydim)

```

```

c ... Error Management:
c -----
c error = 0 ... no problem in time integration
c error = 1 ... problems in evaluation of the time rate, (e.g. undefined
stress state), reduce time integration substeps
c error = 3 ... problems in time integration, reduce abaqus load
increment
c (cut-back)
c error = 10 ... severe error, terminate calculation

```

```

c error=0

```

```

c ... check problem dimensions

```

```

c if (ndi.ne.3) then
c
write(1,*) 'ERROR: this UMAT can be used only for elm.'
write(1,*) 'with 3 direct stress/strain components'
write(1,*) 'noel = ',noel
error=10

```

```

c endif

```

```

c ... check material parameters and move them to array parms(nparms)

```

```

c call check_parms_h(props,nprops,parms,nparms,error)

```

```

c ... print informations about time integration, useful when problems
occur

```

```

c elprsw = .false.
c if (prsw) then

```

```

c ... print only in some defined elements

```

```

c if ((noel.eq.101).and.(npt.eq.1)) elprsw = .false.
c endif

```

```

c ... define number of additional state variables

```

```

c call define_h(nasv)
nyact = 6 + nasv
if (nyact.gt.nydim) then
write(1,*) 'ERROR: nasvdim too small in UMAT'
error=10
endif

```

```

c ... suggested time substep size, and initial excess pore pressure

```

```

c dsub = statev(13)
c pore = -statev(8)

```

```

c ... initialise void ratio

```

```

c if (statev(7) .lt. 0.001) then
ameanstress=-(stress(1)+stress(2)+stress(3))/3
avoid=0
if(Props(16) .le. 10.0) then
if(ameanstress .lt. 0.001) then

```



```

&
endif ! end inittension.eq.0
C
C ... update dsub and nfev
C
if(dsub.le.0.0d0) then
dsub = 0
else if(dsub.ge.dtime) then
dsub = dtime
end if
statev(13)=dsub
statev(10)=dfloat(nfev)
C ... convert solution (stress + cons. tangent) to abaqus format
C update pore pressure and compute total stresses
C
call solout_h(stress,ntens,asv,nasv,ddsdde,
y,nydim,pore,depsv_np1,parms,nparms,DDtan)
C
C ... updated vector of additional state variables to abaqus statev vector
C
do i=1,nasv
statev(i-1+nfasv) = asv(i)
end do
C
C ... transfer additional information to statev vector
C
do i=1,6
sig_np1(i)=y(i)
end do
pp=-((sig_np1(1)+sig_np1(2)+sig_np1(3))/3)
C
statev(8) = -pore
statev(9) = pp

if(inittension.eq.0) then
call calc_statev_h(sig_np1,statev,parms,nparms,nasv,
& nstatv,deps_np1)
end if

C
C -----
C End of time integration
C -----
C
return
end
C -----
C
subroutine check_parms_h(props,nprops,parms,nparms,error)
C checks input material parameters
C
C written 10/2004 (Tamagnini & Sellari)
C -----
implicit none
C
integer nprops,nparms,i,error
C
double precision props(nprops),parms(nprops)
double precision zero,one,four,pi,pi_deg
double precision phi_deg,phi,hs,en,ed0,ec0,eio,alpha,beta
double precision m_R,m_T,r_uc,beta_r,chi,bulk_w,p_t
C
parameter(zero=0.0d0,one=1.0d0,four=4.0d0,pi_deg=180.0d0)
C
nparms=nprops
C
do i=1,nprops
parms(i)=props(i)
enddo
C
C ... recover material parameters
C
phi_deg=parms(1)
hs =parms(3)
en =parms(4)
ed0 =parms(5)
ec0 =parms(6)
eio =parms(7)
alpha =parms(8)
beta =parms(9)
m_R=parms(10)
m_T=parms(11)
r_uc=parms(12)

beta_r=parms(13)
chi=parms(14)
bulk_w=parms(15)
p_t=parms(2)

C
pi=four*datan(one)
phi=phi_deg*pi/pi_deg
parms(1)=phi

C
if(phi.le.zero) then

write(1,*) 'ERROR: subroutine CHECK_PARMS:'
write(1,*) 'phi = ',phi
error = 10
return

end if

if(m_R.lt.zero) then

write(1,*) 'ERROR: subroutine CHECK_PARMS:'
write(1,*) 'm_R = ',m_R
error = 10
return

end if

if(m_T.lt.zero) then

write(1,*) 'ERROR: subroutine CHECK_PARMS:'
write(1,*) 'm_T = ',m_T
error = 10
return

end if

if(r_uc.lt.zero) then

write(1,*) 'ERROR: subroutine CHECK_PARMS:'
write(1,*) 'r_uc = ',r_uc
error = 10
return

end if

if(beta_r.lt.zero) then

write(1,*) 'ERROR: subroutine CHECK_PARMS:'
write(1,*) 'beta_r = ',beta_r
error = 10
return

end if

if(chi.lt.zero) then

write(1,*) 'ERROR: subroutine CHECK_PARMS:'
write(1,*) 'chi = ',chi
error = 10
return

end if

if(bulk_w.lt.zero) then

write(1,*) 'ERROR: subroutine CHECK_PARMS:'
write(1,*) 'bulk_w = ',bulk_w
error = 10
return

end if

if(p_t.lt.zero) then

write(1,*) 'ERROR: subroutine CHECK_PARMS:'
write(1,*) 'p_t = ',p_t
error = 10
return

end if

return
end
C -----

```

```

subroutine define_h(nasv)
-----
implicit none
integer nasv
c
c number of additional state variables
c must be less than 18 (otherwise change nasvdim in umat)
c
c nasv(1) ... del_11 intergranular strain component
c nasv(2) ... del_22 intergranular strain component
c nasv(3) ... del_33 intergranular strain component
c nasv(4) ... del_12 intergranular strain component
c nasv(5) ... del_13 intergranular strain component
c nasv(6) ... del_23 intergranular strain component
c nasv(7) ... void void ratio
c
c modified 6/2005 (Tamagnini, Sellari & Miriano)
c
nasv = 7
return
end
-----
double precision function dot_vect_h(flag,a,b,n)
-----
c dot product of a 2nd order tensor, stored in Voigt notation
c created 10/2004 (Tamagnini & Sellari)
c
c flag = 1 -> vectors are stresses in Voigt notation
c flag = 2 -> vectors are strains in Voigt notation
c flag = 3 -> ordinary dot product between R^n vectors
-----
implicit none
integer i,n,flag
double precision a(n),b(n)
double precision zero, half, one, two, coeff
c
parameter(zero=0.0d0, half=0.5d0, one=1.0d0, two=2.0d0)
c
if(flag.eq.1) then
c
c ... stress tensor (or the like)
c
coeff=two
c
elseif(flag.eq.2) then
c
c ... strain tensor (or the like)
c
coeff=half
c
else
c
c ... standard vectors
c
coeff=one
c
end if
c
dot_vect_h=zero
c
do i=1,n
if(i.le.3) then
dot_vect_h = dot_vect_h+a(i)*b(i)
else
dot_vect_h = dot_vect_h+coeff*a(i)*b(i)
end if
end do
c
return
end
-----
subroutine get_F_sig_q_h(sig,q,nasv,parms,nparms,
& deps,F_sig,F_q,error)
-----
c finds vectors F_sigma and F_q in F(y)
c
c written 6/2005 (Tamagnini, Sellari & Miriano)
-----
implicit none
double precision dot_vect_h
c
integer nparms,nasv,ii
c

```

```

double precision sig(6),q(nasv),parms(nparms),deps(6)
double precision MM(6,6),HH(nasv,6),F_sig(6),F_q(nasv)
double precision LL(6,6),NN(6),norm_D,norm_D2
integer istrain,error
c
c ... compute tangent operators
c
if(parms(10) .le. 0.5) then
istrain=0
else
istrain=1
end if
c
call get_tan_h(deps,sig,q,nasv,parms,nparms,MM,
HH,LL,NN,istrain,error)
c
c ... compute F_sig=MM*deps
c
if (istrain .eq. 1) then
call matmul_h(MM,deps,F_sig,6,6,1)
else
call matmul_h(LL,deps,F_sig,6,6,1)
norm_D2=dot_vect_h(2,deps,deps,6)
norm_D=sqrt(norm_D2)
do ii=1,6
F_sig(ii)=F_sig(ii)+NN(ii)*norm_D
end do
end if
c
c ... compute F_q=HH*deps
c
call matmul_h(HH,deps,F_q,nasv,6,1)
c
return
end
-----
subroutine get_tan_h(deps,sig,q,nasv,parms,nparms,MM,HH,
LL,NN,istrain,error)
-----
c computes matrices M and H for Masin hypoplastic model for clays
c version with intergranular strains
c
c NOTE: stress and strain convention: tension and extension positive
c
c written 6/2005 (Tamagnini & Sellari)
-----
implicit none
integer nparms,nasv,i,j,error
c
double precision dot_vect_h
c
double precision sig(6),q(nasv),parms(nparms),deps(6)
double precision eta(6),eta_dev(6),del(6),void,sig_star(6)
double precision eta_del(6),eta_delta(6),eta_eps(6)
double precision norm_del,norm_del2,norm_deps,norm_deps2,eta_dn2
double precision pp,qq,cos3t,l1,l2,l3,tanpsi
double precision a,a2,FF,fd,fs
double precision num,den,aF,Fa2,eta_n2,norm_m,norm_m2
double precision ll(6,6),lU(6,6)
double precision MM(6,6),HH(nasv,6),LL(6,6),NN(6),AA(6,6),m(6)
integer istrain
double precision m_dir(6),m_dir1(6),Leta(6),H_del(6,6),H_e(6)
double precision load,rho
double precision zero,tiny, half, one, two, three, six, eight, nine
double precision onethird,sqrt3,twosqrt2,sqrt2,oneeight,ln2m1
double precision temp1,temp2,temp3,temp4
double precision phi,hs,en,ed0,ec0,ei0,alpha,beta,r_uc
double precision m_R,m_T,beta_r,chi,bulk_w,p_t,sinphi,sinphi2
double precision ec,ed,ei,bauer,fb,fe,sq2,sq3,sq6,az
c
parameter(zero=0.0d0, one=1.0d0, two=2.0d0, three=3.0d0, six=6.0d0)
parameter(tiny=1.0d-17, half=0.5d0, eight=8.0d0, nine=9.0d0)
parameter(sq2=1.4142135623730951455d0,
& sq3=1.7320508075688771931d0,
& sq6=2.4494897427831778813d0)
c
c ... initialize constants and vectors
c
onethird=one/three
sqrt3=dsqrt(three)

```

```

twosqrt2=two*dsqrt(two)
sqrt2=dsqrt(two)
oneeight=one/eight
onethird=one/three
ln2m1=one/dlog(two)
C
do i=1,6
  do j=1,6
    MM(i,j)=zero
    LL(i,j)=zero
    ll(i,j)=zero
    IU(i,j)=zero
    H_del(i,j)=zero
  end do
  eta_del(i)=zero
  eta_delta(i)=zero
  eta_eps(i)=zero
end do
C
do i=1,nasv
  do j=1,6
    HH(i,j)=zero
  end do
end do
C
C ... fourth order identity tensors in Voigt notation
C
ll(1,1)=one
ll(2,2)=one
ll(3,3)=one
ll(4,4)=half
ll(5,5)=half
ll(6,6)=half
C
IU(1,1)=one
IU(2,2)=one
IU(3,3)=one
IU(4,4)=one
IU(5,5)=one
IU(6,6)=one
C
C ... recover material parameters
C
phi =parms(1)
hs =parms(3)
en =parms(4)
ed0 =parms(5)
ec0 =parms(6)
ei0 =parms(7)
alpha =parms(8)
beta =parms(9)
m_R=parms(10)
m_T=parms(11)
r_uc=parms(12)
beta_r=parms(13)
chi=parms(14)
bulk_w=parms(15)
p_t=parms(2)
C
sinphi=dsin(phi)
sinphi2=sinphi*sinphi
C
C ... recover internal state variables
C
del(1)=q(1)
del(2)=q(2)
del(3)=q(3)
del(4)=q(4)
del(5)=q(5)
del(6)=q(6)
void=q(7)
C
C ... axis translation due to cohesion (p_t>0)
C
sig_star(1)=sig(1)-p_t
sig_star(2)=sig(2)-p_t
sig_star(3)=sig(3)-p_t
sig_star(4)=sig(4)
sig_star(5)=sig(5)
sig_star(6)=sig(6)
C
C ... strain increment and intergranular strain directions
C
norm_deps2=dot_vect_h(2,deps,deps,6)

```

```

norm_del2=dot_vect_h(2,del,del,6)
norm_deps=dsqrt(norm_deps2)
norm_del=dsqrt(norm_del2)
C
if(norm_del.ge.tiny) then
C
  do i=1,6
    eta_del(i)=del(i)/norm_del
  end do
C
end if
C
eta_delta(1)=eta_del(1)
eta_delta(2)=eta_del(2)
eta_delta(3)=eta_del(3)
eta_delta(4)=half*eta_del(4)
eta_delta(5)=half*eta_del(5)
eta_delta(6)=half*eta_del(6)
C
if(norm_deps.ge.tiny) then
C
  do i=1,6
    eta_eps(i)=deps(i)/norm_deps
  end do
C
end if
C
C ... auxiliary stress tensors
C
call inv_sig_h(sig_star,pp,qq,cos3t,I1,I2,I3)
C
if (pp.gt.tiny) then
C
C ... if mean stress is negative, return with MM = 0, HH = 0 and error =
10 (severe)
C
  write(1,*) 'ERROR: subroutine GET_TAN:'
  write(1,*) 'Mean stress is positive (tension): p = ',pp
  error = 10
  return
C
end if
C
eta(1)=sig_star(1)/I1
eta(2)=sig_star(2)/I1
eta(3)=sig_star(3)/I1
eta(4)=sig_star(4)/I1
eta(5)=sig_star(5)/I1
eta(6)=sig_star(6)/I1
C
eta_dev(1)=eta(1)-onethird
eta_dev(2)=eta(2)-onethird
eta_dev(3)=eta(3)-onethird
eta_dev(4)=eta(4)
eta_dev(5)=eta(5)
eta_dev(6)=eta(6)
C
C ... functions a and F
C
eta_dn2=dot_vect_h(1,eta_dev,eta_dev,6)
tanpsi=sqrt3*dsqrt(eta_dn2)
temp1=oneeight*tanpsi*tanpsi+
& (two-tanpsi*tanpsi)/(two+sqrt2*tanpsi*cos3t)
temp2=tanpsi/twosqrt2
C
a=sqrt3*(three-sin(phi))/(twosqrt2*sin(phi))
a2=a*a
FF=dsqrt(temp1)-temp2
C
C ... barotropy and pyknotropy functions
C
bauer=dexp(-(-11/hs)**en)
ed = ed0*bauer
ec = ec0*bauer
ei = ei0*bauer
C
temp1=three+a*a-a*sq3*((ei0-ed0)/(ec0-ed0))**alpha
if(temp1.lt.zero) stop 'factor fb not defined'
fb=hs/en/temp1*(one+ei)/ei*(ei0/ec0)**beta*(-
11/hs)**(one-en)
fe=(ec/void)**beta
fs=fb*fe
C

```



```

        enddo
    C
    C additional state variables
    C
    do i=1,nasv
        y(6+i) = qq(i)
    enddo
    C
    return
end

-----
subroutine inv_eps_h(eps,eps_v,eps_s,sin3t)
-----
C calculate invariants of strain tensor
-----
C
C implicit none
C
integer i
C
double precision eps(6),edev(6),edev2(6),ev3
double precision tredev3,eps_v,eps_s,sin3t
double precision norm2,numer,denom
C
double precision zero,one,two,three,six
double precision onethird,twothirds,sqrt6
C
data zero,one,two,three,six/0.0d0,1.0d0,2.0d0,3.0d0,6.0d0/
C
C ... some constants
C
    onethird=one/three
    twothirds=two/three
    sqrt6=dsqrt(six)
C
C ... volumetric strain
C
eps_v=eps(1)+eps(2)+eps(3)
C
ev3=onethird*eps_v
C
C ... deviator strain
C
    edev(1)=eps(1)-ev3
    edev(2)=eps(2)-ev3
    edev(3)=eps(3)-ev3
    edev(4)=eps(4)/two
    edev(5)=eps(5)/two
    edev(6)=eps(6)/two
C
C ... second invariant
C
    norm2=edev(1)*edev(1)+edev(2)*edev(2)+edev(3)*edev(3)+
&    two*(edev(4)*edev(4)+edev(5)*edev(5)+edev(6)*edev(6))
C
    eps_s=dsqrt(twothirds*norm2)
C
C ... components of (edev_ij)(edev_jk)
C
    edev2(1)=edev(1)*edev(1)+edev(4)*edev(4)+edev(5)*edev(5)
    edev2(2)=edev(4)*edev(4)+edev(2)*edev(2)+edev(6)*edev(6)
    edev2(3)=edev(6)*edev(6)+edev(5)*edev(5)+edev(3)*edev(3)
    edev2(4)=two*(edev(1)*edev(4)+edev(4)*edev(2)+edev(6)*edev(5))
    edev2(5)=two*(edev(5)*edev(1)+edev(6)*edev(4)+edev(3)*edev(5))
    edev2(6)=two*(edev(4)*edev(5)+edev(2)*edev(6)+edev(6)*edev(3))
C
C ... Lode angle
C
    if(eps_s.eq.zero) then
C
        sin3t=-one
C
    else
C
        tredev3=zero
        do i=1,6
            tredev3=tredev3+edev(i)*edev2(i)
        end do
C
        numer=sqrt6*tredev3
        denom=(dsqrt(norm2))**3
        sin3t=numer/denom
    end if
end if
end if
return
end

-----
subroutine inv_sig_h(sig,pp,qq,cos3t,l1,l2,l3)
-----
C calculate invariants of stress tensor
C
C NOTE: Voigt notation is used with the following index conversion
C
C 11 -> 1
C 22 -> 2
C 33 -> 3
C 12 -> 4
C 13 -> 5
C 23 -> 6
-----
C
C implicit none
C
double precision sig(6),sdev(6)
double precision eta(6),eta_d(6),eta_d2(6)
double precision xmin1,xmin2,xmin3
double precision tretadev3,pp,qq,cos3t,l1,l2,l3
double precision norm2,norm2sig,norm2eta,numer,denom
C
double precision half,one,two,three,six
double precision onethird,threehalves,sqrt6,tiny
C
double precision dot_vect_h
C
data half,one/0.5d0,1.0d0/
data two,three,six/2.0d0,3.0d0,6.0d0/
data tiny/1.0d-18/
C
C ... some constants
C
    onethird=one/three
    threehalves=three/two
    sqrt6=dsqrt(six)
C
C ... trace and mean stress
C
    l1=sig(1)+sig(2)+sig(3)
    pp=onethird*l1
C
C ... deviator stress
C
    sdev(1)=sig(1)-pp
    sdev(2)=sig(2)-pp
    sdev(3)=sig(3)-pp
    sdev(4)=sig(4)
    sdev(5)=sig(5)
    sdev(6)=sig(6)
C
C ... normalized stress and dev. normalized stress
C
    if(l1.ne.0) then
        eta(1)=sig(1)/l1
        eta(2)=sig(2)/l1
        eta(3)=sig(3)/l1
        eta(4)=sig(4)/l1
        eta(5)=sig(5)/l1
        eta(6)=sig(6)/l1
    else
        eta(1)=sig(1)/tiny
        eta(2)=sig(2)/tiny
        eta(3)=sig(3)/tiny
        eta(4)=sig(4)/tiny
        eta(5)=sig(5)/tiny
        eta(6)=sig(6)/tiny
    end if
C
    eta_d(1)=eta(1)-onethird
    eta_d(2)=eta(2)-onethird
    eta_d(3)=eta(3)-onethird
    eta_d(4)=eta(4)
    eta_d(5)=eta(5)

```

```

    eta_d(6)=eta(6)
c
c ... second invariants
c
    norm2=dot_vect_h(1,sdev,sdev,6)
    norm2sig=dot_vect_h(1,sig,sig,6)
    norm2eta=dot_vect_h(1,eta_d,eta_d,6)
c
    qq=dsqrt(threehalves*norm2)
    l2=half*(norm2sig-l1*11)
c
c ... components of (eta_d_ij)(eta_d_jk)
c
eta_d2(1)=eta_d(1)*eta_d(1)+eta_d(4)*eta_d(4)+eta_d(5)*eta_d(5)
eta_d2(2)=eta_d(4)*eta_d(4)+eta_d(2)*eta_d(2)+eta_d(6)*eta_d(6)
eta_d2(3)=eta_d(6)*eta_d(6)+eta_d(5)*eta_d(5)+eta_d(3)*eta_d(3)
eta_d2(4)=eta_d(1)*eta_d(4)+eta_d(4)*eta_d(2)+eta_d(6)*eta_d(5)
eta_d2(5)=eta_d(5)*eta_d(1)+eta_d(6)*eta_d(4)+eta_d(3)*eta_d(5)
eta_d2(6)=eta_d(4)*eta_d(5)+eta_d(2)*eta_d(6)+eta_d(6)*eta_d(3)
c
c ... Lode angle
c
    if(norm2eta.lt.tiny) then
c
        cos3t=-one
c
    else
c
        tretadev3=dot_vect_h(1,eta_d,eta_d2,6)
c
        numer=-sqrt6*tretadev3
        denom=(dsqrt(norm2eta))**3
        cos3t=numer/denom
        if(dabs(cos3t).gt.one) then
            cos3t=cos3t/dabs(cos3t)
        end if
c
    end if
c
c ... determinant
c
    xmin1=sig(2)*sig(3)-sig(6)*sig(6)
    xmin2=sig(4)*sig(3)-sig(6)*sig(5)
    xmin3=sig(4)*sig(6)-sig(5)*sig(2)
c
    l3=sig(1)*xmin1-sig(4)*xmin2+sig(5)*xmin3
c
    return
end
-----
subroutine matmul_h(a,b,c,l,m,n)
c-----
c matrix multiplication
c-----
    implicit none
c
    integer i,j,k,l,m,n
c
    double precision a(l,m),b(m,n),c(l,n)
c
    do i=1,l
        do j=1,n
            c(i,j) = 0.0d0
            do k=1,m
                c(i,j) = c(i,j) + a(i,k)*b(k,j)
            enddo
        enddo
    enddo
c
    return
end
-----
subroutine move_asv_h(asv,nasv,qq_n)
c-----
c move internal variables in vector qq_n and changes intergranular
c strain
c from continuum to soil mechanics convention
c
c NOTE: del has always 6 components
c
c written 6/2005 (Tamagnini, Sellari & Miriano)
c-----
    implicit none
    integer nasv,i
    double precision asv(nasv),qq_n(nasv),zero
c
    parameter(zero=0.0d0)
c
    do i=1,nasv
        qq_n(i)=zero
    enddo
c
c ... intergranular strain tensor stored in qq_n(1:6)
c
    do i=1,6
        qq_n(i) = -asv(i)
    enddo
c
c ... void ratio stored in qq_n(7)
c
    qq_n(7) = asv(7)
c
    return
end
-----
subroutine move_eps_h(dstran,ntens,deps,depsv)
c-----
c Move strain increment dstran into deps and computes
c volumetric strain increment
c
c NOTE: all strains negative in compression; deps has always 6
c components
c
c written 7/2005 (Tamagnini, Sellari & Miriano)
c-----
    implicit none
    integer ntens,i
    double precision deps(6),dstran(ntens),depsv
c
    do i=1,ntens
        deps(i) = dstran(i)
    enddo
c
    depsv=deps(1)+deps(2)+deps(3)
c
    return
end
-----
subroutine move_sig_h(stress,ntens,pore,sig)
c-----
c computes effective stress from total stress (stress) and pore pressure
c (pore)
c
c NOTE: stress = total stress tensor (tension positive)
c       pore = exc. pore pressure (undrained conds., compression
c       positive)
c       sig = effective stress (tension positive)
c
c sig has always 6 components
c
c written 7/2005 (Tamagnini, Sellari & Miriano)
c-----
    implicit none
    integer ntens,i
    double precision sig(6),stress(ntens),pore,zero
c
    parameter(zero=0.0d0)
c
    do i=1,6
        sig(i)=zero
    enddo
c
    do i=1,ntens
        if(i.le.3) then
            sig(i) = stress(i)+pore
        else
            sig(i) = stress(i)
        end if
    enddo
c
    return
end
-----

```

```

subroutine norm_res_h(y_til,y_hat,ny,nasv,norm_R)
C-----
C evaluate norm of residual vector Res=||y_hat-y_til||
C
C written 6/2005 (Tamagnini, Sellari & Miriano)
C-----
implicit none
C
integer ny,nasv,ng,k,i,testnan
C
double precision y_til(ny),y_hat(ny),void_til,void_hat,del_void
double precision err(ny),norm_R2,norm_R
double precision norm_sig2,norm_q2,norm_sig,norm_q
double precision sig_hat(6),sig_til(6),del_sig(6)
double precision q_hat(nasv),q_til(nasv),del_q(nasv)
double precision dot_vect_h,zero
C
parameter(zero=0.0d0)
C
ng=6*nasv
k=42+nasv
C
do i=1,ny
err(i)=zero
end do
C
C ... recover stress tensor and internal variables
C
do i=1,6
sig_hat(i)=y_hat(i)
sig_til(i)=y_til(i)
del_sig(i)=dabs(sig_hat(i)-sig_til(i))
end do
C
do i=1,nasv-1
q_hat(i)=y_hat(6+i)
q_til(i)=y_til(6+i)
del_q(i)=dabs(q_hat(i)-q_til(i))
end do
C
void_hat=y_hat(6+nasv)
void_til=y_til(6+nasv)
del_void=dabs(void_hat-void_til)
C
C ... relative error norms
C
norm_sig2=dot_vect_h(1,sig_hat,sig_hat,6)
norm_q2=dot_vect_h(2,q_hat,q_hat,6)
norm_sig=dsqrt(norm_sig2)
norm_q=dsqrt(norm_q2)
C
if(norm_sig.gt.zero) then
do i=1,6
err(i)=del_sig(i)/norm_sig
end do
end if
C
if(norm_q.gt.zero) then
do i=1,nasv-1
err(6+i)=del_q(i)/norm_q
end do
end if
C
err(6+nasv)=del_void/void_hat
C
C ... global relative error norm
C
norm_R2=dot_vect_h(3,err,err,ny)
norm_R=dsqrt(norm_R2)
C
testnan=0
call umatisnan_h(norm_sig,testnan)
call umatisnan_h(norm_q,testnan)
call umatisnan_h(void_hat,testnan)
if(testnan.eq.1) then
norm_R=1.d20
end if
C
return
end
C-----
subroutine perturbate_h(y_n,y_np1,n,nasv,dtsub,err_tol,maxnint,
& DTmin,deps_np1,parms,nparms,nfev,elprsw,theta,ntens,DD,
dtime,
& error)
C-----
C compute numerically consistent tangent stiffness
C
C written 12/2005 (Tamagnini)
C-----
implicit none
C
logical elprsw
C
integer ntens,jj,kk,i
integer n,nasv,nparms,nfev
integer maxnint,error
C
double precision y_n(n),y_np1(n),y_star(n),parms(nparms)
double precision dtsub,err_tol,DTmin, dtime
double precision theta,sig(6),q(nasv)
double precision deps_np1(6),deps_star(6)
double precision dsig(6),DD(6,6),HHtmp(nasv,6)
double precision LL(6,6),NN(6)
integer istrain
double precision zero
C
parameter(zero=0.0d0)
C
C ... initialize DD and y_star
C
if(parms(10) .le. 0.5) then
istrain=0
else
istrain=1
end if
C
do kk=1,6
do jj=1,6
DD(kk,jj)=zero
end do
end do
do i=1,6
sig(i)=y_n(i)
end do
do i=1,nasv
q(i)=y_n(6+i)
end do
C
call push_h(y_n,y_star,n)
C
if(error.ne.10) then
call get_tan_h(deps_np1,sig,q,nasv,parms,nparms,
DD,HHtmp,LL,NN,istrain,error)
end if
if(istrain .eq. 0) then
do kk=1,6
do jj=1,6
DD(kk,jj)=LL(kk,jj)
end do
end do
else
do kk=1,6
do jj=1,6
DD(kk,jj)=parms(10)*LL(kk,jj)
end do
end do
end if
C
return
end
C-----
subroutine push_h(a,b,n)
C-----
C push vector a into vector b
C-----
implicit none
integer i,n
double precision a(n),b(n)
C
do i=1,n
b(i)=a(i)
enddo
C
return
end
C-----

```

```

subroutine rhs_h(y,ny,nasv,parms,nparms,deps,kRK,nfev,error)
c-----
c calculate coefficient kRK from current state y and strain increments
c deps
c Masin hypoplastic model for clays with intergranular strains
c
c written 12/2005 (Tamagnini & Sellari)
c-----
implicit none
c
integer error,ny,nparms,nasv,i,nfev
c
double precision zero,one,two,four
double precision y(ny),kRK(ny),parms(nparms),deps(6)
double precision sig(6),q(nasv)
double precision F_sig(6),F_q(nasv)
c
parameter(zero=0.0d0,one=1.0d0,two=2.0d0,four=4.0d0)
c
c ... update counter for the number of function f(y) evaluations
c
nfev=nfev+1
c
c ... initialize kRK
c
do i=1,ny
kRK(i)=zero
end do
c
c ... recover current state variables (sig,q)
c
do i=1,6
sig(i)=y(i)
end do
c
do i=1,nasv
q(i)=y(6+i)
end do
c
c ... build F_sig(6) and F_q(nasv) vectors and move them into kRK
c
call
get_F_sig_q_h(sig,q,nasv,parms,nparms,deps,F_sig,F_q,error)
if(error.eq.10) return
c
do i=1,6
kRK(i)=F_sig(i)
end do
c
do i=1,nasv
kRK(6+i)=F_q(i)
end do
c
return
end
c-----
subroutine rkf23_update_h(y,n,nasv,dsub,err_tol,maxnint,DTmin,
& deps_np1,parms,nparms,nfev,elprsw,dtime,
& error)
c-----
c
c numerical solution of y'=f(y)
c explicit, adaptive RKF23 scheme with local time step extrapolation
c
c Tamagnini, Sellari & Miriano 6/2005
c
c-----
implicit none
c
logical elprsw
c
integer n,nasv,nparms,i,ksubst,kreject,nfev
integer maxnint,error,error_RKF
c
double precision y(n),parms(nparms),dsub,err_tol,DTmin
double precision zero,one,two,three,four,six
double precision ptnine,onesixth,onethird,twothirds,temp
c
double precision deps_np1(6),y_k(n),y_2(n),y_3(n),y_til(n)
double precision y_hat(n)
double precision T_k,DT_k,dtime
c
double precision kRK_1(n),kRK_2(n),kRK_3(n)
double precision norm_R,S_hull
c
parameter(zero=0.0d0,one=1.0d0,two=2.0d0,three=3.0d0)
parameter(four=4.0d0,six=6.0d0,onehalf=0.5d0,ptnine=0.9d0)
c
c ... initialize y_k vector and other variables
c
do i=1,n
y_k(i)=zero
end do
c
onesixth=one/six
onethird=one/three
twothirds=two/three
c
c ... start of update process
c
error_RKF=0
T_k=zero
DT_k=dsub/dtime
ksubst=0
kreject=0
nfev=0
c
do i=1,n
y_k(i)=y(i)
end do
c
c ... start substepping
c
do while(T_k.lt.one)
c
ksubst=ksubst+1
c
c ... write substepping info
c
write(*,1234) ksubst,T_k,DT_k
1234 format('Substep no.:',i4,' -- T_k = ',d12.4,' -- DT_k = ',d12.4)
c
c ... check for maximum number of substeps
c
if(ksubst.gt.maxnint) then
write(1,*) 'number of substeps ',ksubst,
' is too big, step rejected'
&
error=3
return
end if
c
c ... build RK functions
c
call check_RKF_h(error_RKF,y_k,n,nasv,parms,nparms)
if(error_RKF.eq.1) then
error=3
return
else
call
rhs_h(y_k,n,nasv,parms,nparms,deps_np1,kRK_1,nfev,error)
end if
if(error.eq.10) return
c
c ... find y_2
c
temp=half*DT_k
c
do i=1,n
y_2(i)=y_k(i)+temp*kRK_1(i)
end do
c
call check_RKF_h(error_RKF,y_2,n,nasv,parms,nparms)
if(error_RKF.eq.1) then
error=3
return
else
call
rhs_h(y_2,n,nasv,parms,nparms,deps_np1,kRK_2,nfev,error)
end if
if(error.eq.10) return
c
c ... find y_3
c
do i=1,n

```

```

        y_3(i)=y_k(i)-DT_k*kRK_1(i)+two*DT_k*kRK_2(i)
    end do
c
    call check_RKF_h(error_RKF,y_3,n,nasv,parms,nparms)
    if(error_RKF.eq.1) then
        error=3
        return
    else
        call
rhs_h(y_3,n,nasv,parms,nparms,deps_np1,kRK_3,nfev,error)
    end if
    if(error.eq.10) return
c
c ... approx. solutions of 2nd (y_til) and 3rd (y_hat) order
c
    do i=1,n
        y_til(i)=y_k(i)+DT_k*kRK_2(i)
        y_hat(i)=y_k(i)+DT_k*
&      (onesixth*kRK_1(i)+twothirds*kRK_2(i)+onesixth*kRK_3(i))
    end do
c
c ... local error estimate
c
    call norm_res_h(y_til,y_hat,n,nasv,norm_R)
c                                     check if output y_hat
can be used as an input into the next step
    call check_RKF_h(error_RKF,y_hat,n,nasv,parms,nparms)

    if (error_RKF.ne.0) then
c
c      error=1.d20
c      error_RKF=0
c
c                                     error=3
c                                     return

    end if
c
c ... time step size estimator according to Hull
c
    if(norm_R .ne. 0) then
        S_hull=ptnine*DT_k*(err_tol/norm_R)**onethird
    else
        S_hull=1
    end if
c
    if (norm_R.lt.err_tol) then
c
c ... substep is accepted, update y_k and T_k and estimate new
substep size DT_k
c
    do i=1,n
        y_k(i)=y_hat(i)
    end do
c
        T_k=T_k+DT_k
        DT_k=min(four*DT_k,S_hull)
        dtsub=DT_k*dtime
        DT_k=min((one-T_k),DT_k)
c
    else
c
c ... substep is not accepted, recompute with new (smaller) substep
size DT
c
        DT_k=max(DT_k/four,S_hull)
c
c ... check for minimum step size
c
    if(DT_k.lt.DTmin) then
        write(1,*) 'substep size ',DT_k,
&      ' is too small, step rejected'
        error=3
        return
    end if
c
    end if
c
c ... bottom of while loop
c
    end do
c
c ... recover final state

```

```

c
do i=1,n
    y(i)=y_k(i)
end do

return
end

-----
subroutine check_RKF_h(error_RKF,y,ny,nasv,parms,nparms)
-----
c Checks is RKF23 solout vector y is OK for hypoplasticity
c
implicit none
c
integer error_RKF,ny,nasv,i,nparms,testnan,iopt
c
double precision y(ny),parms(nparms)
double precision sig(6),pmean,sig_star(6)
double precision xN1(3),xN2(3),xN3(3),S(3),P,Q,tmin
double precision p_t,minstress
c
p_t =parms(2)
minstress=p_t/4.d0
do i=1,6
    sig(i)=y(i)
end do

sig_star(1)=sig(1)-p_t
sig_star(2)=sig(2)-p_t
sig_star(3)=sig(3)-p_t
sig_star(4)=sig(4)
c changed order due to prnsig convention different from
abaqus
sig_star(5)=sig(6)
sig_star(6)=sig(5)

pmean=-(sig_star(1)+sig_star(2)+sig_star(3))/3
c
c check for positive mean stress
if(pmean .le. minstress) then
    error_RKF=1
end if
c
c calculate minimum principal stress
c
iopt=0
Call PrnSig_h(iopt, sig_star, xN1, xN2, xN3,
& S(1),S(2),S(3), P, Q)
tmin = 1.0d+20
do i=1,3
    if(tmin .ge. -S(i)) then
        tmin=-S(i)
    endif
enddo
c
c check for tension
c
if(tmin .le. minstress) then
    error_RKF=1
end if
c
c check for NAN
testnan=0
do i=1,ny
    call umatnisan_h(y(i),testnan)
end do
if(testnan.eq.1) error_RKF=1
c
return
end

-----
subroutine solout_h(stress,ntens,asv,nasv,ddsde,y,nydim,
pore,depsv_np1,parms,nparms,DD)
-----
c copy the vector of state variables to umat output
c modified 7/2005 (Tamagnini, Sellari)
c
c NOTE: solid mechanics convention for stress and strain components
c pore is always positive in compression

```

```

-----
implicit none
c
integer nydim,nasv,nparms,ntens,i,j
c
double precision y(nydim),asv(nasv),stress(ntens)
double precision ddsdde(ntens,ntens),DD(6,6)
double precision parms(nparms),bulk_w,pore,depsv_np1
c
bulk_w=parms(15)
c
c ... update excess pore pressure (if undrained conditions),
compression positive
c
pore=pore-bulk_w*depsv_np1
c
c updated total stresses (effective stresses stored in y(1:6))
c
do i=1,ntens
  if (i.le.3) then
    stress(i) = y(i)-pore
  else
    stress(i) = y(i)
  end if
enddo
c
c additional state variables (first 6 components are intergranular
strains)
c
do i=1,nasv
  asv(i) = y(6+i)
enddo
c
c consistent tangent stiffness
c
do j=1,ntens
  do i=1,ntens
    ddsdde(i,j) = DD(i,j)
  enddo
enddo
c
do j=1,3
  do i=1,3
    ddsdde(i,j) = ddsdde(i,j)+bulk_w
  enddo
enddo
return
end
-----
subroutine wrista_h(mode,y,nydim,deps_np1,dtime,coords,statev,
& nstatv,parms,nparms,noel,npt,ndi,nshr,kstep,kinc)
c
c ... subroutine for managing output messages
c
c mode
c
c all = writes:      kstep, kinc, noel, npt
c                   2      = writes also:
message,coords(3),parms(nparms),ndi,nshr,stress(nstress)
c                   deps(nstress),dtime,statev(nstatv)
c                   3      = writes also:
stress(nstress),deps(nstress),dtime,statev(nstatv)
-----
implicit none
c
integer mode,nydim,nstatv,nparms,noel,npt,ndi,nshr,kstep,kinc,i
c
double precision y(nydim),statev(nstatv),parms(nparms)
double precision deps_np1(6),coords(3),dtime
c
c ... writes for mode = 2
c
if (mode.eq.2) then
  write(1,*)
  =====
  write(1,*) 'ERROR: abaqus job failed during call of UMAT'
  write(1,*)
  =====
  write(1,*) 'state dump:'
  write(1,*)
endif
c
c ... writes for all mode values
c
write(1,111) 'Step: ',kstep, 'increment: ',kinc,
& 'element: ', noel, 'Integration point: ',npt
write(1,*)
c
c ... writes for mode = 2
c
if (mode.eq.2) then
  write(1,*) 'Co-ordinates of material point:'
  write(1,104) 'x1 = ',coords(1),' x2 = ',coords(2),' x3 = ',
& coords(3)
  write(1,*)
  write(1,*) 'Material parameters:'
  write(1,*)
  do i=1,nparms
    write(1,105) 'prop(',i,') = ',parms(i)
  enddo
  write(1,*)
  write(1,102) 'No. of mean components: ',ndi
  write(1,102) 'No. of shear components: ',nshr
  write(1,*)
endif
c
c ... writes for mode = 2 or 3
c
if ((mode.eq.2).or.(mode.eq.3)) then
  write(1,*) 'Stresses:'
  write(1,*)
  write(1,101) 'sigma(1) = ',y(1)
  write(1,101) 'sigma(2) = ',y(2)
  write(1,101) 'sigma(3) = ',y(3)
  write(1,101) 'sigma(4) = ',y(4)
  write(1,101) 'sigma(5) = ',y(5)
  write(1,101) 'sigma(6) = ',y(6)
  write(1,*)
  write(1,*) 'Strain increment:'
  write(1,*)
  write(1,101) 'deps_np1(1) = ',deps_np1(1)
  write(1,101) 'deps_np1(2) = ',deps_np1(2)
  write(1,101) 'deps_np1(3) = ',deps_np1(3)
  write(1,101) 'deps_np1(4) = ',deps_np1(4)
  write(1,101) 'deps_np1(5) = ',deps_np1(5)
  write(1,101) 'deps_np1(6) = ',deps_np1(6)
  write(1,*)
  write(1,*) 'Time increment:'
  write(1,*)
  write(1,108) 'dtime = ',dtime
  write(1,*)
  write(1,*) 'Internal variables:'
  write(1,*)
  write(1,109) 'del(1) = ',statev(1)
  write(1,109) 'del(2) = ',statev(2)
  write(1,109) 'del(3) = ',statev(3)
  write(1,109) 'del(4) = ',statev(4)
  write(1,109) 'del(5) = ',statev(5)
  write(1,109) 'del(6) = ',statev(6)
  write(1,109) 'void = ',statev(7)
  write(1,*)
  write(1,*)
endif
101 format(1X,a15,e11.4)
102 format(1X,a25,i1)
103 format(1X,a7,i5)
104 format(1X,3(a5,f10.4,2X))
105 format(1X,a5,i2,a4,f20.3)
106 format(1X,3(a9,f12.4,2X))
107 format(1X,3(a10,f12.4,2X))
108 format(1X,a8,f12.4)
109 format(1X,a6,f10.4)
110 format(1X,a5,f10.4)
111 format(1X,a6,i4,2X,a11,i4,2X,a9,i10,2X,a19,i4)
c
return
end
-----
subroutine calc_statev_h(stress,statev,parms,nparms,nasv,
& nstatv,deps)
c
c computes additional state variables for postprocessing
c
-----

```

```

implicit none
c
logical elprsw
c
integer ntens,jj,kk,i
integer n,nasv,nparms,nfev,nstatv
integer maxnint,error
c
double precision parms(nparms),dot_vect_h
double precision stress(6),statev(nstatv)
double precision deps(6),tmax,tmin
double precision MM(6,6),HHtmp(nasv,6)
double precision LL(6,6),NN(6)
integer istrain
double precision zero,two,four,iopt,three
double precision l1,l2,l3,cos3t,pp,qq
double precision sin2phi,sinphi,sig_star(6),p_t
double precision norm_del,norm_del2,del(6)
c
parameter(zero=0.0d0,two=2.0d0,four=4.0d0,three=3.0d0)
c
c ... calc phimob (statev 11) from Matsuoka-Nakai YS
p_t =parms(2)
do i=1,3
sig_star(i)=stress(i)-p_t
end do
do i=4,6
sig_star(i)=stress(i)
end do
call inv_sig_h(sig_star,pp,qq,cos3t,l1,l2,l3)
if(l3 .ne. 0) then
sin2phi=(9.d0+11*I2/I3)/(1.d0+11*I2/I3)
else
sin2phi=0
end if
if(sin2phi .lt. 0) then
sin2phi=0
end if
if(sin2phi .gt. 1) then
sin2phi=1
end if
sinphi=sqrt(sin2phi)
statev(11)= asin(sinphi)*
! 180.0d0/3.141592d0
c ... calc norm. length of intergr. strain rho (statev 12)
if(parms(10) .le. 0.5) then
istrain=0
else
istrain=1
end if
if(istrain .eq. 1) then
do i=1,6
del(i)=statev(i)
enddo
norm_del2=dot_vect_h(2,del,del,6)
norm_del=dsqrt(norm_del2)
statev(12)=norm_del/parms(12)
else
statev(12)=0
end if
return
end
c-----
subroutine umatisnan_h(chcknum,testnan)
c-----
c
c checks whether number is NaN
c
c-----
double precision chcknum
integer testnan
if (.not.(chcknum .ge. 0. .OR. chcknum .lt. 0.)) testnan=1
if (chcknum .gt. 1.d30) testnan=1
if (chcknum .lt. -1.d30) testnan=1
if (chcknum .ne. chcknum) testnan=1
return
end
c-----
subroutine xit_h
c-----
stop
c
return
end
c-----
Subroutine PrnSig_h(IOpt,S,xN1,xN2,xN3,S1,S2,S3,P,Q)
Implicit Double Precision (A-H,O-Z)
Dimension S(*),xN1(*),xN2(*),xN3(*)
If (iOpt.Eq.1) Then
Call Eig_3_h(0,S,xN1,xN2,xN3,S1,S2,S3,P,Q) ! with
Eigenvectors
Else
Call Eig_3a_h(0,S,S1,S2,S3,P,Q) ! no Eigenvectors
End If
Return
End
c-----
Subroutine Eig_3_h(iOpt,St,xN1,xN2,xN3,S1,S2,S3,P,Q)
Implicit Double Precision (A-H,O-Z)
Dimension St(6),A(3,3),V(3,3),
! xN1(3),xN2(3),xN3(3)
!
! Get Eigenvalues/Eigenvectors for 3*3 matrix
! Wim Bomhof 15/11/01
! PGB : adaption to Principal stress calculation
!
! Applied on principal stresses, directions
! Stress vector St(): XX, YY, ZZ, XY, YZ, ZX
!
A(1,1) = St(1) ! xx
A(1,2) = St(4) ! xy = yx
A(1,3) = St(6) ! zx = xz
A(2,1) = St(4) ! xy = yx
A(2,2) = St(2) ! yy
A(2,3) = St(5) ! zy = yz
A(3,1) = St(6) ! zx = xz
A(3,2) = St(5) ! zy = yz
A(3,3) = St(3) ! zz
! Set V to unity matrix
V(1,1) = 1
V(2,1) = 0
V(3,1) = 0
V(1,2) = 0
V(2,2) = 1
V(3,2) = 0
V(1,3) = 0
V(2,3) = 0
V(3,3) = 1
abs_max_s=0.0
Do i=1,3
Do j=1,3
if (abs(a(i,j)) .Gt. abs_max_s) abs_max_s=abs(a(i,j))
End Do
End Do
Tol = 1d-20 * abs_max_s
it = 0
itmax = 50
Do While (it.Lt.itMax .And.
! abs(a(1,2))+abs(a(2,3))+abs(a(1,3)) .Gt. Tol )
it=it+1
Do k=1,3
If (k .Eq. 1) Then
ip=1
iq=2
Else If (k .Eq.2) Then
ip=2
iq=3
Else
ip=3
iq=1
End If

```

```

ip=1
iq=3
End If
If (abs(a(ip,iq)) .gt. Tol) Then
tau=(a(iq,iq)-a(ip,ip))/(2.0*a(ip,iq))
If (tau .Ge.0.0) Then
sign_tau=1.0
Else
sign_tau=-1.0
End If
t=sign_tau/(abs(tau)+sqrt(1.0+tau*tau))
c=1.0/sqrt(1.0+t*t)
s=t*c
a1p=c*a(1,ip)-s*a(1,iq)
a2p=c*a(2,ip)-s*a(2,iq)
a3p=c*a(3,ip)-s*a(3,iq)
a(1,iq)=s*a(1,ip)+c*a(1,iq)
a(2,iq)=s*a(2,ip)+c*a(2,iq)
a(3,iq)=s*a(3,ip)+c*a(3,iq)
a(1,ip)=a1p
a(2,ip)=a2p
a(3,ip)=a3p

v1p=c*v(1,ip)-s*v(1,iq)
v2p=c*v(2,ip)-s*v(2,iq)
v3p=c*v(3,ip)-s*v(3,iq)
v(1,iq)=s*v(1,ip)+c*v(1,iq)
v(2,iq)=s*v(2,ip)+c*v(2,iq)
v(3,iq)=s*v(3,ip)+c*v(3,iq)
v(1,ip)=v1p
v(2,ip)=v2p
v(3,ip)=v3p

ap1=c*a(ip,1)-s*a(iq,1)
ap2=c*a(ip,2)-s*a(iq,2)
ap3=c*a(ip,3)-s*a(iq,3)
a(iq,1)=s*a(ip,1)+c*a(iq,1)
a(iq,2)=s*a(ip,2)+c*a(iq,2)
a(iq,3)=s*a(ip,3)+c*a(iq,3)
a(ip,1)=ap1
a(ip,2)=ap2
a(ip,3)=ap3
End If ! a(ip,iq)<>0
End Do ! k
End Do ! While
! principal values on diagonal of a
S1 = a(1,1)
S2 = a(2,2)
S3 = a(3,3)
! Derived invariants
P = (S1+S2+S3)/3
Q = Sqrt( ( (S1-S2)**2 + (S2-S3)**2 + (S3-S1)**2 ) / 2 )

! Sort eigenvalues S1 <= S2 <= S3
is1 = 1
is2 = 2
is3 = 3
if (s1.Gt.s2) Then
t = s2
s2 = s1
s1 = t
it = is2
is2 = is1
is1 = it
End If
if (s2.Gt.s3) Then
t = s3
s3 = s2
s2 = t
it = is3
is3 = is2
is2 = it
End If
if (s1.Gt.s2) Then
t = s2
s2 = s1
s1 = t
it = is2
is2 = is1
is1 = it
End If
Do i=1,3
xN1(i) = v(i,is1) ! first column
xN2(i) = v(i,is2) ! second column
xN3(i) = v(i,is3) ! third column

```

```

End Do
Return
End ! Eig_3

Subroutine Eig_3a_h(iOpt,St,S1,S2,S3,P,Q) ! xN1,xN2,xN3,
Implicit Double Precision (A-H,O-Z)
Dimension St(6),A(3,3) ! V(3,3),xN1(3),xN2(3),xN3(3)
!
! Get Eigenvalues ( no Eigenvectors) for 3*3 matrix
! Wim Bomhof 15/11/01
!
! Applied on principal stresses, directions
! Stress vector XX, YY, ZZ, XY, YZ, ZX
!
A(1,1) = St(1) ! xx
A(1,2) = St(4) ! xy = yx
A(1,3) = St(6) ! zx = xz

A(2,1) = St(4) ! xy = yx
A(2,2) = St(2) ! yy
A(2,3) = St(5) ! zy = yz

A(3,1) = St(6) ! zx = xz
A(3,2) = St(5) ! zy = yz
A(3,3) = St(3) ! zz

abs_max_s=0.0
Do i=1,3
Do j=1,3
if (abs(a(i,j)) .Gt. abs_max_s) abs_max_s=abs(a(i,j))
End Do
End Do
Tol = 1d-20 * abs_max_s
If (iOpt.Eq.1) Tol = 1d-50*abs_max_s
it=0
itmax = 50

Do While ( ! it.It.itmax .And.
abs(a(1,2))+abs(a(2,3))+abs(a(1,3)) .Gt. Tol )

it=it+1
Do k=1,3
If (k .Eq. 1) Then
ip=1
iq=2
Else If (k .Eq.2) Then
ip=2
iq=3
Else
ip=1
iq=3
End If

If (abs(a(ip,iq)) .gt. Tol) Then ! ongelijk nul ?
tau=(a(iq,iq)-a(ip,ip))/(2.0*a(ip,iq))
If (tau .Ge.0.0) Then
sign_tau=1.0
Else
sign_tau=-1.0
End If
t=sign_tau/(abs(tau)+sqrt(1.0+tau*tau))
c=1.0/sqrt(1.0+t*t)
s=t*c
a1p=c*a(1,ip)-s*a(1,iq)
a2p=c*a(2,ip)-s*a(2,iq)
a3p=c*a(3,ip)-s*a(3,iq)
a(1,iq)=s*a(1,ip)+c*a(1,iq)
a(2,iq)=s*a(2,ip)+c*a(2,iq)
a(3,iq)=s*a(3,ip)+c*a(3,iq)
a(1,ip)=a1p
a(2,ip)=a2p
a(3,ip)=a3p

ap1=c*a(ip,1)-s*a(iq,1)
ap2=c*a(ip,2)-s*a(iq,2)
ap3=c*a(ip,3)-s*a(iq,3)
a(iq,1)=s*a(ip,1)+c*a(iq,1)
a(iq,2)=s*a(ip,2)+c*a(iq,2)
a(iq,3)=s*a(ip,3)+c*a(iq,3)
a(ip,1)=ap1
a(ip,2)=ap2
a(ip,3)=ap3
End If ! a(ip,iq)<>0
End Do ! k
End Do ! While

```

```

! principal values on diagonal of a
S1 = a(1,1)
S2 = a(2,2)
S3 = a(3,3)
! Derived invariants
P = (S1+S2+S3)/3
Q = Sqrt( ( (S1-S2)**2 + (S2-S3)**2 + (S3-S1)**2 ) / 2 )

if (s1.Gt.s2) Then
  t = s2
  s2 = s1
  s1 = t
End If
if (s2.Gt.s3) Then
  t = s3
  s3 = s2
  s2 = t
End If
if (s1.Gt.s2) Then
  t = s2
  s2 = s1
  s1 = t
End If
Return
End ! Eig_3a

-----
subroutine calc_elasti_h(y,n,nasv,dsub,err_tol,maxnint,DTmin,
&
  &
  &
  dtime,DDtan,youngel,nuel,error)
-----
c
c numerical solution of y'=f(y)
c explicit, adapive RKF23 scheme with local time step extrapolation
c
c Tamagnini, Sellari & Miriano 6/2005
c
-----
implicit none

c
c logical elprsw

integer n,nasv,nparms,i,ksubst,kreject,nfev
integer maxnint,error,error_RKF,tension,j

c
double precision y(n),parms(nparms),dsub,err_tol,DTmin
double precision zero,half,one,two,three,four,six
double precision ptnine,onesixth,onethird,twothirds,temp

c
double precision deps_np1(6),y_k(n),y_2(n),y_3(n),y_til(n)
double precision y_hat(n),DDtan(6,6)
double precision T_k,DT_k,dtime,Il(6,6),krondelta(6)
double precision kRK_1(n),kRK_2(n),kRK_3(n)
double precision norm_R,S_hull,youngel,nuel,F_sig(6)

c
parameter(zero=0.0d0,one=1.0d0,two=2.0d0,three=3.0d0)
parameter(four=4.0d0,six=6.0d0,half=0.5d0,ptnine=0.9d0)

c
c ... initialize y_k vector and other variables
c
do i=1,n
  y_k(i)=zero
end do

c
onesixth=one/six
onethird=one/three
twothirds=two/three

c
c ... fourth order identity tensors in Voigt notation
c
do i = 1,6
  do j=1,6
    Il(i,j)=zero
  end do
end do

Il(1,1)=one
Il(2,2)=one
Il(3,3)=one
Il(4,4)=half
Il(5,5)=half
Il(6,6)=half
c

```

```

krondelta(1)=one
krondelta(2)=one
krondelta(3)=one
krondelta(4)=zero
krondelta(5)=zero
krondelta(6)=zero
c
c ... Elastic stiffness tensor
c
if(youngel.gt.0) then
  do i = 1,6
    do j=1,6
      DDtan(i,j)=(youngel/(1+nuel))*(Il(i,j) +
&
      &
      nuel/(1-2*nuel)*krondelta(i)*krondelta(j));
    end do
  end do
end if

call matmul_h(DDtan,deps_np1,F_sig,6,6,1)
do i=1,6
  y(i)=y(i)+F_sig(i)
end do

return
end
c
-----
SUBROUTINE
SDVINI(STATEV,COORDS,NSTATV,NCRDS,NOEL,NPT,
1 LAYER,KSPT,props,nprops)
-----
c
c The string for the material name may contain 9 characters.
c
c Material constants:
c
-----
props(j)
-----
c
c 1 phi
c 2 p_t
c 3 h_s
c 4 n
c 5 e_d0
c 6 e_c0
c 7 e_i0
c 8 alpha
c 9 beta
c 10 m_R
c 11 m_T
c 12 RR
c 13 beta_r
c 14 chi
c 15 bulk_w
c 16 e0
-----
c
c Solution dependent state variables (statev):
c definition via sdvini
c
c 1 ... del_11 intergranular strain component
c 2 ... del_22 intergranular strain component
c 3 ... del_33 intergranular strain component
c 4 ... del_12 intergranular strain component
c 5 ... del_13 intergranular strain component
c 6 ... del_23 intergranular strain component
c 7 ... void void ratio
c 8 ... pore excess pore pressure (undrained conditions,
bulk_w>0)
c 9 ... p mean stress (o)
c 10 ... nfev number of function evaluation
c 11 ... phi_mob phi_mob in degrees
c 12 ... rho normalised length of intergr. strain rho
c 13 ... dsub suggested substep size
c
c For undrained analyses with penalty approach:
c bulk_w: bulk modulus of water phase
c
Implicit Double Precision (A-H, O-Z)
Dimension statev(nstatv), props(nprops)

```

c initialize state variables

```
statev(1)=1.0d0  
statev(2)=1.0d0  
statev(3)=1.0d0  
statev(4)=1.0d0  
statev(5)=1.0d0  
statev(6)=1.0d0  
statev(7)=0.7392  
statev(8)=0  
statev(9)=0  
statev(10)=0.d0  
statev(11)=0.d0  
statev(12)=0.d0  
statev(13)=0.D0
```

Return

End! StVarIni

**APPENDIX C.**  
**Sample Input code for the abaqus model with the user  
defined material**

```

** m,kg,N,s
*Heading
** Job name: SPd20mm Model name: SPd20mm
** Generated by: Abaqus/CAE 6.13-1
*Preprint, echo=NO, model=NO, history=NO, contact=NO
**
** PARTS
**
*Part, name=Cap
*Node
  1, 0.0500000007, 0.176666662, 0.0250000004
  2, 0.0500000007, 0.211666673, 0.0250000004
  3, 0.0500000007, 0.176666662, 0.0125000002
  4, 0.0500000007, 0.211666673, 0.0125000002
  5, 0.0500000007, 0.176666662, 0.
  6, 0.0500000007, 0.211666673, 0.
  7, 0.075000003, 0.176666662, 0.0250000004
  8, 0.075000003, 0.211666673, 0.0250000004
  9, 0.075000003, 0.176666662, 0.0125000002
 10, 0.075000003, 0.211666673, 0.0125000002
 11, 0.075000003, 0.176666662, 0.
 12, 0.075000003, 0.211666673, 0.
 13, 0.100000001, 0.176666662, 0.0250000004
 14, 0.100000001, 0.211666673, 0.0250000004
 15, 0.100000001, 0.176666662, 0.0125000002
 16, 0.100000001, 0.211666673, 0.0125000002
 17, 0.100000001, 0.176666662, 0.
 18, 0.100000001, 0.211666673, 0.
*Element, type=C3D8
1, 3, 4, 2, 1, 9, 10, 8, 7
2, 5, 6, 4, 3, 11, 12, 10, 9
3, 9, 10, 8, 7, 15, 16, 14, 13
4, 11, 12, 10, 9, 17, 18, 16, 15
*Nset, nset=RBC, generate
  1, 18, 1
*Elset, elset=RBC, generate
  1, 4, 1
** Section: RBC
*Solid Section, elset=RBC, material=RBC
,
*End Part
**
*Part, name=Pile
*Node
  1, -0.150000006, 0., 1.45000005
  2, -0.129999995, 0., 1.45000005
----- truncated -----
*Nset, nset=Pile, generate
  1, 1124, 1
*Elset, elset=Pile, generate
  1, 190, 1
** Section: Pile
*Solid Section, elset=Pile, material=Pile
*End Part
**
*Part, name=Sand
*Node
  1, 0.208090171, -0.0641221479, 0.
  2, 0.205877855, -0.0619098283, 0.
----- truncated -----
*Nset, nset=Soil, generate

```

```

1, 19266, 1
*Elset, elset=Soil, generate
1, 16948, 1
** Section: Soil
*Solid Section, elset=Soil, material=Soil
,
*End Part
**
**
** ASSEMBLY
**
*Assembly, name=Assembly
**
*Instance, name=Pile-1, part=Pile
0.470200002358994, -0.07, 0.
*End Instance
**
*Instance, name=Sand-1, part=Sand
0.130200002342463, 0., 0.
*End Instance
**
*Instance, name=Cap-1, part=Cap
0.255200002358994, -0.246666666666667, 1.5
*End Instance
**
*Node
1, 0.330200016, -0.0700000003, 1.51250005
*Nset, nset=Back, instance=Sand-1
9, 10, 48, 49, 50, 51, 52, 53, 54, 55, 56, 57, 58, 59, 60, 61
----- truncated -----
*Elset, elset=Back, instance=Sand-1
38, 42, 214, 378, 380, 381, 401, 403, 411, 412, 415, 416, 418, 419, 421, 422
----- truncated -----

*Nset, nset=Bottom, instance=Pile-1
5, 6, 57, 58, 59, 60, 61, 62, 63, 64, 77, 78, 79, 80, 81, 82
----- truncated -----
*Nset, nset=Bottom, instance=Sand-1, generate
1, 494, 1
*Elset, elset=Bottom, instance=Pile-1, generate
181, 190, 1
*Elset, elset=Bottom, instance=Sand-1, generate
1, 446, 1
*Nset, nset=Hole, instance=Sand-1
1, 2, 3, 4, 5, 6, 7, 12, 13, 14, 15, 495, 496, 497, 498, 499
----- truncated -----

*Elset, elset=Hole, instance=Sand-1
2, 3, 4, 7, 10, 11, 59, 60, 85, 88, 448, 449, 450, 453, 456, 457
----- truncated -----
*Nset, nset=PH, instance=Pile-1
3, 4, 15, 16, 17, 18, 19, 20, 21, 22, 71, 72, 73, 74, 75, 76
----- truncated -----
*Nset, nset=RP
1,
*Nset, nset=Sides, instance=Sand-1
8, 9, 10, 11, 43, 44, 45, 46, 47, 63, 64, 65, 66, 67, 502, 503
----- truncated -----
nset=Symm, instance=Pile-1
1, 2, 3, 4, 5, 6, 13, 14, 21, 22, 23, 24, 25, 26, 27, 28
----- truncated -----
*Nset, nset=Symm, instance=Sand-1

```

```

6, 7, 8, 11, 16, 17, 18, 19, 20, 21, 22, 23, 24, 25, 26, 27
----- truncated -----
*Elset, elset=Symm, instance=Pile-1
1, 3, 5, 11, 13, 15, 21, 23, 25, 31, 33, 35, 41, 43, 45, 51
----- truncated -----
*Elset, elset=Symm, instance=Sand-1
8, 11, 12, 13, 14, 16, 17, 19, 20, 21, 22, 23, 24, 25, 26, 27
28, 29, 30, 31, 33, 36, 37, 55, 59, 62, 63, 64, 65, 66, 67, *Elset, elset=_Master_Pile_S6,
internal, instance=Pile-1
1, 5, 16, 26, 36, 46, 56, 66, 76, 86, 96, 106, 116, 126, 136, 146
156, 166, 176, 186
*Elset, elset=_Master_Pile_S4, internal, instance=Pile-1
2, 14, 17, 18, 24, 27, 28, 34, 37, 38, 44, 47, 48, 54, 57, 58
----- truncated -----
*Elset, elset=_Master_Pile_S5, internal, instance=Pile-1
4, 7, 8, 12, 22, 32, 42, 52, 62, 72, 82, 92, 102, 112, 122, 132
142, 152, 162, 172, 182
*Elset, elset=_Master_Pile_S3, internal, instance=Pile-1
6, 11, 15, 21, 25, 31, 35, 41, 45, 51, 55, 61, 65, 71, 75, 81
85, 91, 95, 101, 105, 111, 115, 121, 125, 131, 135, 141, 145, 151, 155, 161
165, 171, 175, 181, 185
*Surface, type=ELEMENT, name=Master_Pile
_Master_Pile_S6, S6
_Master_Pile_S4, S4
_Master_Pile_S5, S5
_Master_Pile_S3, S3
*Elset, elset=_Slave_Soil_S5, internal, instance=Sand-1
2, 10, 59, 60, 85, 448, 456, 505, 506, 531, 894, 902, 951, 952, 977, 1340
1348, 1397, 1398, 1423, 1786, 1794, 1843, 1844, 1869, 2232, 2240, 2289, 2290, 2315, 2678, 2686
*Elset, elset=_Slave_Soil_S3, internal, instance=Sand-1, generate
4, 16506, 446
*Elset, elset=_Slave_Soil_S4, internal, instance=Sand-1, generate
88, 16590, 446
*Surface, type=ELEMENT, name=Slave_Soil
_Slave_Soil_S5, S5
_Slave_Soil_S6, S6
_Slave_Soil_S4, S4
_Slave_Soil_S3, S3
** Constraint: RB
*Rigid Body, ref node=_PickedSet31, elset=Cap-1.RBC, tie nset=PH
*Elset, elset=__Slip_Gap_msm_1_S6, internal, instance=Pile-1
1, 5
*Elset, elset=__Slip_Gap_msm_1_S4, internal, instance=Pile-1
2,
*Elset, elset=__Slip_Gap_msm_1_S5, internal, instance=Pile-1
4, 7, 8
*Elset, elset=__Slip_Gap_msm_1_S3, internal, instance=Pile-1
6,
*Surface, type=ELEMENT, name=_Slip_Gap_msm_1, internal
__Slip_Gap_msm_1_S6, S6
__Slip_Gap_msm_1_S4, S4
__Slip_Gap_msm_1_S5, S5
__Slip_Gap_msm_1_S3, S3
*Elset, elset=__Slip_Gap_msm_2_S3, internal, instance=Pile-1
11, 15, 21, 25, 31, 35, 41, 45, 51, 55, 61, 65, 71, 75, 81, 85
91, 95, 101, 105, 111, 115, 121, 125, 131, 135, 141, 145, 151, 155, 161, 165
171, 175, 181, 185
*Elset, elset=__Slip_Gap_msm_2_S5, internal, instance=Pile-1, generate
12, 182, 10
*Elset, elset=__Slip_Gap_msm_2_S4, internal, instance=Pile-1
14, 17, 18, 24, 27, 28, 34, 37, 38, 44, 47, 48, 54, 57, 58, 64
67, 68, 74, 77, 78, 84, 87, 88, 94, 97, 98, 104, 107, 108, 114, 117

```

```

118, 124, 127, 128, 134, 137, 138, 144, 147, 148, 154, 157, 158, 164, 167, 168
174, 177, 178, 184, 187, 188
*Elset, elset=__Slip_Gap_msm_2_S6, internal, instance=Pile-1, generate
16, 186, 10
*Surface, type=ELEMENT, name=__Slip_Gap_msm_2, internal
__Slip_Gap_msm_2_S3, S3
__Slip_Gap_msm_2_S5, S5
__Slip_Gap_msm_2_S4, S4
__Slip_Gap_msm_2_S6, S6
*Elset, elset=__Slip_Gap_ssm_1_S5, internal, instance=Sand-1
2, 10, 59, 60, 85, 448, 456, 505, 506, 531, 894, 902, 951, 952, 977, 1340
1348, 1397, 1398, 1423, 1786, 1794, 1843, 1844, 1869, 2232, 2240, 2289, 2290, 2315, 2678, 2686
----- truncated -----
*Elset, elset=__Slip_Gap_ssm_1_S6, internal, instance=Sand-1
3, 7, 11, 449, 453, 457, 895, 899, 903, 1341, 1345, 1349, 1787, 1791, 1795, 2233
2237, 2241, 2679, 2683, 2687, 3125, 3129, 3133, 3571, 3575, 3579, 4017, 4021, 4025, 4463, 4467
----- truncated -----
*Elset, elset=__Slip_Gap_ssm_1_S3, internal, instance=Sand-1, generate
4, 16506, 446
*Elset, elset=__Slip_Gap_ssm_1_S4, internal, instance=Sand-1, generate
88, 16590, 446
*Surface, type=ELEMENT, name=__Slip_Gap_ssm_1, internal
__Slip_Gap_ssm_1_S5, S5
__Slip_Gap_ssm_1_S6, S6
__Slip_Gap_ssm_1_S4, S4
__Slip_Gap_ssm_1_S3, S3
*End Assembly
**
** MATERIALS
**
*Material, name=Pile
*Density
2600.,
*Elastic
6.86e+10, 0.347
*Material, name=RBC
*Elastic
5e+11, 0.3
*Material, name=Soil
*Density
1442.77,
*Depvar
13,
*User Material, constants=16, unsymm
30., 0., 2.6e+09, 0.35, 0.61, 0.98, 1.1, 0.18
1.1, 0., 0., 0., 0., 0., 0., 0.80
**
** INTERACTION PROPERTIES
**
*Surface Interaction, name=Sip_Gap
1.,
*Friction, slip tolerance=0.005
0.47,
*Surface Behavior, pressure-overclosure=HARD
*Surface Smoothing, name=Slip_Gap
, __Slip_Gap_msm_1, CIRCUMFERENTIAL, 0.3302, -0.07, 0., 0.3302, -0.07, 1.
, __Slip_Gap_msm_2, CIRCUMFERENTIAL, 0.3302, -0.07, 0., 0.3302, -0.07, 1.
__Slip_Gap_ssm_1, , CIRCUMFERENTIAL, 0.3302, -0.07, 1.45, 0.3302, -0.07, 0.45
**
** BOUNDARY CONDITIONS
**
** Name: Back Type: Displacement/Rotation

```

```

*Boundary
Back, 2, 2
** Name: Bottom Type: Displacement/Rotation
*Boundary
Bottom, 1, 1
Bottom, 2, 2
Bottom, 3, 3
Bottom, 4, 4
Bottom, 5, 5
Bottom, 6, 6
** Name: Hole Type: Displacement/Rotation
*Boundary
Hole, 1, 1
Hole, 2, 2
** Name: Sides Type: Displacement/Rotation
*Boundary
Sides, 1, 1
** Name: Symm Type: Symmetry/Antisymmetry/Encastre
*Boundary
Symm, YSYMM
**
** PREDEFINED FIELDS
**
** Name: SW Type: Geostatic stress
*Initial Conditions, type=STRESS, GEOSTATIC
Sand-1.Soil, -20920.2, 0., 0., 1.45, 0.5, 0.5
*Initial Conditions, type=Solution, user
**
** INTERACTIONS
**
** Interaction: Slip_Gap
*Contact Pair, interaction=Slip_Gap, type=SURFACE TO SURFACE, adjust=0.0, geometric correction=Slip_Gap
Slave_Soil, Master_Pile
** -----
**
** STEP: SW
**
*Step, name=SW, nlgeom=YES
SW
*Geostatic
**
** LOADS
**
** Name: SW_GRAVITY Type: Gravity
*Dload
Sand-1.Soil, GRAV, 9.8, 0., 0., -1.
**
** INTERACTIONS
**
** Interaction: Slip_Gap
*Model Change, type=CONTACT PAIR, remove
Slave_Soil, Master_Pile
** Contact Controls for Interaction: Slip_Gap
*Contact Controls, master=Master_Pile, slave=Slave_Soil, reset
*Contact Controls, master=Master_Pile, slave=Slave_Soil, stabilize=1.
**
** OUTPUT REQUESTS
**
*Restart, write, frequency=0
**
** FIELD OUTPUT: F-Output-1
**

```

```

*Output, field, variable=PRESELECT
**
** HISTORY OUTPUT: H-Output-1
**
*Output, history, variable=PRESELECT
*End Step
** -----
**
** STEP: Monotonic
**
*Step, name=Monotonic, nlgeom=YES, inc=1000
*Static
0.001, 6000., 1e-20, 1000.
**
** BOUNDARY CONDITIONS
**
** Name: Back Type: Displacement/Rotation
*Boundary, op=NEW
Back, 2, 2
** Name: Bottom Type: Displacement/Rotation
*Boundary, op=NEW
Bottom, 1, 1
Bottom, 2, 2
Bottom, 3, 3
Bottom, 4, 4
Bottom, 5, 5
Bottom, 6, 6
** Name: Hole Type: Displacement/Rotation
*Boundary, op=NEW
** Name: PH Type: Displacement/Rotation
*Boundary, op=NEW
RP, 1, 1, 0.1
RP, 2, 2
RP, 4, 4
RP, 5, 5
RP, 6, 6
** Name: Sides Type: Displacement/Rotation
*Boundary, op=NEW
Sides, 1, 1
** Name: Symm Type: Symmetry/Antisymmetry/Encastre
*Boundary, op=NEW
Symm, YSYMM
**
** INTERACTIONS
**
** Interaction: Slip_Gap
*Model Change, type=CONTACT PAIR, add
Slave_Soil, Master_Pile
**
*controls, parameters=time incrementation
12, 15, 9, 20, 10, 4, 12, 20, 5, 3, 50
** OUTPUT REQUESTS
**
*Restart, write, frequency=0
**
** FIELD OUTPUT: F-Output-1
**
*Output, field
**
*Output, history

*End Step

```

**APPENDIX D.**  
**Element Test Abaqus for the hypoplastic model**

```

*Heading
** Job name: hpTS Model name: hpTS
** Generated by: Abaqus/CAE 6.13-1
*Preprint, echo=NO, model=NO, history=NO, contact=NO
**
** PARTS
**
*Part, name=Box
*Node
  1, -0.100000001, -0.119999997, 0.5
  2, -0.100000001, 0.379999995, 0.5
  3, -0.100000001, -0.119999997, 0.
  4, -0.100000001, 0.379999995, 0.
  5, 0.400000006, -0.119999997, 0.5
  6, 0.400000006, 0.379999995, 0.5
  7, 0.400000006, -0.119999997, 0.
  8, 0.400000006, 0.379999995, 0.
*Element, type=C3D8
1, 3, 4, 2, 1, 7, 8, 6, 5
*Nset, nset=Box, generate
  1, 8, 1
*Elset, elset=Box
  1,
** Section: S_Soil
*Solid Section, elset=Box, material=TShypo
,
*End Part
**
**
** ASSEMBLY
**
*Assembly, name=Assembly
**
*Instance, name=Box-1, part=Box
*End Instance
**
*Nset, nset=Bottom, instance=Box-1
  3, 4, 7, 8
*Elset, elset=Bottom, instance=Box-1
  1,
*Nset, nset=Left, instance=Box-1, generate
  1, 4, 1
*Elset, elset=Left, instance=Box-1
  1,
*Nset, nset=PorePressure, instance=Box-1
  1, 2, 5, 6
*Nset, nset=Rear, instance=Box-1, generate
  2, 8, 2
*Elset, elset=Rear, instance=Box-1
  1,
*Nset, nset=TopDisplacement, instance=Box-1
  1, 2, 5, 6
*Elset, elset=TopDisplacement, instance=Box-1
  1,
*Elset, elset=_Front_S6, internal, instance=Box-1
  1,

```

```

*Surface, type=ELEMENT, name=Front
_Front_S6, S6
*Elset, elset=_Right_S2, internal, instance=Box-1
1,
*Surface, type=ELEMENT, name=Right
_Right_S2, S2
*Elset, elset=_Top_S5, internal, instance=Box-1
1,
*Surface, type=ELEMENT, name=Top
_Top_S5, S5
*End Assembly
**
** MATERIALS
**
*Material, name=TShypo
*Depvar
13,
*User Material, constants=15
30., 0., 2.6e+09, 0.35, 0.61, 0.98, 1.1, 0.18
1.1, 0.0, 0., 0., 0., 0., 0., 0.80
**
** BOUNDARY CONDITIONS
**
** Name: Bottom Type: Displacement/Rotation
*Boundary
Bottom, 3, 3
** Name: Left Type: Displacement/Rotation
*Boundary
Left, 1, 1
** Name: Rear Type: Displacement/Rotation
*Boundary
Rear, 2, 2
**
** PREDEFINED FIELDS
**
*INITIAL CONDITIONS, TYPE=SOLUTION, USER
** Name: Predefined Field-2 Type: Geostatic stress
*Initial Conditions, type=STRESS, GEOSTATIC
Box-1.Box, -10612., 0., -10612., 0.5, 1., 1.
** -----
**
** STEP: Geostatic
**
*Step, name=Geostatic, nlgeom=NO
*Geostatic
**
** LOADS
**
** Name: Front Type: Pressure
*Dload
Front, P, 10612.
** Name: LoadSurface Type: Pressure
*Dload
Top, P, 10612.
** Name: Right Type: Pressure
*Dload

```

```

Right, P, 10612.
**
** OUTPUT REQUESTS
**
*Restart, write, frequency=0
**
** FIELD OUTPUT: F-Output-1
**
*Output, field, variable=PRESELECT
**
** HISTORY OUTPUT: H-Output-1
**
*Output, history, variable=PRESELECT
*End Step
** -----
**
** STEP: Loading
**
*Step, name>Loading, ngeom=NO, inc=100000
*Static, direct
1, 1500.,
**
** BOUNDARY CONDITIONS
**
** Name: TopDisplacement Type: Displacement/Rotation
*Boundary
TopDisplacement, 3, 3, -0.1
**
** OUTPUT REQUESTS
**
*Restart, write, frequency=0
**
** FIELD OUTPUT: F-Output-1
**
*Output, field, variable=PRESELECT
**
** HISTORY OUTPUT: H-Output-1
**
*Output, history, variable=PRESELECT
*End Step

```